

UC San Diego

UC San Diego Electronic Theses and Dissertations

Title

Reactivity Studies of Carbenes and the Development of a Novel Carbene

Permalink

<https://escholarship.org/uc/item/2xj688k3>

Author

Wang, Victor Tzer

Publication Date

2023

Peer reviewed|Thesis/dissertation

UNIVERSITY OF CALIFORNIA SAN DIEGO

Reactivity Studies of Carbenes and the Development of a Novel Carbene

A dissertation submitted in partial satisfaction of the requirements for the degree of
Doctor of Philosophy

in

Chemistry

by

Victor Tzer Wang

Committee in charge:

Professor Guy Bertrand, Chair
Professor Jennifer Burney
Professor Thomas Bussey
Professor Tadeusz Molinski
Professor Valerie Schmidt

2023

Copyright

Victor Tzer Wang, 2023

All rights reserved

The thesis of Victor Tzer Wang is approved, and it is acceptable in quality and form for publication on microfilm and electronically.

University of California San Diego

2023

DEDICATION

This dissertation is dedicated to my parents and my siblings
who have provided me the love, encouragement, advice, and challenges
that inspire me to dream bigger.

TABLE OF CONENTS

Dissertation Approval Page	iii
Dedication	iv
Table of Contents	v
List of Abbreviations	vii
List of Figures	xi
List of Schemes	xiv
List of Tables	xvii
Acknowledgements	xviii
Vita	xxiv
Abstract of Dissertation	xxv
Chapter 1 General Introduction	1
1.1 What is a Carbene?	1
1.2 Properties of Carbenes	3
1.2.1 HOMO and LUMO energies	3
1.2.2 Singlet-Triplet Gap	11
1.2.3 Steric Environment	12
1.3 Carbene Electronic Diversity	14
1.3.1 Substituent Effects – Electronic Influence	14
1.3.2 Backbone π Effects	17
1.3.3 Backbone σ Effects – Carbene Angle	21
1.4 Carbenes as Useful Chemical Tools	23
1.4.1 Applications as Ligand in Catalysis	23
1.4.2 Applications as Organocatalyst	30
1.4.3 Applications in Main Group Research	36
1.5 Review of Select Carbene Syntheses	44
1.5.1 N-Heterocyclic Carbenes (NHC)	45
1.5.2 1,2,4-triazol-5-ylidenes (Ender's Carbene)	52
1.5.3 Cyclic Alkyl Amino Carbenes (CAAC)	53
1.5.4 Diamido Carbenes (DAC)	55
1.5.5 Mesoionic Carbenes (MIC)	55
1.6 Inventory of Carbenes	57
1.6.1 Nucleophilicity, Electrophilicity, and Ambiphilicity of Carbenes	57
1.6.2 Opportunities for New Carbenes	59
1.7 References	60
Chapter 2 Ambiphilicity of Ring Expanded N-Heterocyclic Carbenes	75
2.1 Introduction	75
2.2 Results and Discussion	77
2.3 Conclusion	83
2.4 Experimental	83
2.4.1 General Methods	83
2.4.2 Synthetic Procedures	84
2.4.3 Crystallographic Data	89

2.4.4 Computational Data	94
2.5 Acknowledgements	103
2.6 References	104
Chapter 3 Synthetic Routes Towards EndersCAAC and isoEndersCAAC	108
3.1 Introduction	108
3.2 Synthetic Work to EndersCAAC	115
3.3 Synthetic Routes to isoEndersCAAC	126
3.4 Conclusion	130
3.5 Experimental	131
3.5.1 General Methods	131
3.5.2 Synthetic Procedures	132
3.5.3 Computational Data	146
3.6 Acknowledgements	148
3.7 References	149
Chapter 4 An Air-Persistent Radical Cation	153
4.1 Introduction	153
4.2 Synthetic Route to 3,3'-Bipyrazolylidene	154
4.3 Characterization	156
4.4 Conclusion	166
4.5 Experimental	167
4.5.1 General Methods	167
4.5.2 Synthetic Procedures	168
4.5.3 Crystallographic Data	173
4.5.4 Computational Data	174
4.6 Acknowledgements	180
4.7 References	180

LIST OF ABBREVIATIONS

Å: Angstrom

Ad: 1-adamantyl

aNHC: Abnormal N-heterocyclic carbene

Ar: Aryl

BICAAC: Bicyclic alkyl(amino)carbene

CAAC: Cyclic (alkyl)(amino)carbene

CAArC: Cyclic (amino)(aryl)carbene

CAASi: Cyclic (alkyl)(amino)silylene

CBA: Cyclic bent allene

CH₂: Methylene

cm⁻¹: Wave numbers

Cod: 1,5-cyclooctadiene

Cy: Cyclohexyl

DAC: N,N'-diamidocarbene

Dbz: Dibenzylideneacetone

DCM: Dichloromethane

Δ_{EST} : Singlet-triplet gap energy

DFT: Density functional theory

Dipp: 2,6-diisopropylphenyl

DippNH₂: 2,6-diisopropylaniline

DMF: Dimethylformamide

DMSO: Dimethyl sulfoxide

E: Main-group functionality

EPR: Electron paramagnetic resonance

Et: Ethyl

EtOAc: ethyl acetate

Et₂O: Diethyl ether

eV: Electron Volt

Fc/Fc⁺: Ferrocene vs Ferrocenium

HMDS: Hexamethyldisilazide

HOMO: Highest occupied molecular orbital

HOTf: Trifluoromethanesulfonic acid, also TfOH

Hz: Hertz

iPr: Isopropyl

IR: Infrared

kcal mol⁻¹: Kilocalories per mole

KHMDS: Potassium hexamethyl disilazane

KOtBu: Potassium tert-butoxide

LDA: Lithium diisopropylamide

LUMO: Lowest unoccupied molecular orbital

Me: Methyl

Mes: Mesityl, 2,4,6-trimethylphenyl

MIC: Mesoionic carbene

NBO: Natural bond order

n-Bu: Normal butyl

n-BuLi: n-butyl lithium

NHC: N-heterocyclic carbene

NMR: Nuclear Magnetic Resonance

OAc: Acetate

OTf: Trifluoromethanesulfonate

OLED: Organic light-emitting diode

p-TsOH: Tosylic acid

%V_{bur}: Percent buried volume

Ph: Phenyl

PhMe: Toluene

Ppm: Parts per million

R: Organic-group functionality

RT: Room temperature

SOMO: Singly occupied molecular orbital

^tBu: Tertbutyl

TEP: Tolman electronic parameter

TfOH: Trifluoromethanesulfonic acid, also HOTf

Tf₂O: Trifluoromethanesulfonic acid anhydride

THF: Tetrahydrofuran

TM: Transition-metal

TMS: Trimethylsilyl

TOF: Turnover frequency

TON: Turnover number

Ts: p-Toluenesulfonate

UV-Vis: Ultraviolet-visible

X: Halogen

LIST OF FIGURES

Figure 1.1. Possible Bonding Configurations of Neutral Carbon Species.	1
Figure 1.2. Electronic Effect of Ligands on Metal Carbonyl Infrared Spectroscopy Shifts.	5
Figure 1.3. Carbene-Phosphinidene Adduct Forms and ³¹ P-NMR Shifts of Selected Carbenes. ...	7
Figure 1.4. Carbene-Selenium Adduct Forms and ⁷⁷ Se-NMR Shifts of Selected Carbenes.	9
Figure 1.5. Sterics Around L Ligands. A) A Carbene Exhibiting Wanzlick Equilibrium Where R Is a Small Substituent, B) A Carbene Exhibiting “Wall-Like” and “Wing-Like” Steric Obstructions, C) “Cone-Shape” Around a Generic Phosphine Ligand.	13
Figure 1.6. Percent Buried Volume. A) Lewis Structure of ^{Dipp} NHC-5, B) Topographic Map of Carbene at 0Å (%V _{bur} is 75.8%), C) Topographic Map of Carbene at 2Å (%V _{bur} is 45.7%).	14
Figure 1.7. CAAC-5 vs NHC Electronics.	15
Figure 1.8. Examples of the Possible Heteroatoms Adjacent to the Carbene Center.	15
Figure 1.9. Lewis and X-Ray Structures of Two Carbenes. A) Diaminocarbene E and B) (Amino)(Phosphino)carbene F.	16
Figure 1.10. Examples of Additional Types of Substituent Effects.	17
Figure 1.11. Difference in HOMO and LUMO Energies of NHC G and NHC H.	18
Figure 1.12. Difference in HOMO and LUMO Energies of NHC G and Enders Carbene I.	19
Figure 1.13. Comparison of NHC G, aNHC J, Enders Carbene I, and MIC K Substituent Effects.	20
Figure 1.14. Difference in HOMO and LUMO Energies of NHC H and DAC L.	21
Figure 1.15. A Simplified Representation of Carbene Electronic Dependence on Carbene Angle. The Blue Bars Indicate the ΔH-L of Each Carbene.	21
Figure 1.16. Energy of Methylene Carbene (CH ₂) Dependence on Carbene Angle. DFT calculations performed with Gaussian16 using UM062x/def2TZVPP. Purple and orange lines represent the calculated energy of the singlet and triplet states of CH ₂ , respectively.	22
Figure 1.17. Bonding Description of A) Phosphine-Metal and B) Carbene-Metal Bonds.	24
Figure 1.18. Select Examples of Ruthenium-Based Olefin Metathesis Catalysts.	26

Figure 1.19. Examples of Unusual Closed Shell Main Groups Species Stabilized by Carbenes. ...	37
Figure 1.20. A Bis-CAAC Stabilized Be ⁰ Species.	38
Figure 1.21. Examples of Molecular Silicon Oxides Stabilized by NHCs.	39
Figure 1.22. Examples of Phosphorus Radicals Stabilized by Carbenes.	41
Figure 1.23. Organic Diradicaloid Species. Examples include the Tschitschibabin radical (A) and the CAAC-stabilized conjugated alkynyl species (B).	43
Figure 1.24. CAAC-Stabilized Carbon-Centered Showing the Effect of Distance on the Mixed Valent Nature of Radical Cations.	44
Figure 1.25. Various Types of Mesoionic Carbenes and their Zwitterionic Forms.	56
Figure 1.26. A Proposed Grouping of Carbenes Based on HOMO and LUMO Values.	57
Figure 2.1. Comparison of NHC-5 and CAAC-5 Electronics and a Comparison of RE-NHCs and CAAC-5 Based on Calculated ΔE_{S-T}	77
Figure 3.1. Comparison of NHC and CAAC Electronic Properties.	109
Figure 3.2. Comparison of NHC and Enders Carbene Electronic Properties.	112
Figure 3.3. Comparison of Enders Carbene, CAAC-5, EndersCAAC, and isoEndersCAAC Electronic Properties.	113
Figure 3.4. Retrosynthetic Analysis of EndersCAAC.	116
Figure 3.5. Comparison of EndersCAAC and ^{Et} CAAC Selenium Adducts.	122
Figure 3.6. Potential Means to Obtain Free EndersCAAC.	125
Figure 3.7. Retrosynthetic Analysis of IsoEndersCAAC.	127
Figure 3.8. Diagram of Bonding Between Atoms as a Possible Explanation for the Lack of Reactivity between Imidazolone 26 and Halogenating Reagents.	129
Figure 3.9. Potential Means to Obtain Free isoEndersCAAC.	130
Figure 4.1. Tetrathiafulvalenes (A), tetraazafulvalenes (B), enetriamines (C), enediamines (D), and the herein reported novel EDA 3,3'-bipyrazolylidene scaffold (1).	154
Figure 4.2. ¹ H- ¹³ C HMQC NMR Spectrum of Dimer 1	157

Figure 4.3. ^1H - ^{13}C HMBC NMR Spectrum of Dimer 1 with Interactions Labelled.	158
Figure 4.4. Homonuclear 2-D NOESY NMR Spectrum of Dimer 1 with Non-Cross Peak Interactions Labelled.	159
Figure 4.5. Summary of 2-D Nuclear Interactions of Dimer 1 by Each Geminal Methyl.	159
Figure 4.6. Cyclic voltammogram of bipyrazolylidene 1 ($n\text{Bu}_4\text{NPF}_6$ 0.1 M in THF, 100 mVs^{-1} , vs. SCE).	160
Figure 4.7. Solid-state structure of dimer 1 (a) top view and (b) side view. Hydrogen atoms omitted for clarity.	163
Figure 4.8. Experimental and simulated room-temperature EPR spectra of $\mathbf{1}^{\bullet+}\cdot\text{SbF}_6$	163
Figure 4.9. Representations of DFT calculated HOMO and LUMO (α -SOMO and β -SOMO for Radical Cation) of Dimer 1 , Radical Cation $\mathbf{1}^{\bullet+}$, and Dication $\mathbf{1}^{2+}$. Hydrogen atoms omitted for clarity.	164
Figure 4.10. Calculated Barrier to Rotation of Radical Cation $\mathbf{1}^{\bullet+}$ and Dication $\mathbf{1}^{2+}$	165
Figure 4.11. Representation of DFT Calculated (a) α -SOMO of Radical Cation $\mathbf{1}^{\bullet+}$ and (b) Spin Densities by Mulliken Population Analysis. As the molecule is symmetric, spin densities are shown only for the right half of radical cation $\mathbf{1}^{\bullet+}$	165

LIST OF SCHEMES

Scheme 1.1. Summary of Singlet and Triplet Carbene. A) Electronic Structure at the Carbene Center. B) Typical Reactivity of Triplet Carbenes, for Singlet Carbenes, see Section 1.4.	2
Scheme 1.2. Synthesis of Metal Carbonyl Compounds Used for TEP Values.	6
Scheme 1.3. Carbene-Phosphinidene Synthetic Procedures Starting from Free Carbene.	8
Scheme 1.4. Carbene-Selenium Adduct Synthetic Procedures.	9
Scheme 1.5. Carbene-Selenium Exchange Between Two Carbenes.	10
Scheme 1.6. Carbene Basicity Method. Proton-Exchange Reaction Example and Accompanying pK_a Scale of Select Carbene Iminium Precursors with Triethylamine for Reference.	11
Scheme 1.7. (Alkyl) (Amino) Carbene Reaction with Carbon Monoxide. A) AAC Forming a Ketene and B) CAAC Forming a Diradical.	18
Scheme 1.8. A General Olefin Metathesis Catalytic Cycle with a Ruthenium Catalyst.	25
Scheme 1.9. Examples of Industrially Important Uses of Olefin Metathesis and Grubbs Catalyst. A) Preparation of a pharmaceutical drug candidate using RCM to form large cycles. B) Preparation of pDCPD with ROMP. C) Upgrading seed oils to biofuels using CM.	27
Scheme 1.10. Catalytic Cycle of a Generic Palladium Cross-Coupling Reaction.	28
Scheme 1.11. Hydroamination and Hydrohydrazination of Alkynes. A) Example hydroamination and hydrohydrazination reactions and a depiction of a Werner Complex. B) Ligands that demonstrate high TON in gold-catalyzed hydroamination and hydrohydrazination reactions.	30
Scheme 1.12. General Catalytic Cycle of the Benzoin Condensation Demonstrating Umpolung. ..	31
Scheme 1.13. Examples of Carbene Organocatalysts that Enable Umpolung Reactivity.	32
Scheme 1.14. A Carbene-Mediated Oxidative Esterification of Aldehydes and its Catalytic Cycle.	33
Scheme 1.15. First Metal-Free Carbonylation Reaction. Note the reaction challenges in red.	34
Scheme 1.16. MIC-Catalyzed Three Component Reaction with SET Pathway.	35
Scheme 1.17. Examples of Isolated or Transient CAAC-Stabilized Boron Species.	37
Scheme 1.18. CAAC-Stabilized Boron Open-Shell Species.	40

Scheme 1.19. Examples of Carbon Radicals Stabilized by Carbenes.	41
Scheme 1.20. Examples of Electron Rich Olefins as a Result of Carbene Dimerization.	42
Scheme 1.21. Various Methods to Generate a Free Carbene.	45
Scheme 1.22. Synthesis of IMes as a Representative Synthetic Procedure for Unsaturated NHCs.	47
Scheme 1.23. Alternate Unsaturated NHC Synthetic Routes. These routes are useful for obtaining highly asymmetrical unsaturated NHCs.	48
Scheme 1.24. General Procedure for the Synthesis of Polycyclic Aromatic NHCs.	48
Scheme 1.25. Synthesis of Unsaturated NHC from Benzimidazole and Syntheses of Carbene Dimers from Benzoxazole and Benzthiazole.	49
Scheme 1.26. Synthesis of SIMes as a Representative Synthetic Procedure for Saturated NHCs and a Method to Functionalize the Saturated NHC Backbone.	50
Scheme 1.27. Facile Syntheses of Asymmetric Saturated NHCs.	51
Scheme 1.28. Two Methods of Generating Saturated NHCs with Larger Ring Sizes.	51
Scheme 1.29. Three Synthetic Routes to Enders Carbenes.	53
Scheme 1.30. Two Methods to Synthesize CAAC and the Synthesis of BiCAAC.	54
Scheme 1.31. General Syntheses of DACs.	55
Scheme 1.32 Two Synthetic Routes to MICs.	56
Scheme 2.1. Reactivity of NHC-6,7,8 and CAAC-5 with p-tolylacetylene.	78
Scheme 2.2. Reactivity of NHC-6,7,8 and CAAC-5 with adamantyl isocyanide.	79
Scheme 2.3. Reactivity of NHC-6,7,8 and CAAC-5 with ammonia.	81
Scheme 2.4. Selenium adducts of Dipp- and Mes- substituted NHC-8.	82
Scheme 2.5. Reactivity of ^{Mes} NHC-8 with ammonia.	82
Scheme 2.6. Reactivity of NHCs and CAAC conjugate salts with NaNH ₂	83
Scheme 3.1. CAAC Reactivity with Small Molecules.	110
Scheme 3.2. A Generic Carbene Catalytic Cycle (A), A Hypothetical CAAC Catalytic Cycle (B), and Examples of Carbene Organocatalysts (C).	111

Scheme 3.3. Synthetic Routes to CAACs Cannot Access EndersCAAC or IsoEndersCAAC.	114
Scheme 3.4. Synthetic Routes to Enders Carbenes Cannot Access EndersCAAC or IsoEndersCAAC.	114
Scheme 3.5. Attempt to Synthesis EndersCAAC via Pathway 2.	117
Scheme 3.6. Attempt to Synthesis EndersCAAC via a Dianion Intermediate.	118
Scheme 3.7. Synthesis to Pyrazolinium 6 En Route to EndersCAAC via Pathway 3.	119
Scheme 3.8. Attempts to Synthesize Free EndersCAAC.	120
Scheme 3.9. Attempts to EndersCAAC Metal Complexes.	121
Scheme 3.10. Attempts to Increase Steric Bulk on the N-Aryl Substituent to Isolate Free EndersCAAC.	123
Scheme 3.11. Attempts to Increase Steric Bulk on the Quaternary Carbon to Isolate Free EndersCAAC.	125
Scheme 3.12. Formation of Imidazolone 21 via Pathway Four En Route to IsoEndersCAAC.	128
Scheme 3.13. Formation of Imidazolone 26 via Pathway Five En Route to IsoEndersCAAC.	128
Scheme 3.14. Attempts to Obtain an IsoEndersCAAC Free Carbene Precursor.	129
Scheme 4.1. Synthesis of Dimer 1	156
Scheme 4.2. Synthesis of Monocation $1^{+} \cdot \text{SbF}_6$ and dication $1^{2+} \cdot 2\text{SbF}_6$	161

LIST OF TABLES

Table 2.1. DFT Calculated Geometric and Thermodynamic Data of CAAC-5 and NHCs.	95
Table 2.2. Cartesian coordinates for the optimized structures of CAAC-5 and NHCs.	95
Table 3.1. DFT Calculated Thermodynamic Data of EndersCAAC and IsoEndersCAAC. Calculated at MO-62x//def2-TZVP.	147
Table 3.2. DFT Calculated Geometric Data of EndersCAAC and IsoEndersCAAC. Calculated at MO-62x//def2-TZVP.	147
Table 4.1. DFT Calculated Thermodynamic Data of 1 , 1⁺ and 1²⁺ Calculated at B3LYP//TZVP. ..	175
Table 4.2. DFT Calculated Geometric Data of 1 , 1⁺ and 1²⁺ . Calculated at B3LYP//TZVP.	176

ACKNOWLEDGEMENTS

Everyone has a unique educational journey. The Ph.D. journey has not been an easy one, or a predictable one. There are so many people that I can acknowledge for their help and support through the last twenty-two years, but I have only so much space and so much memory. To all those who have been there for me, mentioned here or otherwise, I am eternally grateful.

First, I need to thank the Prof. Jennifer Burney, Prof. Thomas Bussey, Prof. Tadeusz Molinski, and Prof. Valerie Schmidt for their service on my Ph.D. committee and for being available for me to talk to and providing insights to my plans.

I need to especially thank Prof. Guy Bertrand for taking me on as one of his students. As someone who came into graduate school with the intention of a non-research career, I was always worried that my future advisor would not be understanding or supportive of my interests in activities outside of producing research and papers. I was pleasantly surprised that we were able to be on similar pages from the beginning. I will always remember your remarks to me, whether in group meetings (“Victor, I don’t know why you tend to choose the hardest ways to go about doing something”) or in casual one-on-one conversations (“at the end of the day, all I want is to be happy, and I have learned that I can’t be happy unless my students are happy”). I was able to learn a lot about chemistry and about working in a complex, collaborative environment from you. I admire the way how you are able to encourage students and researchers to make something of themselves. I am forever grateful and I hope that more of the world can enjoy your amazing way of thinking and your humor.

I am utterly indebted to my family, Dein, Alice, Florence, and York for being part of my entire life. Looking back, I think we are continuously growing together, always caring for each other, and working through our toughest battles together. My parents have done an amazing job

of taking their life history to teach me and my siblings how to be good people and to set ourselves up for success. As a result, I am the first of both sides of my family to earn a Ph.D., something I do not take lightly. Their support for me is something I can never take for granted and one that I will one day return in kind. My siblings and I have had interesting interactions with each other, but underneath it all, we are rooting for the best for one another. As we have moved out of our adolescent years and become our own people, we have grown closer together and become an indispensable support system for each other. Thank you for all your help when I ask for it, particularly when it comes to my writing, and for all your opinions and thoughts, solicited and otherwise.

When I began the last year of my Ph.D. journey, I came in thinking that I was going to keep my head down and focus on all the things I need to do to get across the finish line. I would be a free agent and ready to go wherever life would take me. Then came along Marquise. We started out as strangers attracted to each other and then it bloomed into a full-blown relationship before we knew it. You have been a tremendous source of emotional support for me as I wage my battle against my timeline. My life is more technicolor because you are in it. I am able to explore and enjoy San Diego to a fuller extent because of you. You are the coconut redbull to my vodka, you put a smile on my face every time. Our relationship has grown a lot, just as we both have become closer to fulfilling our potentials. Here's to our futures! I love you so very much. Boop!

The next group on my list is the rest of the Bertrand lab. I have had the pleasure of working with Dr. Michèle Soleilhavoup, Dr. Mohand Melaimi, and Dr. Rodolphe Jazzar, without whom, this lab would not be able to function and who allow a very French spirit to permeate the working environment. From your entertaining stories about the group to talking me down from

Mastering out every year, you all have helped me in countless ways that I'm not sure you have realized. The former students of the lab have inspired and enriched me as a researcher. For this, I need to thank Dr. Erik Romero, Dr. Corey Weinstein, Dr. Jesse Peltier, Dr. Daniel Tolentino, Dr. Adam Vianna, and Dr. François Vermersch. I want to especially call out two amazing people: Dr. Glen Junor for our stimulating conversations and opening my eyes to finding balance and joy while being a busy graduate student, and Dr. Sima Yazdani for her invincible work ethic and being an amazing person to talk to. I want to thank the current and former post-doctoral scholars Dr. Sonia Bajo, Dr. Floriam Mulks, Dr. Ryo Nakano, Dr. Luana Oliveira, Dr. Eder Tomás Gonzales de Mendivil, Dr. Jan Lorkowski, and Dr. Mehdi Abdellaoui for being chemistry wizards and helping me on my projects. I want to specially thank Dr. Ying Kai Loh for being an amazing post-doc and for all the fantastic ideas and conversations we've had. It's been a pleasure observing chemistry at the most dedicated, highest levels. I hope the best for you and your future!

I want to thank the current members of the lab for being so much fun to work with and have complex conversations with: Melinda Serrato, Joseph Yoon, Patrick Yorkigitis, and Levan Gojiashvili. I want to specially thank Alexis Day for being the spirit of the lab and being an example of courage in the face of the unknown. I also need to recognize Sebastian, the first undergrad that I had as a student in the Bertrand lab who was every bit as helpful as I could wish and a really cool guy. I have to recognize Nahal Soltani and the work that she accomplished in the first iteration of the EndersCAAC project. Speaking of, I must also give a massive shoutout to Kai Oppel for being there with me on the final part of the EndersCAAC journey as well, and sharing the bewilderment we constantly face as we run more reactions. I have to thank Vojtech Docekal for being an excellent synthetic chemist and helping me out with the isoEndersCAAC

project as well. I cannot end this section without thanking all the visiting scholars that the Bertrand lab has hosted in my six years. I want to specially thank André Faria-Viera, Dr. Yolanda Garcia, Dr. Shrikant Nilewar, and Dr. Delphine Pinchon for all the fun times we've had in and out of the lab.

The UC San Diego Chemistry Ph.D. program is not just limited to my research lab. The other students in the program have made to my time in the program much more enjoyable. Almost from the beginning, Dr. Kristine Teppang, Dr. Elizabeth Porto, and Dr. Kenneth Han have been part of my core group of people and we've shared so many meals and bottles of wine when we catch up with each other. Dr. Mariam Salib, Dr. John Lopp, and Dr. Gary Arevalo were part of my Pacific Hall Fifth Floor group. Thank you for your friendship and for entertaining me whenever I needed to talk or grab lunch with someone who wasn't in my research group. We made it! Finally, I deeply appreciate Dr. Kenneth Han, Joe Palasz, and Adam Cooper for being fantastic roommates. It's been entertaining and fun living with you all.

Everything at UC San Diego could not have happened without the University of Michigan chapter of my life preceding it. I am indebted to Prof. Rhima Coleman and Prof. Nathaniel Szyczak for taking me into their research labs as an undergraduate researcher. Your labs prepared me well for the work and curiosity I needed to succeed in graduate school. I am grateful to Dr. Eric Dahl for teaching me almost everything he knew about organometallic chemistry work and for challenging me to be better. I have to recognize Dr. Bitá Carrion's role in launching my research career: we were both students in German 101 my first semester of college and before the end of 2017, I was working in Prof. Coleman's lab and have been working in research settings since. Dr. Carrion mentored me on how to conduct experiments and be a respectful member of a research lab. Other key people in my formative research experience are

Dr. Biming Wu and Haitham Maaieh who made working in the Coleman lab a truly eye-opening experience.

I was also a Teaching Assistant for many quarters, and for that, I want to thank all the students that I've had because you all make me a better scientist for helping me to grow in my teaching and communication skill.

In addition to results at the bench and fumehood, I was actively involved with UC San Diego and I have to thank everyone I worked with for making this work less depressing. As part of the Graduate and Professional Student Association (GPSA), I had the pleasure of working with members of the GPSA executives and council: Breana Clark, Anupam, Rachel, Quynh, Erika, Sushil, Tom, Ashley, Julia, Viona, and Mia, to name a few. My experiences leading student advocacy at the state and federal levels will be material I draw on later in life. My experiences working on improving faculty-student mentoring taught me so much about institutional change and strategic patience.

I was also extensively involved at the UC system-wide level. I have to acknowledge the people who do the often-times thankless work of the UC Office of the President and appreciate when they are willing to work with students. I want to extend my admiration to the all the folks at UC Student Association and all the brave UC students who work to make the institution a better place. I must thank my fellow students at the UC Graduate and Professional Council for being amazing people on top of super smart and driven in their quest to make the UC and the US a better place for anybody in graduate school: Dr. Gwen Chodur, Ernesto Arcienega, Dr. Valeria Dominguez, Patriccia Ordoñez-Kim, Dr. Adam Catching, Dr. J. P. Santos, and all the UC Student Regents. The students and people that I have met in my work with GPSA and UCGPC make me feel optimistic about the world and motivate me to keep caring about my passions.

None of the above would have been possible without a deeper, innate drive to learn and succeed. For this, I must thank several teachers in my K-12 years: Ms. Helmholtz and her massive classroom library in third grade at Eaton Elementary, Mr. Buscher and his leadership in Model United Nations at Pacific American School, Mr. and Mrs. Greg Jones and Kristen Jones being voices of ethics and common sense also at Pacific American School.

Chapter 2, in part, is currently being prepared for submission for publication of the material. François Vermersch, Victor T. Wang, Rodolphe Jazzar, and Guy Bertrand “Ambiphilicity of Ring-Expanded N-Heterocyclic Carbenes.” The dissertation author was a co-primary investigator and author of this material.

Chapter 3, in part, is currently being prepared for submission for publication of the material. Victor T. Wang, Mohand Melaimi and Guy Bertrand “EndersCAAC and isoEndersCAAC as Novel Ambiphilic Carbenes” The dissertation author was a primary investigator and author of this material.

Chapter 4, in part, is currently being prepared for submission for publication of the material. Victor T. Wang, Mohand Melaimi, and Guy Bertrand “A 3,3'-Bipyrazolyliidene Air-Persistent Radical Cation.” The dissertation author was a primary investigator and author of this material.

VITA

EDUCATION

Doctor of Philosophy, Chemistry University of California San Diego (Advisor: Prof. Guy Bertrand)	2019-2023
Master of Science, Chemistry University of California San Diego (Advisor: Prof. Guy Bertrand)	2017-2029
Bachelor of Science, Biochemistry University of Michigan, Ann Arbor (Advisor: Prof. Nathaniel Szymczak)	2013-2017

AWARDS AND HONORS

Teaching Assistant Excellence Award (UCSD)	2020
--	------

PUBLICATIONS

1. **Wang, V. T.**, Melaimi, M., Bertrand, G. “3,3’-Bipyrazolylidene: an Air-Persistent Radical Cation” *In preparation 2023*.
2. Vermersch, F., **Wang, V. T.**, Jazzar, R., Bertrand, G. “Ambiphilicity of Ring-Expanded N-Heterocyclic Carbenes” *Submitted 2023*.
3. Carrion, B., Souzanchi, M., **Wang, V.**, Putnam, A., Shikanov, A., Coleman, R. “The Synergistic Effects of Matrix Stiffness and Composition on the Response of Chondroprogenitor Cells in a Three-dimensional Precondensation Microenvironment” 2016, *Adv. Healthc. Mater.* 1192-1202. DOI: <https://doi.org/10.1002/adhm.201501017>

ORAL PRESENTATIONS

Air-Persistent 3,3’-Bipyrazolylidine Radical Cation, ACS National Spring 2022 Meeting (San Diego, March 2022).

TEACHING EXPERIENCE

Chemistry Department Teaching Assistant (UCSD)	2017-2023
Chemistry Department Undergraduate Instructional Assistant (UM)	2016-2017

ACADEMIC SERVICE

UC Graduate and Professional Council (UCGPC) Council Chair	2020-2022
Graduate and Professional Student Association (GPSA) Vice President of Academic Affairs (UCSD)	2020-2021
GPSA Vice President of External Affairs (UCSD)	2019-2020

ABSTRACT OF THE DISSERTATION

Reactivity Studies of Carbenes and the Development of a New Carbene

by

Victor Tzer Wang

Doctor of Philosophy in Chemistry

University of California San Diego, 2023

Professor Guy Bertrand, Chair

Carbenes were thought to be un-isolable chemical species until the isolation of the first phosphinosilyl carbene in 1988 and the subsequent report of the first N-heterocyclic carbene (NHC) in 1991. Since then, carbenes with different electronic and steric properties have been synthesized and used in applications like metal catalysis, organocatalysis, medicine, and optical materials. The more carbenes are investigated, the more fortuitous and paradigm-challenging discoveries are made, advancing the collective knowledge of the structure and reactivity of main group elements. These discoveries are also relevant outside of main group research, often powering the development of more advanced or efficient technologies. As a result, carbene research is valuable. In this dissertation, an NHC's electronic properties, and therefore its reactivity, was found to be closely dependent on its carbene angle, however, increasing carbene

angle was correlated to more steric congestion around the carbene center, introducing a confounding factor that should be carefully considered by future researchers wishing to use saturated ring expanded NHCs. Additionally, this dissertation reports on the synthetic progress towards a novel carbene that aims to combine the excellent leaving group properties of Enders-type carbenes with the highly ambiphilic electronic properties of cyclic (alkyl) (amino) carbenes to create a new carbene organocatalyst. In the process of developing this novel carbene, a new framework for organic reductants was serendipitously discovered. Upon a one electron oxidation of the bipyrazolylidene framework, an air-persistent radical cation is generated.

Chapter 1 General Introduction

1.1 What is a Carbene?

Carbon is an outstandingly versatile element capable of forming strong bonds with almost all non-radioactive elements. Located in the p-block of the periodic table of elements, the electronic ground state configuration of carbon is $1s^2 2s^2 2p^2$. Per this ground state configuration, carbon atoms have four valence electrons. Correspondingly, neutral carbon is commonly encountered with four bonds to two to four other atoms. Less commonly, atoms of carbon can exist in bonding arrangements involving three bonds, two bonds, and even one bond (Figure 1.1). The stability of lower-valent carbon molecules ranges from a fleeting existence as reactive intermediates in chemical reactions to seemingly everlasting: the fewer bonds a carbon atom has, the more reactive the carbon-containing species. Capturing and studying the highly reactive low-valent carbon species is an active field of study that bridges the worlds of main group chemistry, the topics in chemistry concerning metalloid and non-metal elements, and organic chemistry.

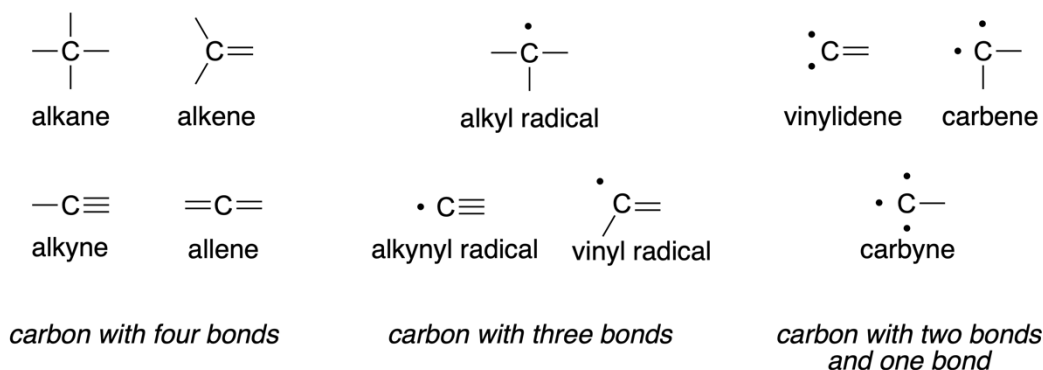
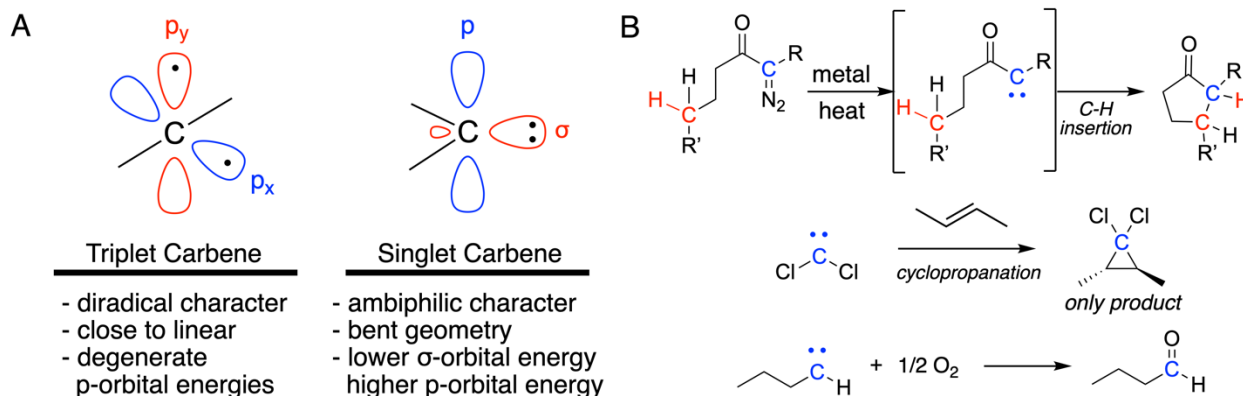


Figure 1.1. Possible Bonding Configurations of Neutral Carbon Species.

Of the low-valent carbon species, carbenes are of particular interest because of their chemical properties. By definition, a carbene is molecule that contains a neutral divalent carbon atom. Given the four valence electrons of an atom of carbon, two valence electrons can

participate in bonding with two adjacent atoms leaving two remaining electrons and two atomic orbitals on the carbon atom. These two remaining electrons can be distributed in two possibilities: one electron in each atomic orbital resulting in a triplet carbene, or both electrons paired together in one orbital (the σ -orbital) leaving the second orbital empty (the p-orbital) resulting in a singlet carbene (Scheme 1.1 A). As it has two unpaired electrons, triplet carbenes behave like diradicals making triplet carbenes short-lived. The reactivity of triplet carbenes include C-H insertions, concerted cyclopropanation reactions, and reactions with other molecules with unpaired electrons (Scheme 1.1 B).¹ With a lone pair and a vacant orbital, singlet carbenes are highly ambiphilic, acting as both an electrophile (electron acceptor) and nucleophile (electron donor). By virtue of not being a biradical, singlet carbenes are less reactive, isolable, and utilized in a wide range of applications (see section 1.4). Hereon, carbenes will refer to singlet carbenes unless otherwise specified.



Scheme 1.1. Summary of Singlet and Triplet Carbene. A) Electronic Structure at the Carbene Center. B) Typical Reactivity of Triplet Carbenes, for Singlet Carbenes, see Section 1.4.

1.2 Properties of Carbenes

As previously mentioned, carbenes are interesting because of their chemical properties, but what specific properties are useful to know?

1.2.1 HOMO and LUMO energies

Carbenes are useful because of their ambiphilic nature, however carbenes can exist in varying levels of nucleophilicity and electrophilicity. The nucleophilicity of a carbene is determined by the energy of its highest occupied molecular orbital (HOMO), the lone pair-filled σ -orbital, whereas its electrophilicity is determined by the energy of its lowest unoccupied molecular orbital (LUMO), the empty p-orbital (Scheme 1.1 A). A strongly nucleophilic carbene has a high energy HOMO; a strongly electrophilic carbene has a low energy LUMO.

Accordingly, carbenes that are both strongly nucleophilic and strongly electrophilic are considered highly ambiphilic. The “ambiphilicity” of a carbene can be defined by the difference between the HOMO and LUMO energies, or the HOMO-LUMO energy gap ($\Delta H-L$). Typically, a smaller $\Delta H-L$ indicates a more reactive carbene. Low HOMO-low LUMO carbenes and high HOMO-high LUMO carbenes have small $\Delta H-L$ as well and are also very reactive. However, because only one component of their electronic structure dominates, these carbenes are labeled as electrophilic and nucleophilic carbenes, respectively.

A small $\Delta H-L$ correlates with a small singlet-triplet gap ($\Delta S-T$) (see Section 1.2.2). Strictly speaking, the $\Delta H-L$ gap measures the energy difference between the carbene lone pair σ -orbital energy and the empty p-orbital. A small $\Delta H-L$ means that the excitation of an electron in the lone pair σ -orbital to the empty p-orbital is more likely than the same excitation in a carbene with a larger $\Delta H-L$. In other words, smaller $\Delta H-L$ indicate that the σ -orbital and p-orbital are

approaching the energy degeneracy of the two p-orbitals of triplet carbenes, allowing a carbene with smaller $\Delta H-L$ to exhibit triplet carbene behavior. Though similar, the $\Delta S-T$ measures the energy difference between the calculated singlet and triplet states under standard conditions and therefore the ability of a carbene to access both states under standard conditions.

Finally, the metal-carbene isolobal analogy attributes some of the transition metal-like chemical properties of carbenes is due to the presence of occupied and unoccupied orbitals at the carbene carbon, much like how transition metal atoms also have occupied and unoccupied d-orbitals. Accordingly, carbenes with smaller $\Delta H-L$ are more likely to exhibit transition metal properties because the carbene orbitals are closer in energy, much like how many d-orbitals are also close in energy or degenerate in energy.

There are several methods to determine the nucleophilicity and electrophilicity of a given carbene. Computationally, the energies of the nucleophilic and electrophilic molecular orbitals can be calculated via software like Gaussian.² Experimentally, there are several methods to 1) evaluate the net electronic properties of a carbene, 2) approximate the nucleophilic component,³ and 3) approximate the electrophilic component.⁴ A few methods relevant to this thesis are described in the following.

Computational density functional theory (DFT) methods can give reasonable HOMO and LUMO energies in electronvolts (eV) and the corresponding $\Delta H-L$. Because computational methods use electron density to calculate the molecular orbitals of a molecule and their corresponding qualities, the energies and shapes of occupied orbitals are generally reliable and correspond to experimental observations. Without a physical entity to base calculations on, unoccupied orbitals and their qualities are calculated using one of two indirect methods: the Hartree-Fock method in which a free electron populates a virtual orbital, and the process is

treated as an electron affinity calculation, or the Kohn-Sham method in which a ground state electron is hypothetically excited to a virtual orbital and the process is treated as an excitation calculation. Deriving the qualities of unoccupied orbitals from either method can lead to inaccurate LUMO energies. In general, calculated HOMO energies are acceptable, but calculated LUMO energies and the resulting $\Delta H-L$ of a carbene are best treated with caution. Nevertheless, DFT calculations give chemists a reasonable method to compare carbenes to one another and other molecular species of interests. For further commentary on using computational methods to study carbenes, refer to Gerbig and Ley.⁵

The Tolman Electronic Parameter (TEP) method⁴ is used to quantify the electronic properties of common metal ligands, L, by measuring the effect the ligand has when bound to a metal carbonyl complex (Figure 1.2). The bound L changes the electron density at the metal center, which in turn changes the amount of π -backbonding of the metal d orbitals into the π^* orbital of carbonyl system, altering the strength of the CO bond. The change in the CO bond is then identified by measuring the resulting CO stretching frequency in infrared (IR) spectroscopy. Accordingly, electron donating ligands result in a bathochromic shift of the CO IR stretching frequency, whereas electron withdrawing ligands result in a hypsochromic shift. The TEP method is popularly used to evaluate the electronic properties of phosphine ligands, which are primarily electron donating.

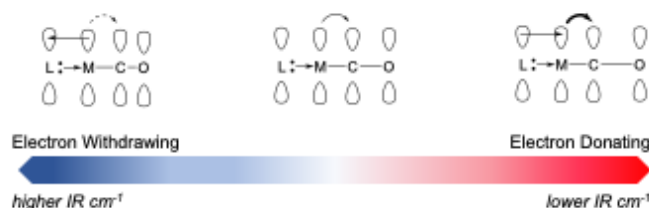
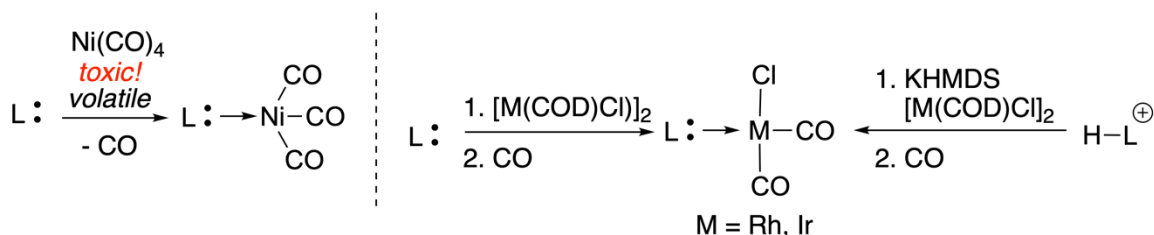


Figure 1.2. Electronic Effect of Ligands on Metal Carbonyl Infrared Spectroscopy Shifts.

In the original method, Ni(L)(CO)₃ metal complexes are prepared and the stretches of the infrared (IR) stretching frequencies are recorded. However, because the starting metal carbonyl Ni(CO)₄ is an extremely toxic liquid, an safer analogous system to evaluate electronic properties was developed using M(L)(CO)₂Cl complexes, where M is rhodium or iridium. The complexes are readily accessed by reacting the ligand with [M(COD)₂Cl]₂ complexes followed by stirring in a CO atmosphere (Scheme 1.2). In the case of carbenes, if the free species is difficult to obtain, the complexes can be obtained by treating the protonated form of the carbene with a suitable base in the presence of [M(COD)₂Cl]₂ complexes followed by stirring in a CO atmosphere. Because the M(L)(CO)₂Cl complexes are planar, the CO trans to the ligand and the CO cis to the ligand are in different electronic environments. Therefore, the TEP values of M(L)(CO)₂Cl complexes are reported as the average of the two CO stretches, ν_{av} , in CH₂Cl₂. Known TEP values for Rh(carbene)(CO)₂Cl complexes range from 2061 cm⁻¹ to 2015 cm⁻¹ (Figure 1.3).⁴



Scheme 1.2. Synthesis of Metal Carbonyl Compounds Used for TEP Values.

While TEP values allow the comparison of carbene electronic properties to that of other ligands, there are a couple deficiencies to keep in mind. The TEP method measures the net electronic properties of the coordinated ligand, meaning that the individual contributions of the electron donating (correlated with HOMO energy) and electron withdrawing (correlated with LUMO energy) effects of ambiphilic molecules like carbenes cannot be determined. The TEP method only indicates whether the net electronic contributions at the metal center is greater or lower compared to other ligands. Another deficiency is that the 46 cm⁻¹ range of values is

relatively small, making it difficult to differentiate the electronic properties of similar carbenes, especially in IR spectroscopy where peak signals can be a couple cm^{-1} wide. Finally, the TEP method is sensitive to the steric environment of the ligand.⁶ Large, bulky ligands can distort the planar geometry of the metal complexes and alter the electronic effect experienced by the CO, resulting in changes to the CO IR stretch, limiting the comparability of the TEP method to ligands that have other parts directed away from the coordinating atom, like phosphines, or ligands that are small enough to not distort the geometry at the planar metal center.

In 2013, the Bertrand group reported a method to evaluate the π -accepting ability, or electrophilicity, of a carbene using nuclear magnetic resonance spectroscopy (NMR).⁷ In this method, carbene-phosphinidene adducts are synthesized and the ^{31}P -NMR chemical shift of the adduct in deuterated benzene is recorded. This method evaluates the degree of back bonding between the phosphinidene phosphorus and the carbene carbon (Figure 1.3). An electron poor phosphorus, meaning a good π -accepting carbene, would result in an adduct form better represented by phosphalkene **A** and a downfield signal. Conversely, a more electron rich phosphorus, meaning a poor π -accepting carbene, would result in an adduct form better represented by phosphide **B** and an upfield ^{31}P -NMR signal.

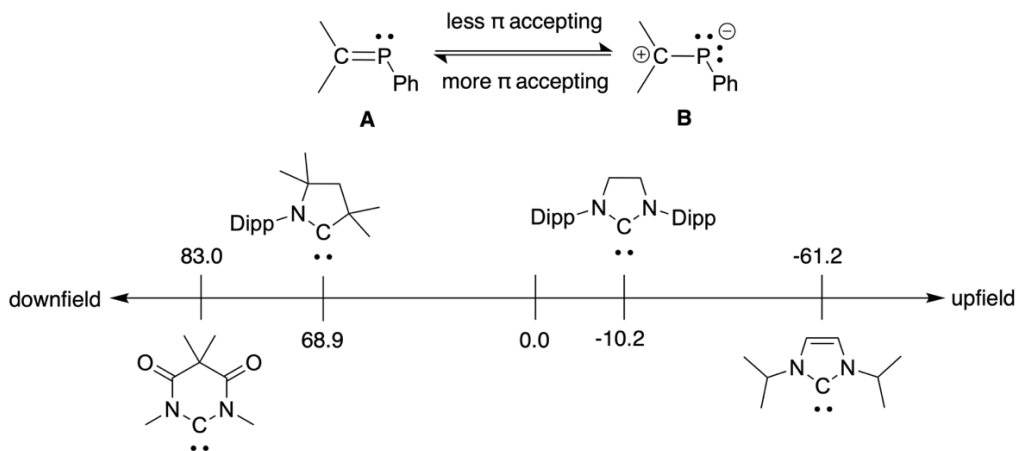
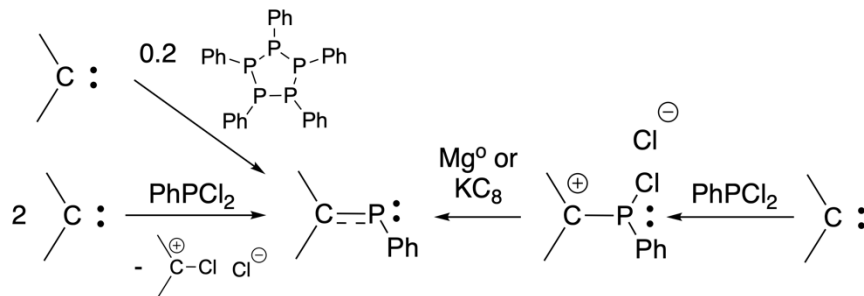


Figure 1.3. Carbene-Phosphinidene Adduct Forms and ^{31}P -NMR Shifts of Selected Carbenes.⁴

The carbene-phosphinidene adducts can be prepared with three methods: reacting free carbene with dichlorophenylphosphine then reduction with potassium graphite or elemental magnesium, reacting two equivalents of the free carbene with dichlorophenylphosphine, or reacting free carbene with pentaphenylcyclophosphane (Scheme 1.3).⁷ Known ³¹P-NMR chemical shift values range from 83.0 ppm to -61.2 ppm.⁴



Scheme 1.3. Carbene-Phosphinidene Synthetic Procedures Starting from Free Carbene.

One of advantages of this method is the larger range of values, making it easier to differentiate carbenes. The ³¹P-NMR method also benefits from high natural abundance of ³¹P (100%), resulting in clear signals. Unfortunately, this method requires isolable free carbene species. This method also can also require more synthetic steps or specialty reagents that are not accessible in some chemistry settings. Finally, the nature of bonding in the carbene-phosphinidene adduct is one in which the first interaction is the carbene lone pair donation to phosphorus, then the backdonation of phosphorus lone pair into the carbene vacant p-orbital occurs. This means that the measurement of the π -accepting ability of the carbene cannot be fully disentangled from the σ -donating ability of the carbene.^{4,7}

Following the Bertrand report in 2013, the Ganter group reported a similar method using ⁷⁷Se-NMR chemical shifts instead of ³¹P-NMR chemical shifts.⁸ The same underlying rationale for using ³¹P-NMR spectroscopy as the π -accepting probe applies for using ⁷⁷Se-NMR spectroscopy, except rather than using carbene-phosphinidene adducts, carbene-selenium are

used instead. Like the carbene-phosphinidene adducts, the π -accepting ability of the carbene determines whether the adduct more resembles the selenourea or selenamide **A** form or the selenide **B** form (Figure 1.4). A carbene with strong π -accepting ability would favor form **A** and a downfield ^{77}Se -NMR signal, whereas a weak π -accepting ability would favor form **B** and an upfield signal.

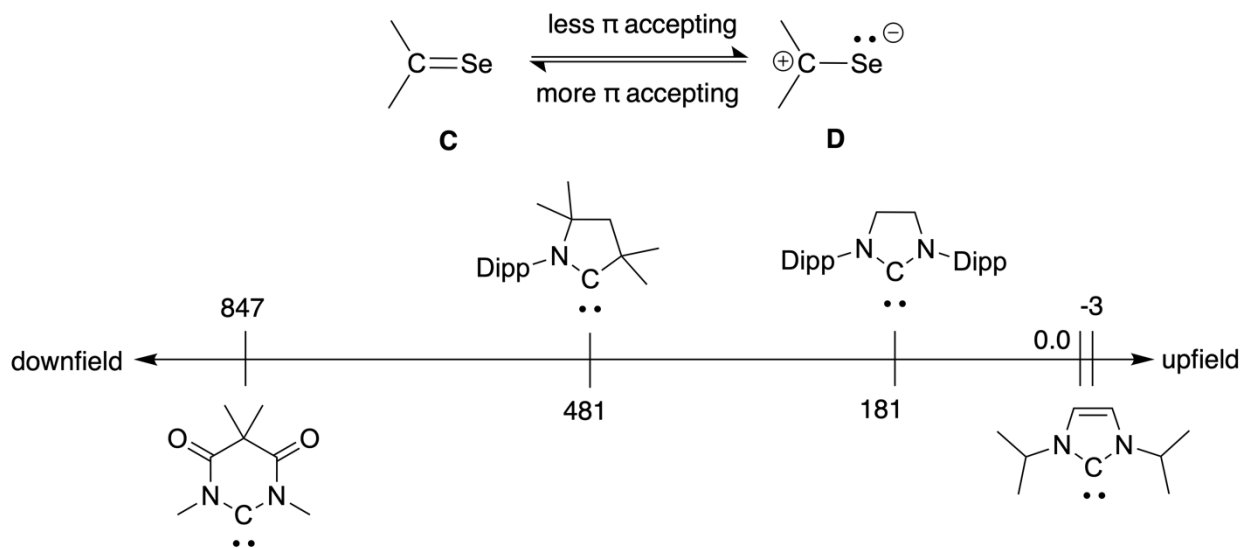
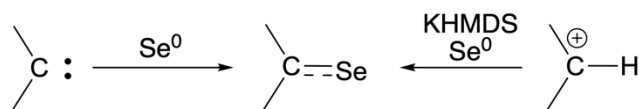


Figure 1.4. Carbene-Selenium Adduct Forms and ^{77}Se -NMR Shifts of Selected Carbenes.⁸

The preparation of the carbene-selenium adduct is straightforward: reacting the free carbene with elemental selenium or the treatment of a protonated carbene with a base in the presence of elemental selenium (Scheme 1.4). Known ^{77}Se -NMR chemical shift values range from 1180 ppm to -4 ppm in acetone- d_6 or 616 ppm to -56 ppm in CDCl_3 .⁴

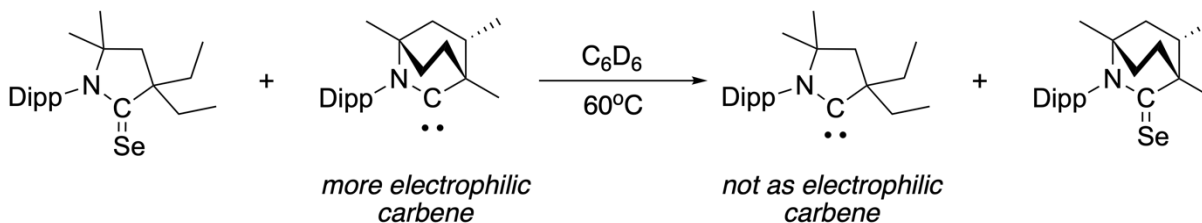


Scheme 1.4. Carbene-Selenium Adduct Synthetic Procedures.

The clear advantage of ^{77}Se -NMR chemical shifts is the preparation of the carbene-selenium adducts proceed with relative ease compared with the preparations of $\text{Rh}(\text{carbene})(\text{CO})_2\text{Cl}$ complexes or carbene-phosphinidene adducts. Additionally, the range of

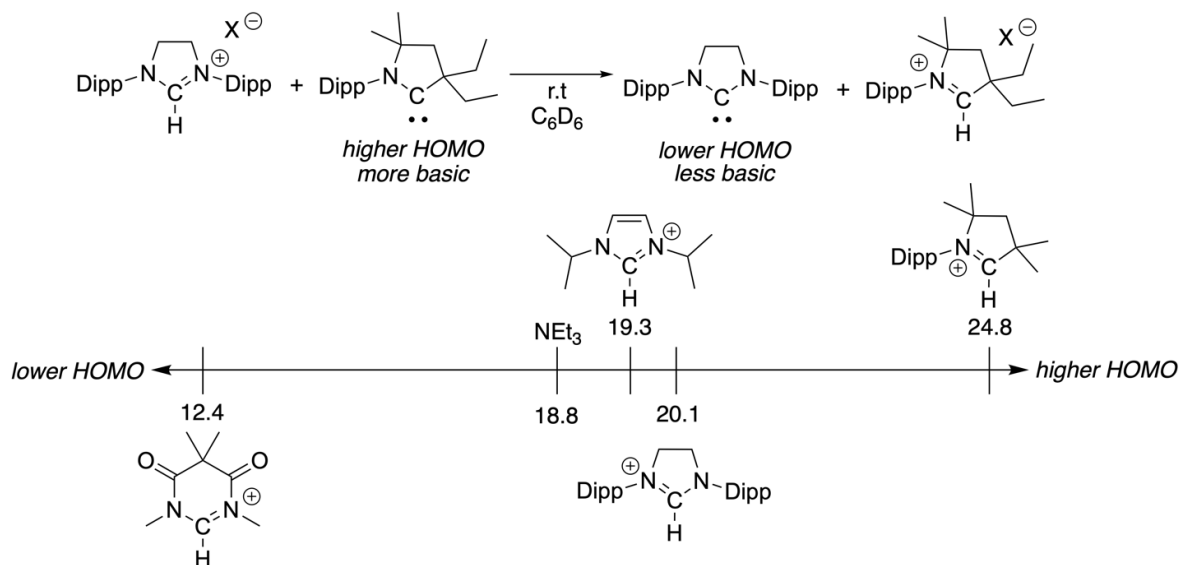
possible values is even greater than that of using ^{31}P -NMR chemical shifts. However, the chemical shift is sensitive to several factors, the most important being solvent, concentration, and temperature. Like the ^{31}P -NMR method, this method also cannot completely disentangle the σ -donating ability of the carbene from its π -accepting ability. Finally, a more recent report has highlighted that non-classical hydrogen bonding interactions between the selenium atom and nearby $\text{sp}^3\text{C-H}$ bonds can influence the chemical shift.^{9,10}

Curiously, in 2017, the Bertrand group reported that reacting a more ambiphilic free carbene with that of a carbene-selenium adduct resulted in an equilibrium in which the more electrophilic carbene is favored to form the carbene-selenium adduct (Scheme 1.5).⁹ The exact mechanism for the exchange reaction remains unreported.



Scheme 1.5. Carbene-Selenium Exchange Between Two Carbenes.⁹

In 2021, the Bertrand group reported an experimentally derived ranking of carbene basicity.³ The relative basicity of each carbene was determined by treating a free carbene with the protonated iminium salt of another carbene; a more basic free carbene can deprotonate the iminium salt or generate an equilibrium (Scheme 1.6). While proton affinity is not perfectly correlated with nucleophilicity, the experimental results demonstrated a basicity order that showed moderate correlation with the order of carbenes ranked by calculated HOMO energy levels. The carbene-carbene proton exchange reaction can be used to demonstrate the relative electron density in the carbene σ -orbital. The approximate pK_a of the carbene iminium precursor can also be calculated.



Scheme 1.6. Carbene Basicity Method. Proton-Exchange Reaction Example and Accompanying pK_a Scale of Select Carbene Iminium Precursors with Triethylamine for Reference.³

1.2.2 Singlet-Triplet Gap

The singlet-triplet energy gap ($\Delta S-T$) describes the relative thermodynamic stability of a carbene with respect to its singlet and triplet states. $\Delta S-T$ values are computationally calculated and are conventionally measured in kilocalories per mole (kcal/mol). A positive $\Delta S-T$ indicates that the carbene ground state is a singlet state, whereas a negative $\Delta S-T$ indicates that the carbene ground state is a triplet state. A smaller $\Delta S-T$ value indicates that the carbene is more likely to access both states under standard conditions, whereas a larger $\Delta S-T$ value indicates that the more energetic state is not thermally accessible. Because triplet carbenes are highly reactive and short-lived, and therefore preclude its use in many applications, stable singlet carbenes must have positive $\Delta S-T$ values that are large enough to prevent room temperature-accessible triplet electronic states. At the same time, the more reactive the free carbene is, the greater the potential for new chemical processes and properties, even when the carbene is bound to another molecular

fragment. Thus, when developing new carbenes, one of the parameters to consider is: which is more desirable, stability or reactivity?

As stated earlier, the $\Delta H-L$ is a modest approximation for the $\Delta S-T$ of a carbene. While a smaller $\Delta H-L$ generally correlates with a smaller $\Delta S-T$, the $\Delta H-L$ describes the relative proximity of the HOMO and LUMO energies, but this value does not directly translate into the thermodynamic propensity of an electron in the HOMO moving into the empty LUMO to create the triplet electronic state, in other words, the $\Delta S-T$.

Unlike the calculated $\Delta H-L$, the calculated $\Delta S-T$ is generally a trustworthy metric because the DFT frequency calculations do not need to utilize a physical approximation to account for virtual orbitals when calculating the energies of the two carbene electronic states. However, the $\Delta S-T$ calculations can be sensitive to the functionals and basis sets that are used in the DFT calculation.

1.2.3 Steric Environment

One last important carbene property is the steric environment that surrounds the carbene center. One can think of a carbene as a homolyzed carbon-carbon double bond, therefore, absent sufficient steric hinderance, carbenes can dimerize into alkenes (Figure 1.5). The equilibrium between the free carbene and its dimer is known as the Wanzlick equilibrium.¹¹ The nature of the substituents around the carbene can create “wing-like” or “wall-like” steric obstruction.¹² This steric environment around the carbene is also very different from that of phosphines, a popular class of L-type ligands which are usually described as “cone-shaped,” and this leads to some advantages of carbenes over phosphines, see section 1.4.1. Increased or decreased steric hinderance around the carbene center can indirectly affect the observed electronic properties of a

carbene by restricting the allowed geometric configurations of other molecules or atoms that the carbene is bound to or by blocking intermolecular interactions with other species that are present.

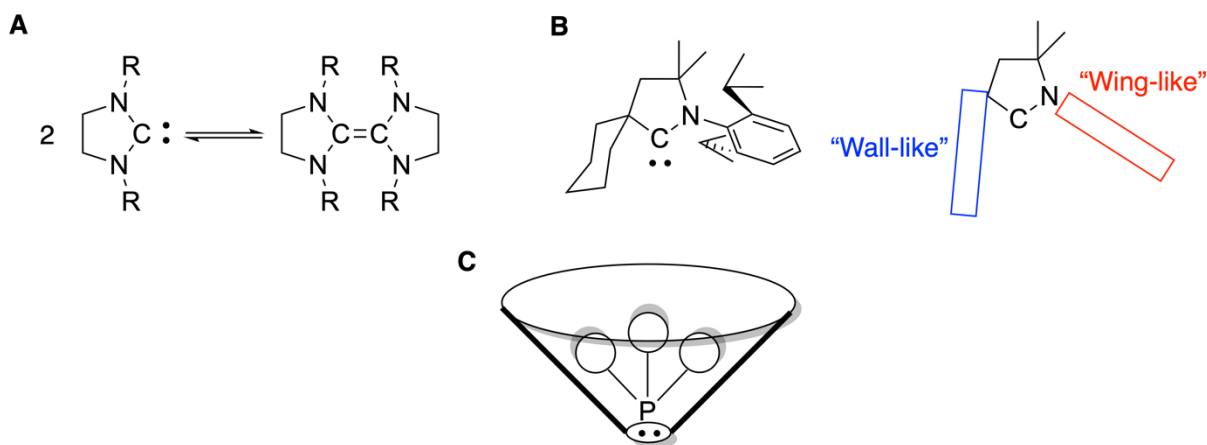


Figure 1.5. Sterics Around L Ligands. A) A Carbene Exhibiting Wanzlick Equilibrium Where R Is a Small Substituent, B) A Carbene Exhibiting “Wall-Like” and “Wing-Like” Steric Obstructions, C) “Cone-Shape” Around a Generic Phosphine Ligand.

Some methods of quantifying the steric environment around a carbene include the buried volume parameter ($\%V_{\text{bur}}$)¹³ which is calculated using the SambVca 2 program from a detailed topographic steric map around the point in question (Figure 1.6).¹⁴ In the $\%V_{\text{bur}}$ method, an approximation of the steric demand of a carbene is calculated from the perspective of a hypothetical metal bound at 2\AA from the carbene. The $\%V_{\text{bur}}$ is then given as a proportion of space that the carbene occupies in a sphere of 3.5\AA radius from the metal center. The SambVca 2 method can also generate a topographic map to give a specific representation of the features in the pocket that the carbene creates. Because they are typically smaller than transition metals, the $\%V_{\text{bur}}$ for main group atoms are calculated in the same way at 1\AA from the carbene center.

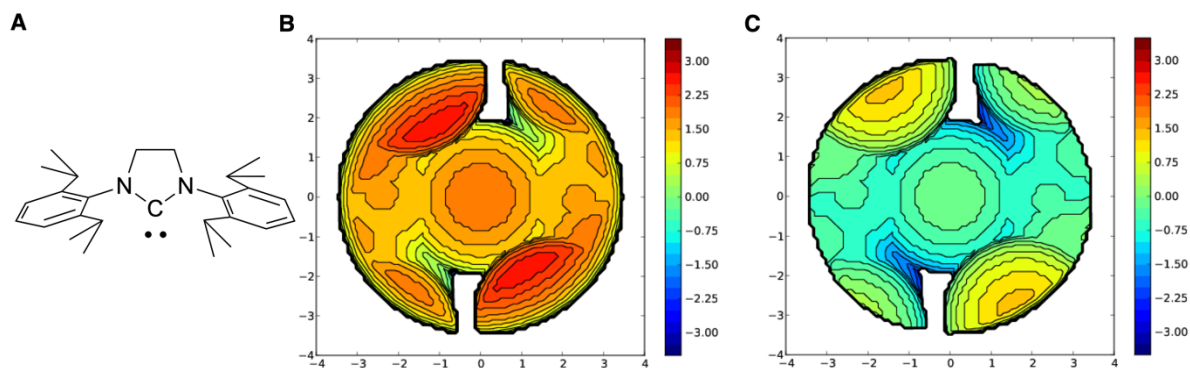


Figure 1.6. Percent Buried Volume. A) Lewis Structure of DippNHC-5 , B) Topographic Map of Carbene at 0 \AA ($\%V_{\text{bur}}$ is 75.8%), C) Topographic Map of Carbene at 2 \AA ($\%V_{\text{bur}}$ is 45.7%).

Given properly positioned steric hindrances, a stereoselective environment can be created around the carbene center or a metal bound to the carbene, allowing molecules to approach the reactive site only from a specific direction, leading to stereoselective reactivity.

1.3 Carbene Electronic Diversity

The discussion of carbene electronic properties above begets another question: what factors influence the electronic properties of a carbene? These factors can increase and/or decrease the carbene HOMO and LUMO energies, but the factors are usually dependent on each other.

1.3.1 Substituent Effects – Electronic Influence

The atoms directly adjacent to the carbene center have the largest effect on the electronic properties of a carbene. This is well illustrated in the difference between an N-heterocyclic carbene (NHC) and a cyclic (alkyl) (amino) carbene (CAAC-5). An NHC is adjacent to two nitrogen atoms, whereas a CAAC-5 is adjacent to one nitrogen atom and one quaternary sp^3

carbon (Figure 1.7).¹⁵ Nitrogen atoms produce a σ -electron withdrawing effect due to the greater electronegativity of the nitrogen atom compared the carbon atom of the carbene, and a π -electron donating effect due to the lone pair on the nitrogen atom donating into the empty p-orbital of the carbene. These two electronic effects help stabilize the HOMO and LUMO of the carbene: lowering the HOMO energy and raising the LUMO energy. A quaternary carbon has neither of stabilizing effect, decreasing the stabilization of the HOMO and decreasing the stabilization of the LUMO, rendering CAACs more ambiphilic, a smaller $\Delta H-L$ compared to that of an NHC.

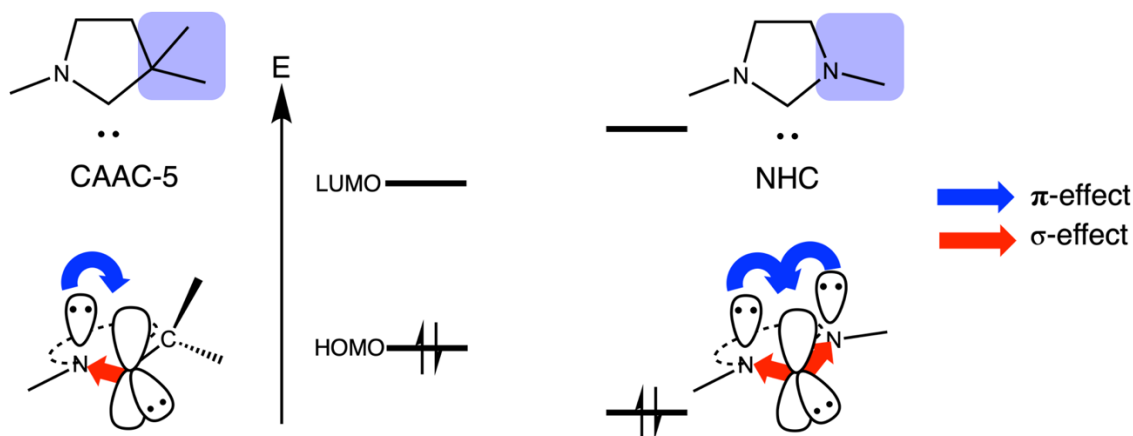


Figure 1.7. CAAC-5 vs NHC Electronics.

Other atoms have different electronic effects.¹⁶ Besides from carbon, amino carbenes with adjacent oxygen,¹⁷ silicon,¹⁸ phosphorus,^{19–21} sulfur,²² and hydrogen²³ atoms have been reported (Figure 1.8). In each of these carbenes, the resulting electronic property can be deduced based on the ability of the adjacent atom's ability to donate or withdraw electron density; σ effects affect the position of the HOMO energy, whereas π effects affect the position of the LUMO energy.

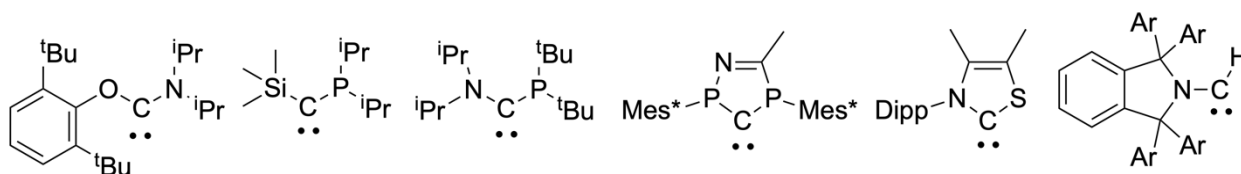


Figure 1.8. Examples of the Possible Heteroatoms Adjacent to the Carbene Center.

For example, phosphorus atoms are expected to be a weak σ -acceptors and weaker π -donating substituent compared to nitrogen atoms, resulting in an electron poor carbene. Indeed, a comparison of the NMR spectra and X-ray crystal structures of acyclic diamino carbene **E** to that of (amino)(phosphino) **F** carbene demonstrate this difference (Figure 1.9). Carbene **E** has a low field carbene ^{13}C -NMR shift of 255.5 ppm in benzene- d_6 . The crystal structure of **E** shows planar nitrogen atoms and short carbon-nitrogen bonds of 1.363Å and 1.381Å in the range typical of C=N double bonds.²⁴ In contrast, the decreased π -donation of the phosphorus atom of carbene **F** manifests in a very low field carbene ^{13}C -NMR shift in the range of 329.7 ppm in THF- d_8 , indicating a more electronically poor carbon atom. The crystal structure of **F** features a pyramidalized phosphorus atom (the sum of bond angles is 304.5°) with its lone pair oriented orthogonal to the carbene p-orbital and a long carbon-phosphorus bond of 1.856Å in the range of C-P single bonds; and, a planar nitrogen atom with a short nitrogen-carbon bond of 1.296Å.¹⁹

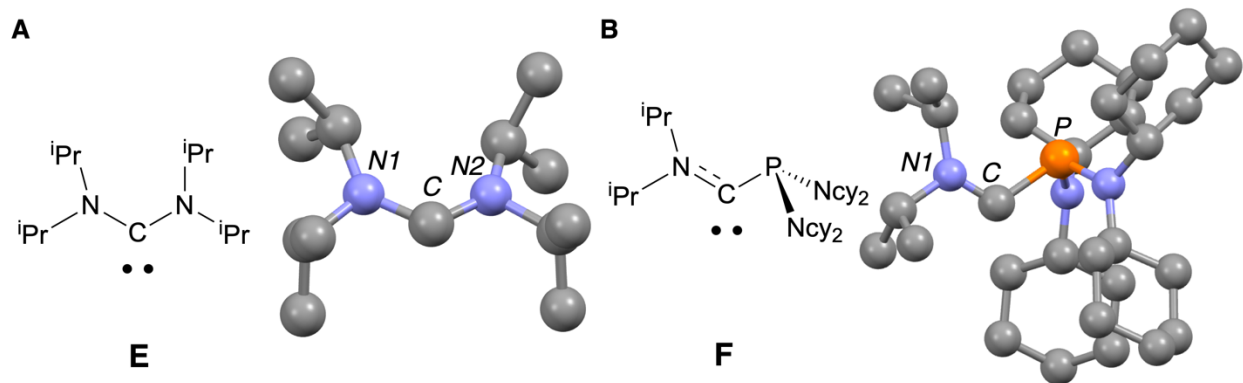


Figure 1.9. Lewis and X-Ray Structures of Two Carbenes. A) Diaminocarbene **E** and B) (Amino)(Phosphino)carbene **F**.

The nature of the atom adjacent to the carbene will also affect the steric environment around the carbene. Bivalent atoms like oxygen and sulfur will confer less steric protection around the carbene center and the resulting carbenes will likely dimerize or exist in a Wanzlick

equilibrium with its dimer. Additional types of substituent effects can include the hybridization²⁵ of the adjacent atoms and the geometric constraints²⁶ of the adjacent atoms (Figure 1.10).

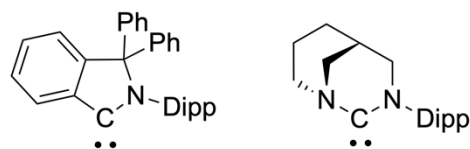


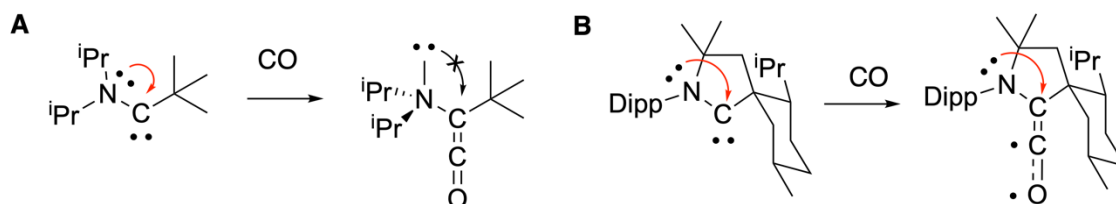
Figure 1.10. Examples of Additional Types of Substituent Effects.

1.3.2 Backbone π Effects

The nature of cyclic backbone, defined as the atoms not carbene adjacent that form the cycle, of a carbene molecule can have a profound effect on the electronics of the carbene. This section will primarily discuss the effect of the backbone on the carbene empty p-orbital. Because of the intrinsic geometry associated with closed rings, the number of atoms in the backbone will also affect the carbene angle (see Section 1.3.3), imparting additional electronic effects that cannot be completely separated from the effects of the backbone.

Before discussing the effect of the backbone on carbene electronics, acyclic carbenes and some of their features must be mentioned.^{23,24,27,28} Due to the absence of the geometric constraints imposed by a cyclic structure, acyclic carbenes possess several attributes that differ from cyclic carbenes. The lack of a ring allows for larger carbene angles than those typically observed in six-membered and smaller carbenes. These large angles introduce more steric hindrance around the carbene and can prevent acyclic carbenes from forming metal complexes.¹⁹ Because greater freedom of rotation exists, there is poorer overlap between lone pairs on adjacent atoms and the carbene p-orbital, resulting in acyclic carbenes that are typically more electrophilic and have smaller $\Delta S-T$ than their cyclic counterparts. The poorer orbital overlap is observed in the carbon monoxide adducts of CAACs and acyclic (alkyl)(amino) carbenes

(AACs): in the AAC-CO adduct, the nitrogen lone pair is orthogonal to the CO orbitals, resulting in a molecule that spectroscopically behaves like a ketene; in the CAAC-CO adduct, the nitrogen lone pair is in plane with the CO orbitals, pushing more electron density into the CO orbitals, resulting in a molecule with diradical behavior (Scheme 1.7).²⁹



Scheme 1.7. (Alkyl) (Amino) Carbene Reaction with Carbon Monoxide. A) AAC Forming a Ketene and B) CAAC Forming a Diradical.

In five-membered NHCs, the hybridization of the backbone has a large impact on the electronic properties at the carbene carbon (Figure 1.11). NHC **G** has a fully unsaturated backbone, leading to a 6π aromatic ring that provides massive stability to the empty p-orbital of the carbene. Conversely, NHC **H** has a fully saturated backbone; with the stabilization of the carbene empty p-orbital no longer present, NHC **H** is much more electrophilic than NHC **G**. Concurrently, the saturated carbon backbone in NHC **H** is weakly electron donating, slightly increasing the carbene HOMO via σ -donation. Overall, NHC **H** is more ambiphilic than NHC **G**.

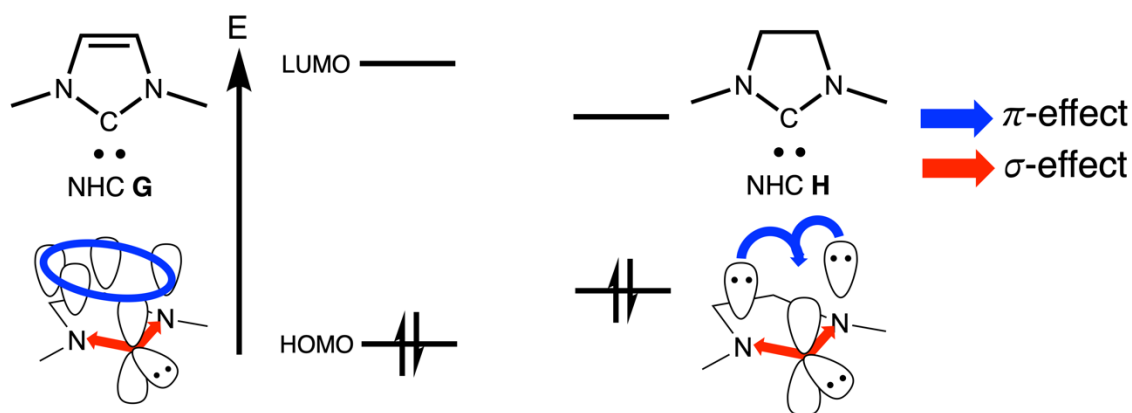


Figure 1.11. Difference in HOMO and LUMO Energies of NHC **G** and NHC **H**.

When comparing the electronic properties of NHC **G** with that of Enders carbene **I**, an NHC-related carbene, the substitution of a carbon with a nitrogen in the backbone primarily alters the HOMO energy (Figure 1.12). As previously mentioned, nitrogen is more electronegative than carbon and possess delocalizable electrons, the presence of nitrogen in the Enders carbene **I** unsaturated backbone decreases the HOMO energy while inducing a mild decrease in the LUMO energy.

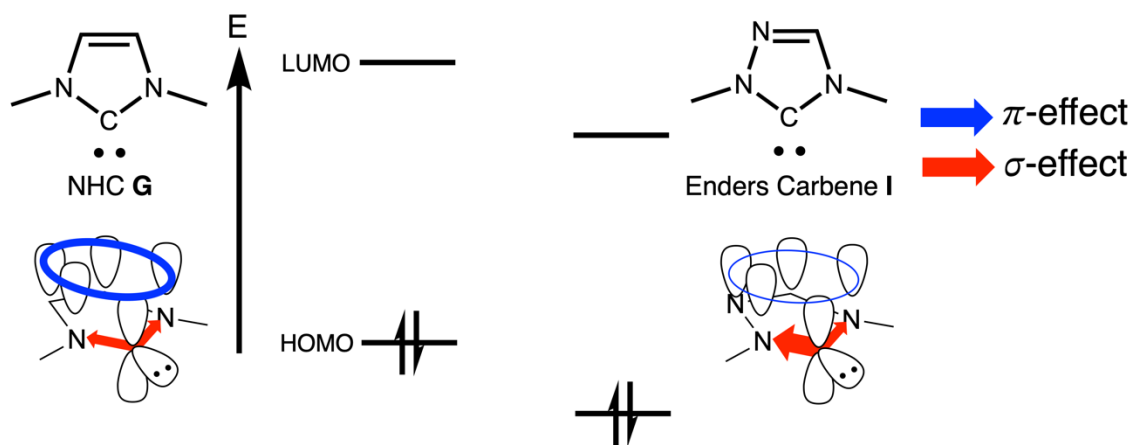


Figure 1.12. Difference in HOMO and LUMO Energies of NHC **G** and Enders Carbene **I**.

Aromaticity due to conjugation with the backbone also explains why mesoionic carbenes (MICs) are strongly nucleophilic carbenes (Figure 1.13). The core structures of abnormal NHC (aNHC) **J** and MIC **K** can be thought of as isomers of NHC **G** and Enders carbene **I**, respectively, in which only one nitrogen is adjacent to the carbenic center. The aromaticity of the system partially fills the carbene “empty” p-orbital, yet without the inductive effect of a second directly adjacent nitrogen, a MIC has a less stabilized σ -orbital which translates into a higher energy HOMO and, therefore, a strongly nucleophilic carbene. The observed differences in the HOMO energies between NHC **G** and aNHC **J**, and Enders Carbene **I** and MIC **K**, are analogous to the differences between an NHC and a CAAC.

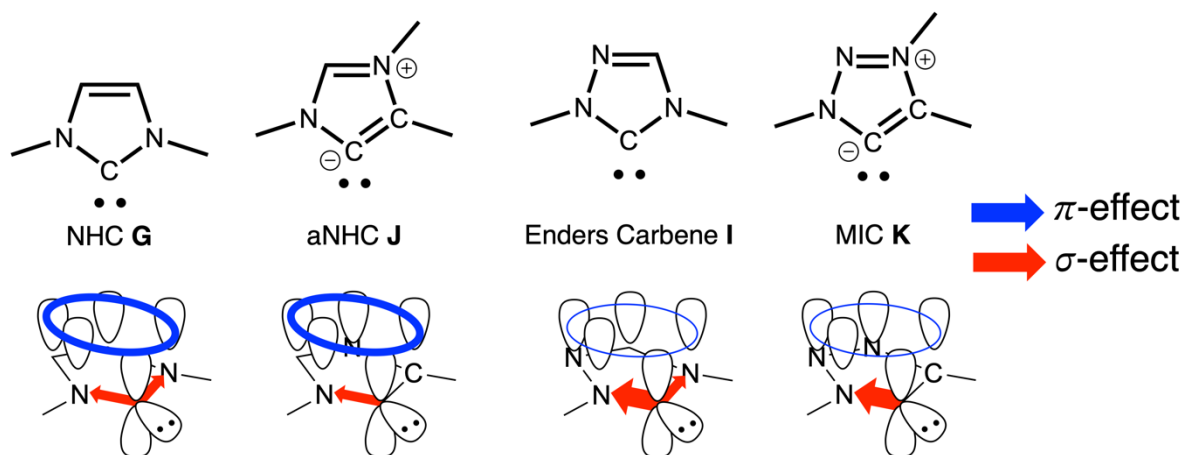


Figure 1.13. Comparison of NHC **G**, aNHC **J**, Enders Carbene **I**, and MIC **K** Substituent Effects.

The carbene backbone can also have a destabilizing effect on the carbene p-orbital if electron withdrawing functional groups interact with the atoms adjacent to the carbene center. For example, mono- and di-amido carbenes (MAC and DAC, respectively) have carbonyl functional groups conjugated to the nitrogen atoms, yielding amide carbene functional groups rather than amino ones (Figure 1.14). The electron-withdrawing nature of the carbonyl of DAC **L** simultaneously pulls electron density away from the carbene p-orbital and inductively withdraws electron density from the carbene σ -orbital.^{30,31} These two effects greatly stabilize the DAC **L** lone pair while also greatly reduce the stabilization of the DAC **L** empty orbital with respect to NHC **H**. As a result, MACs and DACs are strongly electrophilic carbenes. Other motifs that produce electrophilic carbenes by destabilizing the carbene p-orbital include ferrocenophane moieties and boron atoms in the backbone.^{32,33}

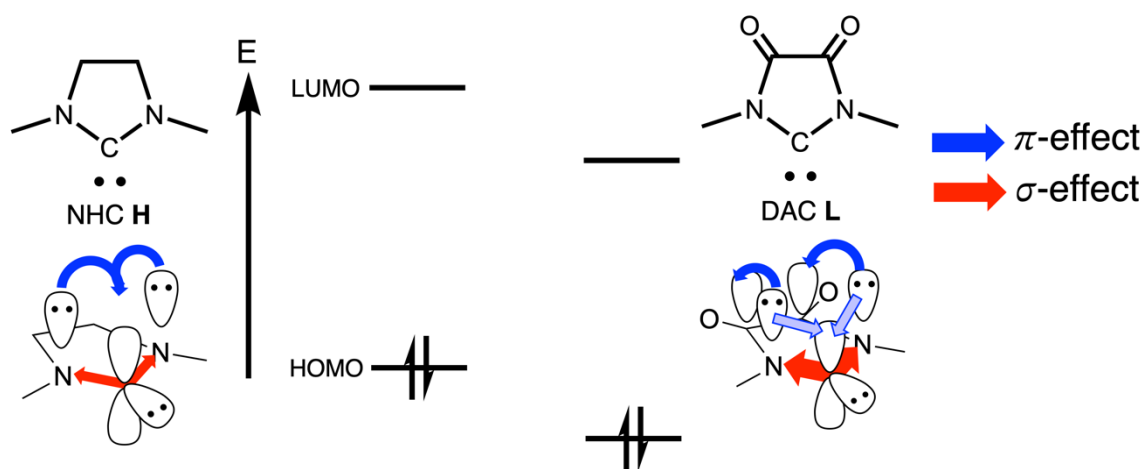


Figure 1.14. Difference in HOMO and LUMO Energies of NHC H and DAC L.

1.3.3 Backbone σ Effects – Carbene Angle

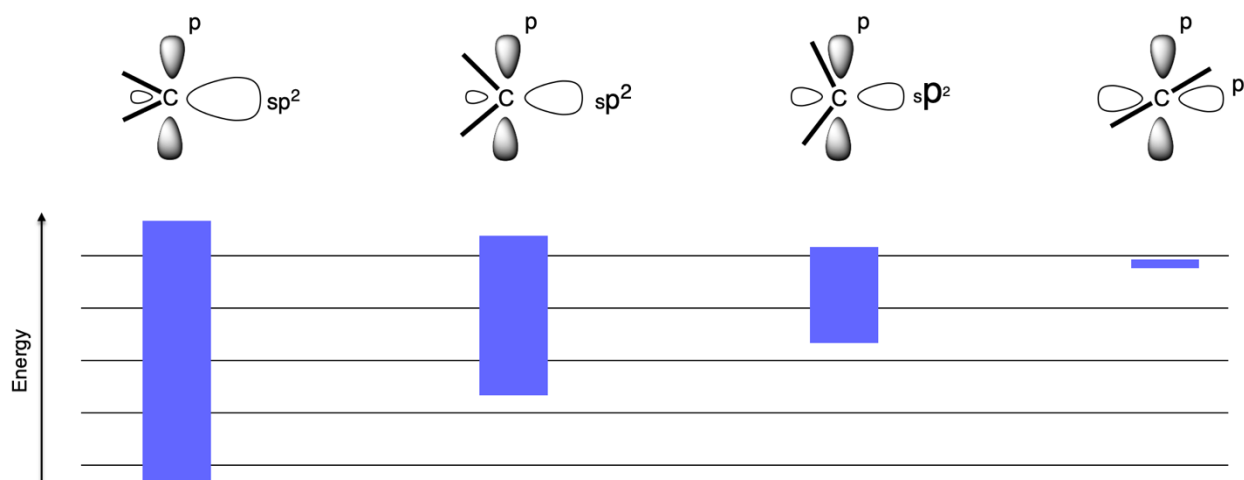


Figure 1.15. A Simplified Representation of Carbene Electronic Dependence on Carbene Angle. The Blue Bars Indicate the $\Delta H-L$ of Each Carbene.

The number of atoms in the backbone can enforce geometric constraints on the carbene angle, which in turn affects the electronics of the carbene (Figure 1.15).³⁴ As the carbene angle decreases, the carbene sp^2 σ -orbital gains more s-orbital character, which stabilizes the orbital and increases $\Delta H-L$, resulting in a less ambiphilic carbene. Conversely, as the carbene angle increases, the σ -orbitals gain more p-orbital character, increasing the nucleophilicity of the

carbene lone pair energy and decreasing $\Delta H-L$, resulting in a more accessible triplet state due to a smaller $\Delta S-T$. An angle sweep calculation of parent methylene carbene demonstrates the effect of the carbene angle on $\Delta S-T$ (Figure 1.16).

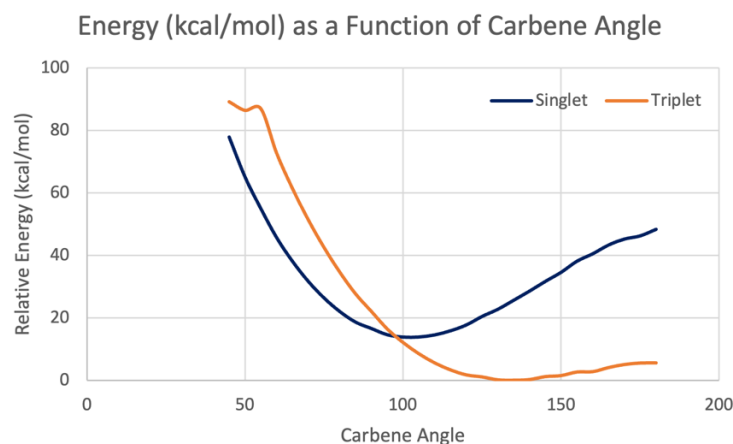


Figure 1.16. Energy of Methylene Carbene (CH_2) Dependence on Carbene Angle. DFT calculations performed with Gaussian16 using UM062x/def2TZVPP. Purple and orange lines represent the calculated energy of the singlet and triplet states of CH_2 , respectively.

Whether a carbene center is in an acyclic or cyclic system affects the carbene angle. Due to the constrained geometry, cyclic carbenes tend to have smaller carbene angles compared to their acyclic versions (see Section 1.3.2).²⁹ The size of the cyclic system influences the carbene angle as increased ring size will increase the carbene angle, and vice versa. However, the correlation between ring size and carbene angle eventually plateaus as an increasing number of sp^3 -hybridized atoms in the ring increases the flexibility of the cyclic system, relaxing the geometric constraints forced by the ring on the carbene angle. As more sp^3 -hybridized atoms are incorporated in the ring, the closer the angle of the cyclic carbene will tend towards the angle of the acyclic analogue. Finally, the size of the atoms in the have a modest effect on the carbene angle: lighter atoms in the cyclic ring result in smaller carbene angles while heavier atoms result in larger carbene angles.

1.4 Carbenes as Useful Chemical Tools

Carbene applications extend beyond cyclopropanations and H-E bond activations. Prior to the isolation of free carbenes, Fischer and Schrock carbenes bound to metal centers were used to effect transformations like [2+2+2] cyclization reactions or the methylenation of carbonyl compounds.³⁵ Since the first report of a free carbene in 1988,¹⁸ chemists have discovered many more applications of carbenes, partly by mimicking “natural” carbenes like thiamine, partly by capitalizing on their unique electronic properties, and partly out of fortuitous observations.^{36–39}

This section will focus on three different ways in which carbenes are used: as ligands in catalysis, as organocatalysts, and as a tool to study atoms featuring uncommon bonding or electronic states.

1.4.1 Applications as Ligand in Catalysis

Carbenes have had the most visible impact in the field of organometallic chemistry as NHCs, CAACs, and other carbenes have become popular ligands in metal catalysis. The variety of chemical transformations metal-carbene complexes can catalyze is astounding.

In many aspects, carbenes are superior metal ligands compared to phosphines, another popular class of neutral metal-binding ligands (Figure 1.17). In both bonding motifs, the lone pair on the bonding atom donates into the metal orbitals. Phosphines can accept some electron density from the metal through its σ^*_{P-M} orbitals. However, carbenes can accept more electron density from the metal through its vacant p-orbital. As a result, carbenes form very strong metal-carbon bonds compared to phosphines. The strong metal-carbon bond means that the carbene ligand is much less likely to dissociate from the metal during the reaction conditions of a

reaction, resulting in metal-carbene complexes that are more robust and long-lived compared with metal-phosphine complexes. Additionally, unlike phosphine ligands, carbenes do not easily undergo oxidations, eliminating a possible catalyst degradation pathway. The steric and electronic properties of a carbene are more easily controlled than that of phosphines ligands. The substituents on the atoms adjacent to the carbene center protrude towards the metal center and can greatly affect the approach of a substrate to the metal, whereas the substituents on phosphorus are pointed away from the metal center. Changing an atom adjacent to the carbene center greatly changes the electronic contribution of the carbene to the electronic properties of the metal center, whereas substituents on phosphine ligands primarily act in an inductive manner, limiting the possible range of electronic contribution from the phosphorus atom to the metal center. Finally, although the preparation of carbenes involves a longer synthetic route, many carbenes can be made without encountering the hazards associated with preparing phosphine ligands from phosphorus trichloride and anionic alkylating or arylating reagents. The synthetic route to many carbenes also allows for increased control over the design of asymmetric carbenes, whereas asymmetric phosphines require more dedicated reaction setups and may still be prone to low enantiomeric excess.

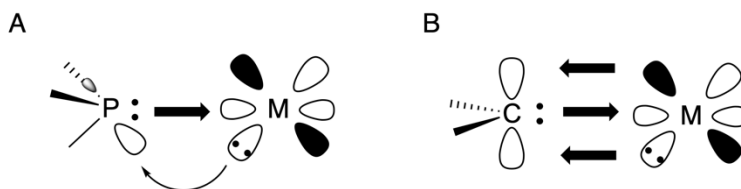
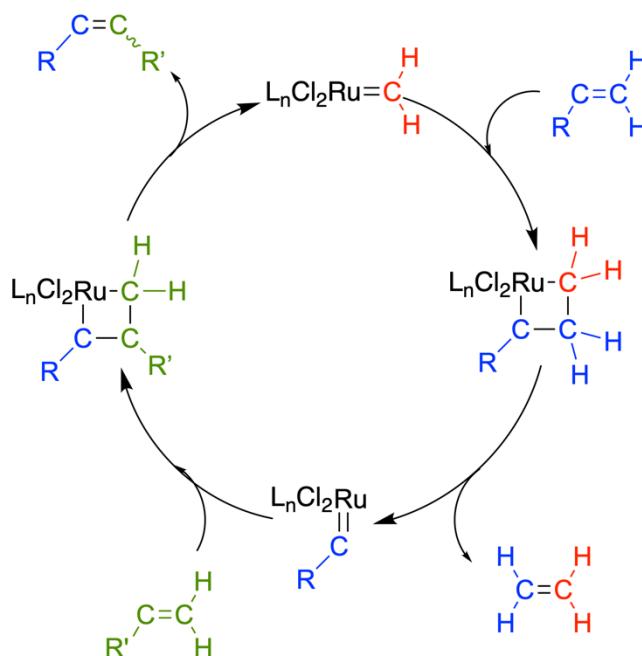


Figure 1.17. Bonding Description of A) Phosphine-Metal and B) Carbene-Metal Bonds.

Below, selected commercially important reactions are briefly discussed to demonstrate the importance of carbenes as ligands in metal-catalyzed reactions.

Olefin Metathesis and Grubbs' Catalyst

Alkenes, also known as olefins, are important chemical functional groups because of their rich reactivity and their presence in both naturally occurring and manufactured molecules. Olefin metathesis is one of the least wasteful and more efficient methods of making alkenes.^{12,40,41} Olefin metathesis is a metal-catalyzed reaction that exchanges fragments of two alkenes via a metallacyclobutane to yield two new alkenes (Scheme 1.8).



Scheme 1.8. A General Olefin Metathesis Catalytic Cycle with a Ruthenium Catalyst.

The most versatile catalyst for olefin metathesis is the Grubbs catalyst, of which there are many generations and iterations (Figure 1.18).⁴²⁻⁴⁴ The first-generation Grubbs catalyst features a pentacoordinate ruthenium active center that has two trans phosphine ligands and a benzylidene carbene that proceeds to form the metallacycle. This catalyst exhibits rapid reaction rates but is water- and air-sensitive and prone to catalyst deactivation. Newer generations of Grubbs catalyst, including the Hoveyda-Grubbs catalysts, replace one of the phosphine ligands with the NHC SIMes, resulting in increased catalytic activity and better water and air tolerances.

These two effects arise from the superior σ -donating ability of NHCs compared to phosphines. First, SIMes is more electron donating than trialkyl phosphines, resulting in increased electron density at ruthenium, increasing the rate of catalyst turnover. Second, the active form of the catalyst is an electron deficient 14-electron metal complex, which NHCs are better able to stabilize than phosphine ligands. A more stable active catalyst is more resistance to attacks on the complex by adventitious water or oxygen in solution. The Hoveyda-Grubbs catalysts do away with phosphine ligands entirely to achieve very fast rates of catalyst turnover.⁴⁵ Variants of Grubbs catalyst containing asymmetric NHC or CAAC ligands have been used to control the resulting *E/Z* stereochemistry of the new alkenes. For further advances, the 2021 review of ruthenium-based olefin metathesis catalysts can be found here.¹²

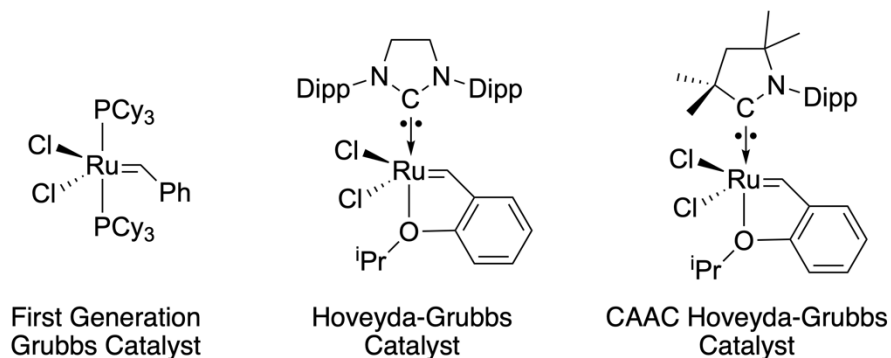
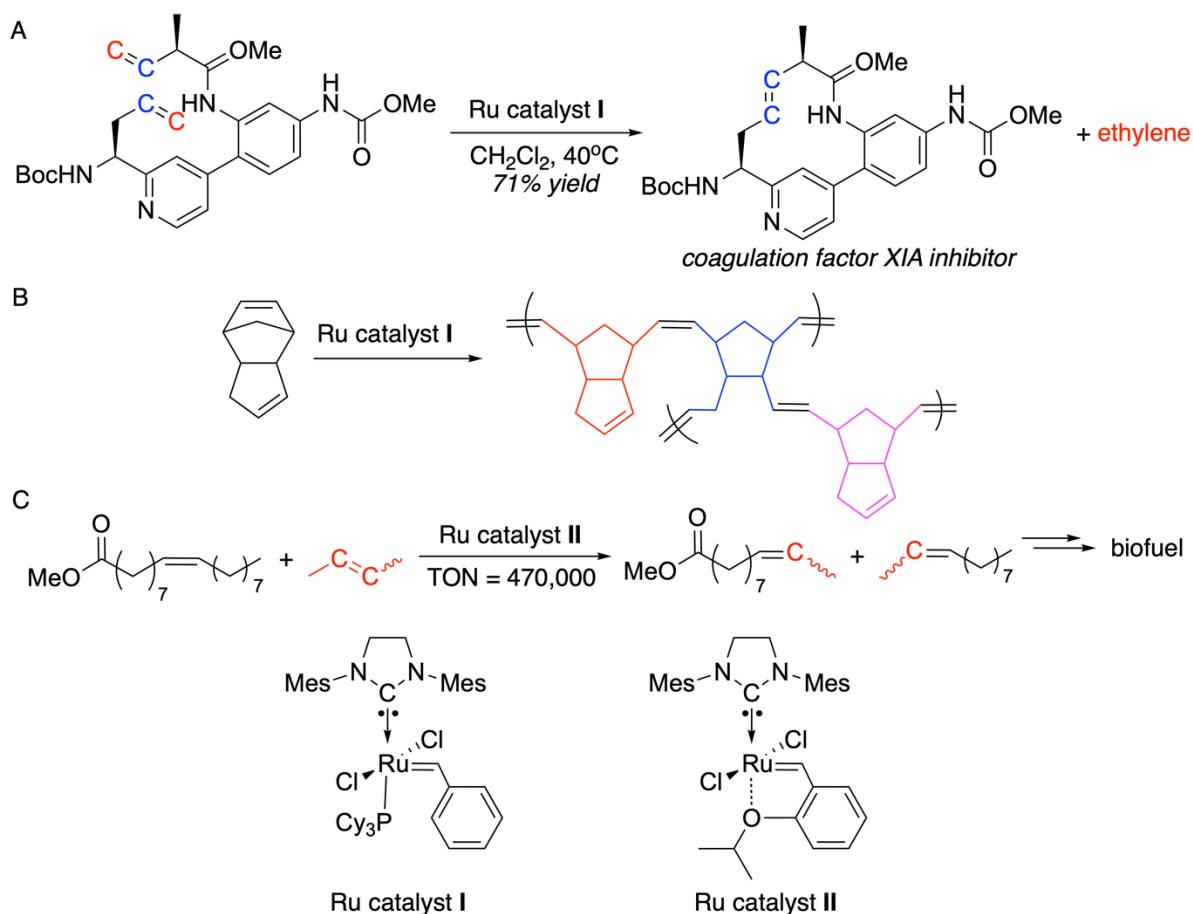


Figure 1.18. Select Examples of Ruthenium-Based Olefin Metathesis Catalysts.

Olefin metathesis and Grubbs catalyst are industrially important (Scheme 1.9).⁴¹ Grubbs catalyst is a powerful tool in the synthesis of small molecules from discovery to the industrial process in both the pharmaceutical and fragrance industries, particularly in using olefin metathesis to perform ring-closing metathesis (RCM) to generate bioactive molecules that contain large rings (Scheme 9A). It has been used to prepare polymers like poly(dicyclopentadiene) (pDCPD) using ring-opening metathesis polymerization (ROMP). pDCPD and related polymers have novel mechanical properties that traditional plastics do not

possess.⁴⁶ Finally, the Grubbs catalyst has been used to upgrade seed oils in a critical cross-metathesis (CM) step that converts the unsaturated fatty acids contained in seed oils to biofuels.⁴⁷

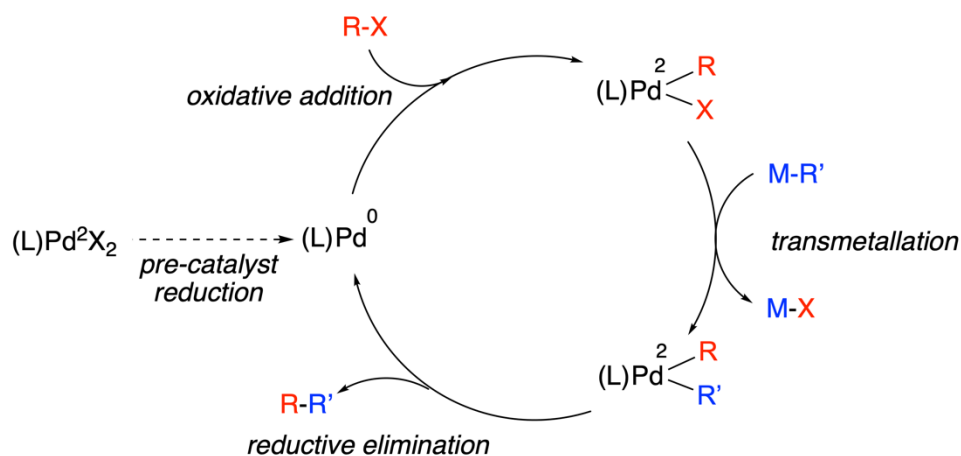


Scheme 1.9. Examples of Industrially Important Uses of Olefin Metathesis and Grubbs Catalyst. A) Preparation of a pharmaceutical drug candidate using RCM to form large cycles. B) Preparation of pDCPD with ROMP. C) Upgrading seed oils to biofuels using CM.

Palladium Cross Coupling Reactions

Carbenes have also been widely used in palladium-catalyzed cross-coupling reactions (Scheme 1.10).⁴⁸ A generic palladium-catalyzed cross-coupling reaction begins with a palladium (0) atom oxidatively adding into a carbon-halogen bond in the electrophilic coupling substrate. Then, the nucleophilic coupling substrate is transferred to the palladium (II) center in a

transmetallation step. Finally, the two organic substrates are combined to yield the coupling product in a reductive elimination step which regenerates the starting palladium (0) catalyst. Through many studies, two factors that facilitate faster reactions rates have been elucidated: a more electron rich palladium (0) center promotes faster oxidative addition rates, a sterically crowded coordination sphere around the palladium promotes reductive elimination over that of a less sterically burdened one.



Scheme 1.10. Catalytic Cycle of a Generic Palladium Cross-Coupling Reaction.

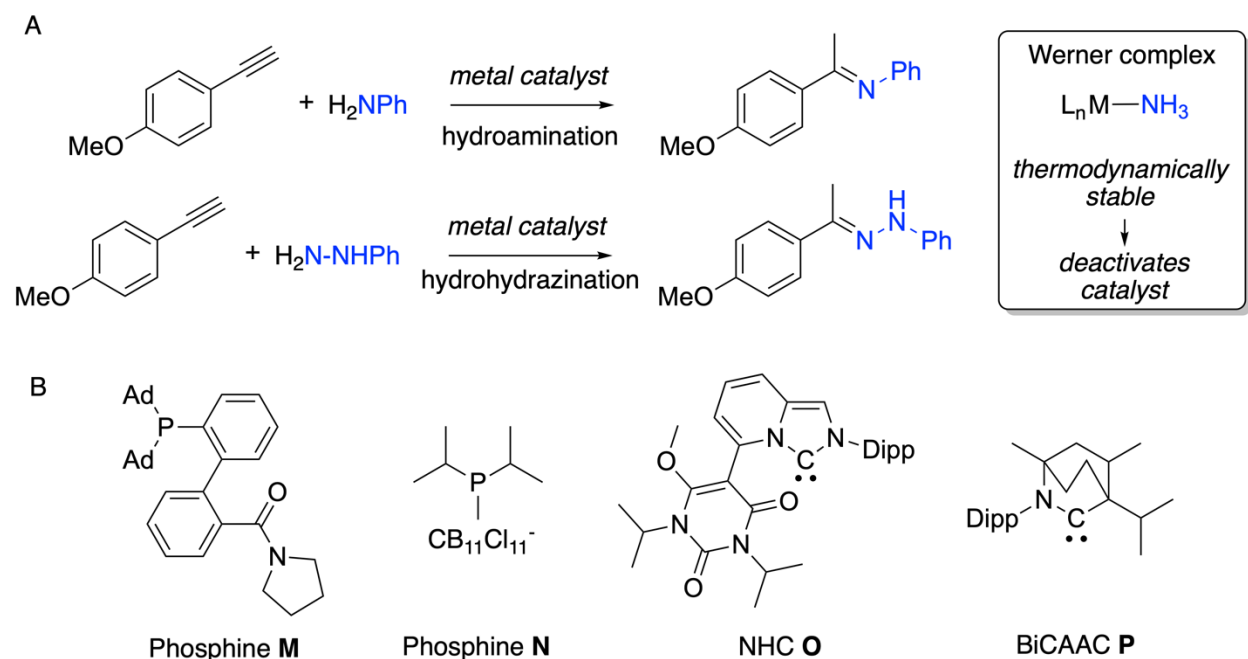
Like in olefin metathesis, palladium cross-coupling reactions are more productive with carbenes as ligands. The advantages are rooted in the increased electron density at the palladium when bound to a carbene, improved catalyst stability via strong carbene-metal bonding, and the substituents on atoms adjacent to the carbene coming closer to the metal center providing more steric pressures on other molecular fragments that are coordinated to the metal. For example, compared with Pd-phosphine complexes, Pd-NHC complexes can perform the Suzuki-Miyaura reaction at much lower temperatures, use aryl chlorides instead of aryl bromide or aryl iodides, and incorporate more sterically demanding substrates.⁹ Similar improvements are observed in the Negishi, Kumada, Hiyama, Sonogashira, Heck, and Buchwald-Hartwig coupling reactions.⁴⁸ Although the Pd-carbene complexes are typically pre-formed, requiring an additional synthetic

step in the catalyst preparation, these complexes have long shelf-life under ambient conditions, unlike many palladium catalysts that are commonly used.

Palladium cross-couplings are even more widely used in industry than olefin metathesis, blowing open the chemical frontier for organic and medicinal chemists in their syntheses of new molecules.

Hydroamination and Hydrohydrazination of Alkynes

Equally as economically valuable as making alkenes, high-yielding methods to construct carbon-nitrogen bonds are important because many natural molecules and pharmaceutical drugs contain nitrogen atoms. Carbon-nitrogen bonds can be further manipulated into value-added chemicals.⁴⁹ However, catalyzing reactions such as the hydroamination and hydrohydrazination of alkynes are difficult. Many metals form thermodynamically stable Werner complexes with amine substrates which effectively deactivates the catalysts. Additionally, electrostatic incompatibility exists between the electron rich nitrogen substrates and electron rich alkyne substrates (Scheme 1.11).⁵⁰ One strategy to overcome these barriers is to use gold complexes that will form (L)Au⁺ active species that activate alkynes. The stability of Au⁺ species in catalysis is the key to preventing catalyst decomposition pathways. Various phosphine, such as phosphines **M** and **N**, and carbene ligands, such as NHC **O**, have been developed with success, relying on secondary coordination sphere interactions to improve catalyst stability.^{51,52} In contrast to designing ever more complicated ligands, in a 2020 study the Bertrand group demonstrated that selecting a carbene, in this case bi-cyclic (alkyl) (amino) carbene (BiCAAC) **P**, with the right electronics and steric bulk can achieve the same turnover number (TON) improvements as using ligands that introduce secondary coordination sphere effects.⁵³



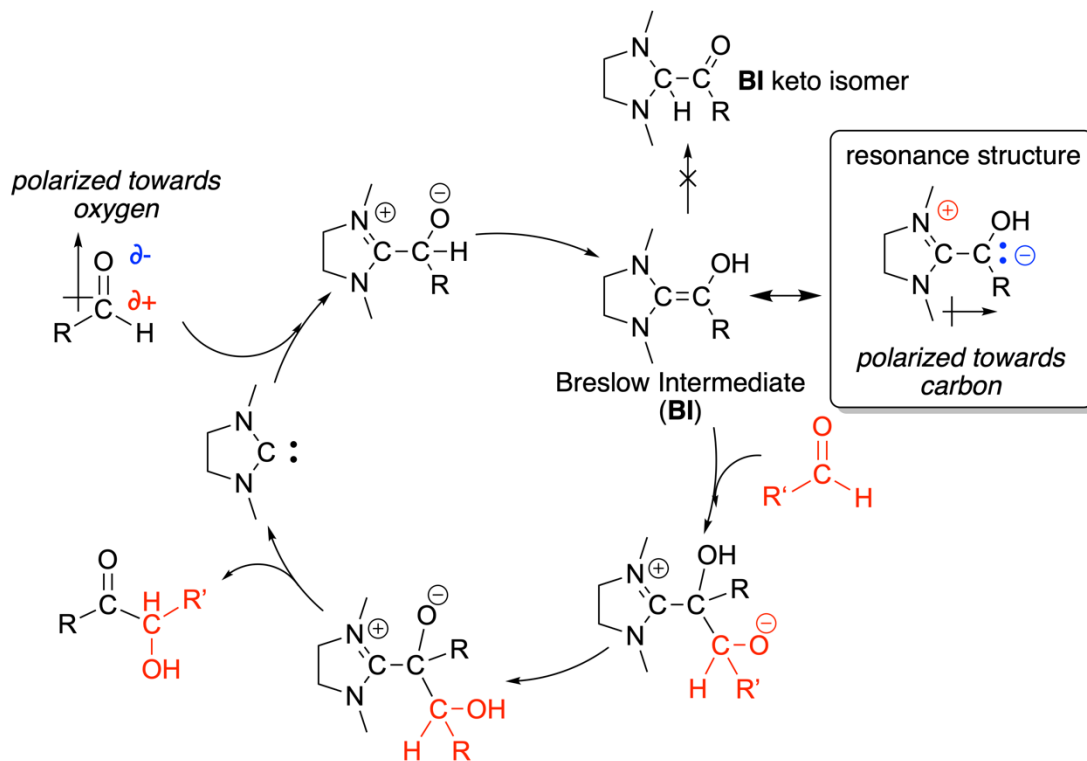
Scheme 1.11. Hydroamination and Hydrohydrazination of Alkynes. A) Example hydroamination and hydrohydrazination reactions and a depiction of a Werner Complex. B) Ligands that demonstrate high TON in gold-catalyzed hydroamination and hydrohydrazination reactions.

1.4.2 Applications as an Organocatalyst

Carbenes as organocatalysts is a rich field for new discoveries and applications because of their unique electronic properties. Due to the variety of electronic properties and structures available, a carbene can be selected or designed to fit the organocatalytic demand. Carbene organocatalysis can be divided by mechanism into three broad categories: carbene-enabled umpolung chemistry, transacylation chemistry, and radical-mediated chemistry. As the following sections demonstrate, many of the carbenes utilized in organocatalysis are good σ -donors and weakly π -acidic. These carbenes are sufficiently nucleophilic enough to form bonds with the starting material, yet remain weak bases, allowing for the elimination and regeneration of the free carbene in the last step of the catalytic cycle.

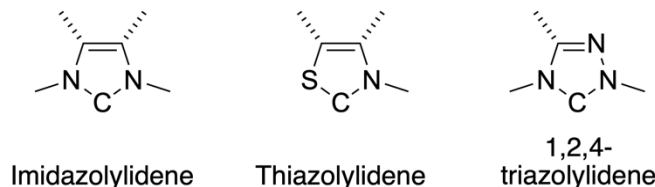
Umpolung Chemistry

Umpolung is the modification of a functional group such that its reactivity is the reverse of its typical electron distribution (Scheme 1.12). For example, the carbonyl function group ordinarily has its electron density unevenly shared towards the oxygen atom due to the difference in electronegativity, making the carbon the electrophilic site and the oxygen the nucleophilic site of the functional group. When a carbene reacts with an aldehyde to form a Breslow intermediate (**BI**), the aldehydic carbon is now a nucleophilic site, as demonstrated by the resonance structure. Upon reacting the **BI** with an electrophile, such as the carbon atom of another carbonyl, and a subsequent proton transfer, the carbene is then released to complete the catalytic cycle. This is the general reaction scheme for the benzoin condensation and Stetter reactions.



Scheme 1.12. General Catalytic Cycle of the Benzoin Condensation Demonstrating Umpolung.

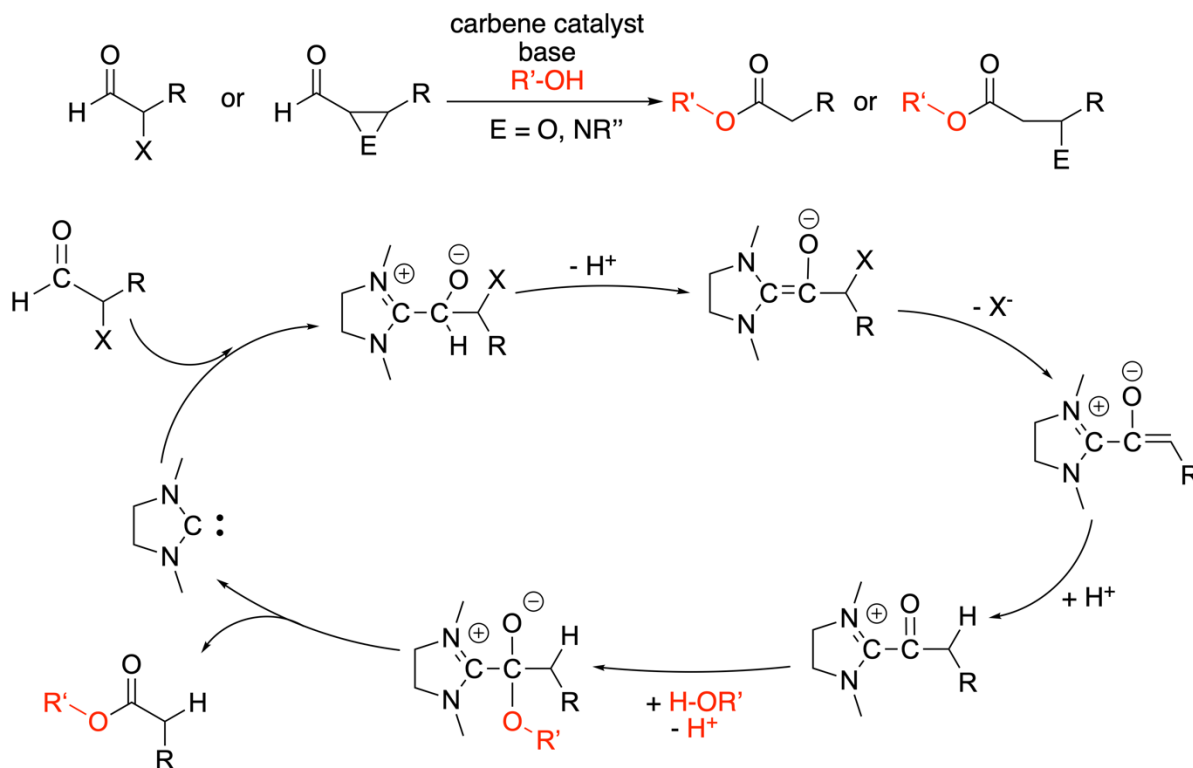
To be a competent organocatalyst for umpolung chemistry, the carbenes must be nucleophilic enough to attack the aldehyde carbon, but not π -acidic enough to tautomerize the **BI** into the keto isomer.⁵⁴ At the same time, the carbene must be a reasonable leaving group in the last step of the reaction, meaning that the carbene must have characteristics of a weak base: moderate nucleophilicity and weak electrophilicity.⁵⁵ As such, the most effective carbenes for benzoin condensations and Stetter reactions are imidazolylienes, thiazolylienes, and 1,2,4-triazolylienes (Scheme 1.13). These carbenes are also capable of asymmetric organocatalysis, or the selective production of one stereoisomer in the formation of new bonds, which leads to the efficient synthesis of molecules with even greater structural complexity, a major objective in the pharmaceutical industry.



Scheme 1.13. Examples of Carbene Organocatalysts that Enable Umpolung Reactivity.

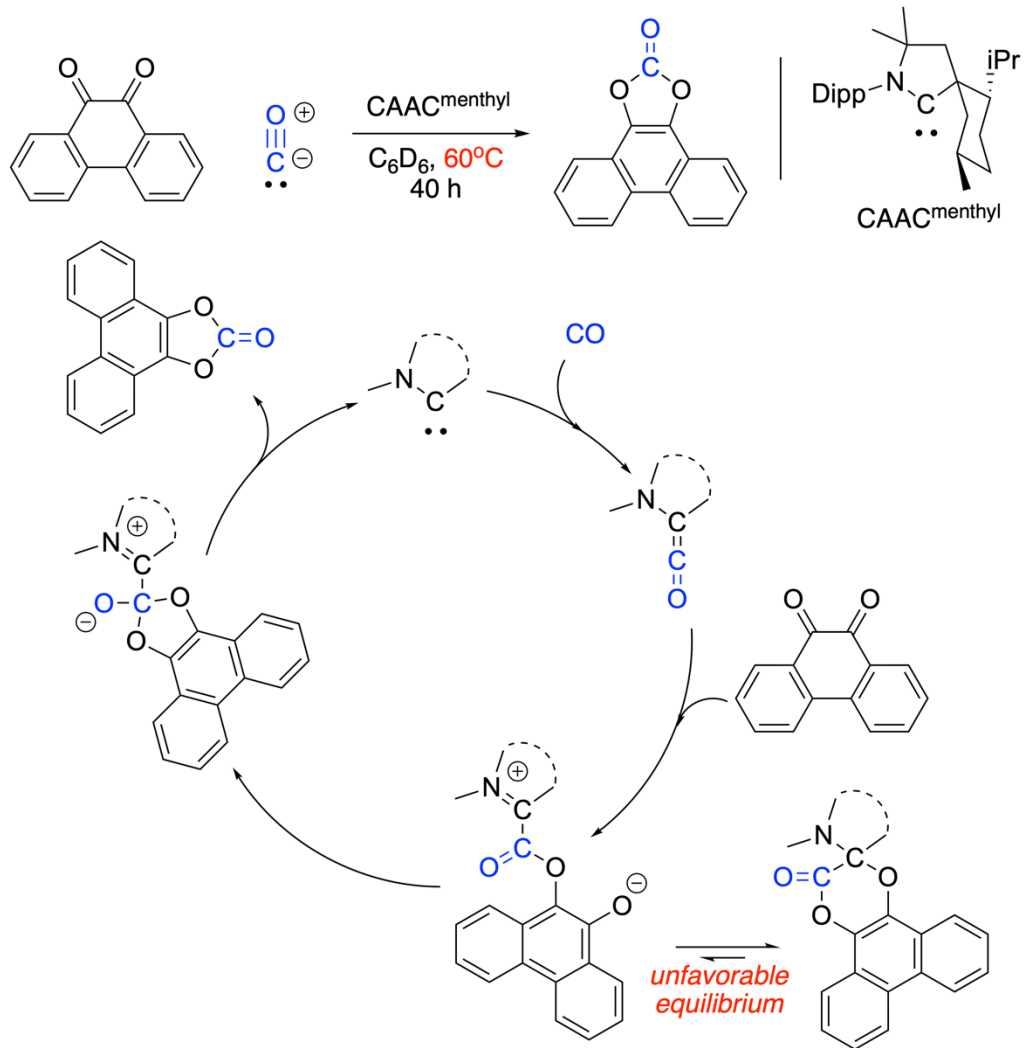
Transacylation Chemistry

Using the same principles as the benzoin condensation and Stetter reaction, carbenes have been applied as tranacylating reagents.⁵⁶ In the oxidative esterification reaction, an imidazolylidene reacts with an α -halogenated, α,β -unsaturated, α -aziridine, or α -epoxide aldehyde to form the corresponding **BI** (Scheme 1.14). Upon releasing a leaving group and tautomerization, the **BI** is transformed into an acyl imidazolium cation. An alcohol then attacks the acyl carbon to release the carbene and yield the corresponding ester. This reaction is a formal oxidation of aldehyde to an ester using a base as the reductant, an economical metal-free process.

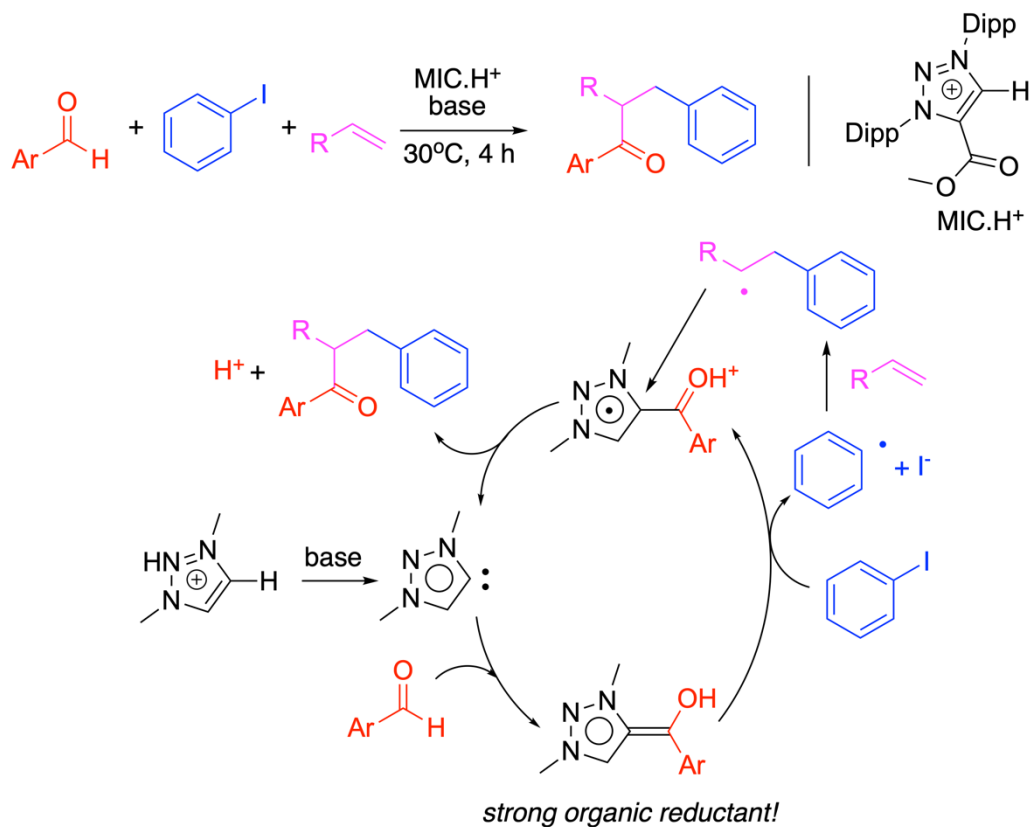


Scheme 1.14. A Carbene-Mediated Oxidative Esterification of Aldehydes and its Catalytic Cycle.

In 2020 the Bertrand group reported a new reaction in which a CAAC catalyzed the synthesis of cyclic carbonates from carbon monoxide and 9,10-phenanthrenequinone (Scheme 1.15).⁵⁷ This is the first example of carbon monoxide as a substrate in metal-free catalysis. The carbene-carbon monoxide ketene adduct is hypothesized to be the key intermediate in the carbonylation catalytic cycle, an adduct that only sufficiently ambiphilic carbenes can form. This reaction is limited by the instability of CAAC at the relatively high temperature required to overcome the lactam resting state of the catalytic cycle. Additionally, only one substrate has been demonstrated to work thus far.



Scheme 1.15. First Metal-Free Carbonylation Reaction. Note the reaction challenges in red.



Scheme 1.16. MIC-Catalyzed Three Component Reaction with SET Pathway.

A recent development in carbene organocatalysis is the use of σ -donating carbenes in single electron transfer (SET) reactions (Scheme 1.16).⁵⁸ Unlike the benzoin condensation and Stetter reactions, in SET reactions, the formed **BI** is used as an organic reductant to reduce an *in situ* oxidant. The generated radicals then couple to form an acyl azolium cation which can then be attacked by a nucleophile to release the product and regenerate the carbene. Previous work in SET reactions utilized weakly reducing **BI**s, requiring specialized reagents as the oxidative partner, limiting practical applications. In 2021, the Bertrand group reported using electron rich 1,2,3-triazolium salts to generate highly reducing **BI**s that were effective at reducing aryl iodides.⁵⁹ In 2022, the group reported a method to synthesize ketones from aldehydes and unactivated alkyl iodides and alkyl bromides, further expanding the scope of the carbene-

mediated SET reactions.⁶⁰ As of the time of writing, the use of carbenes in SET reactions has been used to synthesize ketones from a variety of starting carbonyl substrates.⁶¹

1.4.3 Applications in Main Group Research

Main group research concerns the properties and reactivities of the elements in the p-block of the periodic table and their applications to address technological gaps. Advances in main group chemistry have led to novel materials, new molecular synthesis strategies, and additives that enhance chemical reactions.^{62,63} Carbenes are indispensable in the discovery and isolation of new main group species. Main group species can have unique and uncommon electronic states or chemical reactivities that are predicted by our current understanding of chemistry. Some important main group species are hypothesized chemical reaction intermediates, while some may have desirable properties that can address gaps in our current technology needs. This scientific curiosity motivates the continued importance of main group chemistry research and the discovery of new electronically unusual chemical species in general.

Many of the main group species of interest are extremely reactive and difficult to isolate under ambient conditions. As such, the strategy is to stabilize these species via a supporting framework. Carbenes are fantastic for the isolation of such species because carbenes can act as neutral L-type ligands, can provide sufficient steric protection around the species, and can donate and accept electron density as needed to tame instability. As an ambiphile, carbenes can simultaneously stabilize empty orbitals via σ -donation and stabilize filled orbitals via π -acceptation. Like the phenomena observed with metals, this push-pull effect allows carbenes to form strong bonds with the main group species, decreasing the chance of carbene dissociation,

further adding stability to the system. Additionally, the diversity of carbenes allows us to probe the chemical properties of the studied species under varying electronic and steric environments.

The following selected examples demonstrate how carbenes have been used in the isolation of species with uncommon electronic states.

Closed Shell Species

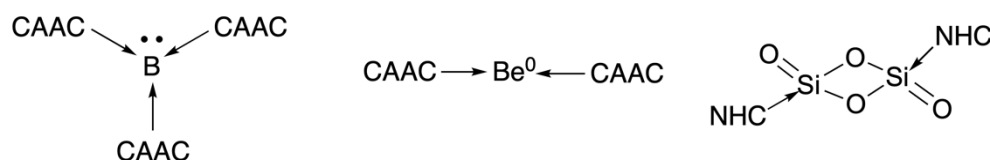
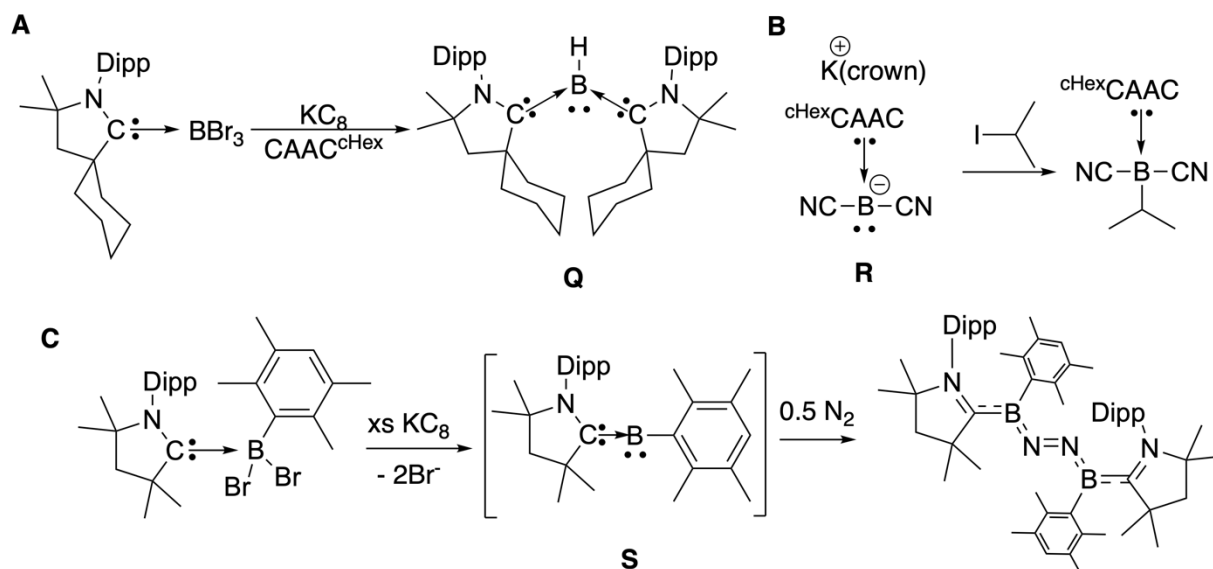


Figure 1.19. Examples of Unusual Closed Shell Main Groups Species Stabilized by Carbenes.

This section will discuss several remarkable main group species with closed shell structures: a nucleophilic borylene, an example of “molecular” beryllium, and the elusive monomeric silicon dioxide (Figure 1.19). In each case, the electronic properties of the supporting carbene allows the isolation of the main group species.



Scheme 1.17. Examples of Isolated or Transient CAAC-Stabilized Boron Species.

Parent borylene, which can exist in two electronic states: as a singlet with one atomic bond, one lone pair, and two empty orbitals, or as a triplet with one atomic bond, two partially filled orbitals and one empty orbital (Scheme 1.17).⁶⁴ In 2011, borylene **Q** was reported and this species can be considered a derivative of the singlet borylene with two CAACs stabilizing the two empty orbitals.⁶⁵ At the same time, the π -acidity of the CAACs also serve to withdraw electron density from the boron atom, providing additional stabilization to tame the nucleophilic electron pair on boron. Borylene **Q** is the first reported example of a nucleophilic boron center, in contrast to the usual electrophilic nature of boron atoms. The nucleophilic nature of CAAC-supported boron species has resulted in remarkable reactivity: boryl anion **R** is capable of alkylation,⁶⁶ and borylene **S** is capable of nitrogen fixation!⁶⁷

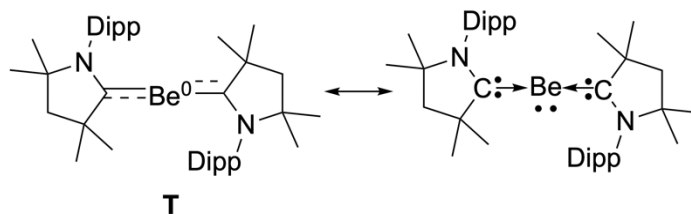


Figure 1.20. A Bis-CAAC Stabilized Be⁰ Species.

The next example is a zero-valent beryllium **T** (Figure 1.20). While monomeric zero-valent transition metal complexes have been investigated,³⁷ the corresponding chemistry for s-block elements remains underexplored. In 2016, Braunschweig *et al* reported the first example of a CAAC-stabilized beryllium(0) species.⁶⁸ In single X-ray crystal studies of the beryllium **T**, the linear C-Be-C bond and the shortened Be-C bonds (1.664Å and 1.659Å versus that of the only other structurally known two-coordinate beryllium complex [(2,6-Mes₂C₆H₃)BeN(SiMe₃)₂] 1.700Å) suggests at least a double bond character between the carbene carbon atoms and the beryllium atom. Interestingly, a computational study⁶⁹ indicated that analogous heavier Group 2 species are unlikely to be stable, owing to their greater reducing nature compared to that of

beryllium. Indeed, in 2016, Turner demonstrated that the attempted reduction of CAAC-MgCl₂ led to decomposition of the CAAC ligands via rearrangements.⁷⁰ However, as the computational study was conducted only with known carbenes, it is feasible that a magnesium(0) complex could be isolated using a novel suitably electrophilic carbene, much like how zero-valent carbene-beryllium complexes are not known with NHCs, but are known with the more π -acidic CAACs.

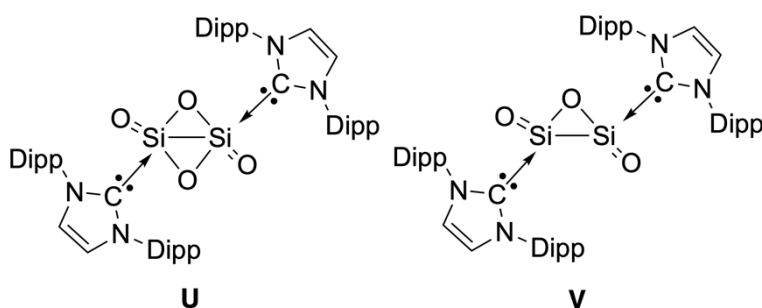


Figure 1.21. Examples of Molecular Silicon Oxides Stabilized by NHCs.

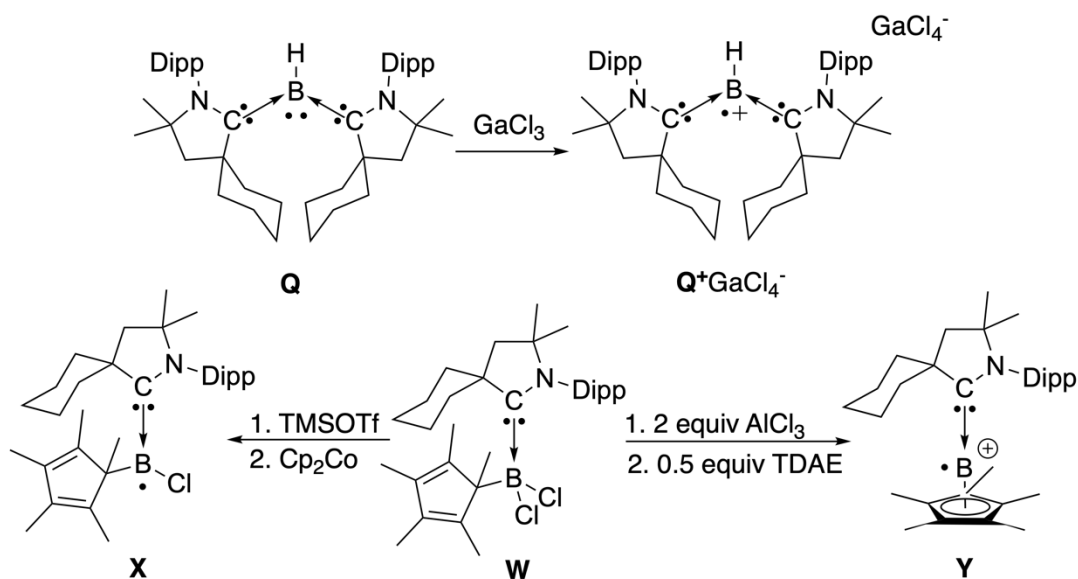
The final example is the molecular silicon dioxide **U** (Figure 1.21). Also known as silica, polymeric forms of SiO₂ are ubiquitous and have many applications as a bulk material. Because of the zwitterionic character of Si-O double bonds and the enthalpically strong Si-O single bonds, contributing to extensive oligomerization, isolation the structure and electronic properties of small silicon-oxide clusters were relatively unknown until Robinson *et al* reported an NHC-stabilized silicon dioxide species **U** and **V** in 2015.⁷¹ These cluster were synthesized by careful introduction of O₂ or N₂O to NHC-stabilized Si₂, respectively. The NHC ligands provided a restricted steric environment that prevented the Si₂O₄ and Si₂O₃ units of **U** and **V**, respectively, from polymerizing further even though computational studies indicated that the Si-O double bonds were heavily polarized towards the oxygen atoms.

Open Shell Species

This section showcases several main group species that have unpaired electrons.

Carbenes are excellent tools in the isolation of radical and radicaloid species because the carbene exhibits push-pull captodative effect abilities with its filled σ -orbital and its empty p-orbital.

Generally, the more π -acidic the carbene, the greater the more delocalized the unpaired electron spin density, and correspondingly the more stabilization the carbene provides.⁷²



Scheme 1.18. CAAC-Stabilized Boron Open-Shell Species.

The number of boron radical species and boron radical chemistry is unknown relative to that of other commonly encountered elements in organic chemistry (C, N, O, S, and P).⁷³ Many of the known boron radical species that have been isolated and studied are stabilized by carbenes (Scheme 1.18). Boron-based radical **Q** was derived from borylene $\text{Q}^+\text{GaCl}_4^-$ (*vide supra*) via a one electron oxidation by GaCl₃.⁶⁵ Another example is the transformation of borondichloride **W** into radicals **X** and **Y**.⁷⁴ The NHC and N-Heterocyclic olefin (NHO) analogs of the borondichloride **W** were also synthesized but did not yield the desired radicals upon treatment

with the same reagents, indicating that the radicals are best stabilized by highly ambiphilic carbenes.

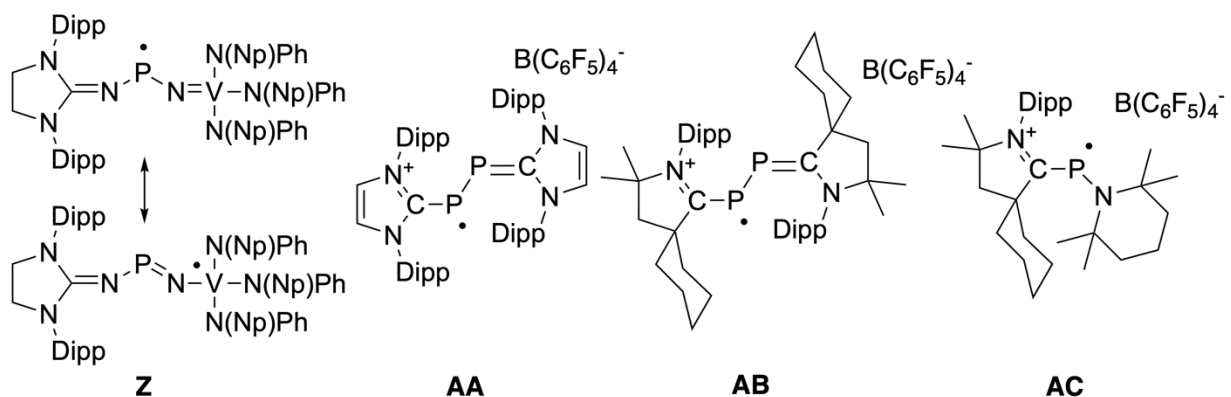
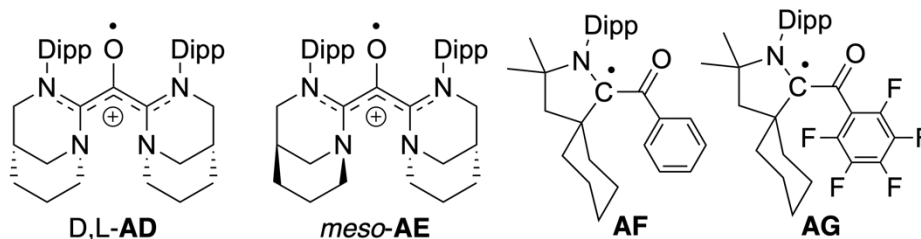


Figure 1.22. Examples of Phosphorus Radicals Stabilized by Carbenes.

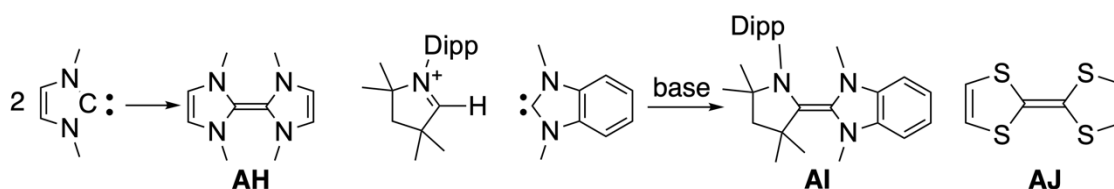
Phosphorus radicals are better understood entities and have physical properties that can have potential applications as photoinitiators and as replacements for tin hydride reagents in industry.⁷⁵ Depending on the nature of the molecule, the spin density of the unpaired electron can be distributed more towards non-phosphorus atoms, like radical **Z**, or reside on the phosphorus atom as a phosphorus-centered radical, like radicals **AA-AC** (Figure 1.22).⁷⁶ Of note are radicals **AA** and **AB** which feature the P_2 fragment, an elusive analogue of the abundant N_2 .



Scheme 1.19. Examples of Carbon Radicals Stabilized by Carbenes.

Carbon-based radicals are more fickle species, in part due to the thermodynamically favorable formation of dimers; carbon-carbon bonds are significantly stronger than that of other homoatomic bonds: nitrogen-nitrogen, oxygen-oxygen, and sulfur-sulfur bonds. The captodative effect is used to somewhat stabilize the carbon-based radical to discourage dimerization. Because

their scaffolds contain components for a captodative system, carbene adducts and carbene dimers have yielded isolable, monomeric carbon-based radicals (Scheme 1.19). Radicals **D,L-AD** and *meso-AE* are the first isolated oxyallyl radicals and are air-stable.⁷⁷ The two radicals were synthesized from the anti-Bredt NHC adduct with CO. The isolation of *meso-AE* shows that only one of the carbene centers is necessary to provide the stability of the captodative effect. Radicals **AF** and **AG** are carbon-based radicals derived from their corresponding carbene-acylium adducts.⁷⁸ Of note, both radicals are stable in solution, but **AG**, with its electron withdrawing C₆F₅ substituent, is also stable in air.⁷⁹



Scheme 1.20. Examples of Electron Rich Olefins as a Result of Carbene Dimerization.

Oxidation of tetraazafulvalenes and tetra- and tri-azaalkenes also result in open-shell species like radicals **AH-AJ**. These highly nitrogen substituted alkenes can be synthesized through the dimerization of small carbenes: tetra-azaalkenes like **AH** are generated via the dimerization of small NHCs; and tri-azaalkenes like **AI** are generated via the addition of a CAAC to a protonated NHC, followed by deprotonation (Scheme 1.20).⁸⁰ Whereas the tri-azaalkenes and the tetrathiafulvalene sulfur analogues **AJ** have three distinct and isolable oxidation states (neutral, radical cation, and dication), most tetra-azaalkenes do not have a stable radical cation, the exception being tethered NHC dimers. The tetrathiafulvalene analogues are weaker reducing agents ($E_{1/2} = +0.32$ V and $+0.71$ V vs SCE) compared to azaalkenes ($E_{1/2} = -1.00$ V vs SCE for **AH**, $E_{1/2} = -0.01$ V and $+0.33$ V vs SCE for **AI**), opening possible applications for the azaalkenes in processes that involve electron transfer.

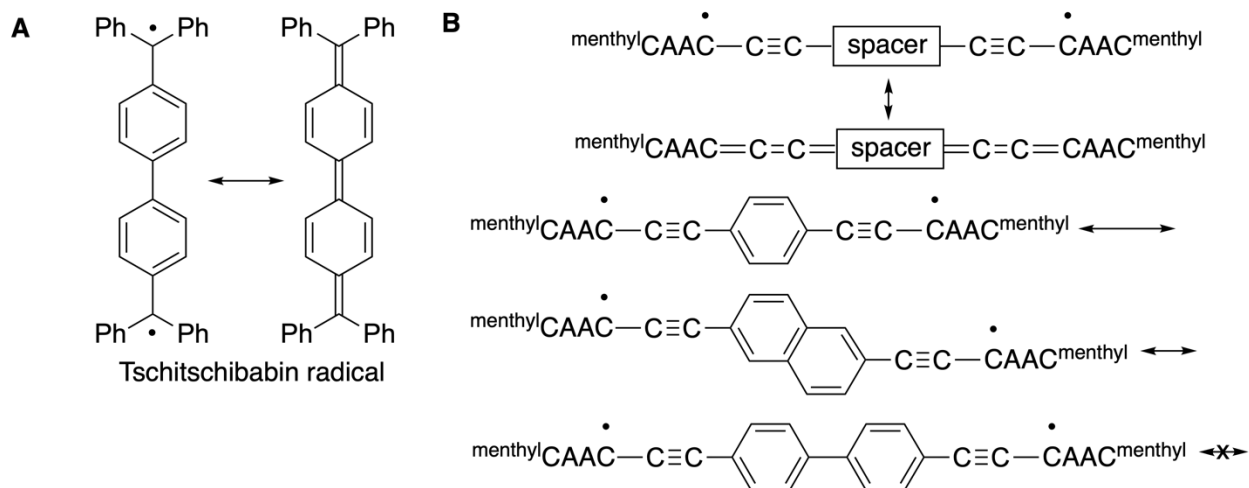


Figure 1.23. Organic Diradicaloid Species. Examples include the Tschitschibabin radical (A) and the CAAC-stabilized conjugated alkynyl species (B).

The final example of carbene applications in open-shell species is their use in investigating the nature of the “diradical paradox”.⁸¹ In 2018, the Bertrand group reacted CAACs with several different alkynes to synthesize Tchitchibabin type diradicals (Figure 1.23) to experimentally determine what factors influence the ground electronic state of these molecules.⁸² The study found that increasing spacer length between the two carbene moieties decreased the energy gap between a molecule’s singlet open shell ground state (biradical with paired spins) and its triplet state (biradical with unpaired spins), while also increased the energy of a molecule’s singlet closed shell state (the cumulenic electronic configuration). Concurrently, the Bertrand group used the same library to investigate the mixed valent character of the analogous radical cations (Figure 24), finding that increasing spacer length transitioned the molecules from type II mixed valent compounds to type III compounds.⁸³

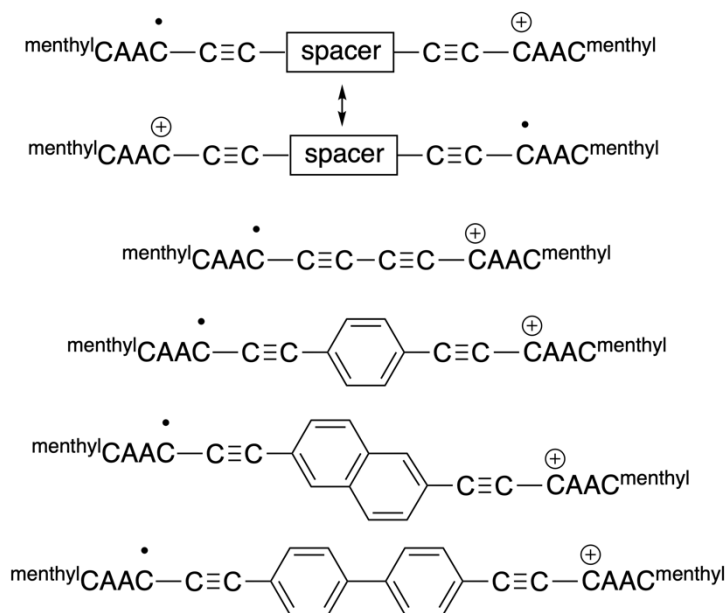


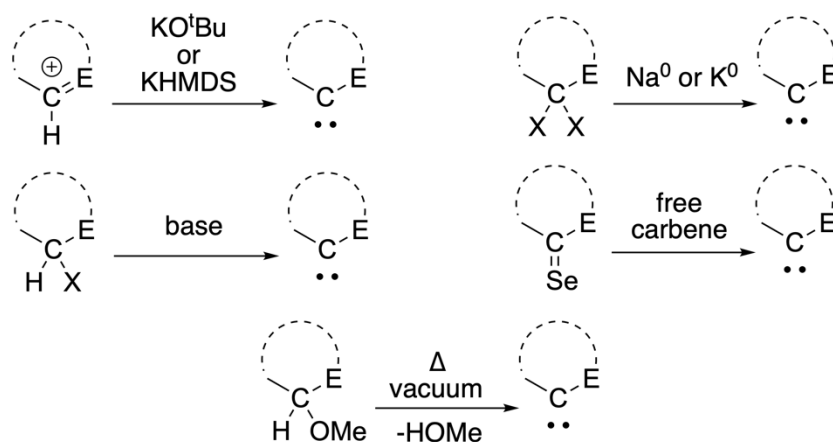
Figure 1.24. CAAC-Stabilized Carbon-Centered Showing the Effect of Distance on the Mixed Valent Nature of Radical Cations.

1.5 Review of Select Carbene Syntheses

Given their astounding diversity, a generic carbene synthetic route does not exist. Instead, each carbene type has a generalized method that usually allow for steric and minor electronic variations. Understanding the method in which the core structures are stitched together reveals which additional functional groups are possible and which are not. Because the synthetic procedure of one core structure is not always adaptable to another, the pursuit of novel types of carbenes can constitute the entire program of a chemistry research group.

Following the synthesis of the core structure, the free carbene is usually generated by a seemingly simple deprotonation, but other methods to yield the carbene are possible (Scheme 1.21). To isolate the free carbene, the deprotonation must be performed under air-free and anhydrous conditions. For strongly nucleophilic carbenes, the cation of the base may prevent the successful deprotonation and isolation of the free carbene. Additionally, nucleophilic carbenes

require stronger bases to deprotonate to overcome the stronger carbene-proton bond. Generally, ambiphilic and electrophilic carbenes require bulky bases as the base could act as a nucleophile and add to the carbene center rather than perform a deprotonation. This obstacle can be overcome by increasing the steric hindrance around the carbene center. More specialized methods of generating carbenes include the following: thermolysis under very low pressure, using alkali metal to reduce a carbene-heteroatom adduct, and a carbene-carbene exchange reaction (see section 1.2.1.6).



Scheme 1.21. Various Methods to Generate a Free Carbene.

The following selected syntheses are provided for commonly encountered carbenes and the carbenes relevant to this thesis. Several in-depth reviews of carbene synthetic routes are available.⁸⁴

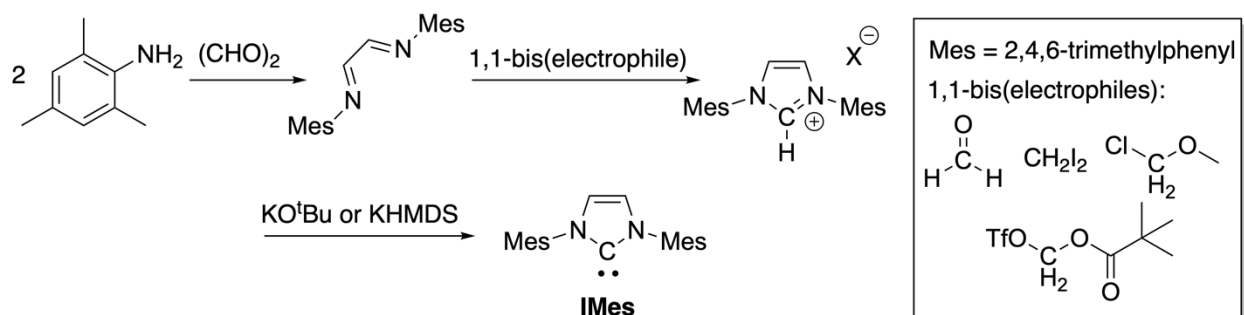
1.5.1 N-Heterocyclic Carbenes (NHC)⁸⁴

In 1991, Arduengo *et al* reported the first X-ray crystal structure of a free carbene.⁸⁵ Five-membered NHCs (NHC-5) are highly popular carbenes (see section 1.4) in part because NHC-5 is synthetically easy to prepare. The protonated precursor to the free NHC is a cyclic formamidine salt. The first and second subsections summarize select procedures to

synthesize symmetric and asymmetric variants of the unsaturated and saturated NHCs, respectively. The last subsection discusses the synthesis of ring expanded NHCs (re-HNCs). As 2,3,4-triazol-5-ylidenes, or Enders carbenes are special cases of NHCs, they are discussed in section 1.5.2.

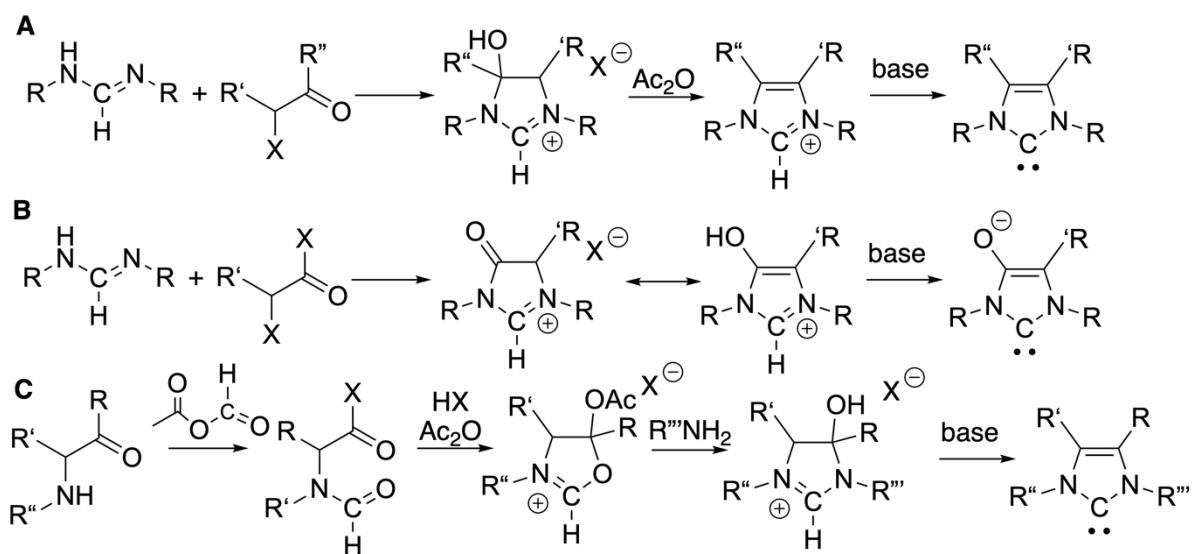
Imidazol-2-ylidenes (Unsaturated NHCs)

The unsaturated NHCs are the most synthetically accessible, with most synthesized in three steps (Scheme 1.22). The most common synthetic route for an unsaturated NHC begins with installing the nitrogen substituents on an α,β -dicarbonyl, followed by cyclization with a C-1 source, and finally deprotonation. The synthesis of NHC **IMes** is representative of a general procedure for the synthesis of symmetric unsaturated NHCs. **IMes** is synthesized by a condensation between two equivalents of 2,4,6-trimethylaniline (mesitylaniline, Mes) with glyoxal, followed by a cyclization with paraformaldehyde under acidic conditions, and then resulting imidazolium salt is deprotonated with a strong base like potassium tert-butoxide (KO^tBu) or potassium bis(trimethylsilyl)amide (KHMDs). Apart from paraformaldehyde, other reported C-1 sources are 1,1-bis(electrophiles), which include, in order of increasing electrophilicity, methylene iodide, chloromethyl ether, and *in situ* generated trifluoromethylsulfonyloxymethyl pivalate. These C-1 sources succeed in generating imidazolium salts when the diimine intermediates are electron poor.



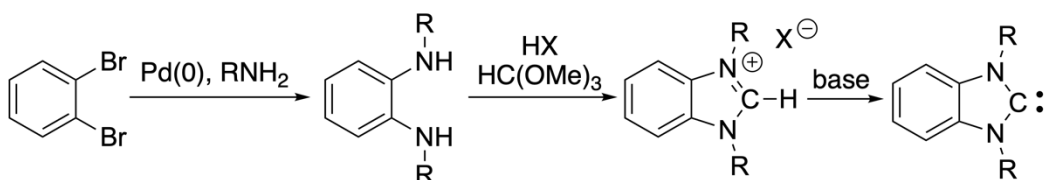
Scheme 1.22. Synthesis of IMes as a Representative Synthetic Procedure for Unsaturated NHCs.

Unsaturated NHCs with non-hydrogen substituents on the backbone have lengthier synthetic procedures and generally utilize one of three strategies (Scheme 1.23). The first procedure forms the core structure by cyclizing a pre-formed formamidine with an alpha-halo ketone followed by dehydration using acetic anhydride. The second procedure is similar: a cyclization of a pre-formed formamidine with an alpha-halo acid chloride or an alpha-halo ester forms a carbonyl-containing backbone, which is then aromatized through keto-enol tautomerization to form the carbene precursor. The third procedure installs the second nitrogen as the last part of forming the core structure: the first step N-formylates a beta-aminoketone, which is then cyclized under acidic conditions to form an acetal intermediate, the oxazolium salt is then refluxed with a primary amine to form a hemiaminal intermediate, and finally dehydrated with acetic anhydride or strong acid to yield the desired carbene precursor. All three procedures can be used to synthesize asymmetric unsaturated NHCs where the substituents on the nitrogen are different. The first and second procedures may not be regioselective, whereas the third procedure yields only the desired asymmetric carbene.



Scheme 1.23. Alternate Unsaturated NHC Synthetic Routes. These routes are useful for obtaining highly asymmetrical unsaturated NHCs.

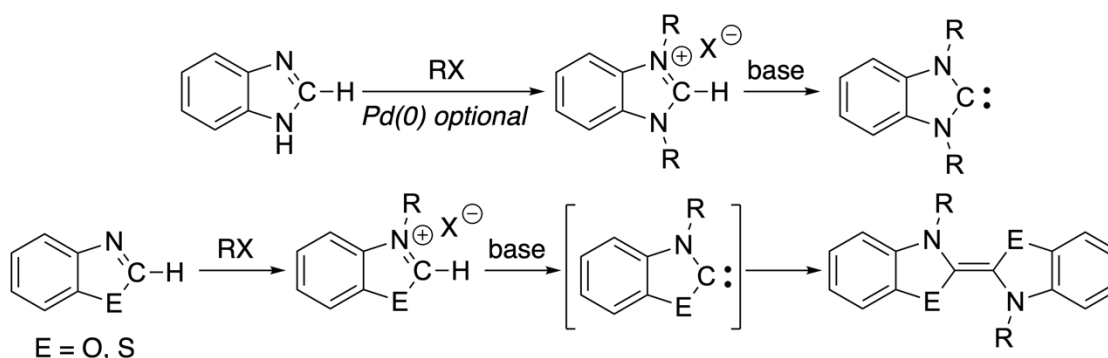
Unsaturated NHCs that are part of polycyclic aromatic systems are generally synthesized via N-substituted aromatic diamines (Scheme 1.24). The diamines are prepared from Buchwald-Hartwig aminations or nucleophilic aromatic substitutions. The remainder of the synthetic strategy follows that of the **IMes** synthesis: cyclization of the diamine intermediate with triethyl formate, a C-1 source, to yield the desired fused imidazolium salt.



Scheme 1.24. General Procedure for the Synthesis of Polycyclic Aromatic NHCs.

The synthesis of benzannulated NHCs deserves a special mention because of their widely available starting materials and synthetic ease (Scheme 1.25). For example, to reach the benzimidazolium salt carbene precursors, benzimidazole is refluxed with the appropriate alkyl halide in the presence of a mild base, or benzimidazole is reacted with the appropriate aryl halide in a Buchwald-Hartwig amination reaction. The same procedure can be used to obtain

benzoxazolium and benzthiazolium salts. Lastly, deprotonation of the benzannulated salts with an alkoxide base or KHMDS generates the free benzimidazolylidene carbene. With the benzoxazolylidene and benzthiazolylidene carbenes, the lack of steric bulk around the carbene center leads to a Wanzlick equilibrium between the free carbene and its thermodynamically favored dimer, whereas the equilibrium is shifted towards the free carbene in benzimidazolylidene carbenes with sufficient sterically bulky substituents on the carbene adjacent nitrogen atoms.

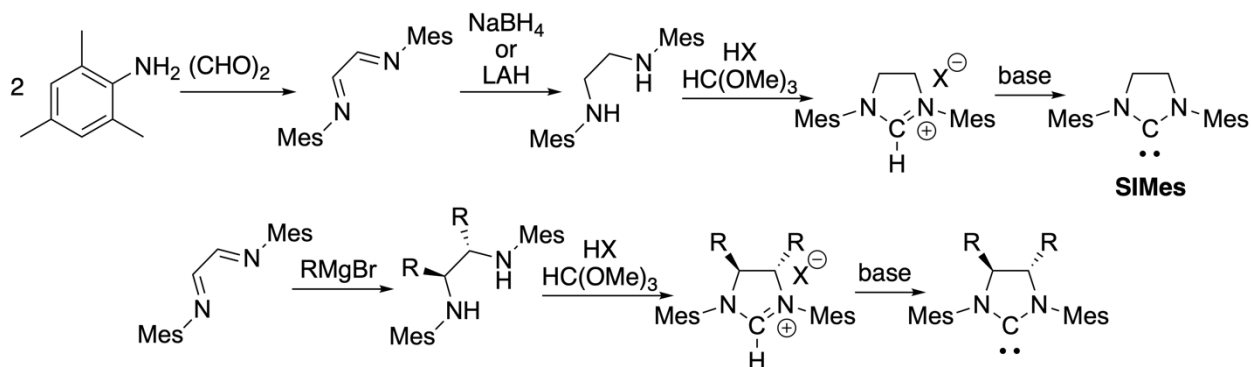


Scheme 1.25. Synthesis of Unsaturated NHC from Benzimidazole and Syntheses of Carbene Dimers from Benzoxazole and Benzthiazole.

Imidazoline-2-ylidenes (Saturated NHCs)

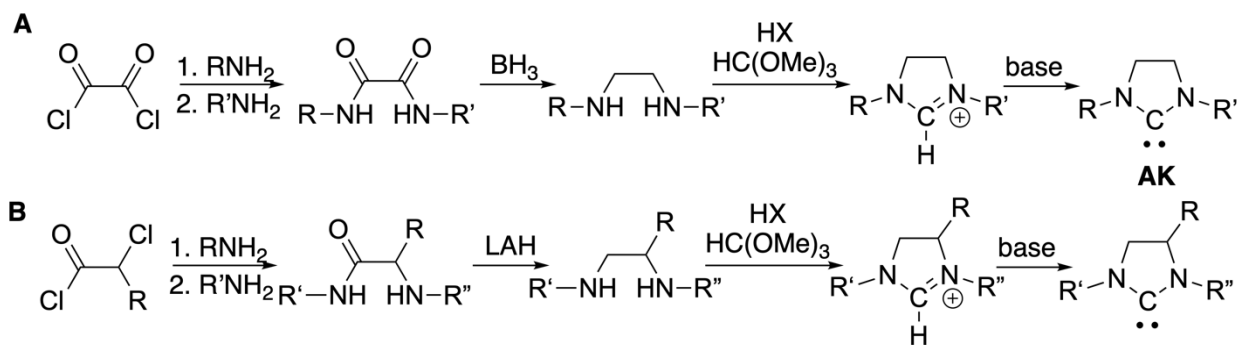
The synthesis of simple saturated NHCs follows a similar procedure to that of the unsaturated NHCs. The general strategy is to first form the desired N,N'-disubstituted ethan-1,2-diamine and then cyclize to the imidazolinium salt (Scheme 1.26). The simplest procedure starts with a diimine intermediate formed from the condensation of two equivalents of an amine with glyoxal, which is then reduced with sodium borohydride or lithium aluminum hydride to yield a diamine, cyclized with triethyl orthoformate under acidic conditions to yield the imidazolinium salt, and finally deprotonated to yield the free saturated NHC. The synthesis of NHC **SIMes** is

representative of a general procedure for the synthesis of symmetric unsaturated NHCs. Other routes to diamines provide variation in the substitution patterns on the saturated NHC backbone. For example, the addition of Grignard reagents to diimines will yield the respective *trans*-diamines.



Scheme 1.26. Synthesis of SIMes as a Representative Synthetic Procedure for Saturated NHCs and a Method to Functionalize the Saturated NHC Backbone.

The synthetic routes to asymmetric diamines typically rely on acylation and alkylation steps to provide regioselectivity (Scheme 1.27). In the synthesis of NHC **AK**, oxalyl chloride is sequentially reacted with two different amines to generate the oxalyldiamide intermediate, which is then reduced to the amines with BH_3 and cyclized with triethyl orthoformate to form the desired asymmetric imidazolium salt. A higher yielding process starts with chloroacetyl chloride or a substituted bromoacetyl bromide reacted sequentially with two different amines, followed by reduction of the amide with lithium aluminum hydride to the diamine intermediate, which is then cyclized and deprotonated to yield the asymmetric saturated NHC. When diamine stereochemistry is important, the installation of the nitrogen substituents on diamine substrates with defined stereochemistry can be performed with Buchwald-Hartwig amination to avoid the use of lithium aluminum hydride, which would give racemic diamines.

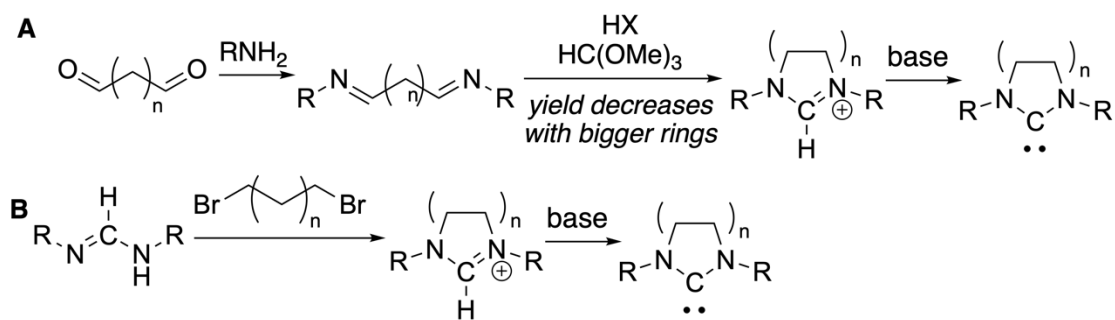


Scheme 1.27. Facile Syntheses of Asymmetric Saturated NHCs.

The typical C-1 source for generating saturated NHCs is a trialkyl orthoformate. Paraformaldehyde and other C-1 sources mentioned in section 1.5.1.1 can also be used with diamine, however, treatment of the resulting intermediate with N-bromosuccinimide to oxidize the C2 carbon is required into the yield proper imidazolium salt precursor.

Ring-expanded NHCs (re-NHCs)

NHCs with more than 5 atoms in the core structure can be synthesized using several methods, however, the carbenes become progressively more difficult to synthesize with increasing backbone atoms and flexibility (Scheme 1.28).



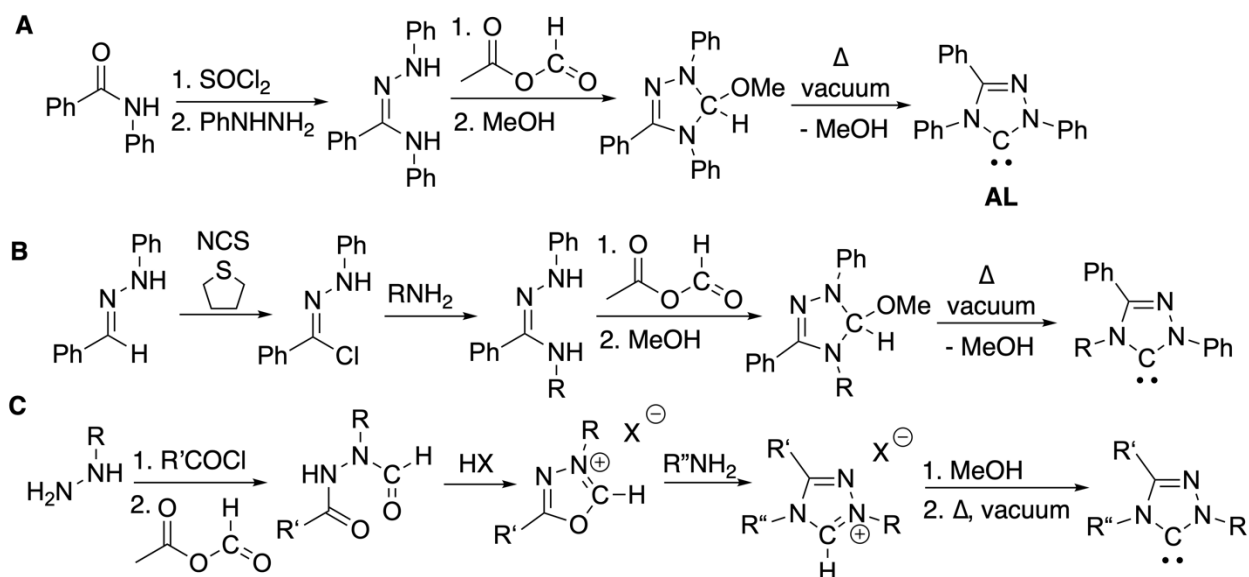
Scheme 1.28. Two Methods of Generating Saturated NHCs with Larger Ring Sizes.

Using the appropriate bisaldehyde, one can follow the simple saturated NHC procedure to synthesize the respective re-NHC. However, as the ring size increases, the efficiency of the ring closure with triethyl formate or paraformaldehyde decreases. The alternative method is to

alkylate formamidines with the appropriate dibromo molecules, however, this may require considerable reaction time.⁸⁶

1.5.2 1,2,4-triazol-5-ylidenes (Ender's Carbene)

Enders carbene was first prepared by Enders *et al* in 1995.⁸⁷ The Enders carbene is a subcategory of unsaturated NHC-5s defined by the presence of an imine (C-N double bond) in the backbone (Scheme 1.29A). The backbone nitrogen not only introduces synthetic challenges but also changes the electronic properties at the carbene center, see sections 1.4.2 and 1.6.1. The synthesis of Enders carbene **AL**⁸⁸ begins by treating an amide with thionyl chloride to form the corresponding imidoyl chloride, to which phenyl hydrazine is added. The resulting imidohydrazone is cyclized using formic acetic mixed anhydride as the C-1 source to generate a 1,2,4-triazolium salt, then treated with methanol to generate the methoxytriazoline intermediate. Heating the methoxytriazoline intermediate under vacuum causes the elimination of methanol, generating the free carbene. A similar procedure (Scheme 1.29B) has been reported in which oxidation of a hydrazone yields a hydrazoneyl chloride, is then reacted with a primary amine, cyclized with triethyl orthoformate under acidic conditions, and then deprotonated with KO^tBu in THF to yield the free carbene.⁸⁹ This synthetic route is amenable when the hydrazine starting material is easily accessible.



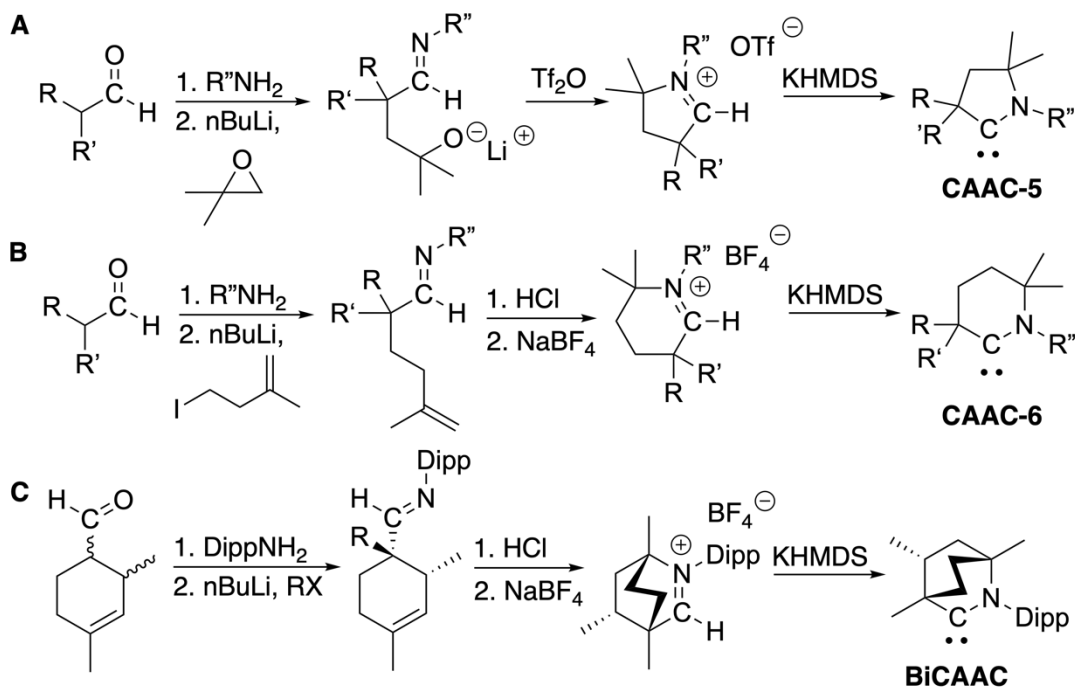
Scheme 1.29. Three Synthetic Routes to Enders Carbenes.

Another strategy to synthesize Enders carbene is to install the N-substituted aniline fragment last via heterocycle conversion to complete the core structure (Scheme 1.29C). When installing the N-substituted aniline last, a hydrazine is first acylated, then formylated, and cyclized to form a 1,3,4-oxadiazolium salt. The salt is then heated in the presence of a primary amine that generates the desired 1,2,4-triazolium salt precursor.⁸⁴ However, this procedure cannot access annulated Enders carbenes.

1.5.3 Cyclic Alkyl Amino Carbenes (CAAC)⁹⁰

The first cyclic (alkyl)(amino) carbene (CAAC) was reported in 2005 by Bertrand *et al.*¹⁵ In this report, the atoms of the five-member ring core are stitched together and then cyclized to form the pyrrolidolinium salt carbene precursor (Scheme 1.30A). The CAAC-5 synthesis begins with the condensation of an α,α -disubstituted aldehyde with aniline to form an imine intermediate, which is then deprotonated with *n*-butyllithium (*n*BuLi) and reacted with a 2,2-disubstituted epoxide to yield an imine alcoholate. The alcoholate intermediate is then treated

with triflic anhydride to yield the pyrrolidolinium salt. The pyrrolidolinium is deprotonated with KHMDS to generate free **CAAC-5**. The most difficult step in this synthesis is the thorough removal of THF solvent prior to the addition of triflic anhydride; THF polymerizes upon addition of triflic anhydride, greatly reducing yield and complicating the isolation of the carbene precursor.



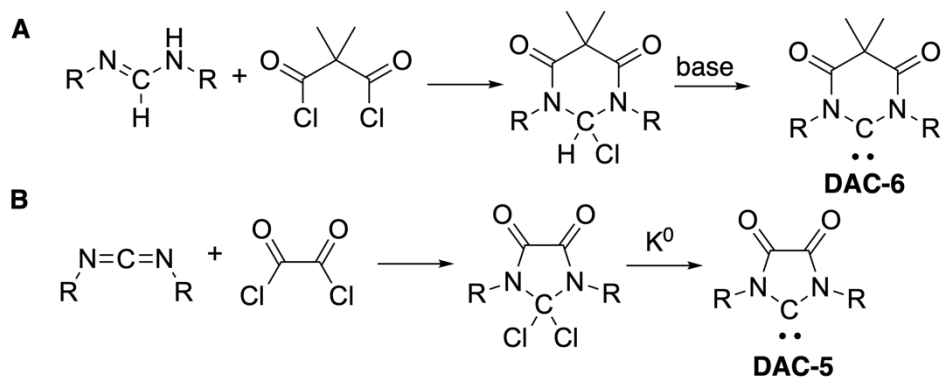
Scheme 1.30. Two Methods to Synthesize CAAC and the Synthesis of BiCAAC.

A later reported “hydroiminiumium” procedure obtains a higher yield using an acid-mediated cyclization step (Scheme 1.30B).⁹¹ In the proposed mechanism of the acid cyclization step, the imine nitrogen is first protonated before transferring the proton to the alkene, generating a tertiary carbocation. The carbocation is then attacked by the imine lone pair to form the pyrrolidolinium salt. This route has also been used to synthesize the six-membered **CAAC-6**.⁹ Because N-alkylated iminiums are too basic to transfer the proton to the alkene, the hydroiminiumium procedure is limited to producing N-aryl substituted CAACs.

The “hydroiminium” route can also be used to synthesize bicyclic CAAC structures **BICAAC** (Scheme 1.30C).⁹²

1.5.4 Diamido Carbenes (DAC)

Diamido carbenes (DACs) were first reported in 2008 by César and Lavigne.⁹³ A general synthetic strategy to access DACs begins by reacting a formamidine with a diacid chloride, followed by deprotonation (Scheme 1.31A). This strategy has successfully yielded six-membered DAC (**DAC-6**). A modified procedure is needed to generate the free five-membered DAC (**DAC-5**):⁹⁴ an *N,N'*-diarylated carbodiimide is reacted with oxalyl chloride to yield a gem-dichloro five-membered ring intermediate, which is then treated with potassium mirror in order to yield free DAC-5 (Scheme 1.31B).



Scheme 1.31. General Syntheses of DACs.

1.5.5 Mesoionic Carbenes (MIC)

Mesoionic carbenes (MICs) are carbenes in which “there are no reasonable canonical resonance forms... that can be drawn showing a carbene without additional charges.”⁹⁵ Because of this definition, several molecules are included in this class of carbenes such as the abnormal NHC (aNHC) and cyclic bent allene (CBA) (Figure 1.25). Because of their unique electronic

properties and applications (see Section 1.4), this section will only focus on the synthetic methods to access 1,2,4-trisubstituted-1,2,3-triazole MICs.

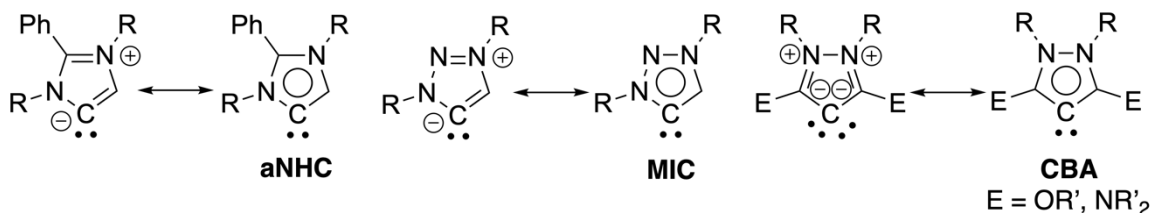
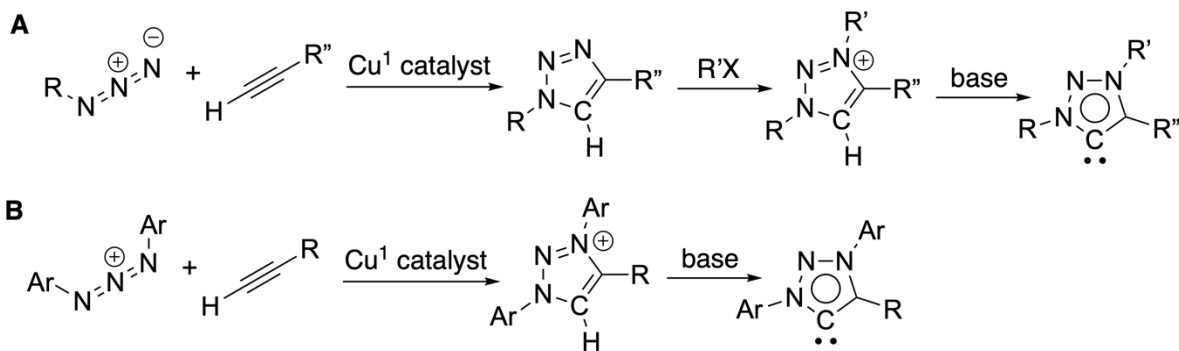


Figure 1.25. Various Types of Mesoionic Carbenes and their Zwitterionic Forms.

The key step in synthesizing the MIC core structure is a copper-catalyzed 1,3-dipolar cycloaddition reaction between an alkyne and an azide, also known as the click reaction (Scheme 1.32A). The resulting 1,2,3-triazole is then alkylated at the N3 position and finally deprotonated with KHMDS or KO^tBu. A variation of this procedure also utilizes the click reaction by reacting an alkyne or haloalkene with a 1,3-diaza-2-azoniaallene salt under copper-free conditions (Scheme 1.32B). This method is particularly suitable for when aryl substituents are desired on at the N3 position.



Scheme 1.32. Two Synthetic Routes to MICs.

Using various terminal alkynes, a variety of substituents can be installed on at the C4 position, resulting in markedly different reactivity in different MIC applications.^{96,97}

1.6 Inventory of Carbenes

As evident, there are a lot of carbenes. There are also a lot of carbene applications, with no universal, one size fits all, carbene. Given the ones already discussed thus far, how can chemists select the appropriate carbene for a specific application? Furthermore, can we use a classification system to evaluate the currently available carbenes and determine if there are any unoccupied chemical niches?

The two most important determinants that influence the application of a carbene are the HOMO and LUMO energies and the corresponding $\Delta H-L$. One way to classify these carbenes is to sort them into four electronic groups as depicted in Figure 1.26.

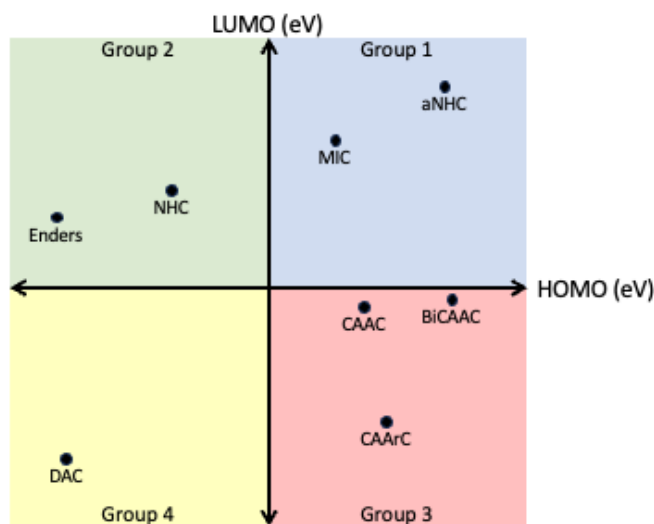


Figure 1.26. A Proposed Grouping of Carbenes Based on HOMO and LUMO Values.

1.6.1 Nucleophilicity, Electrophilicity, and Ambiphilicity of Carbenes

The carbenes in the upper right quadrant (Group 1) are ones with high HOMO energy and high LUMO energy, resulting in highly nucleophilic carbenes. Members of this category include MICs and aNHCs. These carbenes are exceptionally electron-rich as demonstrated by

their strong sigma-donating abilities as metal ligands⁹⁸ and in the use of MIC Breslow intermediates as organic electron donors.^{59–61} These carbenes also tend to feature an aromatic system that greatly reduces their π -accepting abilities, as evident in the difficulties of MIC in forming phosphinidene and selenium adducts.

The upper left quadrant (Group 2) contains carbenes that possess low HOMO energy and high LUMO energy. Members of this category include NHCs and Enders carbenes. These carbenes are not as basic or as π -acidic as the other carbenes, making them suitable leaving groups in organocatalytic reactions. Even though Group 2 carbenes are not as π -accepting as the other two carbene groups, carbenes in this category form strong bonds with metals and have been employed in many metal-catalyzed reactions. The Group 2 carbenes have also been used in the isolation of novel main group species.

Moving to the next row, the lower left quadrant (Group 3) contains carbenes that have high HOMO energy and low LUMO energy. Members of this quadrant include CAACs and CAACs. These carbenes form even stronger bonds with metals and can greatly improve the reaction conditions and substrate scope in many metal-catalyzed reactions. More noteworthy is their applications in main group research. The highly ambiphilic nature of Group 3 carbenes helps stabilize many unusual molecular species and the carbenes have excelled in the isolation of even different oxidation states of molecules. Finally, because the HOMO and LUMO energies are close together, the Group 3 carbenes have been described as having “metal-like” reactivity, as evidenced in their reactivity with small molecules like H_2 ,⁹⁹ CO ,²⁹ and NH_3 .⁹⁹

1.6.2 Opportunities for New Carbenes

Finally, the lower right quadrant (Group 4) contains carbenes that have low HOMO energy and low LUMO energy, resulting in highly electrophilic carbenes. Group 4 has the fewest carbenes, of which the most prominent are the DACs. Like CAACs, DAC can react with a variety of small molecules, although in different ways. For example, DACs react reversibly with CO and NH₃, and with alkenes in a [2+1] fashion,^{31,100} whereas CAACs have been demonstrated to react with alpha-beta unsaturated carbonyls to form Breslow-type structures. Finally, DACs are known to react with aromatic compounds upon UV irradiation. Also, at elevated temperatures, DACs can activate C-H bonds on its N-aryl groups.

As there are fewer examples of group 4 carbenes, the chemistry of carbenes with the low HOMO and low LUMO energy combination is relatively under investigated. The low HOMO energy suggests group 4 carbenes would be about as basic as NHCs and allow group 4 carbenes to function as good leaving groups, a desirable property in organocatalysis as this would allow the release of the final product while regenerating the carbene catalyst. At the same time, the low LUMO energy would result in a small HOMO-LUMO gap, enabling electrophilic-mediated activation of small molecules, as mentioned above with DAC. These two properties logically lead to the tantalizing possibility of organocatalyzed reactions that can use small gaseous molecules like CO, NH₃, H₂, ethylene, and others as starting materials. Presently, catalytic reactions that use these feedstocks require the use of rare earth metals like palladium, ruthenium, iridium, gold, and others that are toxic, expensive, and sensitive to ambient oxygen and moisture, necessitating extra precautions and work from small-scale academic to large-scale industrial settings if these reactions are to be performed.

Thus, group 4 carbenes present an exciting opportunity to test the extent of the metal-carbene isolobal analogy, with the potential to at least add to the everyday chemist's toolkit, if not to lead a transformation of the chemistry landscape away from transition metals to more abundant, environmentally friendly main group tools.

1.7 References

- (1) Wang, Z.; Tzouras, N. V.; Nolan, S. P.; Bi, X. Silver N-Heterocyclic Carbenes: Emerging Powerful Catalysts. *Trends Chem.* **2021**, *3* (8), 674–685.
<https://doi.org/10.1016/j.trechm.2021.04.006>.
- (2) Frisch, M. J.; Trucks, G. W.; Cheeseman, J. R.; Scalmani, G.; Caricato, M.; Hratchian, H. P.; Li, X.; Barone, V.; Bloino, J.; Zheng, G.; Vreven, T.; Montgomery, J. A.; Petersson, G. A.; Scuseria, G. E.; Schlegel, H. B.; Nakatsuji, H.; Izmaylov, A. F.; Martin, R. L.; Sonnenberg, J. L.; Peralta, J. E.; Heyd, J. J.; Brothers, E.; Ogliaro, F.; Bearpark, M.; Robb, M. A.; Mennucci, B.; Kudin, K. N.; Staroverov, V. N.; Kobayashi, R.; Normand, J.; Rendell, A.; Gomperts, R.; Zakrzewski, V. G.; Hada, M.; Ehara, M.; Toyota, K.; Fukuda, R.; Hasegawa, J.; Ishida, M.; Nakajima, T.; Honda, Y.; Kitao, O.; Nakai, H. Gaussian 09.
- (3) Vermersch, F.; Yazdani, S.; Junor, G. P.; Grotjahn, D. B.; Jazzar, R.; Bertrand, G. Stable Singlet Carbenes as Organic Superbases. *Angew. Chem. Int. Ed.* **2021**, *60* (52), 27253–27257. <https://doi.org/10.1002/anie.202111588>.
- (4) Huynh, H. V. Electronic Properties of N-Heterocyclic Carbenes and Their Experimental Determination. *Chem. Rev.* **2018**, *118* (19), 9457–9492.
<https://doi.org/10.1021/acs.chemrev.8b00067>.

- (5) Gerbig, D.; Ley, D. Computational Methods for Contemporary Carbene Chemistry. *WIREs Comput. Mol. Sci.* **2013**, *3* (3), 242–272. <https://doi.org/10.1002/wcms.1124>.
- (6) Setiawan, D.; Kalescky, R.; Kraka, E.; Cremer, D. Direct Measure of Metal–Ligand Bonding Replacing the Tolman Electronic Parameter. *Inorg. Chem.* **2016**, *55* (5), 2332–2344. <https://doi.org/10.1021/acs.inorgchem.5b02711>.
- (7) Back, O.; Henry-Ellinger, M.; Martin, C. D.; Martin, D.; Bertrand, G. ³¹P NMR Chemical Shifts of Carbene-Phosphinidene Adducts as an Indicator of the π -Accepting Properties of Carbenes. *Angew. Chem. - Int. Ed.* **2013**, *52* (10), 2939–2943. <https://doi.org/10.1002/anie.201209109>.
- (8) Liske, A.; Verlinden, K.; Buhl, H.; Schaper, K.; Ganter, C. Determining the π -Acceptor Properties of N-Heterocyclic Carbenes by Measuring the ⁷⁷Se NMR Chemical Shifts of Their Selenium Adducts. *Organometallics* **2013**, *32* (19), 5269–5272. <https://doi.org/10.1021/om400858y>.
- (9) Weinstein, C. M.; Junor, G. P.; Tolentino, D. R.; Jazzar, R.; Melaimi, M.; Bertrand, G. Highly Ambiphilic Room Temperature Stable Six-Membered Cyclic (Alkyl)(Amino)Carbenes. *J. Am. Chem. Soc.* **2018**, *140* (29), 9255–9260. <https://doi.org/10.1021/jacs.8b05518>.
- (10) Junor, G. P.; Lorkowski, J.; Weinstein, C. M.; Jazzar, R.; Pietraszuk, C.; Bertrand, G. The Influence of C(Sp³)H–Selenium Interactions on the ⁷⁷Se NMR Quantification of the π -Accepting Properties of Carbenes. *Angew. Chem.* **2020**, *132* (49), 22212–22217. <https://doi.org/10.1002/ange.202010744>.

- (11) Böhm, V. P. W.; Herrmann, W. A. The “Wanzlick Equilibrium.” *Angew. Chem. Int. Ed.* **2000**, *39* (22), 4036–4038. [https://doi.org/10.1002/1521-3773\(20001117\)39:22<4036::AID-ANIE4036>3.0.CO;2-L](https://doi.org/10.1002/1521-3773(20001117)39:22<4036::AID-ANIE4036>3.0.CO;2-L).
- (12) Morvan, J.; Mauduit, M.; Bertrand, G.; Jazzar, R. Cyclic (Alkyl)(Amino)Carbenes (CAACs) in Ruthenium Olefin Metathesis. *ACS Catal.* **2021**, *11* (3), 1714–1748. <https://doi.org/10.1021/acscatal.0c05508>.
- (13) Clavier, H.; Correa, A.; Cavallo, L.; Escudero-Adán, E. C.; Benet-Buchholz, J.; Slawin, A. M. Z.; Nolan, S. P. [Pd(NHC)(Allyl)Cl] Complexes: Synthesis and Determination of the NHC Percent Buried Volume (%Vbur) Steric Parameter. *Eur. J. Inorg. Chem.* **2009**, *2009* (13), 1767–1773. <https://doi.org/10.1002/ejic.200801235>.
- (14) Falivene, L.; Credendino, R.; Poater, A.; Petta, A.; Serra, L.; Oliva, R.; Scarano, V.; Cavallo, L. SambVca 2. A Web Tool for Analyzing Catalytic Pockets with Topographic Steric Maps. *Organometallics* **2016**, *35* (13), 2286–2293. <https://doi.org/10.1021/acs.organomet.6b00371>.
- (15) Lavallo, V.; Canac, Y.; Präsang, C.; Donnadiu, B.; Bertrand, G. Stable Cyclic (Alkyl)(Amino)Carbenes as Rigid or Flexible, Bulky, Electron-Rich Ligands for Transition-Metal Catalysts: A Quaternary Carbon Atom Makes the Difference. *Angew. Chem. - Int. Ed.* **2005**, *44* (35), 5705–5709. <https://doi.org/10.1002/anie.200501841>.
- (16) Melaimi, M.; Soleilhavoup, M.; Bertrand, G. Stable Cyclic Carbenes and Related Species beyond Diaminocarbenes. *Angew. Chem. Int. Ed.* **2010**, *49* (47), 8810–8849. <https://doi.org/10.1002/anie.201000165>.
- (17) Alder, Roger. W.; Butts, C. P.; Orpen, A. G. Stable Aminooxy- and Aminothiocarbenes. *J. Am. Chem. Soc.* **1998**, *120* (44), 11526–11527. <https://doi.org/10.1021/ja9819312>.

- (18) Igau, A.; Grutzmacher, H.; Baceiredo, A.; Bertrand, G. Analogous α,α' -Bis-Carbenoid, Triply Bonded Species: Synthesis of a Stable λ^3 -Phosphino Carbene- λ^5 -Phosphaacetylene. *J. Am. Chem. Soc.* **1988**, *110* (19), 6463–6466. <https://doi.org/10.1021/ja00227a028>.
- (19) Merceron, N.; Miqueu, K.; Baceiredo, A.; Bertrand, G. Stable (Amino)(Phosphino)Carbenes: Difunctional Molecules. *J. Am. Chem. Soc.* **2002**, *124* (24), 6806–6807. <https://doi.org/10.1021/ja026556z>.
- (20) Merceron-Saffon, N.; Gornitzka, H.; Baceiredo, A.; Bertrand, G. α,β -(Phosphino)(Aminocarbene) and α,ω -(Phosphino)(Oxyaminocarbene): New Bidentate Ligands for Transition Metal Complexes. *J. Organomet. Chem.* **2004**, *689* (8), 1431–1435. <https://doi.org/10.1016/j.jorganchem.2004.02.002>.
- (21) Martin, D.; Baceiredo, A.; Gornitzka, H.; Schoeller, W. W.; Bertrand, G. A Stable P-Heterocyclic Carbene. *Angew. Chem. Int. Ed.* **2005**, *44* (11), 1700–1703. <https://doi.org/10.1002/anie.200462239>.
- (22) Arduengo III, A. J.; Goerlich, J. R.; Marshall, W. J. A Stable Thiazol-2-Ylidene and Its Dimer. *Liebigs Ann.* **1997**, *1997* (2), 365–374. <https://doi.org/10.1002/jlac.199719970213>.
- (23) Nakano, R.; Jazzar, R.; Bertrand, G. A Crystalline Monosubstituted Carbene. *Nat. Chem.* **2018**, *10* (12), 1196–1200. <https://doi.org/10.1038/s41557-018-0153-1>.
- (24) Alder, R. W.; Allen, P. R.; Murray, M.; Orpen, A. G. Bis(Diisopropylamino)Carbene. *Angew. Chem. Int. Ed. Engl.* **1996**, *35* (10), 1121–1123. <https://doi.org/10.1002/anie.199611211>.
- (25) Rao, B.; Tang, H.; Zeng, X.; Liu, L.; Melaimi, M.; Bertrand, G. Cyclic (Amino)(Aryl)Carbenes (CAArCs) as Strong σ -Donating and π -Accepting Ligands for

- Transition Metals. *Angew. Chem. - Int. Ed.* **2015**, *54* (49), 14915–14919.
<https://doi.org/10.1002/anie.201507844>.
- (26) Martin, D.; Lassauque, N.; Donnadieu, B.; Bertrand, G. A Cyclic Diaminocarbene with a Pyramidalized Nitrogen Atom: A Stable N-Heterocyclic Carbene with Enhanced Electrophilicity. *Angew. Chem. Int. Ed.* **2012**, *51* (25), 6172–6175.
<https://doi.org/10.1002/anie.201202137>.
- (27) Lavallo, V.; Mafhouz, J.; Canac, Y.; Donnadieu, B.; Schoeller, W. W.; Bertrand, G. Synthesis, Reactivity, and Ligand Properties of a Stable Alkyl Carbene. *J. Am. Chem. Soc.* **2004**, *126* (28), 8670–8671. <https://doi.org/10.1021/ja047503f>.
- (28) Merceron-Saffon, N.; Baceiredo, A.; Gornitzka, H.; Bertrand, G. Synthesis of Carbenes Through Substitution Reactions at a Carbene Center. *Science* **2003**, *301* (5637), 1223–1225. <https://doi.org/10.1126/science.1086860>.
- (29) Lavallo, V.; Canac, Y.; Donnadieu, B.; Schoeller, W. W.; Bertrand, G. CO Fixation to Stable Acyclic and Cyclic Alkyl Amino Carbenes: Stable Amino Ketenes with a Small HOMO–LUMO Gap. *Angew. Chem.* **2006**, *118* (21), 3568–3571.
<https://doi.org/10.1002/ange.200600987>.
- (30) Blake, G. A.; Moerdyk, J. P.; Bielawski, C. W. Tuning the Electronic Properties of Carbenes: A Systematic Comparison of Neighboring Amino versus Amido Groups. *Organometallics* **2012**, *31* (8), 3373–3378. <https://doi.org/10.1021/om3001586>.
- (31) Moerdyk, J. P.; Schilter, D.; Bielawski, C. W. *N, N'*-Diamidocarbenes: Isolable Divalent Carbons with Bona Fide Carbene Reactivity. *Acc. Chem. Res.* **2016**, *49* (8), 1458–1468.
<https://doi.org/10.1021/acs.accounts.6b00080>.

- (32) Siemeling, U.; Färber, C.; Bruhn, C.; Leibold, M.; Selent, D.; Baumann, W.; Hopffgarten, M. von; Goedecke, C.; Frenking, G. N-Heterocyclic Carbenes Which Readily Add Ammonia, Carbon Monoxide and Other Small Molecules, *Chem. Sci.* **2010**, *1* (6), 697–704. <https://doi.org/10.1039/C0SC00451K>.
- (33) Lu, W.; Li, Y.; Ganguly, R.; Kinjo, R. Alkene–Carbene Isomerization Induced by Borane: Access to an Asymmetrical Diborene. *J. Am. Chem. Soc.* **2017**, *139* (14), 5047–5050. <https://doi.org/10.1021/jacs.7b02251>.
- (34) Walsh, A. D. 466. The Electronic Orbitals, Shapes, and Spectra of Polyatomic Molecules. Part I. AH₂ Molecules. *J. Chem. Soc. Resumed* **1953**, No. 0, 2260. <https://doi.org/10.1039/jr9530002260>.
- (35) Dötz, K. H.; Stendel, J. Jr. Fischer Carbene Complexes in Organic Synthesis: Metal-Assisted and Metal-Templated Reactions. *Chem. Rev.* **2009**, *109* (8), 3227–3274. <https://doi.org/10.1021/cr900034e>.
- (36) Melaimi, M.; Jazzar, R.; Soleilhavoup, M.; Bertrand, G. Cyclic (Alkyl)(Amino)Carbenes (CAACs): Recent Developments. *Angew. Chem. - Int. Ed.* **2017**, *56* (34), 10046–10068. <https://doi.org/10.1002/anie.201702148>.
- (37) Jazzar, R.; Soleilhavoup, M.; Bertrand, G. Cyclic (Alkyl)- and (Aryl)-(Amino)Carbene Coinage Metal Complexes and Their Applications. *Chem. Rev.* **2020**, *120* (9), 4141–4168. <https://doi.org/10.1021/acs.chemrev.0c00043>.
- (38) Hopkinson, M. N.; Richter, C.; Schedler, M.; Glorius, F. An Overview of N-Heterocyclic Carbenes. *Nature* **2014**, *510* (7506), 485–496. <https://doi.org/10.1038/nature13384>.

- (39) Bellotti, P.; Koy, M.; Hopkinson, M. N.; Glorius, F. Recent Advances in the Chemistry and Applications of N-Heterocyclic Carbenes. *Nat. Rev. Chem.* **2021**, *5* (10), 711–725. <https://doi.org/10.1038/s41570-021-00321-1>.
- (40) Phillips, J. H. Latest Industrial Uses of Olefin Metathesis. In *Organometallic Chemistry in Industry*; Colacot, T. J., Seechurn, C. C. C. J., Eds.; Wiley, 2020; pp 259–282. <https://doi.org/10.1002/9783527819201.ch10>.
- (41) Hughes, D.; Wheeler, P.; Ene, D. Olefin Metathesis in Drug Discovery and Development—Examples from Recent Patent Literature. *Org. Process Res. Dev.* **2017**, *21* (12), 1938–1962. <https://doi.org/10.1021/acs.oprd.7b00319>.
- (42) Grubbs, R. H. Olefin-Metathesis Catalysts for the Preparation of Molecules and Materials (Nobel Lecture). *Angew. Chem. Int. Ed.* **2006**, *45* (23), 3760–3765. <https://doi.org/10.1002/anie.200600680>.
- (43) Chauvin, Y. Olefin Metathesis: The Early Days (Nobel Lecture). *Angew. Chem. Int. Ed.* **2006**, *45* (23), 3740–3747. <https://doi.org/10.1002/anie.200601234>.
- (44) Schrock, R. R. Multiple Metal–Carbon Bonds for Catalytic Metathesis Reactions (Nobel Lecture). *Angew. Chem. Int. Ed.* **2006**, *45* (23), 3748–3759. <https://doi.org/10.1002/anie.200600085>.
- (45) Kajetanowicz, A.; Grela, K. Nitro and Other Electron Withdrawing Group Activated Ruthenium Catalysts for Olefin Metathesis Reactions. *Angew. Chem. Int. Ed.* **2021**, *60* (25), 13738–13756. <https://doi.org/10.1002/anie.202008150>.
- (46) Kovačič, S.; Slugovc, C. Ring-Opening Metathesis Polymerisation Derived Poly(Dicyclopentadiene) Based Materials. *Mater. Chem. Front.* **2020**, *4* (8), 2235–2255. <https://doi.org/10.1039/D0QM00296H>.

- (47) Marx, V. M.; Sullivan, A. H.; Melaimi, M.; Virgil, S. C.; Keitz, B. K.; Weinberger, D. S.; Bertrand, G.; Grubbs, R. H. Cyclic Alkyl Amino Carbene (Caac) Ruthenium Complexes as Remarkably Active Catalysts for Ethenolysis. *Angew. Chem. - Int. Ed.* **2015**, *54* (6), 1919–1923. <https://doi.org/10.1002/anie.201410797>.
- (48) C. Fortman, G.; P. Nolan, S. N-Heterocyclic Carbene (NHC) Ligands and Palladium in Homogeneous Cross-Coupling Catalysis: A Perfect Union. *Chem. Soc. Rev.* **2011**, *40* (10), 5151–5169. <https://doi.org/10.1039/C1CS15088J>.
- (49) Klinkenberg, J. L.; Hartwig, J. F. Catalytic Organometallic Reactions of Ammonia. *Angew. Chem. - Int. Ed.* **2011**, *50* (1), 86–95. <https://doi.org/10.1002/cmdc.201700488>.
- (50) Severin, R.; Doye, S. The Catalytic Hydroamination of Alkynes. *Chem. Soc. Rev.* **2007**, *36* (9), 1407–1420. <https://doi.org/10.1039/b600981f>.
- (51) Wang, Y.; Wang, Z.; Li, Y.; Wu, G.; Cao, Z.; Zhang, L. A General Ligand Design for Gold Catalysis Allowing Ligand-Directed Anti-Nucleophilic Attack of Alkynes. *Nat. Commun.* **2014**, *5* (1), 3470. <https://doi.org/10.1038/ncomms4470>.
- (52) Tang, Y.; Benaissa, I.; Huynh, M.; Vendier, L.; Lugan, N.; Bastin, S.; Belmont, P.; César, V.; Michelet, V. An Original L-Shape, Tunable N-Heterocyclic Carbene Platform for Efficient Gold(I) Catalysis. *Angew. Chem. Int. Ed.* **2019**, *58* (24), 7977–7981. <https://doi.org/10.1002/anie.201901090>.
- (53) Yazdani, S.; Junor, G. P.; Peltier, J. L.; Gembicky, M.; Jazzar, R.; Grotjahn, D. B.; Bertrand, G. Influence of Carbene and Phosphine Ligands on the Catalytic Activity of Gold Complexes in the Hydroamination and Hydrohydrazination of Alkynes. *ACS Catal.* **2020**, *10* (9), 5190–5201. <https://doi.org/10.1021/acscatal.0c01352>.

- (54) Martin, D.; Canac, Y.; Lavallo, V.; Bertrand, G. Comparative Reactivity of Different Types of Stable Cyclic and Acyclic Mono- and Diamino Carbenes with Simple Organic Substrates. *J. Am. Chem. Soc.* **2014**, *136* (13), 5023–5030.
<https://doi.org/10.1021/ja412981x>.
- (55) Enders, D.; Niemeier, O.; Henseler, A. Organocatalysis by N-Heterocyclic Carbenes. **2007**, 5606–5655. <https://doi.org/10.1021/cr068372z>.
- (56) J. Ryan, S.; Candish, L.; W. Lupton, D. Acyl Anion Free N -Heterocyclic Carbene Organocatalysis. *Chem. Soc. Rev.* **2013**, *42* (12), 4906–4917.
<https://doi.org/10.1039/C3CS35522E>.
- (57) Peltier, J. L.; Tomás-Mendivil, E.; Tolentino, D. R.; Hansmann, M. M.; Jazzar, R.; Bertrand, G. Realizing Metal-Free Carbene-Catalyzed Carbonylation Reactions with CO. *J. Am. Chem. Soc.* **2020**, *142* (43), 18336–18340. <https://doi.org/10.1021/jacs.0c09938>.
- (58) Ishii, T.; Nagao, K.; Ohmiya, H. Recent Advances in N-Heterocyclic Carbene-Based Radical Catalysis. *Chem. Sci.* **2020**, *11* (22), 5630–5636.
<https://doi.org/10.1039/D0SC01538E>.
- (59) Liu, W.; Vianna, A.; Zhang, Z.; Huang, S.; Huang, L.; Melaimi, M.; Bertrand, G.; Yan, X. Mesoionic Carbene-Breslow Intermediates as Super Electron Donors: Application to the Metal-Free Arylacylation of Alkenes. *Chem Catal.* **2021**, *1* (1), 196–206.
<https://doi.org/10.1016/j.checat.2021.03.004>.
- (60) Zhang, Z.; Huang, S.; Li, C.-Y.; Zhao, L.-L.; Liu, W.; Melaimi, M.; Bertrand, G.; Yan, X. The Triplet State of Deprotonated Mesoionic Carbene Breslow Intermediates Is Thermally Accessible: Distal Difunctionalization of Aldehydes. *Chem Catal.* **2022**, *2* (12), 3517–3527. <https://doi.org/10.1016/j.checat.2022.09.047>.

- (61) Liu, C.; Zhang, Z.; Zhao, L.-L.; Bertrand, G.; Yan, X. Mesoionic Carbene-Catalyzed Formyl Alkylation of Aldehydes. *Angew. Chem. Int. Ed.* **2023**, *62* (24), e202303478. <https://doi.org/10.1002/anie.202303478>.
- (62) Power, P. P. Main-Group Elements as Transition Metals. *Nature* **2010**, *463* (7278), 171–177. <https://doi.org/10.1038/nature08634>.
- (63) Bertrand, G. Introduction to Main Group Chemistry. *Chem. Rev.* **2010**, *110* (7), 3851–3851. <https://doi.org/10.1021/cr1001657>.
- (64) Braunschweig, H.; Dewhurst, R.; Gessner, V. Transition Metal Borylene Complexes. *Chem. Soc. Rev.* **2013**, *42* (8), 3197–3208. <https://doi.org/10.1039/C3CS35510A>.
- (65) Kinjo, R.; Donnadieu, B.; Celik, M. A.; Frenking, G.; Bertrand, G. Synthesis and Characterization of a Neutral Tricoordinate Organoboron Isoelectronic with Amines. *Science* **2011**, *333* (6042), 610–613. <https://doi.org/10.1126/science.1207573>.
- (66) Ruiz, D. A.; Ung, G.; Melaimi, M.; Bertrand, G. Deprotonation of a Borohydride: Synthesis of a Carbene-Stabilized Boryl Anion. *Angew. Chem. Int. Ed.* **2013**, *52* (29), 7590–7592. <https://doi.org/10.1002/anie.201303457>.
- (67) Légaré, M.-A.; Bélanger-Chabot, G.; Dewhurst, R. D.; Welz, E.; Krummenacher, I.; Engels, B.; Braunschweig, H. Nitrogen Fixation and Reduction at Boron. *Science* **2018**, *359* (6378), 896–900. <https://doi.org/10.1126/science.aaq1684>.
- (68) Arrowsmith, M.; Braunschweig, H.; Celik, M. A.; Dellermann, T.; Dewhurst, R. D.; Ewing, W. C.; Hammond, K.; Kramer, T.; Krummenacher, I.; Mies, J.; Radacki, K.; Schuster, J. K. Neutral Zero-Valent s-Block Complexes with Strong Multiple Bonding. *Nat. Chem.* **2016**, *8* (9), 890–894. <https://doi.org/10.1038/nchem.2542>.

- (69) A. Couchman, S.; Holzmann, N.; Frenking, G.; D. Wilson, D. J.; L. Dutton, J. Beryllium Chemistry the Safe Way: A Theoretical Evaluation of Low Oxidation State Beryllium Compounds. *Dalton Trans.* **2013**, 42 (32), 11375–11384.
<https://doi.org/10.1039/C3DT50563D>.
- (70) Turner, Z. R. Chemically Non-Innocent Cyclic (Alkyl)(Amino)Carbenes: Ligand Rearrangement, C–H and C–F Bond Activation. *Chem. - Eur. J.* **2016**, 22 (32), 11461–11468. <https://doi.org/10.1002/chem.201602264>.
- (71) Wang, Y.; Chen, M.; Xie, Y.; Wei, P.; Schaefer, H. F.; Schleyer, P. V. R.; Robinson, G. H. Stabilization of Elusive Silicon Oxides. *Nat. Chem.* **2015**, 7 (6), 509–513.
<https://doi.org/10.1038/nchem.2234>.
- (72) D. Martin, C.; Soleilhavoup, M.; Bertrand, G. Carbene-Stabilized Main Group Radicals and Radical Ions. *Chem. Sci.* **2013**, 4 (8), 3020–3030.
<https://doi.org/10.1039/C3SC51174J>.
- (73) Curran, D. P.; Solovyeu, A.; Makhlof Brahmī, M.; Fensterbank, L.; Malacria, M.; Lacôte, E. Synthesis and Reactions of N-Heterocyclic Carbene Boranes. *Angew. Chem. Int. Ed.* **2011**, 50 (44), 10294–10317. <https://doi.org/10.1002/anie.201102717>.
- (74) Huang, J.-S.; Lee, W.-H.; Shen, C.-T.; Lin, Y.-F.; Liu, Y.-H.; Peng, S.-M.; Chiu, C.-W. Cp*-Substituted Boron Cations: The Effect of NHC, NHO, and CAAC Ligands. *Inorg. Chem.* **2016**, 55 (23), 12427–12434. <https://doi.org/10.1021/acs.inorgchem.6b02336>.
- (75) Livshits-Kritsman, Y.; Tumanskii, B.; Ménard, G.; Dobrovetsky, R. Isolable Cyclic (Alkyl)(Amino)Carbene–Phosphonyl Radical Adducts. *Chem. Commun.* **2020**, 56 (9), 1341–1344. <https://doi.org/10.1039/C9CC09244G>.

- (76) Das, B.; Makol, A.; Kundu, S. Phosphorus Radicals and Radical Ions. *Dalton Trans.* **2022**, 51 (33), 12404–12426. <https://doi.org/10.1039/D2DT01499H>.
- (77) Martin, D.; Moore, C. E.; Rheingold, A. L.; Bertrand, G. An Air-Stable Oxyallyl Radical Cation. *Angew. Chem. Int. Ed.* **2013**, 52 (27), 7014–7017. <https://doi.org/10.1002/anie.201302841>.
- (78) Mahoney, J. K.; Martin, D.; Moore, C. E.; Rheingold, A. L.; Bertrand, G. Bottleable (Amino)(Carboxy) Radicals Derived from Cyclic (Alkyl)(Amino) Carbenes. *J. Am. Chem. Soc.* **2013**, 135 (50), 18766–18769. <https://doi.org/10.1021/ja4104765>.
- (79) Mahoney, J. K.; Martin, D.; Thomas, F.; Moore, C. E.; Rheingold, A. L.; Bertrand, G. Air-Persistent Monomeric (Amino)(Carboxy) Radicals Derived from Cyclic (Alkyl)(Amino) Carbenes. *J. Am. Chem. Soc.* **2015**, 137 (23), 7519–7525. <https://doi.org/10.1021/jacs.5b04414>.
- (80) *NHC-CAAC Heterodimers with Three Stable Oxidation States - Munz - 2016 - Angewandte Chemie - Wiley Online Library.* <https://onlinelibrary.wiley.com/doi/full/10.1002/ange.201607537> (accessed 2023-08-01).
- (81) Ravat, P.; Baumgarten, M. “Tschitschibabin Type Biradicals”: Benzenoid or Quinoid? *Phys. Chem. Chem. Phys.* **2015**, 17 (2), 983–991. <https://doi.org/10.1039/C4CP03522D>.
- (82) Hansmann, M. M.; Melaimi, M.; Munz, D.; Bertrand, G. Modular Approach to Kekulé Diradicaloids Derived from Cyclic (Alkyl)(Amino)Carbenes. *J. Am. Chem. Soc.* **2018**, 140 (7), 2546–2554. <https://doi.org/10.1021/jacs.7b11183>.
- (83) Hansmann, M. M.; Melaimi, M.; Bertrand, G. Organic Mixed Valence Compounds Derived from Cyclic (Alkyl)(Amino)Carbenes. *J. Am. Chem. Soc.* **2018**, 140 (6), 2206–2213. <https://doi.org/10.1021/jacs.7b11184>.

- (84) Benhamou, L.; Chardon, E.; Lavigne, G.; Bellemin-Laponnaz, S.; César, V. Synthetic Routes to N-Heterocyclic Carbene Precursors. *Chem. Rev.* **2011**, *111* (4), 2705–2733. <https://doi.org/10.1021/cr100328e>.
- (85) Arduengo, A. J.; Harlow, R. L.; Kline, M. A Stable Crystalline Carbene. *J. Am. Chem. Soc.* **1991**, *113* (1), 361–363. <https://doi.org/10.1021/ja00001a054>.
- (86) Iglesias, M.; Beetstra, D. J.; Knight, J. C.; Ooi, L.-L.; Stasch, A.; Coles, S.; Male, L.; Hursthouse, M. B.; Cavell, K. J.; Dervisi, A.; Fallis, I. A. Novel Expanded Ring N-Heterocyclic Carbenes: Free Carbenes, Silver Complexes, And Structures. *Organometallics* **2008**, *27* (13), 3279–3289. <https://doi.org/10.1021/om800179t>.
- (87) Enders, D.; Breuer, K.; Raabe, G.; Runsink, J.; Teles, J. H.; Melder, J.-P.; Ebel, K.; Brode, S. Preparation, Structure, and Reactivity of 1,3,4-Triphenyl-4,5-Dihydro-1H-1,2,4-Triazol-5-Ylidene, a New Stable Carbene. *Angew. Chem. Int. Ed. Engl.* **1995**, *34* (9), 1021–1023. <https://doi.org/10.1002/anie.199510211>.
- (88) Enders, D.; Breuer, K.; Kallfass, U.; Balensiefer, T. Preparation and Application of 1,3,4-Triphenyl-4,5-Dihydro-1H-1,2,4-Triazol-5-Ylidene, A Stable Carbene. *Synthesis* **2003**, *2003* (8), 1292–1295. <https://doi.org/10.1055/s-2003-39409>.
- (89) Yatham, V. R.; Harnying, W.; Kootz, D.; Neudörfl, J.-M.; Schlörer, N. E.; Berkessel, A. 1,4-Bis-Dipp/Mes-1,2,4-Triazolylidenes: Carbene Catalysts That Efficiently Overcome Steric Hindrance in the Redox Esterification of α - and β -Substituted α,β -Enals. *J. Am. Chem. Soc.* **2016**, *138* (8), 2670–2677. <https://doi.org/10.1021/jacs.5b11796>.
- (90) Paul, U. S. D.; Radius, U. What Wanzlick Did Not Dare To Dream: Cyclic (Alkyl)(Amino)Carbenes (CAACs) as New Key Players in Transition-Metal Chemistry. *Eur. J. Inorg. Chem.* **2017**, *2017* (28), 3362–3375. <https://doi.org/10.1002/ejic.201700397>.

- (91) Jazzar, A. R.; Bourg, J. B.; Dewhurst, R. D.; Donnadiou, B.; Bertrand, G.; Jazzar, R.; Bourg, J. B.; Dewhurst, R. D.; Donnadiou, B.; Bertrand, G. Intramolecular “Hydroiminiumation and -Amidiniumation” of Alkenes: A Convenient, Flexible, and Scalable Route to Cyclic Iminium and Imidazolium Salts. *J. Org. Chem.* **2007**, *72* (9), 3492–3499. <https://doi.org/10.1021/jo0703909>.
- (92) Tomás-Mendivil, E.; Hansmann, M. M.; Weinstein, C. M.; Jazzar, R.; Melaimi, M.; Bertrand, G. Bicyclic (Alkyl)(Amino)Carbenes (BICAACs): Stable Carbenes More Ambiphilic than CAACs. *J. Am. Chem. Soc.* **2017**, *139* (23), 7753–7756. <https://doi.org/10.1021/jacs.7b04640>.
- (93) César, V.; Lugan, N.; Lavigne, G. A Stable Anionic N-Heterocyclic Carbene and Its Zwitterionic Complexes. *J. Am. Chem. Soc.* **2008**, *130* (34), 11286–11287. <https://doi.org/10.1021/ja804296t>.
- (94) Moerdyk, J. P.; Bielawski, C. W. Reductive Generation of Stable, Five-Membered N,N'-Diamidocarbenes. *Chem. Commun.* **2014**, *50* (35), 4551–4553. <https://doi.org/10.1039/c4cc00846d>.
- (95) Guisado-Barrios, G.; Soleilhavoup, M.; Bertrand, G. 1H-1,2,3-Triazol-5-Ylidenes: Readily Available Mesoionic Carbenes. *Acc. Chem. Res.* **2018**, *51* (12), 3236–3244. <https://doi.org/10.1021/acs.accounts.8b00480>.
- (96) Bouffard, J.; Keitz, B. K.; Tonner, R.; Guisado-Barrios, G.; Frenking, G.; Grubbs, R. H.; Bertrand, G. Synthesis of Highly Stable 1,3-Diaryl-1H-1,2,3-Triazol-5-Ylidenes and Their Applications in Ruthenium-Catalyzed Olefin Metathesis. *Organometallics* **2011**, *30* (9), 2617–2627. <https://doi.org/10.1021/om200272m>.

- (97) Bezuidenhout, D. I.; Kleinhans, G.; Guisado-Barrios, G.; Liles, D. C.; Ung, G.; Bertrand, G. Isolation of a Potassium Bis(1,2,3-Triazol-5-Ylidene)Carbazolide: A Stabilizing Pincer Ligand for Reactive Late Transition Metal Complexes. *Chem. Commun.* **2014**, *50* (19), 2431–2433. <https://doi.org/10.1039/c3cc49385g>.
- (98) Lavallo, V.; Dyker, C. A.; Donnadiou, B.; Bertrand, G. Synthesis and Ligand Properties of Stable Five-Membered-Ring Allenes Containing Only Second-Row Elements. *Angew. Chem.* **2008**, *120* (29), 5491–5494. <https://doi.org/10.1002/ange.200801176>.
- (99) Frey, G. D.; Lavallo, V.; Donnadiou, B.; Schoeller, W. W.; Bertrand, G. Facile Splitting of Hydrogen at a Single Carbon Center. *Science* **2007**, *316* (April), 439–441.
- (100) Hudnall, T. W.; Bielawski, C. W. An N , N ' -Diamidocarbene : Studies in C - H Insertion , Reversible Carbonylation , and Transition-Metal Coordination Chemistry. **2009**, *373* (2), 16039–16041.

Chapter 2 Ambiphilicity of Ring Expanded N-Heterocyclic Carbenes

1.1 Introduction

Thanks to growing efforts in main group chemistry, the activation of enthalpically strong bonds and industrially relevant small molecules is no longer restricted to transition-metals.^{1,2} This is the case for a select few singlet carbenes which have been shown to activate such molecules providing a suitable stereo-electronic environment.³⁻⁶ Notably, in 2006, our group discovered that the cyclic (alkyl) (amino) carbenes (CAAC-5),⁷ a class of highly ambiphilic carbenes with low lying LUMO and high HOMO character, could react with carbon monoxide to give the corresponding ketenes.⁸ We later explored their reactivity with more challenging molecules such as H₂,⁹ P₄,¹⁰ and ammonia.⁴ Today, the propensity of CAACs to effect strong bond activation is well established across a broad range of functionalities (Si-H, C-H, B-H ...) ¹¹⁻¹³ and has even been illustrated in catalytic reaction.^{14,15} In comparison, similar reactivities are much less developed with N-heterocyclic carbenes (NHC-5s), the popular class of singlet carbenes introduced by Arduengo in 1991.¹⁶ Akin to their lack of reactivity with CO, NHC-5s are not as ambiphilic as CAAC-5 owing to the two σ -withdrawing, π -donating amino groups stabilizing the carbene center. Since 1991, a number of ring-expanded N-heterocyclic carbenes (RE-NHCs) containing more than five- atoms of carbons in the backbone have emerged.¹⁷⁻¹⁹ As expected, RE-NHCs display a larger N-C_{NHC}-N bond angle (\angle_{carb}) imposing greater steric constraint toward the carbene center²⁰⁻²² a feature used to enhance catalytic activity.²³ Arguably

less emphasized, it also increases the p-character of the sp^2 hybridized σ -orbital, effectively raising the HOMO concomitantly to the number of atoms in the backbone (see Section 2.4.4, Computational Data). Comparatively, the LUMO is less affected since ring size does not significantly disrupt the planarization of the α -amino fragments leaving mesomeric stabilization of the p_π orbital by the nitrogen's lone pair nearly identical. The ambiphilicity of a carbene centre can be estimated computationally by considering the Singlet-Triplet gap (ΔE_{S-T}) (Figure 2.1). As expected, it confirms a trend between the ring size and a higher ambiphilic character of RE-NHCs compared to NHC-5. Interestingly, the data also suggests that the ambiphilicity of NHC-8 and NHC-9 should compare to that of CAAC-5. While the saturated NHC-9 remain to be reported, herein we discuss the ambiphilic nature of RE-NHCs (NHC-6, -7, -8) through their reaction with small molecules.

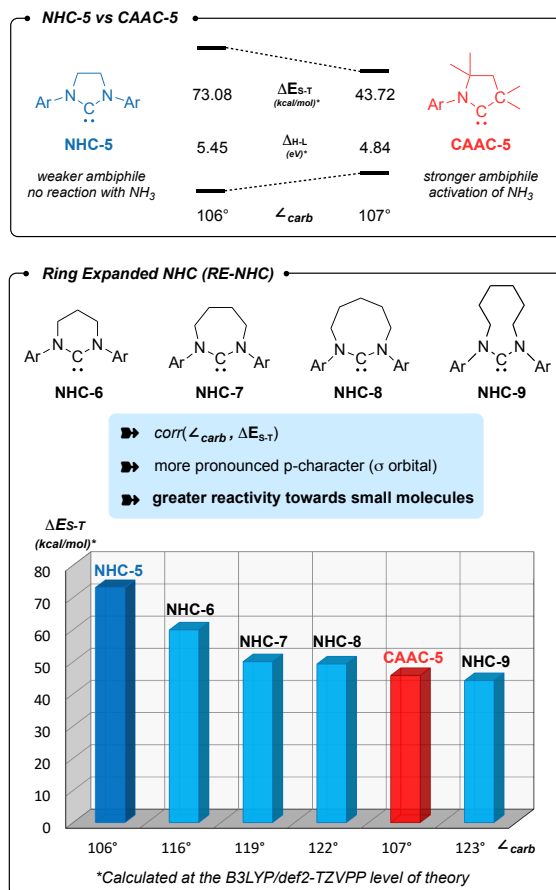
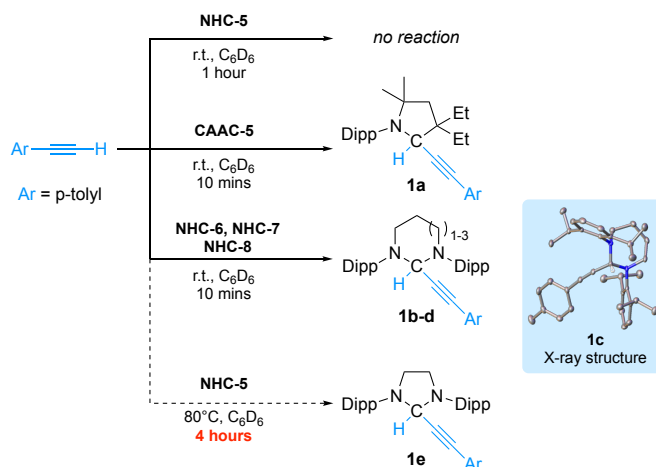


Figure 2.1. Comparison of NHC-5 and CAAC-5 Electronics and a Comparison of RE-NHCs and CAAC-5 Based on Calculated ΔE_{S-T} .

1.2 Results and Discussion

To compare experimentally the ambiphilicity of RE-NHC with that of CAAC-5, we first considered the activation of sp-hybridized CH bonds which has been reported with CAACs²⁴ but is seldomly described with NHCs (one example has been reported using acetylene gas).²⁵ We first examined the reaction of p-tolylacetylene ($pK_a(\text{DMSO}) = 28.8$ vs. 25 for acetylene) with NHC-5 at room temperature in benzene solution (Scheme 2.1). In this case no reaction was observed within 2h, in marked contrast reaction with CAAC-5 afforded the oxidative addition

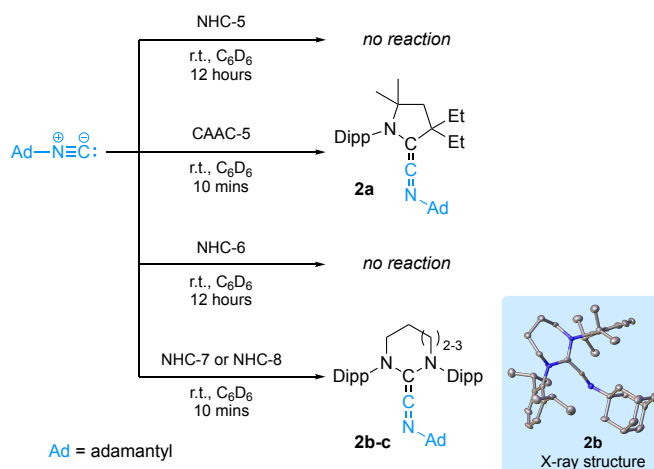
product **1a** within minutes. Under the same conditions a rapid and clean reaction was also observed with NHC-6,²² NHC-7,²² and NHC-8.¹⁹ NMR spectroscopy suggested the formation of adducts **1b-d** with diagnostic signals at 6.04 ppm, 5.87 ppm, 5.64 ppm by ¹H NMR and 72.3 ppm, 73.9 ppm and 77.1 ppm by ¹³C NMR for NHC-6, -7 and -8 respectively. X-ray quality crystals of adduct **1c** confirmed this reactivity. Puzzled by the significant difference in reactivity observed between NHC-5 and these RE-NHCs, we re-evaluated the reaction of NHC-5 with p-tolylacetylene and observed very slow conversion to adduct **1e** upon performing the reaction at 80°C over 4h. This reactivity is consistent with the order of decreasing singlet-triplet gap: NHC-5 > NHC-6 > NHC-7 > NHC-8 and illustrates the stronger σ -donating ability of RE-NHCs compared to traditional 5-membered NHCs.



Scheme 2.1. Reactivity of NHC-6,7,8 and CAAC-5 with p-tolylacetylene

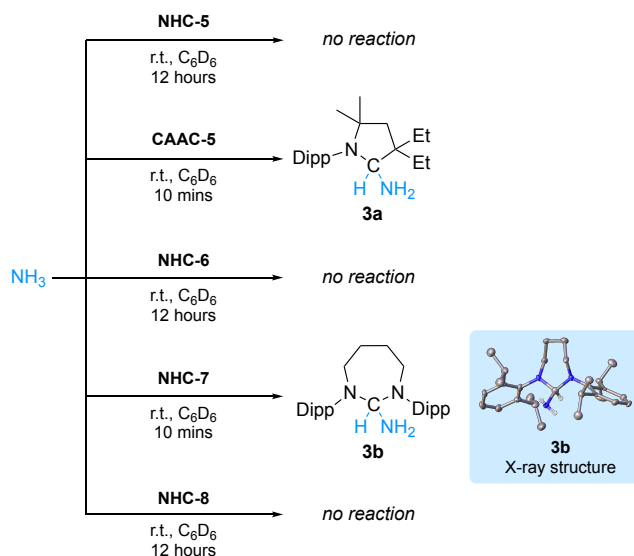
These initial results prompted us to search for more challenging molecules to activate. Unlike CAACs, which belong to the push–spectator category, NHCs are not supposed to be sufficiently ambiphilic to react with CO. As proposed by Frenking,²⁶ the stability and the formation of ketenes *via* carbonylation of carbenes highly depends on the corresponding singlet/triplet gap. This is also the case with isocyanides, the isoelectronic equivalent of carbon monoxide. Examples of diamino ketenimines reported in the literature are scarce and include

Anti-Bredt NHC²⁷ and diamidocarbenes (DAC)^{28–30} whose enhanced electrophilicity results from reduced donation of the nitrogen lone-pair to the empty p-type orbital of the carbene carbon. Curious to probe the reactivity of RE-NHCs for the same, we considered their reaction and that of NHC-5 or CAAC-5 with adamantyl isocyanide (Scheme 2.2). As expected, no reaction was observed with NHC-5 after 16h at room temperature in benzene solution.³¹ This result contrasts with CAAC-5 which afforded the ketenimine **2a** cleanly within minutes. Performing the same reaction with free NHC-6 did not yield in any observable reaction even after prolonged reaction time. More interestingly repeating the same reaction with NHC-7 and NHC-8 led to the clean formation of compound **2b** and **2c**, with diagnostic signal for the central carbon of ketenimines at 216.9 ppm and 211.5 ppm, respectively, by ¹³C NMR. We confirmed the structure of compound **2b** by X-ray crystallography. Of interest the solid-state structure revealed a pronounced bent geometry (C_{NHC}-C-N angle: 158.5°) compared to that of diamido cyclohexylketenimine (C_{DAC}-C-N angle: 173.8°)²⁹ with a longer C_{NHC}-C_{ket} bond (133.8 pm vs. 129.7 pm for DAC). This observation is in agreement with a zwitterionic resonance form of **2c**, in which the π-system connecting carbene carbon and the isonitrile carbon is highly polarized is not negligible.



Scheme 2.2. Reactivity of NHC-6,7,8 and CAAC-5 with adamantyl isocyanide.

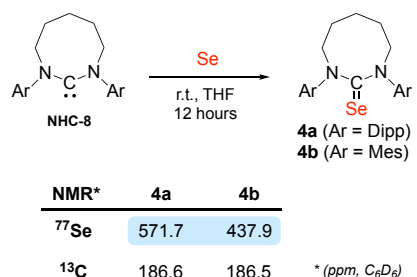
Taken together the reaction of RE-NHCs with terminal alkynes and isocyanide support that NHC-7 and NHC-8 belong to the class of strongly ambiphilic carbenes as suggested by their smaller singlet-triplet. To deconvolute these results further, we wondered if RE-NHCs, notwithstanding their lower electrophilicity could compare with CAAC-5 in the activation of ammonia.⁴ Diaminocarbenes are generally considered not nucleophilic enough for ammonia activation and have even been generated in liquid NH₃.³² We confirmed this lack of reactivity by pressurizing a benzene solution of free NHC-5 with 2 atmospheres of ammonia (Scheme 2.3). In agreement with literature precedent, we confirmed the reactivity of CAAC-5 under the same conditions leading to the ammonia adduct **3a**. Switching to RE-NHCs, no reaction was observed with NHC-6 despite prolonged reaction time, while NHC-7 led to the clean formation of product **3b** with distinctive signals by ¹H and ¹³C NMR spectroscopy at $\delta = 5.25$ ppm and 85.8 ppm respectively. We attributed these signals to adduct **3b**, resulting from the formal oxidative addition of NH₃ by free NHC-7. This result was confirmed by single crystals X-ray diffraction. Surprisingly no reaction was observed with NHC-8. While the lack of reactivity of NHC-5 and NHC-6 with ammonia is in good agreement with a higher singlet-triplet gap, the same rational is not straightforward with NHC-8.



Scheme 2.3. Reactivity of NHC-6,7,8 and CAAC-5 with ammonia.

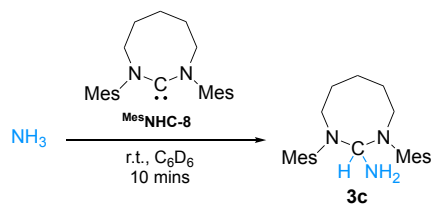
We previously reported that the steric environment of CAAC-5 is a determining factor in controlling the reversibility of E-H bond activation (E = N-H, P-H).¹⁵ Compared to CAAC-5 ($\angle_{\text{carb}} = 106^\circ$), NHC-8 is more sterically constrained around the carbene carbon due to its large N-C_{NHC}-N bond angle ($\angle_{\text{carb}} = 122^\circ$)¹⁹ which might explain its lack of reactivity with ammonia despite favourable electronics. To probe this hypothesis, we prepared the N-Mesityl (-Mes) substituted NHC-8 (^{Mes}NHC-8) expecting that its steric profile should be smaller than that of NHC-8. This is apparent in the solid state, when considering the sterics maps (see Section 2.4.4, Computational Data) and percent buried volumes %V_{bur} (%) around the carbene carbon which shows that ^{Mes}NHC-8 (77.2%) has a smaller steric profile compared to NHC-8 (80.1%), closer to that of NHC-7 (78.4.%). It is also apparent in solution when considering the unusual ⁷⁷Se NMR downfield shift of NHC-8-Se adduct **4a** (571.1 ppm) with respect to ^{Mes}NHC-8-Se adduct **4b** (437.9 ppm) (Scheme 2.4). ⁷⁷Se NMR is a spectroscopic marker for highlighting non-classical bonding (NCB) interactions between pendant N-Dipp substituents and the selenium atom. Taken altogether these observations suggests that with NHC-8 the activation sphere of the carbene centre is largely occupied by the N-Dipp isopropyl substituents.³³ Note that comparing

the reactivity of N-tolyl and N-Dipp 8-membered NHCs with silver chloride, Cavell and co-workers observed that in very large ring NHCs the steric environment provided by N-dipp substituents can become so overwhelming as to prevent coordination.¹⁹

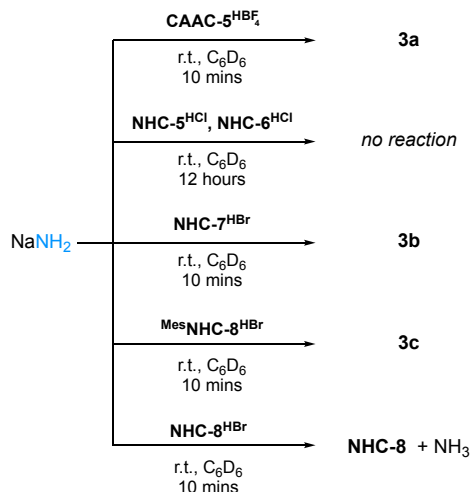


Scheme 2.4. Selenium adducts of Dipp- and Mes- substituted NHC-8.

Having confirmed ^{Mes}NHC-8 to be less sterically hindered than NHC-8 and NHC-7, we evaluated its reactivity with ammonia. Gratifyingly in this case rapid formation of the corresponding ammonia adduct was observed when performing the reaction in C₆D₆ under 2 atmospheres of ammonia (Scheme 2.5). To confirm these results, we also investigated the reactivity of sodium amide with the corresponding iminium salt conjugate acids which provided the expected reactivities resulting from electrophilic addition of NH₂⁻ (Scheme 2.6). Note that under these conditions, reaction of NHC-8^{HBr} with NaNH₂ afforded free NHC-8 and ammonia. Altogether these results suggest the activation of ammonia in NHC-8s is likely reversible and controlled by steric parameters.



Scheme 2.5. Reactivity of ^{Mes}NHC-8 with ammonia.



Scheme 2.6. Reactivity of NHCs and CAAC conjugate salts with NaNH₂.

1.3 Conclusions

N-heterocyclic carbenes, the popular class of singlet carbenes introduced by Arduengo in 1991 are not expected to be very ambiphilic owing to the two σ -withdrawing, π -donating amino groups stabilizing the carbene centre. However, our experimental data demonstrate that ring-expanded N-heterocyclic carbenes belong this exclusive class of ambiphilic carbenes. Through the activation of ammonia, we have identified NHC-8 as the most ambiphilic N-heterocyclic carbene considered herein. Our results also showcase that as with CAACs, the steric environment in RE-NHCs is a determining factor in controlling the reversibility of E-H bond activation. We expect that these results will have far reaching implications in the design and applications of large ring singlet carbene skeletons.

2.4 Experimental

2.4.1 General Methods

All manipulations were performed using standard glovebox and Schlenk techniques. Glassware was dried in an oven overnight at 150 °C or flame-dried, and solvent were dried and degassed before use. Benzene, THF, diethyl ether, and n-pentane were freshly distilled over Na metal. Hexanes, dichloromethane, and chloroform were freshly distilled over CaH₂. All reactions with free carbenes were performed in an argon-filled glovebox. Ammonia gas was not dried prior to use.

Deuterium-labeled solvents (d₆-benzene (C₆D₆) and d₈-THF) were purchased from Cambridge Isotope Laboratories and were freshly distilled over Na metal. NMR: Multinuclear NMR data were recorded on a Varian INOVA 500 MHz or a JOEL ECZL 400 MHz at UCSD. Chemical shifts (δ) are reported in parts per million (ppm) and are referenced to residual solvent signals (¹H, ¹³C). Coupling constants J are given in hertz (Hz). NMR multiplicities are abbreviated as follows: s = singlet, d = doublet, t = triplet, q = quartet, sext = sextet, sept = septet, m = multiplet, br = broad. All spectra were recorded at 298 K unless otherwise noted.

Single crystal X-Ray diffraction data were collected on a Bruker Apex II-CCD detector using either Mo-K α radiation ($\lambda = 0.71073 \text{ \AA}$) or Cu-K α ($\lambda = 1.54178$). Crystals were selected under oil, mounted on nylon loops then immediately placed in a cold stream of N₂. Structures were solved and refined using SHELXTL and Olex2 software. All hydrogen atoms were included in the refinement in calculated positions depending on the connecting carbon atoms. Visualized structures were generated with Mercury or Avogadro.

2.4.2 Synthetic Procedures

CAAC-5,⁷ NHC-5,³⁴ NHC-6,¹⁷ NHC-7,¹⁸ and NHC-8¹⁹ iminium precursors and carbenes were prepared according to known literature procedures and matched reported spectroscopic

data. CAAC-5 derivative molecule **1a**, **2a**, and **3a**³⁵ matched previously reported spectroscopic data.

1b: C₆D₆ (0.7 mL) was added to a J Young NMR tube containing NHC-6 (40 mg, 1.0 eq) and 4-ethynyltoluene (13 μL, 1.05 eq). The tube was shaken for 10 minutes at room temperature. NMR of the resulting colorless solution showed quantitative formation of the adduct. ¹H NMR (500 MHz, C₆D₆) δ = 7.15-7.19 (m, 4H), 7.03 (dd, 2H, J=6.5Hz), 6.55 (d, 2H, J=8.0Hz), 6.46 (d, 2H, J=8.0Hz), 6.07 (s, 1H), 4.48 (sept, 2H, J=7.0Hz), 3.93 (sept, 2H, J=6.5Hz), 3.38 (m, 4H), 3.13 (m, 2H), 1.69 (s, 3H), 1.36 (d, 6H, J=7.0Hz), 1.36 (d, 6H, J=7.0Hz), 1.29 (d, 6H, J=7.0Hz), 1.24 (d, 6H, J=7.0Hz), 1.23 (m, 2H) ¹³C{¹H} NMR (125 MHz, C₆D₆) δ = 151.0, 149.5, 144.7, 137.9, 131.3, 128.9, 127.4, 124.4, 123.6, 119.9, 88.3, 86.0, 72.3, 52.2, 30.0, 28.6, 27.6, 25.6, 24.9, 24.8, 23.9, 21.1.

1c: C₆D₆ (0.7 mL) was added to a J Young NMR tube containing NHC-7 (47 mg, 1.0 eq) and 4-ethynyltoluene (14 μL, 1.05 eq). The tube was shaken for 10 minutes at room temperature. NMR of the resulting colorless solution showed quantitative formation of the adduct. Slow evaporation of C₆D₆ under argon gave colorless crystals. ¹H NMR (500 MHz, C₆D₆) δ = 7.29-7.33 (m, 6H), 7.06 (d, 2H, J=7.0Hz), 6.79 (d, 2H, J=7.0Hz), 5.87 (s, 1H), 4.30 (sept, 2H, J=6.5Hz), 3.93 (sept, 2H, J=6.5Hz), 3.92 (m, 4H), 1.99 (s, 3H), 1.95-2.05 (m, 2H), 1.72-1.78 (m, 2H), 1.53 (d, 6H, J=6.5Hz), 1.45 (d, 6H, J=6.5Hz), 1.45 (d, 6H, J=6.5Hz), 1.41 (d, 6H, J=6.5Hz) ¹³C{¹H} NMR (125 MHz, C₆D₆) δ = 150.1, 148.8, 145.3, 137.7, 131.9, 129.0, 127.2, 124.9, 124.6, 120.9, 89.6, 86.9, 73.9, 52.9, 30.4, 28.6, 28.3, 25.4, 24.7, 24.7, 24.1, 20.6.

1d: C₆D₆ (1.0 mL) was added to a 20 mL scintillation vial equipped with a magnetic mini stir bar containing NHC-8 (51 mg, 1.0 eq) and 4-ethynyltoluene (13 μL, 1.05 eq). The reaction was stirred for 30 minutes at room temperature. NMR of the resulting colorless solution showed

quantitative formation of the adduct. Slow evaporation of C_6D_6 under argon gave colorless crystals. 1H NMR (400 MHz, C_6D_6) δ = 7.11-7.16 (m, 6H), 7.00 (d, 2H, $J=7.9$ Hz), 6.73 (d, 2H, $J=7.4$ Hz), 5.63 (s, 1H), 4.33 (m, 2H, $J=6.5$ Hz), 3.81 (m, 2H), 3.66 (m, 4H), 1.93 (s, 3H), 1.90-1.94 (m, 4H), 1.64 (m, 2H), 1.36 (d, 12H, $J=6.9$ Hz), 1.31 (d, 12H, $J=6.9$ Hz), $^{13}C\{^1H\}$ NMR (100 MHz, C_6D_6) δ = 149.7, 148.5, 147.4, 137.9, 131.8, 129.1, 127.0, 124.9, 89.1, 86.2, 77.1, 53.1, 30.7, 28.9, 26.1, 25.2, 25.0, 24.4.

1e: C_6D_6 (0.7 mL) was added under argon to a J Young NMR tube containing free carbene NHC-5 (39 mg, 1.0 eq) and 4-ethynyltoluene (13 μ L, 1.05 eq). The tube was shaken for 5 minutes at room temperature then heated at 80°C. NMR of the resulting colorless solution showed quantitative formation of the adduct after 4 hours. 1H NMR (500 MHz, C_6D_6) δ = 7.22-7.29 (m, 4H), 7.16-7.19 (m, 4H), 6.69 (d, 2H, $J=8.0$ Hz), 5.96 (s, 1H), 4.39 (sept, 2H, $J=7.0$ Hz), 3.87 (m, 2H), 3.59 (sept, 2H, $J=7.0$ Hz), 3.56 (m, 2H), 1.90 (s, 3H), 1.43 (d, 6H, $J=7.0$ Hz), 1.33 (d, 6H, $J=7.0$ Hz), 1.32 (d, 6H, $J=7.0$ Hz), 1.32 (d, 6H, $J=7.0$ Hz) $^{13}C\{^1H\}$ NMR (125 MHz, C_6D_6) δ = 152.0, 149.8, 139.4, 138.0, 132.1, 129.1, 128.0, 124.6, 124.5, 120.7, 89.4, 85.1, 73.0, 52.3, 28.5, 28.4, 25.7, 24.7, 24.0, 23.8, 20.6.

2b: C_6D_6 (0.7 mL) was added under argon to a J Young NMR tube containing free carbene NHC-7 (37.1 mg, 1.0 eq) and adamantyl isocyanide (10.9 mg, 1.05 eq). The tube was shaken for 10 minutes at room temperature. NMR of the resulting colorless solution showed quantitative formation of the corresponding ketenimine. Slow evaporation of C_6D_6 under argon gave colorless crystals. 1H NMR (500 MHz, C_6D_6) δ = 7.20 (t, 1H, $J=7.0$ Hz), 7.17 (dd, 4H, $J=7.0$ Hz), 7.11 (t, 1H, $J=7.0$ Hz), 3.83 (m, 4H), 3.73 (sept, 2H, $J=7.0$ Hz), 3.63 (sept, 2H, $J=7.0$ Hz), 1.86 (m, 4H), 1.61 (m, 2H), 1.58 (d, 6H, $J=7.0$ Hz), 1.52 (m, 2H), 1.43 (t, 8H, $J=7.0$ Hz), 1.38 (m, 1H), 1.33 (d, 6H, $J=7.0$ Hz), 1.32 (d, 6H, $J=7.0$ Hz), 1.21 (d, 6H, $J=7.0$ Hz)

$^{13}\text{C}\{^1\text{H}\}$ NMR (125 MHz, C_6D_6) $\delta = 216.9, 148.7, 146.1, 143.6, 126.9, 124.6, 124.2, 124.1, 59.3, 55.1, 42.4, 36.2, 30.6, 29.5, 28.4, 28.2, 25.3, 25.1, 24.0, 23.4$.

2c: C_6D_6 (0.7 mL) was added under argon to a J Young NMR tube containing free carbene NHC-8 (43 mg, 1.0 eq) and adamantyl isocyanide (16 mg, 1.05 eq). The tube was shaken for 10 minutes at room temperature. NMR of the resulting colorless solution showed quantitative formation of the corresponding ketenimine. Slow evaporation of C_6D_6 under argon gave off-white crystals. ^1H NMR (500 MHz, C_6D_6) $\delta = 7.20$ (t, 1H, $J=7.0\text{Hz}$), 7.17 (dd, 4H, $J=7.0\text{Hz}$), 7.11 (t, 1H, $J=7.0\text{Hz}$), 3.83 (m, 4H), 3.73 (sept, 2H, $J=7.0\text{Hz}$), 3.63 (sept, 2H, $J=7.0\text{Hz}$), 1.86 (m, 4H), 1.61 (m, 2H), 1.58 (d, 6H, $J=7.0\text{Hz}$), 1.52 (m, 2H), 1.43 (t, 8H, $J=7.0\text{Hz}$), 1.38 (m, 1H), 1.33 (d, 6H, $J=7.0\text{Hz}$), 1.32 (d, 6H, $J=7.0\text{Hz}$), 1.21 (d, 6H, $J=7.0\text{Hz}$) $^{13}\text{C}\{^1\text{H}\}$ NMR (125 MHz, C_6D_6) $\delta = 216.9, 148.7, 146.1, 143.6, 126.9, 124.6, 124.2, 124.1, 59.3, 55.1, 42.4, 36.2, 30.6, 29.5, 28.4, 28.2, 25.3, 25.1, 24.0, 23.4$.

3b: In a dry pressure Schlenk under argon, free NHC-7 (35 mg) was dissolved in anhydrous THF. The solution was degassed 3 times. NH_3 (1 bar) was added at -47°C . Then the solution was stirred overnight from -47°C to room temperature. The solvent was removed under vacuum and NHC-7(H)(NH_2) adduct was obtained as a yellowish solid – quantitative reaction. Slow diffusion of pentane into a saturated solution of NHC-7(H)(NH_2) adduct in C_6D_6 under argon gave colorless crystals. ^1H NMR (500 MHz, C_6D_6) $\delta = 7.18$ (t, 2H, $J=7.5\text{Hz}$), 7.10-7.12 (m, 4H), 5.25 (t, 1H, $J=6.0\text{Hz}$), 3.99 (sept, 2H, $J=6.5\text{Hz}$), 3.78 (sept, 2H, $J=6.5\text{Hz}$), 3.64 (m, 4H), 1.69 (m, 2H), 1.57 (m, 2H) 1.27 (d, 6H, $J=7.5\text{Hz}$), 1.26 (d, 6H, $J=7.5\text{Hz}$), 1.24 (d, 6H, $J=7.5\text{Hz}$), 1.23 (d, 6H, $J=7.5\text{Hz}$) $^{13}\text{C}\{^1\text{H}\}$ NMR (125 MHz, C_6D_6) $\delta = 149.9$ (C), 148.5 (C), 145.3 (C), 127.0 (CH), 125.0 (CH), 124.8 (CH), 85.8 (CH), 51.6 (CH_2), 30.6 (CH_2), 28.3 (CH), 28.0 (CH), 25.0 (CH_3), 24.6 (CH_3), 24.1 (CH_3), 24.0 (CH_3).

3c: In an argon-filled glovebox, C₆D₆ (0.7 mL) was added under argon to a J Young NMR tube containing free carbene ^{Mes}NHC-8 (35 mg, 1.0 eq) and brought out of the glovebox. On a Schlenk line, the solution was degassed 3 times at 0°C. NH₃ was added at -78°C. The solution was allowed to slowly warm to room temperature and the NMR tube was inverted multiple times for 1 minute. NMR of the resulting colorless solution showed formation of the corresponding NHC-8(H)(NH₂) adduct. ¹H NMR (500 MHz, C₆D₆) δ = 7.18 (t, 2H, J=7.5Hz), 7.10-7.12 (m, 4H), 5.25 (t, 1H, J=6.0Hz), 3.99 (sept, 2H, J=6.5Hz), 3.78 (sept, 2H, J=6.5Hz), 3.64 (m, 4H), 1.69 (m, 2H), 1.57 (m, 2H) 1.27 (d, 6H, J=7.5Hz), 1.26 (d, 6H, J=7.5Hz), 1.24 (d, 6H, J=7.5Hz), 1.23 (d, 6H, J=7.5Hz) ¹³C{¹H} NMR (125 MHz, C₆D₆) δ = 149.9 (C), 148.5 (C), 145.3 (C), 127.0 (CH), 125.0 (CH), 124.8 (CH), 85.8 (CH), 51.6 (CH₂), 30.6 (CH₂), 28.3 (CH), 28.0 (CH), 25.0 (CH₃), 24.6 (CH₃), 24.1 (CH₃), 24.0 (CH₃).

4a: C₆D₆ (1.0 mL) was added to a 20 mL scintillation vial equipped with a magnetic mini stir bar containing NHC-8 iminium bromide salt (51 mg, 1.0 eq), KHMDS (20 mg, 1 eq), and elemental selenium (15 mg, 2.0 eq). The reaction was stirred overnight at room temperature. Slow evaporation of C₆D₆ under argon gave off-white crystals. ¹H NMR (400 MHz, C₆D₆) δ = 7.08-7.15 (m, 2H), 7.03 (m, 4H), 3.51 (m, 4H), 3.14 (sept, 4H), 1.61 (m, 6H), 1.48 (d, 12H), 1.22 (d, 12H) ¹³C{¹H} NMR (100 MHz, C₆D₆) δ = 186.57, 147.49, 144.56, 127.77(?), 124.92, 55.55, 29.48, 26.13, 24.94, 24.71, 24.52 ⁷⁷Se NMR (76.27 MHz, C₆D₆) δ = 571.73 (76.27 MHz, CDCl₃) δ = 548.72

4b: C₆D₆ (1.0 mL) was added to a 20 mL scintillation vial equipped with a magnetic mini stir bar containing ^{Mes}NHC-8 iminium bromide salt (43 mg, 1.0 eq), KHMDS (20 mg, 1 eq), and elemental selenium (15 mg, 2.0 eq). The reaction was stirred overnight at room temperature. Slow evaporation of C₆D₆ under argon gave off-white crystals. ¹H NMR (400 MHz, C₆D₆) δ =

6.82 (s, 4H), 3.41-3.38 (m, 4H), 2.34 (s, 12H), 2.15 (s, 6H), 1.63 (m, 4H), 1.29 (m, 2H). $^{13}\text{C}\{^1\text{H}\}$ NMR (125 MHz, C_6D_6) δ = 183.9, 147.2, 136.0, 134.6, 130.2, 54.2, 26.2, 24.1, 21.1, 19.5. ^{77}Se NMR (76.27 MHz, C_6D_6) δ = 437.88

2.4.3 Crystallographic Data

Olex2 software³⁶ was used for the resolution, refinement, and generation of crystallographic information files of every structure. The structures were solved with the ShelXS9³⁷ structure solution program using Direct Methods and refined with the ShelXL9³⁶ refinement package using Least Squares minimization. During the final stages of the refinements, all the positional parameters and the anisotropic temperature factors of all the non-H atoms were refined. The H atoms were geometrically located and their coordinates were refined riding on their parent atoms.

Molecule 1c	
Empirical formula	$\text{C}_{38}\text{H}_{50}\text{N}_2$
Formula weight	534.80
Temperature/K	100.0
Crystal system	triclinic
Space group	P-1
a/Å	9.9626(2)
b/Å	12.7843(2)
c/Å	13.6552(2)
$\alpha/^\circ$	69.2430(10)
$\beta/^\circ$	75.6740(10)
$\gamma/^\circ$	87.5200(10)
Volume/Å ³	1573.84(5)
Z	2
$\rho_{\text{calc}}/\text{cm}^3$	1.129
μ/mm^{-1}	0.482
F(000)	584.0
Crystal size/mm ³	0.05 × 0.05 × 0.04
Radiation	$\text{CuK}\alpha$ ($\lambda = 1.54178$)
2 Θ range for data collection/ $^\circ$	7.146 to 136.57

Index ranges	-11 ≤ h ≤ 11, -15 ≤ k ≤ 15, -16 ≤ l ≤ 16
Reflections collected	17967
Independent reflections	5563 [R _{int} = 0.0422, R _{sigma} = 0.0425]
Data/restraints/parameters	5563/0/370
Goodness-of-fit on F ²	1.036
Final R indexes [I ≥ 2σ (I)]	R ₁ = 0.0397, wR ₂ = 0.0965
Final R indexes [all data]	R ₁ = 0.0486, wR ₂ = 0.1023
Largest diff. peak/hole / e Å ⁻³	0.22/-0.21

Molecule 1d

Empirical formula	C ₃₉ H ₅₂ N ₂
Formula weight	548.82
Temperature/K	273.15
Crystal system	triclinic
Space group	P-1
a/Å	10.2570(7)
b/Å	12.6644(7)
c/Å	13.8843(9)
α/°	68.028(2)
β/°	75.974(2)
γ/°	87.399(2)
Volume/Å ³	1620.63(18)
Z	2
ρ _{calc} /cm ³	1.125
μ/mm ⁻¹	0.064
F(000)	600.0
Crystal size/mm ³	0.025 × 0.012 × 0.01
Radiation	MoKα (λ = 0.71073)
2θ range for data collection/°	5.092 to 50.76
Index ranges	-10 ≤ h ≤ 12, -13 ≤ k ≤ 15, -15 ≤ l ≤ 16
Reflections collected	8944
Independent reflections	5511 [R _{int} = 0.0486, R _{sigma} = 0.1017]
Data/restraints/parameters	5511/0/380
Goodness-of-fit on F ²	1.035
Final R indexes [I ≥ 2σ (I)]	R ₁ = 0.0578, wR ₂ = 0.1202
Final R indexes [all data]	R ₁ = 0.1052, wR ₂ = 0.1406
Largest diff. peak/hole / e Å ⁻³	0.23/-0.22

Compound 2b

Empirical formula	C ₄₆ H ₆₃ N ₃
-------------------	--

Formula weight	657.99
Temperature/K	100.00
Crystal system	monoclinic
Space group	P2 ₁ /c
a/Å	20.277(3)
b/Å	10.5458(12)
c/Å	18.401(2)
α/°	90
β/°	92.839(6)
γ/°	90
Volume/Å ³	3930.0(8)
Z	4
ρ _{calc} /g/cm ³	1.112
μ/mm ⁻¹	0.478
F(000)	1440.0
Crystal size/mm ³	0.23 × 0.15 × 0.01
Radiation	CuKα (λ = 1.54178)
2Θ range for data collection/°	4.364 to 144.908
Index ranges	-24 ≤ h ≤ 24, -12 ≤ k ≤ 12, -22 ≤ l ≤ 22
Reflections collected	64029
Independent reflections	7157 [R _{int} = 0.1170, R _{sigma} = 0.0793]
Data/restraints/parameters	7157/0/450
Goodness-of-fit on F ²	1.089
Final R indexes [I >= 2σ (I)]	R ₁ = 0.0714, wR ₂ = 0.1465
Final R indexes [all data]	R ₁ = 0.0986, wR ₂ = 0.1601
Largest diff. peak/hole / e Å ⁻³	0.34/-0.34

Compound 2c

Empirical formula	C ₄₇ H ₆₅ N ₃
Formula weight	672.02
Temperature/K	273.15
Crystal system	monoclinic
Space group	P2 ₁ /c
a/Å	10.1396(4)
b/Å	20.3171(8)
c/Å	19.4251(7)
α/°	90
β/°	100.0250(10)
γ/°	90
Volume/Å ³	3940.6(3)
Z	4

$\rho_{\text{calc}}/\text{cm}^3$	1.133
μ/mm^{-1}	0.065
F(000)	1472.0
Crystal size/ mm^3	$0.024 \times 0.023 \times 0.01$
Radiation	MoK α ($\lambda = 0.71073$)
2Θ range for data collection/ $^\circ$	5.312 to 51.448
Index ranges	$-12 \leq h \leq 12, -24 \leq k \leq 24, -23 \leq l \leq 23$
Reflections collected	55840
Independent reflections	7503 [$R_{\text{int}} = 0.0799, R_{\text{sigma}} = 0.0446$]
Data/restraints/parameters	7503/2/480
Goodness-of-fit on F^2	1.026
Final R indexes [$I \geq 2\sigma(I)$]	$R_1 = 0.0441, wR_2 = 0.0961$
Final R indexes [all data]	$R_1 = 0.0665, wR_2 = 0.1063$
Largest diff. peak/hole / $e \text{ \AA}^{-3}$	0.21/-0.28
Compound 3b	
Empirical formula	C ₂₉ H ₄₅ N ₃
Formula weight	435.68
Temperature/K	100.15
Crystal system	monoclinic
Space group	P2 ₁ /c
a/ \AA	10.4427(9)
b/ \AA	24.913(2)
c/ \AA	11.5295(9)
$\alpha/^\circ$	90
$\beta/^\circ$	116.382(4)
$\gamma/^\circ$	90
Volume/ \AA^3	2687.2(4)
Z	4
$\rho_{\text{calc}}/\text{cm}^3$	1.077
μ/mm^{-1}	0.470
F(000)	960.0
Crystal size/ mm^3	$0.04 \times 0.021 \times 0.01$
Radiation	CuK α ($\lambda = 1.54178$)
2Θ range for data collection/ $^\circ$	9.268 to 138.388
Index ranges	$-12 \leq h \leq 12, -29 \leq k \leq 30, -13 \leq l \leq 13$
Reflections collected	25294
Independent reflections	4946 [$R_{\text{int}} = 0.0628, R_{\text{sigma}} = 0.0432$]
Data/restraints/parameters	4946/0/305
Goodness-of-fit on F^2	1.032
Final R indexes [$I \geq 2\sigma(I)$]	$R_1 = 0.0479, wR_2 = 0.1204$
Final R indexes [all data]	$R_1 = 0.0645, wR_2 = 0.1317$
Largest diff. peak/hole / $e \text{ \AA}^{-3}$	0.42/-0.22

Molecule 4a	
Empirical formula	C ₃₆ H ₅₀ N ₂ Se
Formula weight	589.74
Temperature/K	273.15
Crystal system	monoclinic
Space group	P2 ₁ /c
a/Å	15.9260(9)
b/Å	15.8347(8)
c/Å	14.3550(8)
α/°	90
β/°	116.049(2)
γ/°	90
Volume/Å ³	3252.4(3)
Z	4
ρ _{calc} /g/cm ³	1.204
μ/mm ⁻¹	1.180
F(000)	1256.0
Crystal size/mm ³	0.03 × 0.02 × 0.01
Radiation	MoKα (λ = 0.71073)
2θ range for data collection/°	5.676 to 50.758
Index ranges	-19 ≤ h ≤ 19, -19 ≤ k ≤ 19, -17 ≤ l ≤ 17
Reflections collected	70350
Independent reflections	5970 [R _{int} = 0.0917, R _{sigma} = 0.0401]
Data/restraints/parameters	5970/0/360
Goodness-of-fit on F ²	1.023
Final R indexes [I ≥ 2σ (I)]	R ₁ = 0.0320, wR ₂ = 0.0768
Final R indexes [all data]	R ₁ = 0.0425, wR ₂ = 0.0824
Largest diff. peak/hole / e Å ⁻³	0.42/-0.49

Molecule 4b	
Empirical formula	C ₂₄ H ₃₂ N ₂ Se
Formula weight	427.494
Temperature/K	100.00
Crystal system	monoclinic
Space group	C2/c
a/Å	19.8071(9)
b/Å	13.3759(7)
c/Å	17.5615(8)
α/°	90

$\beta/^\circ$	110.970(2)
$\gamma/^\circ$	90
Volume/ \AA^3	4344.5(4)
Z	8
$\rho_{\text{calc}}/\text{g}/\text{cm}^3$	1.307
μ/mm^{-1}	1.739
F(000)	1792.7
Crystal size/ mm^3	$0.1 \times 0.067 \times 0.055$
Radiation	Mo K α ($\lambda = 0.71073$)
2Θ range for data collection/ $^\circ$	3.76 to 52.88
Index ranges	$-24 \leq h \leq 24, -16 \leq k \leq 16, -21 \leq l \leq 21$
Reflections collected	44841
Independent reflections	4459 [$R_{\text{int}} = 0.0474, R_{\text{sigma}} = 0.0225$]
Data/restraints/parameters	4459/0/250
Goodness-of-fit on F^2	1.037
Final R indexes [$I \geq 2\sigma(I)$]	$R_1 = 0.0218, wR_2 = 0.0539$
Final R indexes [all data]	$R_1 = 0.0254, wR_2 = 0.0555$
Largest diff. peak/hole / $e \text{\AA}^{-3}$	0.34/-0.29

2.4.4 Computational Data

All calculations were performed with the Gaussian16 program package.³⁸ The theoretical approach is based on the framework of density functional theory (DFT). All calculations were performed with the B3LYP functional and employing Weigend and Ahlrich's def2-TZVPP basis set.³⁹ The singlet and triplet states of each carbene were fully optimized without constraints at the aforementioned level of theory. The Gibbs energy corrections from frequency calculations and dispersion corrections were added to the single-point energies to obtain the Gibbs free energies in solution. Gibbs free reaction energies and enthalpies were calculated for standard conditions ($P = 1 \text{ atm}, T = 298 \text{ K}$) and are unscaled and are given in the following Table 2.1. The $\%V_{\text{bur}}$ was calculated using the SambVca 2 program⁴⁰ and measured at a distance of 0 \AA from the carbene carbon. Cartesian coordinates for the optimized structures are given in the following Table 2.2.

Table 2.1. DFT Calculated Geometric and Thermodynamic Data of CAAC-5 and NHCs.

Carbene	ΔE_{S-T} (kcal/mol)	Singlet LUMO (eV) Singlet HOMO (eV)	ΔE_{H-L} (eV)	Carbene angle (°)
CAAC-5	45.72	-0.448 -5.290	4.842	107.3
NHC-5	73.08	-0.359 -5.805	5.446	106.3
NHC-6	59.89	-0.342 -5.322	4.980	116.0
NHC-7	50.02	-0.358 -5.103	4.745	118.7
NHC-8	49.29	-0.384 -5.110	4.726	122.1
NHC-9	44.13	-0.360 -5.033	4.673	123.2

Table 2.2. Cartesian coordinates for the optimized structures of CAAC-5 and NHCs.

Carbene	Coordinates								
CAAC-5 singlet	C	-1.33181	-0.07661	-1.04389	C	3.60801	0.19134	-0.01714	
	C	-2.78932	-0.17973	-0.62513	H	4.6885	0.2514	0.00031	
	C	-2.77351	-0.45341	0.90599	C	2.97987	-1.04264	-0.04801	
	H	-3.53022	0.12154	1.44005	H	3.58113	-1.94079	-0.08184	
	H	-2.97969	-1.50788	1.09509	C	1.58935	-1.1488	-0.06088	
	C	-1.3577	-0.10728	1.39875	C	0.67824	2.59354	-0.284	
	C	-3.48192	1.14972	-0.97893	H	-0.37121	2.39684	-0.08838	
	H	-3.39138	1.35431	-2.0455	C	1.11613	3.73555	0.64232	
	H	-3.04845	1.99363	-0.44094	H	1.06516	3.44832	1.69318	
	H	-4.54311	1.09923	-0.72493	H	0.46865	4.60231	0.49835	
	C	-3.46873	-1.31661	-1.40045	H	2.13733	4.05902	0.43625	
	H	-4.51296	-1.4183	-1.09431	C	0.77564	3.01604	-1.76094	
	H	-2.97073	-2.27107	-1.22188	H	1.80881	3.23099	-2.04044	
	H	-3.43897	-1.12106	-2.47214	H	0.18467	3.91718	-1.93791	
	C	-1.29707	1.24903	2.10908	H	0.40107	2.22679	-2.41196	
	H	-1.83488	1.17996	3.05576	C	0.95793	-2.52043	-0.2612	
	H	-1.75831	2.04109	1.52257	H	-0.10432	-2.43961	-0.04662	
	H	-0.27015	1.53552	2.33361	C	1.53471	-3.60418	0.65889	
	C	-0.7825	-1.16932	2.33561	H	0.98265	-4.53676	0.52895	
	H	0.25811	-0.96401	2.58707	H	1.47271	-3.31832	1.70942	
H	-0.84755	-2.16796	1.90969	H	2.58067	-3.81615	0.43342		
H	-1.354	-1.16886	3.2651	C	1.07372	-2.9342	-1.73928		
C	0.83265	0.03796	-0.01111	H	2.1192	-3.0342	-2.03715		
C	1.45256	1.30027	-0.06818	H	0.60329	-2.1931	-2.38484		
C	2.84729	1.3474	-0.05274	H	0.58311	-3.89576	-1.90462		
H	3.34537	2.30649	-0.09086	N	-0.61511	-0.05379	0.04614		
CAAC-5 triplet	C	-1.28246	0.57811	-1.01322	C	3.34246	-1.4734	-0.17851	
	C	-2.74397	0.69528	-0.69859	H	4.31692	-1.9429	-0.21987	
	C	-2.6613	0.58515	0.86494	C	2.19864	-2.25051	-0.08743	
	H	-3.32187	1.30427	1.34988	H	2.29275	-3.32823	-0.07212	
	H	-2.98401	-0.41251	1.1649	C	0.93223	-1.67166	-0.02312	

Table 2.2. Cartesian coordinates for the optimized structures of CAAC-5 and NHCs (Continued).

	C	-1.1796	0.7902	1.30321	C	1.91949	2.04146	-0.37464
	C	-3.3384	2.03947	-1.16005	H	0.88289	2.34083	-0.25223
	H	-3.28477	2.12421	-2.24625	C	2.76028	2.80556	0.65797
	H	-2.79864	2.88448	-0.735	H	2.48038	2.54273	1.67894
	H	-4.38856	2.11945	-0.86687	H	2.62422	3.88194	0.53707
	C	-3.59819	-0.44324	-1.28948	H	3.82535	2.59571	0.54542
	H	-4.63551	-0.36749	-0.95194	C	2.32799	2.43158	-1.80531
	H	-3.21386	-1.41962	-0.99616	H	3.36691	2.16713	-2.0112
	H	-3.59755	-0.39476	-2.37932	H	2.22251	3.50872	-1.94984
	C	-0.91082	2.26395	1.64922	H	1.70086	1.92866	-2.54164
	H	-1.56337	2.57892	2.46591	C	-0.28945	-2.57805	-0.01069
	H	-1.10033	2.91327	0.79591	H	-1.1541	-1.95757	0.21337
	H	0.11895	2.41143	1.972	C	-0.21652	-3.6784	1.05765
	C	-0.81616	-0.07431	2.50815	H	-1.1546	-4.23586	1.0879
	H	0.24176	0.01719	2.75605	H	-0.03589	-3.26569	2.05076
	H	-1.0393	-1.12498	2.33703	H	0.57898	-4.39508	0.84868
	H	-1.39099	0.25556	3.37502	C	-0.52097	-3.1902	-1.40284
	C	0.8299	-0.26165	-0.03277	H	0.31386	-3.83092	-1.69331
	C	1.98531	0.53363	-0.18726	H	-0.62839	-2.41318	-2.15953
	C	3.23	-0.09556	-0.2415	H	-1.42768	-3.79882	-1.40835
	H	4.12407	0.5042	-0.35107	N	-0.45453	0.36062	0.06308
NHC-5 singlet	N	-1.07505	-0.04006	0.51939	C	2.71339	3.838	0.47081
	N	1.07504	0.04001	0.5194	H	2.98552	3.55308	1.48827
	C	0.	0.	-0.28662	H	2.02235	4.68097	0.52857
	C	-0.75778	-0.10656	1.96866	H	3.61705	4.19256	-0.02721
	H	-1.04729	-1.07934	2.37413	C	-2.42856	-0.15966	0.06904
	H	-1.29704	0.66086	2.52391	C	-3.23884	0.98889	0.02416
	C	0.75775	0.10649	1.96868	C	-4.56072	0.84965	-0.39756
	H	1.04727	1.07927	2.37417	H	-5.1997	1.72163	-0.44722
	H	1.297	-0.66095	2.52391	C	-5.06776	-0.38564	-0.76738
	C	2.42854	0.15964	0.06903	H	-6.09504	-0.47366	-1.0969
	C	2.92921	1.42229	-0.29752	C	-4.25572	-1.50766	-0.71969
	C	4.25565	1.50767	-0.71977	H	-4.65961	-2.46581	-1.01845
	H	4.6595	2.46584	-1.01855	C	-2.92926	-1.4223	-0.2975
	C	5.06771	0.38567	-0.7675	C	-2.06151	-2.6714	-0.28531
	H	6.09497	0.4737	-1.09708	H	-1.13567	-2.42564	0.23261
	C	4.56071	-0.84963	-0.39765	C	-2.71344	-3.83807	0.47063
	H	5.19971	-1.72159	-0.4473	H	-2.98551	-3.55332	1.48816
	C	3.23884	-0.98889	0.02412	H	-2.02243	-4.68109	0.52823
	C	2.70793	-2.36922	0.38028	H	-3.61713	-4.19252	-0.0274
	H	1.68461	-2.24816	0.73223	C	-1.67679	-3.08212	-1.71585
	C	3.51271	-3.02994	1.50942	H	-1.15434	-2.27098	-2.22183
	H	3.54316	-2.40036	2.40004	H	-2.56219	-3.33724	-2.30168
	H	4.54333	-3.22469	1.20839	H	-1.02192	-3.95572	-1.70024
	H	3.06507	-3.98644	1.78591	C	-2.70789	2.36922	0.38025
	C	2.64778	-3.27614	-0.85909	H	-1.68459	2.24814	0.73227
	H	2.03648	-2.82724	-1.64169	C	-3.51268	3.03007	1.50931
	H	2.21667	-4.24588	-0.60232	H	-3.54315	2.40058	2.39999
	H	3.64358	-3.45277	-1.26966	H	-4.54329	3.22481	1.20824
	C	2.06147	2.6714	-0.28529	H	-3.06503	3.98659	1.78571

Table 2.2. Cartesian coordinates for the optimized structures of CAAC-5 and NHCs (Continued).

	H	1.13561	2.42563	0.23258	C	-2.64763	3.27604	-0.85918
	C	1.67683	3.08223	-1.7158	H	-2.03625	2.8271	-1.64169
	H	1.15442	2.27111	-2.22187	H	-2.21656	4.24582	-0.60245
	H	2.56226	3.33739	-2.30157	H	-3.6434	3.45262	-1.26986
	H	1.02195	3.95582	-1.70016				
NHC-5 triplet	N	-1.24902	0.32586	0.44966	C	2.36882	3.96653	0.07441
	N	1.0559	0.10195	0.493	H	2.46168	3.73609	1.13681
	C	-0.0714	0.44282	-0.2682	H	1.65346	4.78433	-0.03281
	C	-0.86321	0.23854	1.8744	H	3.33907	4.32891	-0.27019
	H	-1.08768	-0.7643	2.2473	C	-2.45349	-0.27243	-0.02484
	H	-1.39342	0.96384	2.49512	C	-3.6492	0.46734	0.11705
	C	0.65426	0.50473	1.86222	C	-4.84061	-0.09148	-0.34075
	H	0.86135	1.56733	2.03355	H	-5.76395	0.46302	-0.23329
	H	1.18862	-0.08057	2.60868	C	-4.86298	-1.33386	-0.95369
	C	2.40611	0.33443	0.07181	H	-5.79546	-1.74702	-1.31558
	C	2.82241	1.54703	-0.51958	C	-3.68135	-2.04501	-1.10055
	C	4.15633	1.66696	-0.9122	H	-3.70773	-3.01842	-1.57294
	H	4.48833	2.58694	-1.37542	C	-2.46648	-1.54819	-0.63254
	C	5.06965	0.64698	-0.70595	C	-1.21751	-2.40661	-0.77553
	H	6.10091	0.76936	-1.01077	H	-0.40094	-1.90446	-0.26281
	C	4.6544	-0.5295	-0.1039	C	-1.38655	-3.78244	-0.11122
	H	5.37055	-1.32506	0.05571	H	-1.66719	-3.6846	0.93849
	C	3.32916	-0.71354	0.28454	H	-0.45046	-4.34192	-0.16105
	C	2.92135	-2.03779	0.91423	H	-2.15366	-4.38164	-0.60404
	H	1.84857	-1.99018	1.09304	C	-0.80288	-2.55654	-2.24775
	C	3.61496	-2.26561	2.26653	H	-0.63107	-1.58338	-2.7083
	H	3.42408	-1.44351	2.95801	H	-1.57316	-3.07043	-2.82601
	H	4.69704	-2.35195	2.15096	H	0.11823	-3.1368	-2.32973
	H	3.2571	-3.18726	2.72977	C	-3.66598	1.86093	0.72886
	C	3.17156	-3.22103	-0.03306	H	-2.63266	2.13572	0.93452
	H	2.6581	-3.07895	-0.98442	C	-4.43923	1.89408	2.05664
	H	2.80891	-4.14899	0.41347	H	-4.03486	1.17769	2.77331
	H	4.23437	-3.35022	-0.245	H	-5.49277	1.64977	1.90776
	C	1.89997	2.74164	-0.72617	H	-4.38999	2.88793	2.50619
	H	0.91042	2.46668	-0.36147	C	-4.21799	2.90856	-0.25029
	C	1.73511	3.08531	-2.21422	H	-3.65391	2.90932	-1.18341
	H	1.35045	2.23184	-2.77331	H	-4.15315	3.90734	0.18613
	H	2.6827	3.38281	-2.66701	H	-5.26538	2.72214	-0.49359
	H	1.03391	3.91283	-2.33759				
NHC-6 singlet	N	-1.14132	0.00275	0.69449	C	3.16388	-3.58381	0.65625
	N	1.14075	-0.06178	0.69683	H	2.6151	-4.50447	0.864
	C	0.00038	-0.02801	-0.01769	H	3.46363	-3.14666	1.61003
	C	-1.24016	0.00432	2.16676	H	4.07319	-3.85859	0.11927
	H	-2.15705	-0.51095	2.45215	C	1.85463	-3.25071	-1.48747
	H	-1.32343	1.03351	2.53337	H	1.31474	-4.1825	-1.30759
	C	-0.02429	-0.68041	2.76905	H	2.71547	-3.48066	-2.11821
	H	-0.0198	-0.55992	3.85273	H	1.20092	-2.57674	-2.04003
	H	-0.06718	-1.75123	2.55991	C	1.24287	-0.09321	2.16937
	H	1.41576	0.91799	2.55307	C	-2.91372	1.34692	-0.35679
	H	2.11326	-0.69075	2.44118	C	-4.14993	1.40089	-1.00152

Table 2.2. Cartesian coordinates for the optimized structures of CAAC-5 and NHCs (Continued).

	C	-2.39678	0.08667	-0.01096	H	-4.56261	2.36133	-1.2815
	C	-3.10281	-1.09426	-0.30226	C	-2.16922	2.64221	-0.07157
	C	-4.33389	-0.98768	-0.94837	H	-1.23696	2.38486	0.42821
	H	-4.88862	-1.88516	-1.18937	C	-2.9608	3.56604	0.8672
	C	-4.85829	0.24733	-1.29464	H	-2.37888	4.45936	1.10264
	H	-5.81555	0.30997	-1.79595	H	-3.89708	3.89323	0.41176
	C	-2.55904	-2.4737	0.03789	H	-3.20775	3.0659	1.80492
	H	-1.61305	-2.33624	0.55857	C	-1.7947	3.36787	-1.3727
	C	-3.49632	-3.2527	0.97352	H	-1.2109	4.2644	-1.15582
	H	-3.04961	-4.21005	1.24905	H	-1.20181	2.72201	-2.01948
	H	-4.45555	-3.46236	0.49734	H	-2.68326	3.67684	-1.92613
	H	-3.69891	-2.69806	1.89108	C	3.04523	1.16585	-0.25982
	C	-2.25644	-3.28046	-1.23431	C	4.28273	1.14087	-0.9037
	H	-1.81296	-4.24502	-0.97914	H	4.79447	2.07181	-1.11011
	H	-1.56054	-2.74391	-1.87823	C	2.43761	2.50576	0.12738
	H	-3.16543	-3.47378	-1.80684	H	1.46616	2.31005	0.57844
	C	2.39931	-0.05682	-0.00847	C	3.29513	3.24533	1.16646
	C	2.97874	-1.27884	-0.39394	H	2.80986	4.17487	1.47077
	C	4.21434	-1.2506	-1.03979	H	3.45437	2.63842	2.05898
	H	4.67228	-2.17932	-1.35427	H	4.27653	3.50157	0.76346
	C	4.86638	-0.054	-1.29106	C	2.18873	3.38737	-1.10578
	H	5.82592	-0.05286	-1.79192	H	1.69365	4.31635	-0.81639
	C	2.29275	-2.61578	-0.15852	H	3.1236	3.65234	-1.60257
	H	1.38791	-2.42598	0.41593	H	1.55622	2.87492	-1.82974
NHC-6 triplet	N	-1.17568	0.04207	0.72877	C	2.43221	-3.63323	0.86459
	N	1.22376	-0.0189	0.7643	H	1.75068	-4.45338	1.09953
	C	0.0504	0.46073	0.21656	H	2.65482	-3.1031	1.79167
	C	-1.24185	0.27259	2.18857	H	3.36498	-4.06838	0.50038
	H	-2.13511	-0.22323	2.56863	C	1.4374	-3.46691	-1.45516
	H	-1.33208	1.34523	2.41051	H	0.7204	-4.25604	-1.22266
	C	0.0135	-0.29284	2.86148	H	2.30767	-3.94037	-1.91301
	H	0.00424	-0.02066	3.91918	H	0.98604	-2.80879	-2.1981
	H	-0.00511	-1.38259	2.79862	C	1.30395	0.22411	2.21226
	H	1.4308	1.29203	2.43679	C	-2.83143	1.47627	-0.45147
	H	2.17217	-0.30824	2.60114	C	-4.03111	1.55699	-1.16008
	C	-2.38926	0.20671	-0.02598	H	-4.38219	2.52327	-1.49813
	C	-3.14787	-0.94984	-0.3036	C	-2.06748	2.76133	-0.16324
	C	-4.34689	-0.81129	-1.00147	H	-1.16997	2.49805	0.39462
	H	-4.94195	-1.68916	-1.21708	C	-2.88908	3.73345	0.69773
	C	-4.78774	0.42947	-1.43163	H	-2.29501	4.61555	0.94482
	H	-5.71852	0.51743	-1.97714	H	-3.78591	4.07484	0.17764
	C	-2.70331	-2.33534	0.13968	H	-3.20634	3.2675	1.63177
	H	-1.7111	-2.22478	0.57456	C	-1.59306	3.43965	-1.45737
	C	-3.62995	-2.90767	1.2243	H	-1.00409	4.32934	-1.22628
	H	-3.26357	-3.87666	1.56937	H	-0.9702	2.76563	-2.04572
	H	-4.64374	-3.05159	0.84544	H	-2.4335	3.75066	-2.08062
	H	-3.69297	-2.24421	2.08798	C	3.25738	0.87615	-0.31074
	C	-2.58566	-3.30825	-1.04264	C	4.43352	0.62818	-1.01989
	H	-2.19409	-4.26972	-0.70478	H	5.10103	1.44922	-1.24719
	H	-1.9141	-2.91984	-1.80835	C	2.92892	2.30202	0.10824

Table 2.2. Cartesian coordinates for the optimized structures of CAAC-5 and NHCs (Continued).

	H	-3.55365	-3.49507	-1.51106	H	1.94375	2.29249	0.57123
	C	2.40977	-0.2108	-0.0195	C	3.93369	2.84061	1.13902
	C	2.7174	-1.51017	-0.47014	H	3.64994	3.84414	1.4621
	C	3.90184	-1.7044	-1.17888	H	3.98126	2.20209	2.02208
	H	4.16109	-2.69706	-1.523	H	4.93983	2.89947	0.71973
	C	4.75929	-0.64833	-1.44711	C	2.8331	3.24226	-1.10327
	H	5.67687	-0.81989	-1.99511	H	2.52922	4.24081	-0.78323
	C	1.80942	-2.69484	-0.18157	H	3.79047	3.33782	-1.61828
	H	0.88938	-2.29507	0.24181	H	2.09937	2.88033	-1.82357
NHC-7 singlet	C	0.01006	-0.02613	0.00511	H	1.54591	0.41759	2.71241
	N	-1.13238	0.18796	0.68423	H	2.30384	-1.06695	2.19123
	C	-1.23938	0.59777	2.10727	H	5.06687	1.62668	-0.87812
	C	-0.99814	-0.5216	3.11344	H	5.66871	-0.42678	-2.09012
	C	0.26075	-1.33145	2.78178	H	4.16036	-2.36767	-2.04551
	C	1.3734	-0.50291	2.14723	H	0.94527	-2.46283	-0.15265
	N	1.15088	-0.20429	0.69751	H	0.57189	-3.80192	-2.18274
	C	2.3644	-0.26308	-0.0914	H	2.05096	-3.16921	-2.90401
	C	3.21313	0.85747	-0.11888	H	0.69979	-2.0802	-2.56842
	C	4.40227	0.7732	-0.84394	H	1.82554	-4.75745	-0.18444
	C	4.74372	-0.38008	-1.53005	H	3.36337	-4.20442	-0.83989
	C	3.89153	-1.47242	-1.5001	H	2.88404	-3.72961	0.78668
	C	2.69652	-1.44292	-0.78201	H	1.88989	2.041	1.0456
	C	1.80056	-2.67182	-0.79083	H	2.4577	4.24118	0.13127
	C	1.24878	-2.94531	-2.19818	H	3.73498	3.54524	-0.86187
	C	2.51244	-3.90968	-0.22345	H	2.0527	3.12538	-1.17898
	C	2.87367	2.1591	0.59395	H	-5.06915	-1.34412	-1.15263
	C	2.77396	3.33511	-0.38968	H	-5.59145	0.85127	-2.12859
	C	-2.33361	0.36139	-0.10605	H	-4.02903	2.72822	-1.84076
	C	-3.21293	-0.72201	-0.27446	H	-0.82819	2.49813	0.06991
	C	-4.38283	-0.51988	-1.0083	H	-0.40216	4.04173	-1.79709
	C	-4.67921	0.71375	-1.56251	H	-1.90095	3.54853	-2.583
	C	-3.79753	1.76963	-1.39499	H	-0.59128	2.38116	-2.3764
	C	-2.61644	1.61941	-0.66949	H	-1.98588	-2.04988	0.83109
	C	-1.67467	2.8074	-0.53958	H	-2.4619	-4.10911	-0.42596
	C	-1.10943	3.2175	-1.90821	H	-1.93381	-2.82271	-1.51846
	C	-2.92468	-2.10697	0.28483	H	-3.63908	-3.26179	-1.42767
	C	-2.72782	-3.13444	-0.84061	H	3.57498	3.37973	2.25294
	C	3.87027	2.47299	1.721	H	4.8757	2.63293	1.32762
	C	-4.00825	-2.57177	1.26945	H	3.92621	1.65857	2.44454
	C	-2.34136	3.99978	0.16386	H	-3.74258	-3.53886	1.70122
	H	-0.52065	1.404	2.27432	H	-4.13838	-1.86021	2.0863
	H	-2.2277	1.02946	2.25217	H	-4.97527	-2.68614	0.77686
	H	-0.9022	-0.06486	4.10239	H	-1.62458	4.81283	0.29471
	H	-1.86345	-1.18424	3.1626	H	-3.18008	4.39049	-0.4148
	H	0.65124	-1.79406	3.69069	H	-2.72082	3.72228	1.1485
	H	0.01403	-2.15127	2.1057				
NHC-7 triplet	C	-0.14742	-0.71702	0.00954	H	1.99073	-1.70503	2.28107
	N	-1.1798	-0.03515	0.63779	H	1.58087	-2.91443	1.06974
	C	-1.05263	0.19244	2.07553	H	4.86334	1.72613	0.38133
	C	-0.80249	-1.08157	2.93024	H	5.45988	0.87472	-1.84711

Table 2.2. Cartesian coordinates for the optimized structures of CAAC-5 and NHCs (Continued).

	C	-0.10532	-2.27708	2.25457	H	4.06441	-0.84046	-2.92199
	C	1.22473	-1.99861	1.55892	H	1.01743	-2.33314	-1.36882
	N	1.08213	-0.89816	0.58473	H	0.60036	-2.3262	-3.79077
	C	2.27983	-0.42739	-0.06714	H	1.9505	-1.2212	-4.04974
	C	3.09321	0.5306	0.57128	H	0.53677	-0.68968	-3.13426
	C	4.23342	0.98388	-0.09173	H	2.07284	-4.08706	-2.71606
	C	4.57489	0.50491	-1.34564	H	3.50161	-3.09338	-2.9852
	C	3.78298	-0.45827	-1.94947	H	3.13052	-3.67313	-1.36348
	C	2.63612	-0.95158	-1.32814	H	1.84748	0.62543	2.28221
	C	1.8347	-2.04258	-2.02624	H	2.28633	2.95451	2.93552
	C	1.19479	-1.53635	-3.32757	H	3.47381	3.12884	1.64631
	C	2.68808	-3.29444	-2.28601	H	1.77609	2.88225	1.24667
	C	2.78102	1.07871	1.95575	H	-5.50818	-0.14559	-0.91123
	C	2.56644	2.5996	1.94176	H	-5.23419	1.97365	-2.127
	C	-2.27136	0.50156	-0.11497	H	-3.07674	3.15306	-2.07602
	C	-3.50177	-0.18636	-0.15215	H	-0.08643	1.91756	-0.20791
	C	-4.55648	0.369	-0.87707	H	0.75404	3.20516	-2.1191
	C	-4.4053	1.56043	-1.56676	H	-0.8618	3.30086	-2.81656
	C	-3.18642	2.22033	-1.53794	H	-0.0517	1.73972	-2.68077
	C	-2.10591	1.71357	-0.81756	H	-2.75814	-1.78763	1.00982
	C	-0.80451	2.49961	-0.78188	H	-4.15533	-3.59076	0.10128
	C	-0.20946	2.69648	-2.18356	H	-3.32558	-2.73668	-1.20425
	C	-3.70891	-1.51404	0.55876	H	-5.03986	-2.44805	-0.90673
	C	-4.07953	-2.63605	-0.4233	H	3.58764	1.03542	3.97533
	C	3.86494	0.69431	2.9759	H	4.82527	1.14838	2.7257
	C	-4.74821	-1.4065	1.68545	H	4.01289	-0.38568	3.01537
	C	-0.98639	3.84992	-0.06984	H	-4.83867	-2.35648	2.21625
	H	-0.24135	0.90563	2.25767	H	-4.47343	-0.6388	2.41036
	H	-1.96941	0.677	2.40945	H	-5.73477	-1.15092	1.29442
	H	-0.22959	-0.77381	3.80986	H	-0.03373	4.37935	-0.00429
	H	-1.75911	-1.44715	3.30901	H	-1.68569	4.49309	-0.60717
	H	0.06987	-3.0453	3.0125	H	-1.37022	3.71709	0.9426
	H	-0.78323	-2.719	1.52405				
NHC-8 singlet	C	0.00018	0.03429	0.02125	C	2.09223	4.20491	0.44565
	C	-1.5121	-0.25007	2.12847	C	3.11319	-1.91905	-0.1106
	H	-2.5948	-0.14171	2.20112	N	1.16304	0.19414	0.7017
	H	-1.09111	0.59981	2.66468	H	2.78726	4.71985	-0.22587
	C	-1.11856	-1.5687	2.80822	H	2.64449	3.93783	1.35267
	H	-1.34378	-1.45853	3.87838	H	1.31403	4.92479	0.72197
	H	-1.77041	-2.36928	2.43768	C	-2.18617	-3.97782	-0.63438
	C	0.33901	-2.00116	2.62544	H	-2.70368	-3.95617	0.33065
	H	0.51104	-2.90037	3.2297	H	-1.41653	-4.75619	-0.58901
	H	0.48839	-2.30917	1.58554	H	-2.91406	-4.28548	-1.3926
	C	-2.34042	-0.2854	-0.19314	C	-0.81805	-2.64771	-2.32033
	C	-3.27801	0.77302	-0.24479	H	-0.78972	-2.41805	-0.20264
	C	-4.43187	0.60952	-1.02047	H	-1.521	-2.80753	-3.14566
	H	-5.16016	1.41419	-1.06535	H	-0.08136	-3.45843	-2.34635
	C	-4.65621	-0.55544	-1.74532	H	-0.3016	-1.69799	-2.48348
	H	-5.55585	-0.66335	-2.34454	C	3.00599	-2.81571	-1.35883
	C	-3.71345	-1.57585	-1.70589	H	2.82909	-3.85745	-1.06791

Table 2.2. Cartesian coordinates for the optimized structures of CAAC-5 and NHCs (Continued).

	H	-3.88226	-2.47834	-2.2858	H	3.92675	-2.79096	-1.95166
	C	-2.55025	-1.47042	-0.93195	H	2.18364	-2.49499	-2.00288
	C	-3.07119	2.10063	0.48292	C	4.26203	-2.39403	0.79999
	C	-1.54627	-2.61688	-0.96327	H	2.17891	-2.02549	0.44258
	N	-1.17634	-0.15285	0.67133	H	4.35177	-1.77309	1.69714
	C	1.4231	0.34095	2.16809	H	5.22512	-2.35613	0.27951
	H	2.41195	0.79575	2.25926	H	4.09947	-3.4301	1.11754
	H	0.72629	1.0727	2.57973	C	-4.12475	2.3331	1.58425
	C	1.40963	-0.96562	2.99308	H	-5.13223	2.39663	1.15914
	H	1.31393	-0.68757	4.05188	H	-3.92836	3.27272	2.11252
	H	2.38759	-1.44912	2.8963	H	-4.13155	1.52646	2.32389
	C	2.31058	0.53429	-0.13173	C	-3.06259	3.28553	-0.5028
	C	2.48327	1.87943	-0.53133	H	-2.08634	2.07364	0.95723
	C	3.61106	2.21442	-1.28929	H	-2.32483	3.13522	-1.29448
	H	3.7482	3.24221	-1.61221	H	-2.81956	4.21659	0.02164
	C	4.55688	1.25698	-1.64033	H	-4.04046	3.42153	-0.97676
	H	5.4284	1.53671	-2.22543	C	0.68179	3.34354	-1.49086
	C	4.37335	-0.06139	-1.24289	H	0.73604	2.55502	0.49072
	H	5.10743	-0.81043	-1.52567	H	0.17681	2.46141	-1.8945
	C	3.25735	-0.4496	-0.4886	H	1.35264	3.73851	-2.26185
	C	1.46073	2.9666	-0.21612	H	-0.06928	4.111	-1.2745
NHC-8 triplet	C	-0.04524	0.51846	0.4461	C	3.08563	3.5668	0.90112
	C	-1.67035	0.05794	2.18989	C	2.52446	-2.31212	-0.35897
	H	-2.75779	0.17586	2.22291	N	1.24051	0.06823	0.77104
	H	-1.23546	0.98813	2.57794	H	3.97288	3.89539	0.34853
	C	-1.27332	-1.12699	3.09311	H	3.42623	2.93206	1.72513
	H	-1.36988	-0.79336	4.13616	H	2.61395	4.45666	1.3328
	H	-2.01285	-1.92647	2.96197	C	-2.82131	-3.52847	0.22517
	C	0.10934	-1.75741	2.86451	H	-3.11495	-3.06709	1.17301
	H	0.17348	-2.63821	3.5159	H	-2.27611	-4.45192	0.45072
	H	0.1466	-2.13745	1.83958	H	-3.73928	-3.80335	-0.30659
	C	-2.32058	-0.06093	-0.22109	C	-1.51097	-3.26412	-1.92418
	C	-3.01486	1.1445	-0.49031	H	-1.05702	-2.33795	-0.04489
	C	-4.08091	1.11242	-1.39814	H	-2.36603	-3.60119	-2.52009
	H	-4.62654	2.02787	-1.60822	H	-0.90298	-4.14681	-1.70011
	C	-4.45374	-0.06481	-2.03713	H	-0.91595	-2.5905	-2.54775
	H	-5.28582	-0.06793	-2.73563	C	2.25265	-3.21378	-1.57645
	C	-3.75073	-1.2365	-1.78057	H	1.87113	-4.18742	-1.24989
	H	-4.04274	-2.15365	-2.28344	H	3.16236	-3.40069	-2.1573
	C	-2.67752	-1.25921	-0.8809	H	1.51398	-2.76742	-2.24733
	C	-2.65819	2.47533	0.16936	C	3.59243	-2.94972	0.55202
	C	-1.9547	-2.57537	-0.62111	H	1.59728	-2.23361	0.21369
	N	-1.2601	-0.0952	0.76903	H	3.78194	-2.3378	1.4392
	C	1.62133	0.29387	2.19171	H	4.5447	-3.06379	0.02185
	H	2.68498	0.55079	2.22497	H	3.27456	-3.944	0.88562
	H	1.07054	1.16897	2.56057	C	-3.77001	2.95742	1.1223
	C	1.37305	-0.91802	3.11566	H	-4.70363	3.14502	0.58056
	H	1.38456	-0.55232	4.15219	H	-3.47702	3.89244	1.61265
	H	2.22687	-1.60043	3.02783	H	-3.9841	2.22043	1.90237
	C	2.29173	0.2483	-0.21453	C	-2.33988	3.55977	-0.87759

Table 2.2. Cartesian coordinates for the optimized structures of CAAC-5 and NHCs (Continued).

	C	2.71516	1.54797	-0.58836	H	-1.74605	2.3279	0.7533
	C	3.7675	1.67008	-1.50459	H	-1.5497	3.23052	-1.5575
	H	4.10365	2.66076	-1.79664	H	-2.00352	4.47811	-0.3838
	C	4.39423	0.55218	-2.04342	H	-3.21783	3.81416	-1.48111
	H	5.21044	0.67033	-2.75063	C	1.58194	3.75573	-1.1297
	C	3.97036	-0.71742	-1.66895	H	1.22585	2.53659	0.57848
	H	4.46524	-1.58908	-2.08689	H	0.88264	3.23315	-1.78837
	C	2.92072	-0.8959	-0.75869	H	2.39813	4.14426	-1.74834
	C	2.09653	2.8226	-0.01782	H	1.06202	4.61609	-0.69461
NHC-9 singlet	N	1.17354	-0.20428	0.59429	H	-2.25966	-1.91471	0.33100
	C	1.46247	-0.48508	2.02442	C	-1.31458	3.03904	-0.24821
	C	1.23499	-1.94610	2.43796	C	-0.64655	3.65480	-1.48697
	H	0.89654	0.20218	2.63922	H	-0.17055	2.88366	-2.09202
	H	2.50989	-0.24923	2.19362	H	0.11455	4.37810	-1.18914
	C	-0.14487	-2.52947	2.12533	H	-1.37013	4.17838	-2.11375
	H	1.44503	-2.02371	3.51030	C	-1.92963	4.13065	0.64252
	H	1.99015	-2.55797	1.93944	H	-1.16469	4.84480	0.95421
	C	-1.31144	-2.00719	2.97394	H	-2.38310	3.70762	1.54000
	H	-0.35518	-2.36874	1.06978	H	-2.70494	4.68711	0.11294
	H	-0.09679	-3.61382	2.25270	H	-0.52774	2.55068	0.32288
	C	-1.35823	-0.49967	3.24399	C	2.54182	-1.32231	-1.16352
	H	-1.26972	-2.48926	3.95549	C	3.30187	0.77395	-0.15373
	H	-2.24972	-2.33666	2.52448	C	4.46057	0.69806	-0.92487
	C	-1.50076	0.52511	2.08447	C	4.67578	-0.35407	-1.79888
	H	-0.49341	-0.24059	3.85350	C	3.71580	-1.34334	-1.91867
	H	-2.21653	-0.31493	3.89495	H	5.20072	1.48393	-0.84973
	C	0.00917	0.05898	-0.01893	H	5.58091	-0.39642	-2.39072
	N	-1.15541	0.22616	0.64459	H	3.87870	-2.15480	-2.61558
	H	-0.96721	1.43477	2.37219	C	1.52945	-2.43551	-1.38296
	H	-2.54883	0.80516	2.03475	C	2.11984	-3.82574	-1.10240
	C	2.34626	-0.25794	-0.26373	H	1.34771	-4.59109	-1.20234
	C	-2.24371	0.63458	-0.24280	H	2.53093	-3.89106	-0.09390
	C	-3.20672	-0.30226	-0.65669	H	2.92047	-4.07512	-1.80075
	C	-4.26065	0.13415	-1.46145	C	0.93583	-2.36328	-2.79824
	C	-4.37278	1.45729	-1.84965	H	0.70748	-2.27821	-0.69183
	C	-3.41248	2.36803	-1.44113	H	0.18666	-3.14525	-2.93742
	C	-2.33839	1.98288	-0.64016	H	0.45988	-1.39728	-2.96276
	H	-5.00444	-0.57924	-1.79167	H	1.70431	-2.50180	-3.56108
	H	-5.19914	1.77665	-2.47135	C	3.10732	1.99648	0.73642
	H	-3.49653	3.40050	-1.75412	C	3.05800	3.28771	-0.09628
	C	-3.14169	-1.77452	-0.28613	H	2.29338	3.22782	-0.86921
	C	-4.36349	-2.21643	0.53438	H	4.01327	3.48273	-0.58602
	H	-4.26241	-3.25961	0.84112	H	2.83339	4.14422	0.54282
	H	-5.28475	-2.13195	-0.04446	C	4.18520	2.10558	1.82703
	H	-4.48425	-1.60961	1.43301	H	5.17513	2.25038	1.39140
	C	-2.96897	-2.66252	-1.52796	H	4.22925	1.21011	2.44815
	H	-3.83608	-2.60012	-2.18779	H	3.98388	2.95783	2.47907
	H	-2.85053	-3.70811	-1.23575	H	2.14196	1.90440	1.23072
	H	-2.09145	-2.36588	-2.10100				

Table 2.2. Cartesian coordinates for the optimized structures of CAAC-5 and NHCs (Continued).

NHC-9 triplet	N	1.09677	-0.95886	0.30405	H	-2.86515	-1.56769	0.30271
	C	1.53078	-2.17287	1.03902	C	-0.46432	2.88101	1.06031
	C	0.64018	-3.40709	0.87281	C	0.60495	3.57942	0.20816
	H	1.64080	-1.93356	2.09895	H	1.08317	2.87846	-0.47569
	H	2.52521	-2.42686	0.67347	H	1.37788	4.01044	0.84705
	C	-0.85792	-3.25405	1.14778	H	0.18169	4.39268	-0.38379
	H	1.05699	-4.18549	1.52231	C	-1.06708	3.85420	2.08768
	H	0.75027	-3.77488	-0.15097	H	-0.28442	4.24889	2.73874
	C	-1.30975	-2.90601	2.57645	H	-1.81102	3.36060	2.71459
	H	-1.25617	-2.52717	0.44545	H	-1.55395	4.70231	1.60267
	H	-1.32614	-4.20878	0.89073	H	0.03905	2.08923	1.61202
	C	-1.04282	-1.49743	3.13504	C	1.84606	-0.40503	-1.96775
	H	-0.86219	-3.62726	3.26858	C	3.26176	0.21341	-0.06553
	H	-2.38886	-3.08388	2.62913	C	4.19572	0.72618	-0.96531
	C	-1.68026	-0.31464	2.40666	C	3.97961	0.68413	-2.33327
	H	0.02691	-1.31119	3.22966	C	2.81112	0.12672	-2.82394
	H	-1.43422	-1.47217	4.15644	H	5.10713	1.17150	-0.58813
	C	0.25605	-0.05893	0.94964	H	4.71823	1.08829	-3.01349
	N	-1.12857	-0.06335	1.05507	H	2.64581	0.09865	-3.89300
	H	-1.56116	0.58219	3.02842	C	0.58992	-1.02109	-2.56313
	H	-2.75390	-0.47521	2.29484	C	0.91247	-2.30559	-3.34302
	C	2.08296	-0.36894	-0.58016	H	-0.00365	-2.76680	-3.71766
	C	-1.89537	0.87423	0.25088	H	1.42481	-3.03441	-2.71334
	C	-3.01891	0.40175	-0.46474	H	1.55547	-2.10006	-4.20106
	C	-3.72645	1.29155	-1.27160	C	-0.17839	-0.02347	-3.44192
	C	-3.36185	2.62270	-1.37228	H	-0.05573	-1.29556	-1.73116
	C	-2.29288	3.08803	-0.62730	H	-1.09801	-0.47618	-3.81645
	C	-1.55397	2.24550	0.20481	H	-0.44995	0.87054	-2.88072
	H	-4.57899	0.93216	-1.83304	H	0.40921	0.28735	-4.30761
	H	-3.91703	3.29585	-2.01254	C	3.56183	0.30308	1.42626
	H	-2.03255	4.13696	-0.67811	C	3.80112	1.75033	1.88304
	C	-3.52094	-1.03245	-0.37521	H	2.95286	2.38610	1.63472
	C	-4.93973	-1.09817	0.21467	H	4.69020	2.18045	1.41918
	H	-5.24887	-2.13696	0.34670	H	3.94585	1.78362	2.96472
	H	-5.66871	-0.61714	-0.43949	C	4.75460	-0.58356	1.82180
	H	-4.99341	-0.60316	1.18532	H	5.67326	-0.24676	1.33794
	C	-3.46471	-1.75976	-1.72637	H	4.59684	-1.62471	1.53956
	H	-4.11156	-1.28371	-2.46516	H	4.91587	-0.54757	2.90107
	H	-3.79463	-2.79456	-1.61515	H	2.68508	-0.04843	1.96519
	H	-2.45223	-1.76966	-2.12842				

2.5 Acknowledgements

Chapter 2 is adapted, in part from François L. Vermersch, Victor T. Wang, Rodolphe Jazzar, and Guy Bertrand “Ambiphilicity of Ring Expanded N-Heterocyclic Carbenes”.

Permission to use images and data was obtained from François L. Vermersch, Rodolphe Jazzar, and Guy Bertrand. The dissertation author was the co-first author of the manuscript.

2.6 References

- (1) Power, P. P. Main-Group Elements as Transition Metals. *Nature* **2010**, *463* (7278), 171–177. <https://doi.org/10.1038/nature08634>.
- (2) Chu, T.; Nikonov, G. I. Oxidative Addition and Reductive Elimination at Main-Group Element Centers. *Chem. Rev.* **2018**, *118* (7), 3608–3680. <https://doi.org/10.1021/acs.chemrev.7b00572>.
- (3) Martin, D.; Soleilhavoup, M.; Bertrand, G. Stable Singlet Carbenes as Mimics for Transition Metal Centers. *Chem. Sci.* **2011**, *2* (3), 389–399. <https://doi.org/10.1039/C0SC00388C>.
- (4) Frey, G. D.; Lavallo, V.; Donnadiou, B.; Schoeller, W. W.; Bertrand, G. Facile Splitting of Hydrogen and Ammonia by Nucleophilic Activation at a Single Carbon Center. *Science* **2007**, *316* (5823), 439–441. <https://doi.org/10.1126/science.1141474>.
- (5) Hudnall, T. W.; Moerdyk, J. P.; Bielawski, C. W. Ammonia N–H Activation by a N,N'-Diamidocarbene. *Chem. Commun.* **2010**, *46* (24), 4288. <https://doi.org/10.1039/c0cc00638f>.
- (6) Moerdyk, J. P.; Bielawski, C. W. Reductive Generation of Stable, Five-Membered N,N'-Diamidocarbenes. *Chem. Commun.* **2014**, *50* (35), 4551–4553. <https://doi.org/10.1039/c4cc00846d>.
- (7) Lavallo, V.; Canac, Y.; Präsang, C.; Donnadiou, B.; Bertrand, G. Stable Cyclic (Alkyl)(Amino)Carbenes as Rigid or Flexible, Bulky, Electron-Rich Ligands for Transition-Metal Catalysts: A Quaternary Carbon Atom Makes the Difference. *Angew. Chem. - Int. Ed.* **2005**, *44* (35), 5705–5709. <https://doi.org/10.1002/anie.200501841>.
- (8) Lavallo, V.; Canac, Y.; Donnadiou, B.; Schoeller, W. W.; Bertrand, G. CO Fixation to Stable Acyclic and Cyclic Alkyl Amino Carbenes: Stable Amino Ketenes with a Small HOMO-LUMO Gap. *Angew. Chem. - Int. Ed.* **2006**, *45* (21), 3488–3491. <https://doi.org/10.1002/anie.200600987>.
- (9) Frey, G. D.; Lavallo, V.; Donnadiou, B.; Schoeller, W. W.; Bertrand, G. Facile Splitting of Hydrogen at a Single Carbon Center. *Science* **2007**, *316* (April), 439–441.
- (10) Masuda, J. D.; Schoeller, W. W.; Donnadiou, B.; Bertrand, G. Carbene Activation of P4 and Subsequent Derivatization. *Angew. Chem. Int. Ed.* **2007**, *46* (37), 7052–7055. <https://doi.org/10.1002/anie.200703055>.
- (11) Frey, G. D.; Masuda, J. D.; Donnadiou, B.; Bertrand, G. Activation of Si–H, B–H, and P–H Bonds at a Single Nonmetal Center. *Angew. Chem. Int. Ed.* **2010**, *49* (49), 9444–9447. <https://doi.org/10.1002/anie.201005698>.
- (12) Zhukhovitskiy, A. V.; Mavros, M. G.; Queeney, K. T.; Wu, T.; Van Voorhis, T.; Johnson, J. A. Reactions of Persistent Carbenes with Hydrogen-Terminated Silicon Surfaces. *J. Am. Chem. Soc.* **2016**, *138* (27), 8639–8652. <https://doi.org/10.1021/jacs.6b04962>.
- (13) Würtemberger-Pietsch, S.; Schneider, H.; Marder, T. B.; Radius, U. Adduct Formation, B–H Activation and Ring Expansion at Room Temperature from Reactions of HBcat with

- NHCs. *Chem. – Eur. J.* **2016**, *22* (37), 13032–13036.
<https://doi.org/10.1002/chem.201603328>.
- (14) Peltier, J. L.; Tomás-Mendivil, E.; Tolentino, D. R.; Hansmann, M. M.; Jazzar, R.; Bertrand, G. Realizing Metal-Free Carbene-Catalyzed Carbonylation Reactions with CO. *J. Am. Chem. Soc.* **2020**, *142* (43), 18336–18340. <https://doi.org/10.1021/jacs.0c09938>.
- (15) Tolentino, D. R.; Neale, S. E.; Isaac, C. J.; Macgregor, S. A.; Whittlesey, M. K.; Jazzar, R.; Bertrand, G. Reductive Elimination at Carbon under Steric Control. *J. Am. Chem. Soc.* **2019**, *141* (25), 9823–9826. <https://doi.org/10.1021/jacs.9b04957>.
- (16) Arduengo, A. J.; Harlow, R. L.; Kline, M. A Stable Crystalline Carbene. *J. Am. Chem. Soc.* **1991**, *113* (1), 361–363. <https://doi.org/10.1021/ja00001a054>.
- (17) Iglesias, M.; Beetstra, D. J.; Knight, J. C.; Ooi, L.-L.; Stasch, A.; Coles, S.; Male, L.; Hursthouse, M. B.; Cavell, K. J.; Dervisi, A.; Fallis, I. A. Novel Expanded Ring N-Heterocyclic Carbenes: Free Carbenes, Silver Complexes, And Structures. *Organometallics* **2008**, *27* (13), 3279–3289. <https://doi.org/10.1021/om800179t>.
- (18) Kolychev, E. L.; Portnyagin, I. A.; Shuntikov, V. V.; Khrustalev, V. N.; Nechaev, M. S. Six- and Seven-Membered Ring Carbenes: Rational Synthesis of Amidinium Salts, Generation of Carbenes, Synthesis of Ag(I) and Cu(I) Complexes. *J. Organomet. Chem.* **2009**, *694* (15), 2454–2462. <https://doi.org/10.1016/j.jorganchem.2009.03.014>.
- (19) Lu, W. Y.; Cavell, K. J.; Wixey, J. S.; Kariuki, B. First Examples of Structurally Imposing Eight-Membered-Ring (Diazocanylidene) N-Heterocyclic Carbenes: Salts, Free Carbenes, and Metal Complexes. *Organometallics* **2011**, *30* (21), 5649–5655.
<https://doi.org/10.1021/om200467x>.
- (20) Page, M. J.; Lu, W. Y.; Poulten, R. C.; Carter, E.; Algarra, A. G.; Kariuki, B. M.; Macgregor, S. A.; Mahon, M. F.; Cavell, K. J.; Murphy, D. M.; Whittlesey, M. K. Three-Coordinate Nickel(I) Complexes Stabilised by Six-, Seven- and Eight-Membered Ring N-Heterocyclic Carbenes: Synthesis, EPR/DFT Studies and Catalytic Activity. *Chem. – Eur. J.* **2013**, *19* (6), 2158–2167. <https://doi.org/10.1002/chem.201202950>.
- (21) Cervantes-Reyes, A.; Rominger, F.; Rudolph, M.; Hashmi, A. S. K. Gold(I) Complexes with Eight-Membered NHC Ligands: Synthesis, Structures and Catalytic Activity. *Adv. Synth. Catal.* **2020**, *362* (12), 2523–2533. <https://doi.org/10.1002/adsc.202000281>.
- (22) Hall, J. W.; Bouchet, D.; Mahon, M. F.; Whittlesey, M. K.; Cazin, C. S. J. Synthetic Access to Ring-Expanded N-Heterocyclic Carbene (RE-NHC) Copper Complexes and Their Performance in Click Chemistry. *Organometallics* **2021**, *40* (9), 1252–1261.
<https://doi.org/10.1021/acs.organomet.1c00039>.
- (23) Falivene, L.; Cao, Z.; Petta, A.; Serra, L.; Poater, A.; Oliva, R.; Scarano, V.; Cavallo, L. Towards the Online Computer-Aided Design of Catalytic Pockets. *Nat. Chem.* **2019**, *11* (10), 872–879. <https://doi.org/10.1038/s41557-019-0319-5>.
- (24) Turner, Z. R. Chemically Non-Innocent Cyclic (Alkyl)(Amino)Carbenes: Ligand Rearrangement, C–H and C–F Bond Activation. *Chem. - Eur. J.* **2016**, *22* (32), 11461–11468. <https://doi.org/10.1002/chem.201602264>.
- (25) Arduengo III, A. J.; Calabrese, J. C.; Davidson, F.; Rasika Dias, H. V.; Goerlich, J. R.; Krafczyk, R.; Marshall, W. J.; Tamm, M.; Schmutzler, R. C–H Insertion Reactions of Nucleophilic Carbenes. *Helv. Chim. Acta* **1999**, *82* (12), 2348–2364.
[https://doi.org/10.1002/\(SICI\)1522-2675\(19991215\)82:12<2348::AID-HLCA2348>3.0.CO;2-M](https://doi.org/10.1002/(SICI)1522-2675(19991215)82:12<2348::AID-HLCA2348>3.0.CO;2-M).

- (26) Goedecke, C.; Leibold, M.; Siemeling, U.; Frenking, G. When Does Carbonylation of Carbenes Yield Ketenes? A Theoretical Study with Implications for Synthesis. *J. Am. Chem. Soc.* **2011**, *133* (10), 3557–3569. <https://doi.org/10.1021/ja109812r>.
- (27) Martin, D.; Lassauque, N.; Donnadiou, B.; Bertrand, G. A Cyclic Diaminocarbene with a Pyramidalized Nitrogen Atom: A Stable N-Heterocyclic Carbene with Enhanced Electrophilicity. *Angew. Chem. Int. Ed.* **2012**, *51* (25), 6172–6175. <https://doi.org/10.1002/anie.201202137>.
- (28) Braun, M.; Frank, W.; Reiss, G. J.; Ganter, C. An N-Heterocyclic Carbene Ligand with an Oxalamide Backbone. *Organometallics* **2010**, *29* (20), 4418–4420. <https://doi.org/10.1021/om100728n>.
- (29) Hudnall, T. W.; Bielawski, C. W. An N, N' -Diamidocarbene : Studies in C - H Insertion , Reversible Carbonylation , and Transition-Metal Coordination Chemistry. **2009**, *373* (2), 16039–16041.
- (30) César, V.; Labat, S.; Miqueu, K.; Sotiropoulos, J.-M.; Brousses, R.; Lugan, N.; Lavigne, G. The Ambivalent Chemistry of a Free Anionic N-Heterocyclic Carbene Decorated with a Malonate Backbone: The Plus of a Negative Charge. *Chem. – Eur. J.* **2013**, *19* (50), 17113–17124. <https://doi.org/10.1002/chem.201303184>.
- (31) Kim, Y.; Liu, L. L.; Stephan, D. W. N-Heterocyclic Carbene Derived 3-Azabutadiene as a π -Base in Classic and Frustrated Lewis Pair Chemistry. *Chem. – Eur. J.* **2019**, *25* (29), 7110–7113. <https://doi.org/10.1002/chem.201901609>.
- (32) Herrmann, W. A.; Gooßen, L. J.; Spiegler, M. Functionalized Imidazoline-2-Ylidene Complexes of Rhodium and Palladium. *J. Organomet. Chem.* **1997**, *547* (2), 357–366. [https://doi.org/10.1016/S0022-328X\(97\)00434-8](https://doi.org/10.1016/S0022-328X(97)00434-8).
- (33) Junor, G. P.; Lorkowski, J.; Weinstein, C. M.; Jazsar, R.; Pietraszuk, C.; Bertrand, G. The Influence of C(Sp³)H–Selenium Interactions on the ⁷⁷Se NMR Quantification of the π -Accepting Properties of Carbenes. *Angew. Chem.* **2020**, *132* (49), 22212–22217. <https://doi.org/10.1002/ange.202010744>.
- (34) Arduengo, A. J.; Krafczyk, R.; Schmutzler, R.; Craig, H. A.; Goerlich, J. R.; Marshall, W. J.; Unverzagt, M. Imidazolylidenes, Imidazolynylidenes and Imidazolidines. *Tetrahedron* **1999**, *55* (51), 14523–14534. [https://doi.org/10.1016/S0040-4020\(99\)00927-8](https://doi.org/10.1016/S0040-4020(99)00927-8).
- (35) Hansmann, M. M.; Melaimi, M.; Bertrand, G. Crystalline Monomeric Allenyl/Propargyl Radical. *J. Am. Chem. Soc.* **2017**, *139* (44), 15620–15623. <https://doi.org/10.1021/jacs.7b09622>.
- (36) Dolomanov, O. V.; Bourhis, L. J.; Gildea, R. J.; Howard, J. a. K.; Puschmann, H. OLEX2: A Complete Structure Solution, Refinement and Analysis Program. *J. Appl. Crystallogr.* **2009**, *42* (2), 339–341. <https://doi.org/10.1107/S0021889808042726>.
- (37) Sheldrick, G. M. A Short History of SHELX. *Acta Crystallogr. A* **2008**, *64* (1), 112–122. <https://doi.org/10.1107/S0108767307043930>.
- (38) Frisch, M. J.; Trucks, G. W.; Cheeseman, J. R.; Scalmani, G.; Caricato, M.; Hratchian, H. P.; Li, X.; Barone, V.; Bloino, J.; Zheng, G.; Vreven, T.; Montgomery, J. A.; Petersson, G. A.; Scuseria, G. E.; Schlegel, H. B.; Nakatsuji, H.; Izmaylov, A. F.; Martin, R. L.; Sonnenberg, J. L.; Peralta, J. E.; Heyd, J. J.; Brothers, E.; Ogliaro, F.; Bearpark, M.; Robb, M. A.; Mennucci, B.; Kudin, K. N.; Staroverov, V. N.; Kobayashi, R.; Normand, J.; Rendell, A.; Gomperts, R.; Zakrzewski, V. G.; Hada, M.; Ehara, M.; Toyota, K.; Fukuda, R.; Hasegawa, J.; Ishida, M.; Nakajima, T.; Honda, Y.; Kitao, O.; Nakai, H. Gaussian 09.

- (39) Weigend, F.; Ahlrichs, R. Balanced Basis Sets of Split Valence, Triple Zeta Valence and Quadruple Zeta Valence Quality for H to Rn: Design and Assessment of Accuracy. *Phys. Chem. Chem. Phys.* **2005**, 7 (18), 3297–3305. <https://doi.org/10.1039/B508541A>.
- (40) Falivene, L.; Credendino, R.; Poater, A.; Petta, A.; Serra, L.; Oliva, R.; Scarano, V.; Cavallo, L. SambVca 2. A Web Tool for Analyzing Catalytic Pockets with Topographic Steric Maps. *Organometallics* **2016**, 35 (13), 2286–2293. <https://doi.org/10.1021/acs.organomet.6b00371>.

Chapter 3 Synthetic Routes Towards

EndersCAAC and isoEndersCAAC

3.1 Introduction

First reported in 2005, CAACs have become established as a carbene favorite in a variety of uses from metal-binding ligands, to stabilizing unusual main group species, to organic light emitting diode (OLED) materials, to even as a potential pharmaceutical agent.^{1,2} The electronic properties of CAACs are its most distinguishing feature: CAACs are strongly nucleophilic and strongly electrophilic. These two electronic properties arise from the nitrogen and quaternary carbon adjacent to the CAAC carbene center (Figure 3.1). This contrasts with the highly popular Arduengo NHC which have two nitrogen atoms adjacent to the carbene center which decreases the nucleophilicity and electrophilicity of the NHC carbene carbon. For further discussion on the impact of adjacent carbenes on the electronic properties of carbenes, refer to Chapter 1.3.1 “Substituent Effects – Electronic Influence”. When used to stabilize uncommon or unusual molecular fragments like electron-rich, low-valent metals (Cu^0 , Fe^0 , Be^0 , etc)^{3,4} or like main group species (see Chapter 1.4.3 “Applications in Main Group Research”), carbenes function as a donating L-type ligand with its σ -orbital, but the electron donation is tempered by the partially filled carbene p-orbital which allows carbenes to also receive electron density from the molecular species, providing further stabilization. Because the CAAC p-orbital is less filled due to fewer adjacent nitrogen atoms, CAACs engage in greater electron back-bonding than NHCs, forming a stronger, more stabilizing bond between CAAC and the molecular fragment than an

NHC could ever achieve. In particular, this effect allows CAACs to stabilize electron-rich molecular species better than NHCs can.

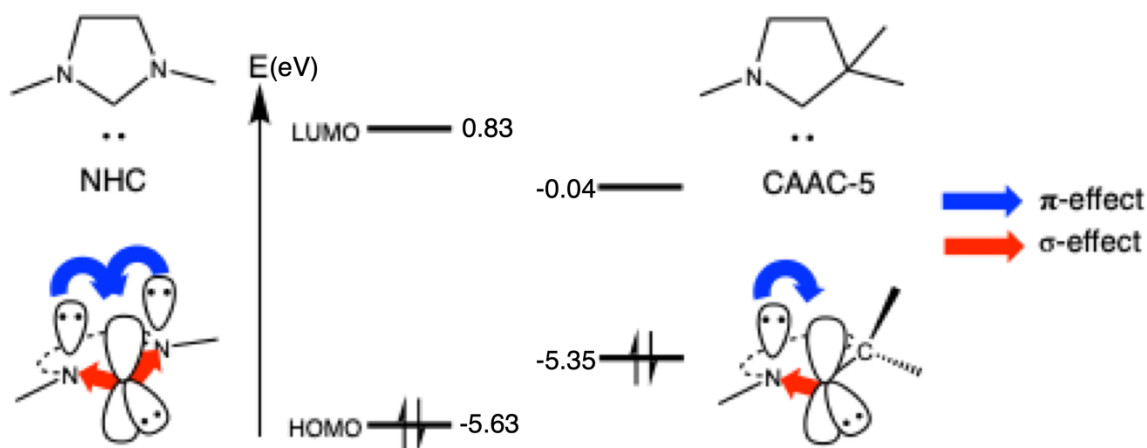
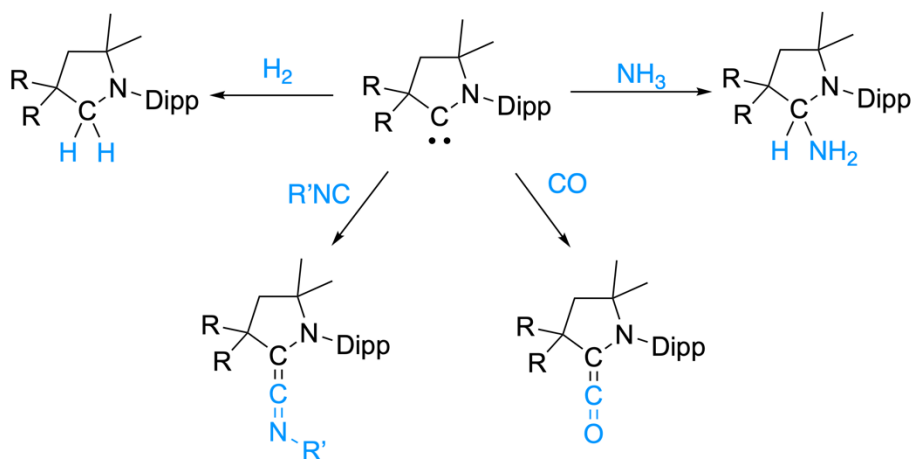


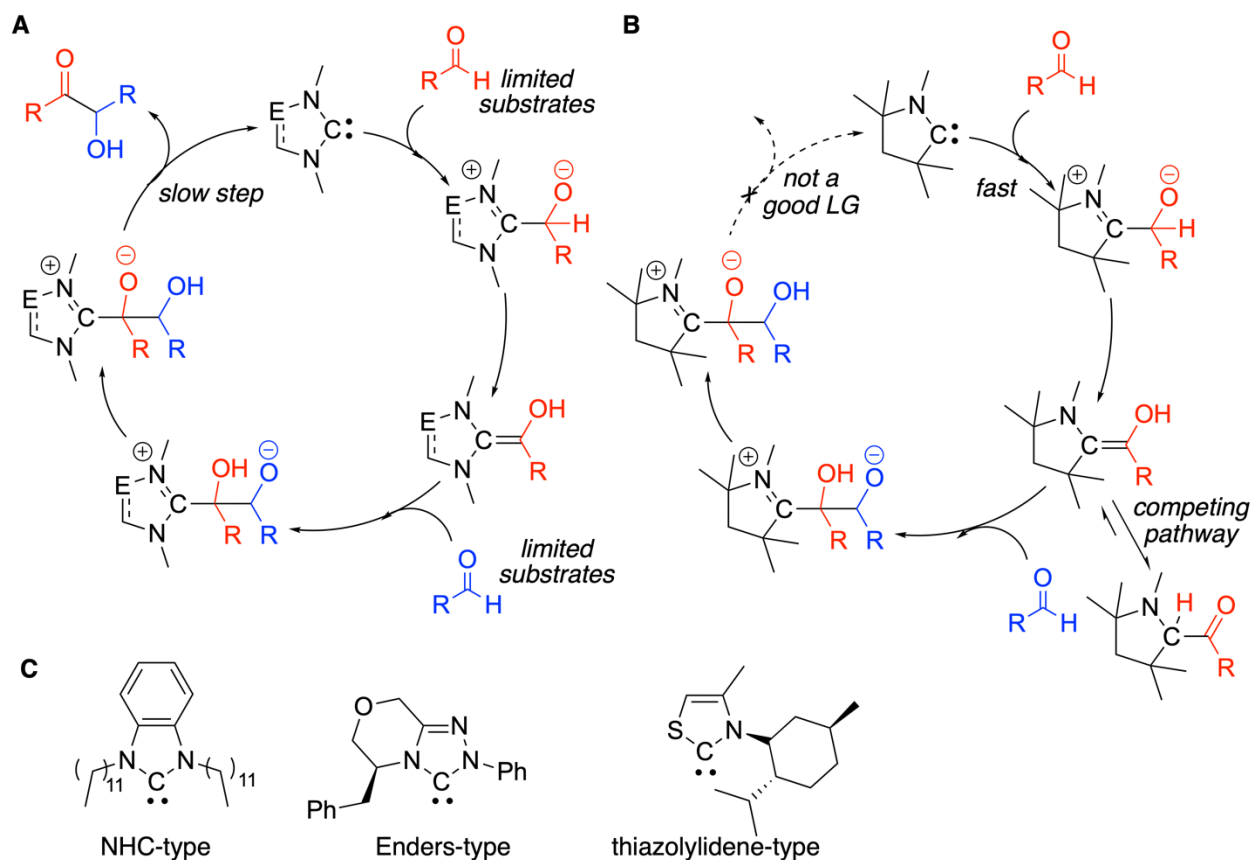
Figure 3.1. Comparison of NHC and CAAC Electronic Properties.

In an application of the isolobal analogy,⁵ the energies of a CAAC HOMO and LUMO and the corresponding small $\Delta H-L$ resembles the filled and empty d-orbitals of transition metals. As a result, carbenes exhibit transition metal-like reactivity such as reacting with small molecules like H_2 , NH_3 , CO , and isonitriles^{6,7} and engaging in reductive elimination mechanisms (Scheme 3.1).⁸ These reactivities are highly unusual not only for carbon-based molecules, but for other carbenes as well. The few carbenes that can react with these types of substrates are carbenes that are highly electrophilic, like DACs and the ferrocene-NHC.⁹⁻¹¹ Reactivity with these kinds of substrates is well documented with transition metals and are also known in limited examples in other low-valent p-block molecules.¹²



Scheme 3.1. CAAC Reactivity with Small Molecules.

CAACs also differ in reactivity from other carbenes in that CAACs are terrible organocatalysts. Compared with NHC- and the Enders carbene-type carbenes, CAACs have only been reported to catalyze two reactions without the presence of metals.^{8,13} In general, to be a successful organocatalyst the carbene needs to be sufficiently nucleophilic to attack the active site of a substrate, but also act as a sufficiently good leaving group in order to regenerate the active free carbene species and close the catalytic cycle (Scheme 3.2). The prime examples of organocatalytic carbenes are NHCs, Enders carbenes, and thiazolyliene carbenes. For example, these carbenes are nucleophilic enough to attack carbonyl carbons, yet also are relatively weak bases such that the free carbene can be regenerated in the last step without too much difficulty. However, NHCs, Enders carbenes, and thiazolyliene carbenes have a limited substrate scope of the most reactive carbonyl reagents and relatively weak electrophiles. The field of carbene organocatalysis can benefit greatly with a new carbene that can activate small molecules for use in catalytic reactions and could herald a new era of chemistry in which transition metals play an increasingly small role. Decreased use of transition metals, particularly the noble metals and rare earth metals, can result in financial savings and further reduce the environmental impact of chemistry.



Scheme 3.2. A Generic Carbene Catalytic Cycle (A), A Hypothetical CAAC Catalytic Cycle (B), and Examples of Carbene Organocatalysts (C).

How can we have a carbene that has an adjacent quaternary carbon (small $\Delta H-L$) and function as a good leaving group? A possible solution lies in the differences between an NHC and the Enders carbene (Figure 3.2). The Enders carbene is structurally like an unsaturated NHC but it is a more efficient organocatalyst for benzoin condensations, Stetter reactions, and similar umpolung reactions compared to NHCs. Enders carbenes excel at these reactions because they are better leaving groups compared to NHCs. The presence of the imine $C=N$ bond in the backbone of an NHC acts in a σ -withdrawing effect upon the carbene σ -orbital electrons, further lowering the Enders carbene HOMO and nucleophilicity. Concomitantly, the $C=N$ bond also acts in a π -withdrawing manner upon the nitrogen adjacent to the carbene, decreasing the donation of the nitrogen lone pair into the vacant carbene p -orbital and lowering the LUMO of the Enders

carbene. The lowering of the LUMO energy allows the Enders carbene to maintain a similar $\Delta H-L$ as an NHC.

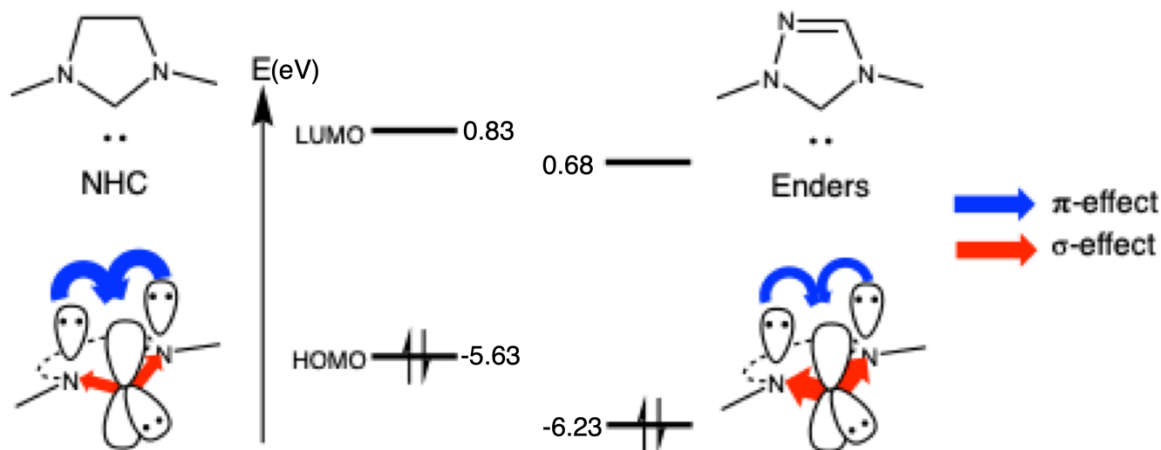


Figure 3.2. Comparison of NHC and Enders Carbene Electronic Properties.

We hypothesize that we can use an imine C=N bond in the backbone of a CAAC to produce a novel CAAC-like carbene with lowered HOMO and LUMO energies and a similar small $\Delta H-L$. Indeed, when performing DFT calculations on two hypothetical Enders carbene-CAAC hybrids (EndersCAAC and isoEndersCAAC), we observed a drop in the HOMO and LUMO energies are a small $\Delta H-L$ like that of CAAC (Figure 3.3). This *in silico* finding provides a promising lead to an organocatalytic CAAC-like carbene. However, the synthetic challenge remains.

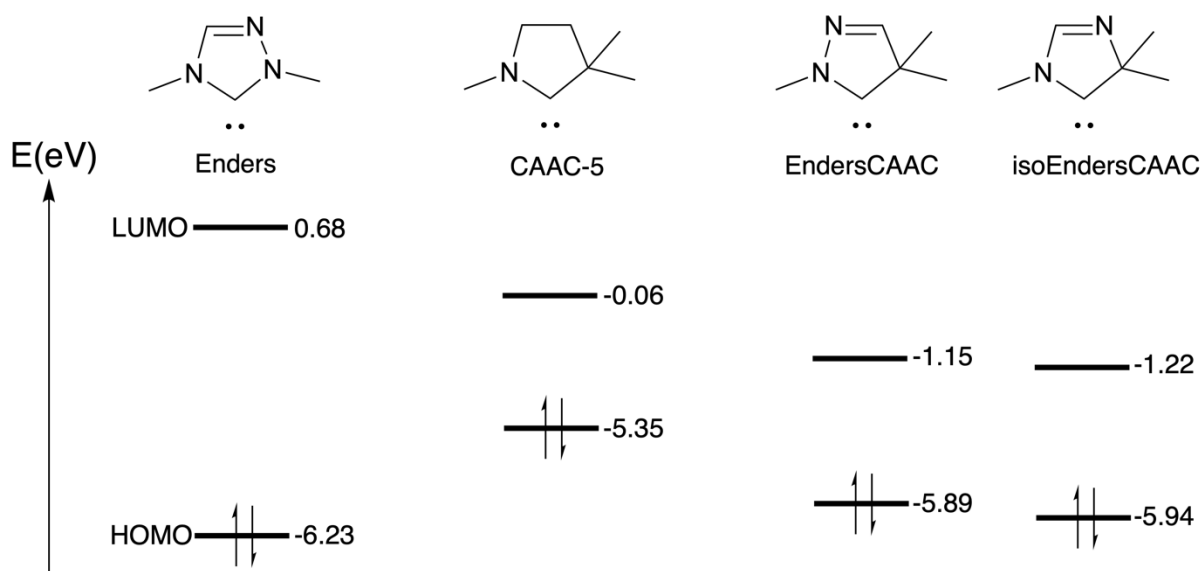
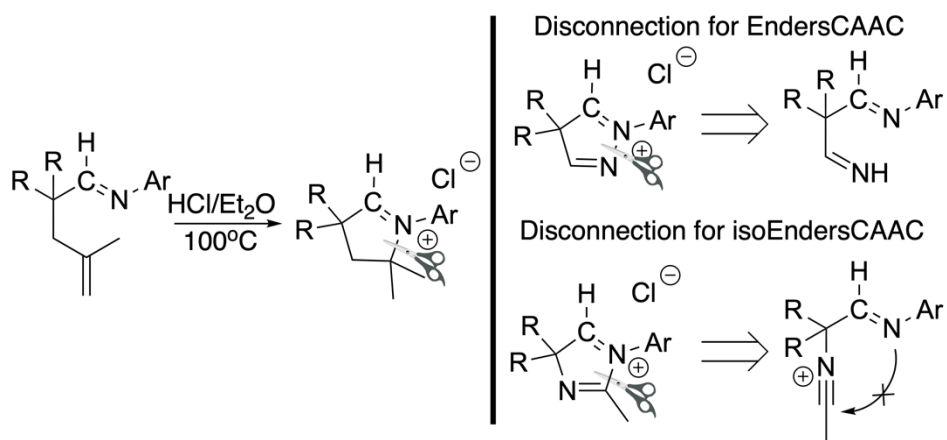


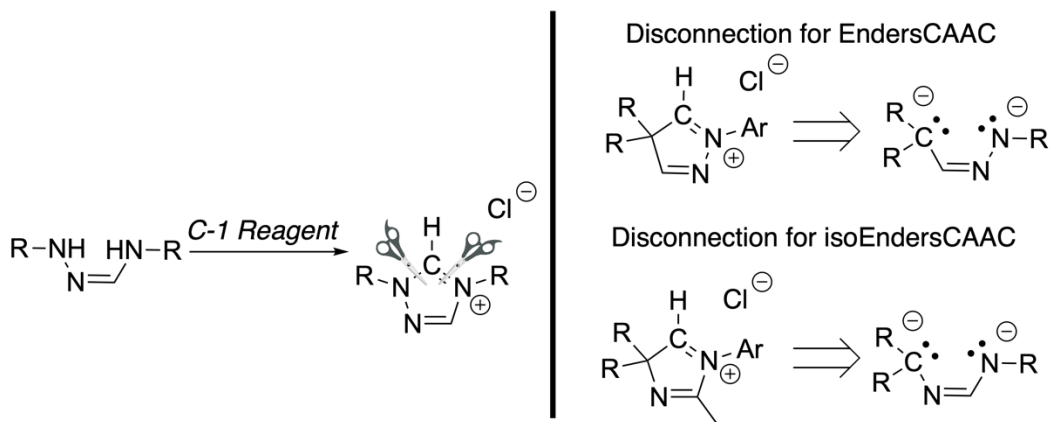
Figure 3.3. Comparison of Enders Carbene, CAAC-5, EndersCAAC, and isoEndersCAAC Electronic Properties.

An analysis of the current methods to synthesize CAACs and Enders carbenes prove that these methods cannot be used to synthesize EndersCAAC or isoEndersCAAC. CAACs are produced by deprotonating their corresponding iminium salt, which in turn is obtained through one of two methods: the alkylation of an epoxide followed by Tf₂O-mediated ring closure, or by the more commonly used hydroiminium ring closure between an alkene and an imine (Scheme 3.3).¹⁴ The hydroiminium methods cannot access EndersCAAC because the required disconnection bond is an N-N bond, which cannot be formed using acid-catalyzed cyclization. IsoEndersCAAC cannot be synthesized by the hydroiminium route either as this route would require a nitrilium and imine that cannot be positioned correctly for the key proton-transfer step and subsequent nucleophilic cyclization to occur.



Scheme 3.3. Synthetic Routes to CAACs Cannot Access EndersCAAC or IsoEndersCAAC.

The synthetic routes to Enders carbene all install the carbenic carbon from a C-1 reagent source, relying on the two nitrogen atoms adjacent to the carbene carbon (Scheme 3.4).¹⁵ Without a second nitrogen atom, any route to EndersCAAC or isoEndersCAAC using this method would require generating a carbanion on the eventual quaternary carbon to attack the carbon derived from the C-1 source, transformations that may require functional groups that are incompatible under strongly basic reaction conditions. In the below section, an attempt was made using this synthetic approach for EndersCAAC, but it quickly became apparent that it would not work. As a result, the bulk of this chapter details the different strategies that were attempted to synthesize EndersCAAC and isoEndersCAAC.



Scheme 3.4. Synthetic Routes to Enders Carbenes Cannot Access EndersCAAC or IsoEndersCAAC.

3.2 Synthetic Work towards EndersCAAC

Since the EndersCAAC pyrazolyliidinium salt precursor cannot be synthesized using the CAAC hydroiminiumation method, a retrosynthetic analysis of the EndersCAAC pyrazolylidene ring was performed. The free carbene follows a retrosynthetic route to a pyrazolyliidinium salt, which in turn comes from a pyrazolinone. From here, there are three possible disconnection pathways to obtain the pyrazolinone (Figure 3.4): 1) disconnections at the N2-C3 and C4-C5 bonds, 2) disconnections at the N1-C5, N2-C3, and C3-C4 bonds, and 3) disconnections at the N1-C5 and N2-C3 bonds. The first pathway is a 1,3-dipolar cycloaddition between a nitrile imine and disubstituted ketene, a reaction with no known literature precedent involving two highly reactive molecules. The second pathway is analogous to the Enders carbene synthetic route. The second pathway entails a hydrazone condensation, followed by N-formylation, and deprotonation of the alpha proton to form a stabilized carbanion that then attacks the formyl carbon to form a hemiaminal. The third pathway is a double condensation between a hydrazine and a beta-ketoester. The 1,3-dipolar cycloaddition pathway was deemed unlikely to succeed because both reagents need to be generated *in situ* and used immediately and because of reaction condition incompatibility. The nitrile imine is generated from the deprotonation of hydrazonoyl chlorides and reverts to the hydrazonoyl chloride in the presence of acidic protons, which are generated in the process of making ketenes. Initially, the second pathway was more attractive than the third pathway because it also paralleled the reported synthesis of cyclic (alkyl) (amino) silylenes (CAASi), which used a Si-1 reagent source rather than a C-1 source to form the low-valent main group species.¹⁶

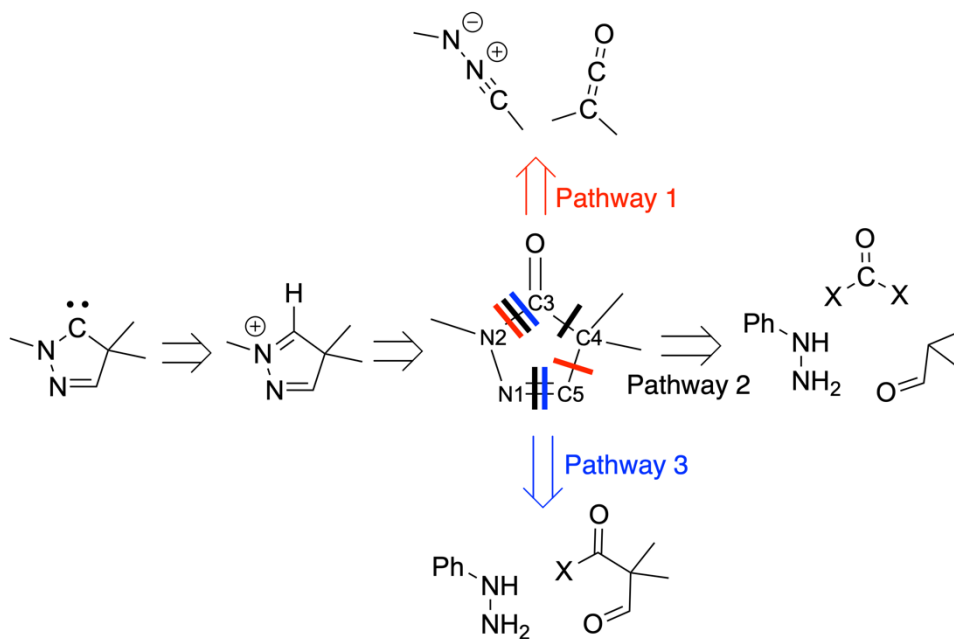
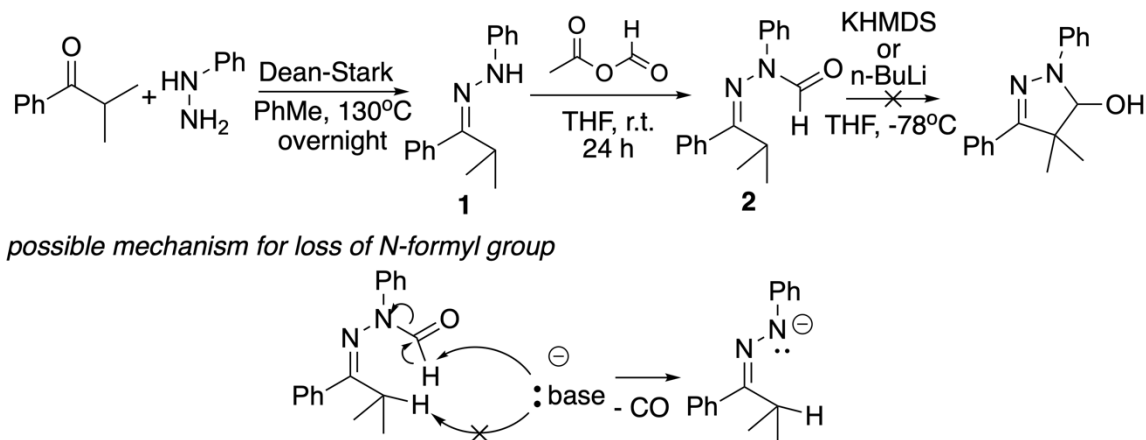


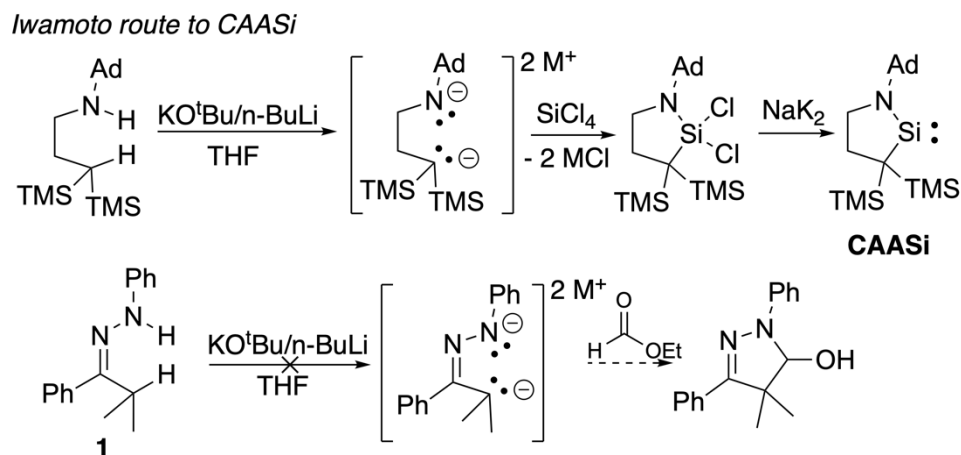
Figure 3.4. Retrosynthetic Analysis of EndersCAAC.

We pursued the second pathway (Scheme 3.5) starting the condensation of phenyl hydrazine and isobutyrophenone to form hydrazone **1** as a white solid. Hydrazone **1** was then reacted with formic acetic anhydride to yield N-formyl hydrazone **2** as a white solid. Attempts to deprotonate the alpha carbon of N-formyl hydrazone **2** with KMHDS or n-BuLi yielded only hydrazone **1** upon work-up. During the addition of n-BuLi to the reaction mixture, gas evolution was observed, possibly indicating that the base was deprotonating the formyl hydrogen and generating CO rather than the base deprotonating the alpha carbon.



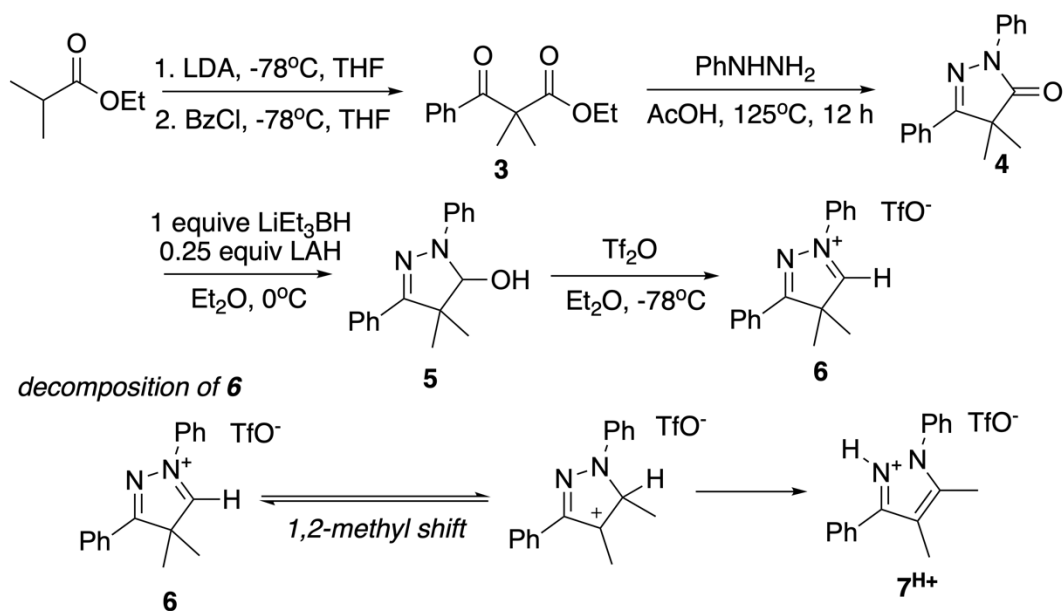
Scheme 3.5. Attempt to Synthesis EndersCAAC via Pathway 2.

With N-formyl hydrazone cyclization unlikely, two equivalents of n-BuLi/KO^tBu were added to phenylhydrazone **1** to attempt to produce the doubly deprotonated species and react it with a C-1 source *in situ* (Scheme 3.6). However, these reactions only yielded phenylhydrazone **1** upon work-up. It is likely that the first deprotonation of the N-H bond succeeds, but the additional electron density in the monoanion species greatly increases the alpha C-H bond pK_a, preventing the second deprotonation from occurring. In the synthesis of CAASi, Iwamoto *et al* were successful in using a geminal bis(trimethylsilyl) group to stabilize the generated carbanion and facilitate the resulting attack on their Si-1 source.¹⁶ The hydrazone C=N bond positioned adjacent to an anionic nitrogen atom likely could not provide the same carbanion-stabilizing effect as the geminal bis(trimethylsilyl) group of Iwamoto's system, causing the cyclization with a C-1 source to fail.



Scheme 3.6. Attempt to Synthesis EndersCAAC via a Dianion Intermediate.

Having exhausted the second pathway, we turned our attention to the third pathway (Scheme 3.7). We began with a Claisen condensation of ethyl isobutyrate and benzoyl chloride yielded ketoester **3** as a viscous, yellow oil. Ketoester **3** was then cyclized with phenylhydrazine in refluxing acetic acid to yield pyrazolone **4** as an off-white solid. Pyrazolone **4** can then be reduced with lithium aluminum hydride or lithium triethylborohydride to yield hemiaminal **5** as a white solid. Treating hemiaminal **5** with one equivalent of triflic anhydride (Tf_2O) in diethyl ether quantitatively yields pyrazolinium salt **6** as an off-white fluffy solid. In our work, we discovered that pyrazolinium **6** will rearrange into pyrazolium **7**^{H+} through a 1,2-methyl shift and a subsequent deprotonation. This process is thought to be catalyzed by the presence of adventitious triflic acid not removed during workup, or by the basic imine nitrogen in the backbone. As a result, it is not recommended to store pyrazolinium **6** for greater than one day.

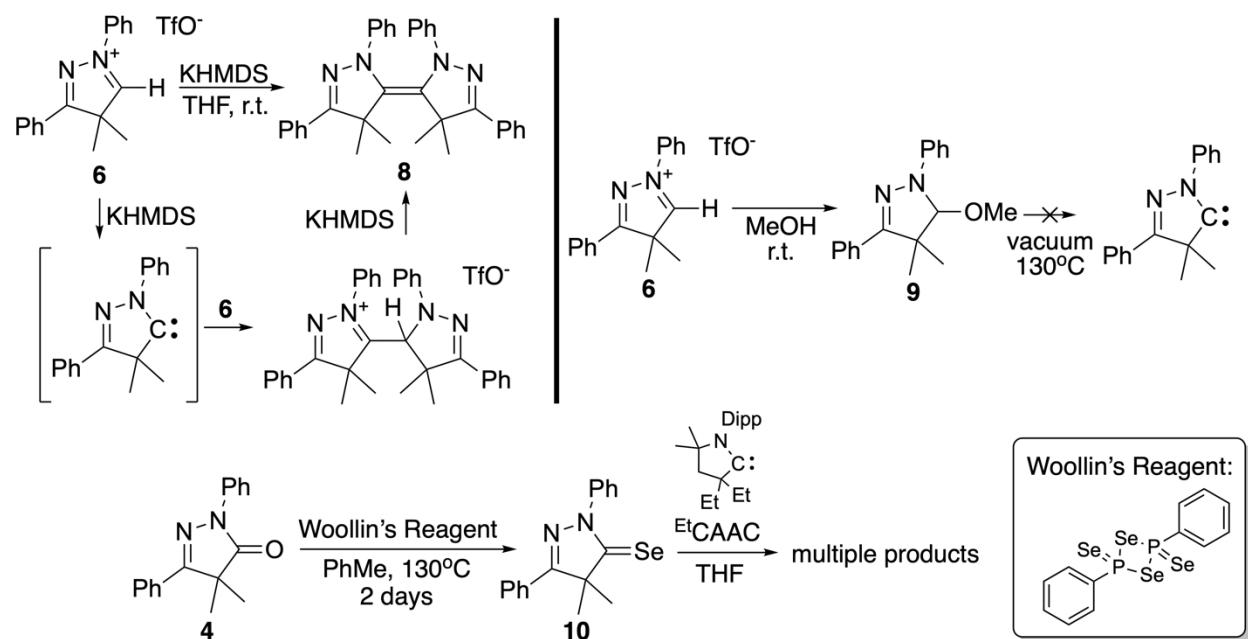


Scheme 3.7. Synthesis to Pyrazolinium **6** En Route to EndersCAAC via Pathway 3.

Deprotonation of pyrazolinium **6** with KHMDS quantitatively yielded an intensely yellow oil that was identified as bipyrazolylidene **8**, which is the dimer of EndersCAAC. As the literature establishes, carbene dimerization occurs through the reaction of the free carbene with an equivalent of the starting iminium salt and a subsequent deprotonation rather than direct carbene-carbene addition.^{17,18} Given this mechanism, we attempted to isolate free EndersCAAC through non-iminium routes (Scheme 3.8). Pyrazolinium **6** was reacted with methanol to generate the EndersCAAC(HOMe) adduct **9**. Adduct **9** was then subjected to vacuum pyrolysis conditions similar to the conditions used in the formation of triphenyl Enders carbene¹⁹ in an attempt to eliminate methanol from adduct **9** to generate free EndersCAAC. The attempted vacuum pyrolysis resulted in the decomposition of adduct **9** to dark, tarry residue. Hemiaminal **5** was also subjected to similar conditions to eliminate water to generate free EndersCAAC, but this too was not successful. Inspired by a 2018 report by the Bertrand group in which selenium exchange occurred between two carbenes,²⁰ EndersCAAC(Se) adduct **10** was synthesized by refluxing pyrazolinone **4** with Woollin's reagent in toluene. Adduct **10** was then reacted with one

equivalent of ^{Et}CAAC, but the reaction produced multiple products, one of which was pyrazole

6.

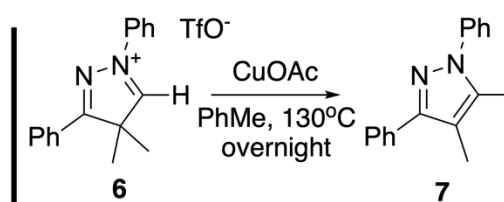
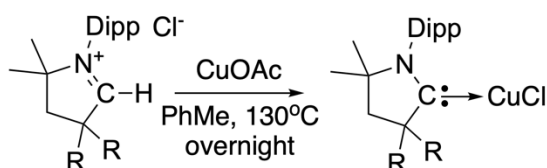


Scheme 3.8. Attempts to Synthesize Free EndersCAAC.

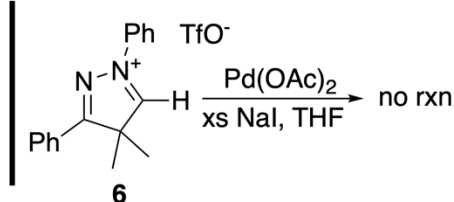
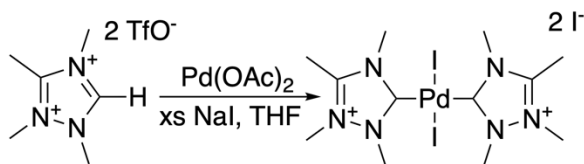
As obtaining free EndersCAAC seemed unlikely, we turned our attention to synthesizing other adducts of EndersCAAC to at the very least gather indirect data of EndersCAAC, particularly of its electronic properties (Scheme 3.9). Recent reports by Jana *et al*²¹ and Bertrand *et al*²² suggested a facile route to the EndersCAAC(Cu)Cl complex from carbene iminium precursors, but subjecting pyrazolinium **6** to the same conditions as that of the Bertrand paper yielded only pyrazole **7**. We hypothesize that pyrazolinium **6** undergoes the 1,2-methyl shift readily at high temperatures, precluding the formation of any acetate or copper-coordinated intermediates that would lead to the CuCl-carbene complex. Attempting a palladium metalation under reaction conditions from an older report by the Bertrand group resulted in the recovery of starting material.²³ Attempting to break up dimer **8** by refluxing with [Rh(COD)Cl]₂ to generate a biscarbene-rhodium complex²⁴ yielded only starting material. We hypothesize that this reaction

only can occur when a Wanzlick equilibrium exists between the free carbene and its dimer, as in the case with dimethyl-benzimidazolylidene. The EndersCAAC dimer **8** is not an electron rich enough alkene to dissociate into its free carbenes. Thus far, the characterization of EnderCAAC's electronic properties is the ^{77}Se -NMR shift of adduct **10**. The selenium atom of adduct **10** has a chemical shift of which is more downfield compared to the selenium adduct of $^{\text{Et}}\text{CAAC}$ (δ 481ppm),²⁵ indicating that the selenium atom has more π -back bonding with EndersCAAC than with $^{\text{Et}}\text{CAAC}$ (Figure 3.5).

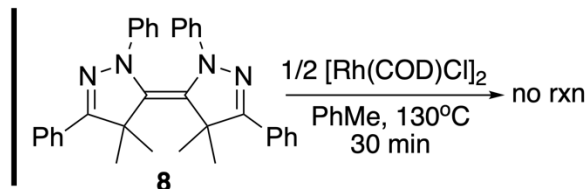
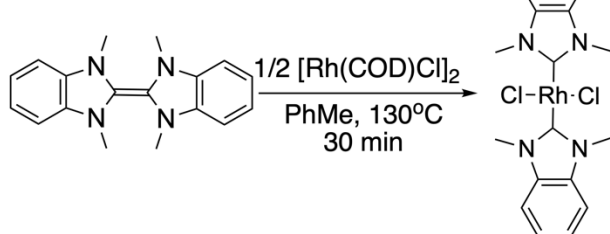
Bertrand CuCl metallation



Bertrand Pd metallation



Lappert Rh metallation



Scheme 3.9. Attempts to EndersCAAC Metal Complexes.

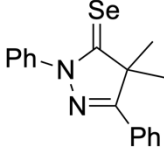
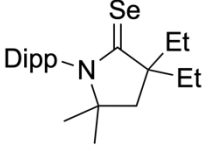
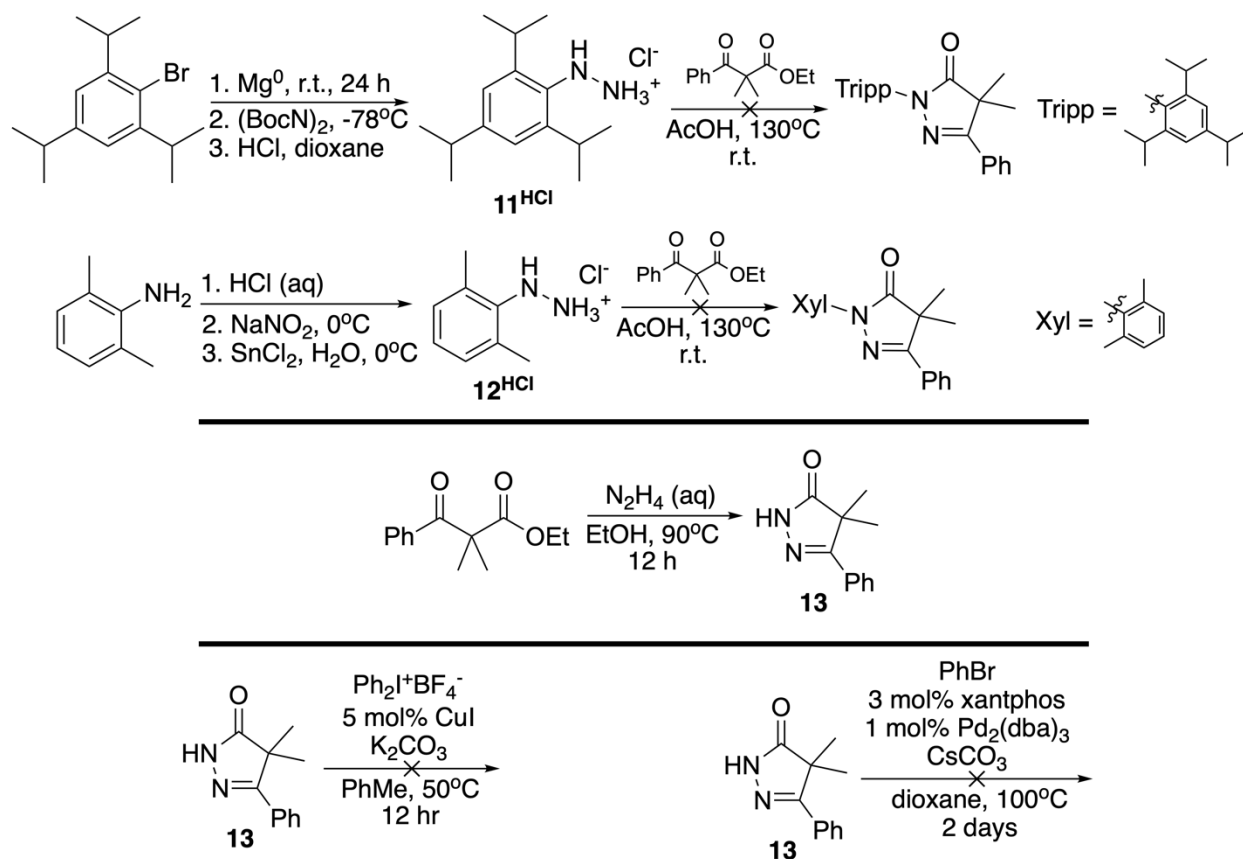
	 <p style="text-align: center;">10</p>	 <p style="text-align: center;">EtCAAC(Se)</p>
⁷⁷ Se NMR	δ 501 ppm (CDCl ₃)	δ 481 ppm (d ₆ -acetone)
¹³ C NMR	δ 206 ppm (CDCl ₃)	δ 217 ppm (C ₆ D ₆)

Figure 3.5. Comparison of EndersCAAC and EtCAAC Selenium Adducts.

As retrosynthetic pathway 3 has proven a reasonable method to obtain the structural motif of EndersCAAC, we decided to revisit the synthesis to add steric bulk around the carbene center in hopes of isolating a free carbene. We envisioned adding steric bulk to the N-aryl group or adding steric bulk to the quaternary carbon may finally allow the isolation of a free EndersCAAC.

Increasing the steric demand on the N-aryl group seemed the likeliest route to the free carbene, afterall, ^{Me}CAAC with an N-2,6-diisopropylphenyl (Dipp) group is isolable and does not dimerize (Scheme 3.10). N-2,4,6-trisopropylphenyl (Tripp) hydrazine hydrochloride **11**^{HCl} was synthesized following a literature reported preparation,²⁶ but hydrazine **11** failed to cyclize with beta-ketoester **4**. We next tried to cyclize N-2,6-dimethylphenyl hydrazine hydrochloride **12**^{HCl}²⁷ with beta-ketoester **4**, but again, the reaction failed and only yielded degradation products. We next attempted to install an aryl group with metal-catalyzed C-N coupling reactions on pyrazolone **13** with a diphenyliodonium salt or phenyl bromide, however starting material was recovered in both palladium²⁸ and copper²⁹ catalyzed reactions. We suspect that the neighboring nitrogen atom of pyrazolone **13** may coordinate to the metal catalyst, preventing the cross-coupling reaction from proceeding. While the N-arylation of pyrazolone **13** may proceed

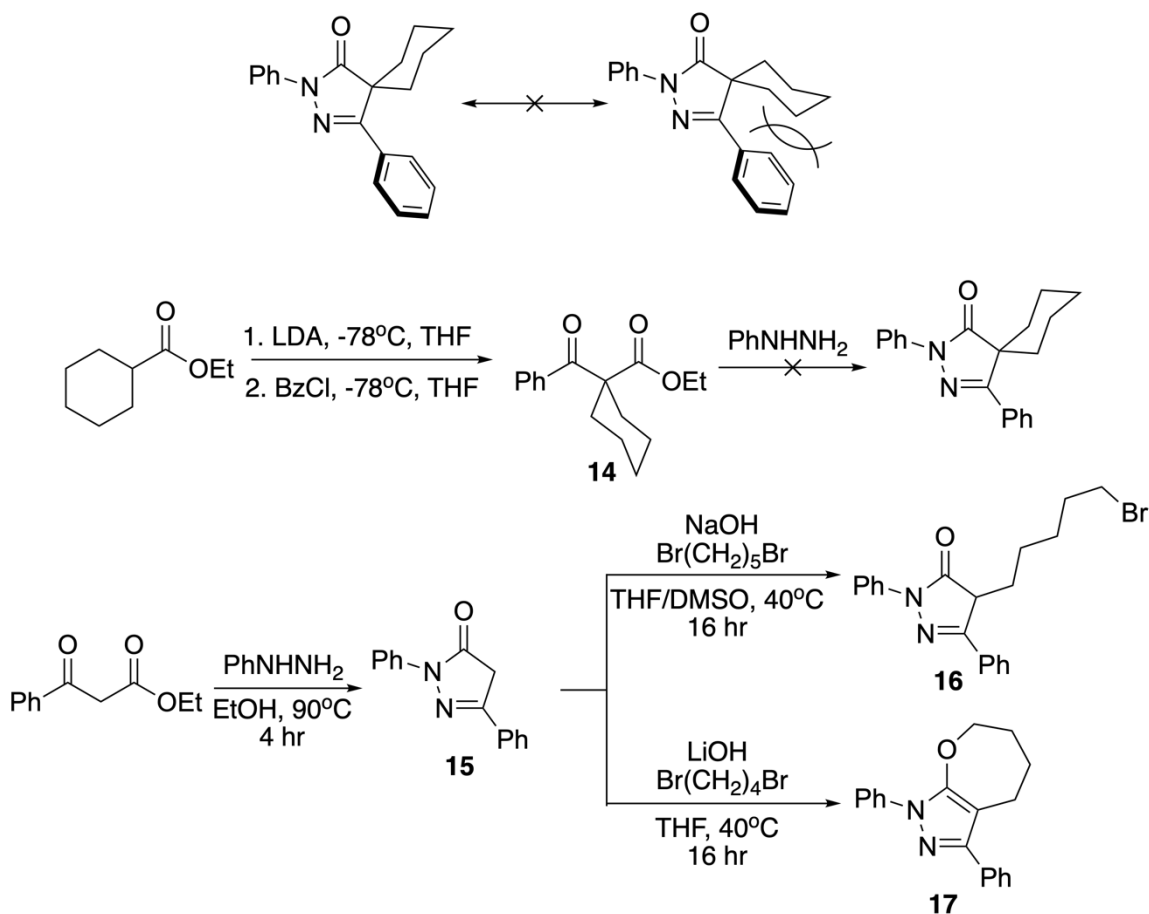
with a more suitable reaction condition, metal ligand, or arylating reagent, we decided to turn our attention to increasing the steric demand on the quaternary carbon.



Scheme 3.10. Attempts to Increase Steric Bulk on the N-Aryl Substituent to Isolate Free EndersCAAC.

To increase the steric demand on the quaternary carbon, we attempted two strategies: to pre-install the substituents onto the beta-ketoester prior to cyclization, and post-cyclization modification (Scheme 3.11). To increase the steric demand from the geminal dimethyl groups in pyrazolone **4**, a spiro-cyclohexyl group was chosen because the C-phenyl group in the backbone would force a cyclohexyl chair conformation in which the cyclohexyl group is pointing out in the same direction as the carbene σ -orbital, providing a consistent source of steric pressure. Additionally, the spiro-cyclohexyl group may suppress 1,2-alkyl shifts at the iminium intermediate because such a rearrangement would form a thermodynamically unfavorable 7-

membered ring. The synthesis of beta-ketoester **14** was achieved using a modified procedure of beta-ketoester **4**. However, beta-ketoester **14** did not react with phenylhydrazine at all, not even the hydrazone condensation product. Situated between a phenyl group on one side and a ring and ester substituted quaternary carbon on the other side, it is possible that the ketone of beta-ketoester **14** is simply inaccessible to nucleophilic attack by the terminal hydrazine nitrogen. We then attempted to form the quaternary carbon post-cyclization. Commercially available ethyl benzoacetate and phenylhydrazine were cyclized to form pyrazolone **15**. Pyrazolone **15** was then reacted with 1,5-dibromopentane in the presence of a base, but no desired spiro-cyclohexyl pyrazolone product was formed only pyrazolone **16**; the second ring-closing alkylation was not achieved. Even modifying the conditions did not yield the desired pyrazolone product.³⁰ Additionally, pyrazolone **15** was reacted with 1,4-dibromobutane to hopefully obtain the spiro-cyclopentyl pyrazolone, but the only product that was observed was bicycle **17**.



Scheme 3.11. Attempts to Increase Steric Bulk on the Quaternary Carbon to Isolate Free EndersCAAC.

While the above attempts to obtain a free EndersCAAC were unsuccessful, other strategies to increase steric bulk around the carbene center may be more successful. Strategies that have not been tried are introducing an N-alkyl group and changing the C-phenyl group to a functional group that is less sterically bulky (Figure 3.6). Due to time constraints, the author was not able to conduct reactions to investigate these approaches.

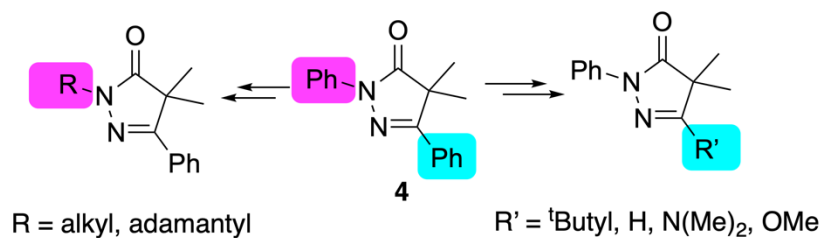


Figure 3.6. Potential Means to Obtain Free EndersCAAC.

3.2 Synthetic Work towards isoEndersCAAC

Like the EndersCAAC situation, a retrosynthetic analysis of the isoEndersCAAC imidazolylidene ring was performed because the existing strategies to synthesize CAACs and Enders carbene cannot be applied. The free carbene follows a retrosynthetic route to an imidazolium salt, which in turn is obtained from an imidazolone. Unlike the pyrazolinone, there are five possible disconnection pathways, of which, this chapter will only discuss pathways four and five (Figure 3.7): 1) disconnections that flow from the reaction of an N-oxide and an aryl isocyanate, 2) disconnections that flow from a 1,3-dipolar cycloaddition between a nitrile ylide and an aryl isocyanate, 3) disconnections at the N1-C5 and N4-C5 bonds to form the ring from a 4-atom fragment and a 1-atom fragment, 4) disconnections at the N4-C5 bond, and 5) disconnections at the N1-C2 and N4-C5 bonds to form the ring from a 3-atom fragment and a 2-atom fragment. The fourth pathway involves a Staudinger reaction to form the ring, a reaction that has precedent in recent literature.³¹ The fifth pathway comprises two acylation reactions to reach the imidazolone.

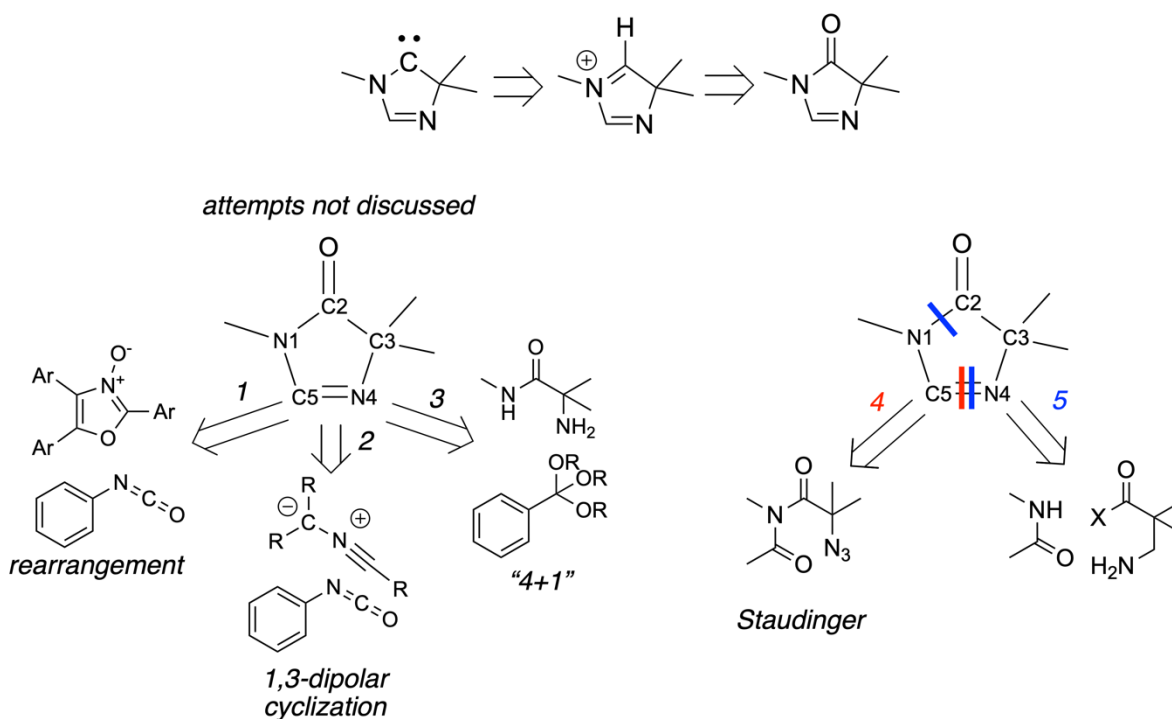
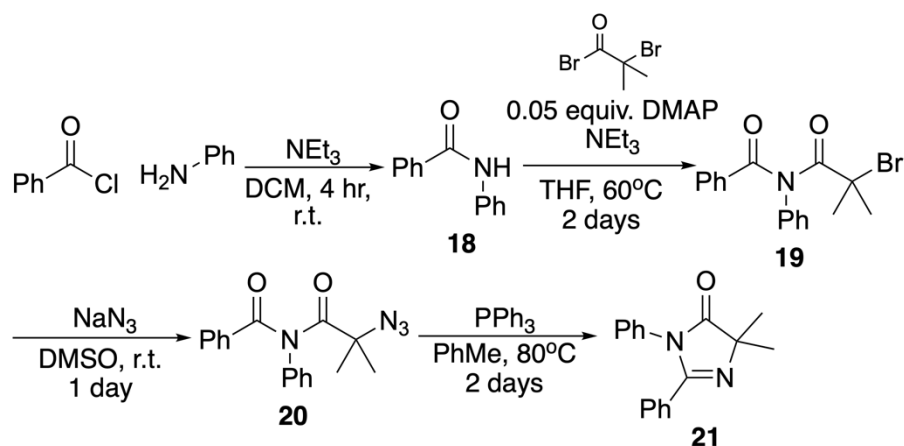


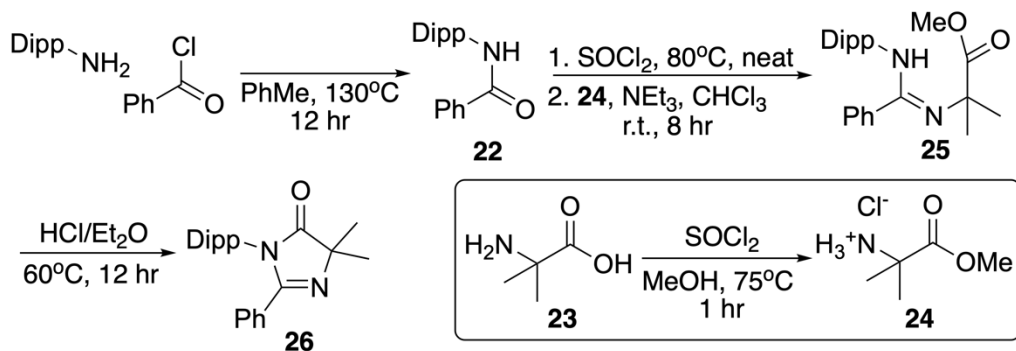
Figure 3.7. Retrosynthetic Analysis of IsoEndersCAAC.

Pathway four (Scheme 3.12) began with the formation of benzanilide **18** and subsequent acylation of the amide nitrogen with 2-bromo-2-methylpropanoyl bromide in the presence of DMAP to yield imide **19**. The alkyl bromide of imide **19** is then converted to the azide in imide **20**. Reacting imide **20** with triphenylphosphine resulted in ring closure and the formation of imidazolone **21**. While pathway four provides imidazolone **21** a short number of synthetic steps, the reactions can be lengthy, particularly the synthesis of the imide. Additionally, as imidazolone **21** is an isomer of pyrazolone **4** and the derived EndersCAAC dimerizes, we opted to synthesize an imidazolone with more steric bulk around the carbene center.



Scheme 3.12. Formation of Imidazolone **21** via Pathway Four En Route to IsoEndersCAAC.

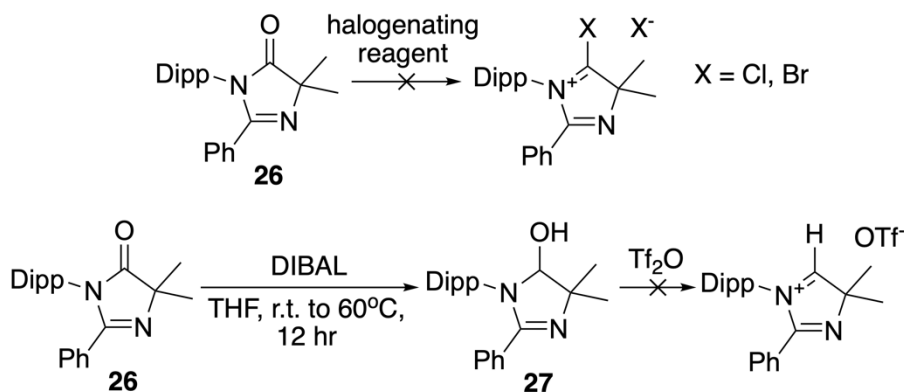
Pathway five provides an alternative route to imidazolones (Scheme 3.13). This pathway begins with the formation of benzanilide **22** which is then treated with SOCl_2 to form an *in situ* imidoyl chloride that is then reacted with amino ester **24** in the presence of NEt_3 to form amidine **25**. Amino ester **24** is formed by a simple esterification of α,α -amino acid **23**. Amidine **25** is then heated in anhydrous HCl to form imidazolone **26**. Pathway five provides a small advantage over pathway four because pathway five can tolerate different functional groups and substituent steric bulkiness, particularly of the N-aryl group, more than pathway four.



Scheme 3.13. Formation of Imidazolone **26** via Pathway Five En Route to IsoEndersCAAC.

With imidazolones **21** and **26** on hand, we turned our attention to converting the imidazolones to a carbene precursor (Scheme 3.14). Inspired by carbene halogen-exchange reports,²⁰ we attempted to deoxyhalogenate imidazolone **26** to form the corresponding

haloiminium with a variety of reagents (SOCl_2 , $(\text{COCl})_2$, $\text{DMF}/(\text{COCl})_2$, PCl_3 , PBr_3 , PCl_5 , POCl_3) to no avail. The halogenation reagents preferentially react with amides and lactams because of the large partial negative charges on the amide oxygen due to the electron-donating abilities of the amine nitrogen atom. However, with imidazolone **26**, we hypothesize that the amide oxygen may not be nucleophilic because the amide nitrogen atom is instead donating its electron density into the $\text{C}=\text{N}$ bond in the backbone. As a result, the amide oxygen is not nucleophilic and will resist reacting with halogenating reagents (Figure 3.8). Next, we attempted to reduce imidazolone **26** to a hemiaminal with hydride reagents. Of these reagents, only diisobutylaluminum hydride (DIBAL) produced hemiaminal **27** in low yield. Attempts to convert hemiaminal **27** to an imidazolium with Tf_2O were unsuccessful. Initially, we thought that a 1,2-hydride shift may have occurred, like with pyrazolinium **6**, but the expected imidazole methyl peaks were not observed by NMR.



Scheme 3.14. Attempts to Obtain an IsoEndersCAAC Free Carbene Precursor.

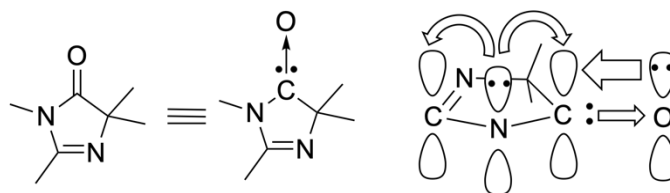


Figure 3.8. Diagram of Bonding Between Atoms as a Possible Explanation for the Lack of Reactivity between Imidazolone **26** and Halogenating Reagents.

While free isoEndersCAAC has not been obtained as of this dissertation, the work thus far towards this carbene has formed a strong foundation for future work. There are two potential ways to move forward. First, like EndersCAAC, the dimethyl substituents on the quaternary carbon can be exchanged for a spiro cyclohexyl group by making the corresponding amino ester. The added steric bulk may facilitate the successful formation of the imidazolium precursor to the free carbene. However, this may make the imidazolone reduction to the hemiaminal more difficult. A second method to obtain the imidazolium precursor is to form the hemiaminal methyl ether and add acid. From the imidazolone, one can imagine a simple deprotonation with KHMDS would yield the free carbene.

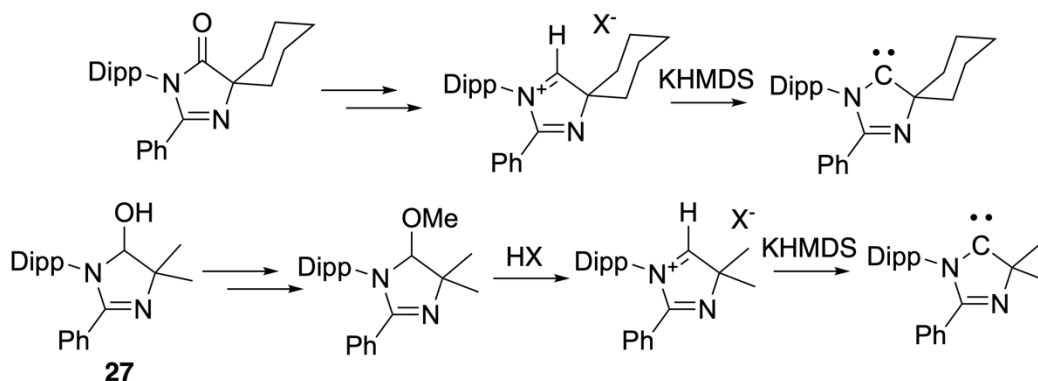


Figure 3.9. Potential Means to Obtain Free isoEndersCAAC.

3.4 Conclusion

The syntheses of EndersCAAC and isoEndersCAAC has been challenging and highlights the continued demand for new synthetic routes to carbenes. This work demonstrates that carbenes have not been completely “tamed” and that carbenes can be as synthetically challenging to obtain as other main group species. The difficulties associated with obtaining free EndersCAAC or free isoEndersCAAC may be a direct consequence of the electrophilic and weak base properties that made them attractive in the first place. The decreased HOMO and

LUMO levels that are due to the presence of a C=N bond in the backbone also led to issues in maintaining stable molecules. In 5-membered cyclic carbenes, when four atoms are planar and conjugated, the energy barrier for a rearrangement is small due to the massive increase in stability that aromatic rings provide. Additionally, as the C=N bond in the backbone withdraws electron density from the carbene center, the increased electrophilicity also imposes a penalty as it is more likely that a base will add to the carbene center rather than deprotonate the iminium hydrogen atom to generate a carbene. The increased electrophilicity also allows the free carbene to quickly react with another iminium in a reaction and form the dimer. In the course of the work and effort that has been put into this thesis chapter, we have ruled out the generality of several approaches to carbenes that seemed promising: the halogen- and selenium-exchange reactions, vacuum pyrolysis of carbenes with decreased nucleophilicity, and several of the direct metalation of carbene methods.

Finally, despite failing to capture and characterize the elusive carbenes, this project was still fruitful because of in the process of synthesizing free EndersCAAC, the novel carbene dimer **8** was discovered and exhibits properties that may be of interest to other researchers, see Chapter 4.

3.5 Experimental

3.5.1 General Methods

All manipulations were performed using standard glovebox and Schlenk techniques. Glassware was dried in an oven overnight at 150 °C or flame-dried, and solvent were dried and degassed before use. Benzene, THF, diethyl ether, and n-pentane were freshly distilled over Na metal. Hexanes, dichloromethane, and chloroform were freshly distilled over CaH₂.

Deuterium-labeled solvents (d_6 -benzene (C_6D_6) and d -chloroform ($CDCl_3$) were purchased from Cambridge Isotope Laboratories and were freshly distilled over CaH_2 . NMR: Multinuclear NMR data were recorded on a Varian INOVA 500 MHz or a JOEL ECZL 400 MHz at UCSD. Chemical shifts (δ) are reported in parts per million (ppm) and are referenced to residual solvent signals (1H , ^{13}C). Coupling constants J are given in hertz (Hz). NMR multiplicities are abbreviated as follows: s = singlet, d = doublet, t = triplet, q = quartet, sext = sextet, sept = septet, m = multiplet, br = broad. All spectra were recorded at 298 K unless otherwise noted.

3.5.2 Synthetic Procedures

1: To a 100 mL round bottom flask equipped with a magnetic stir bar, isobutyrophenone (10.0 mL, 0.067 mol, 1.0 equivalent), phenylhydrazine (7.9 mL, 0.080 mol, 1.2 equivalents), and toluene (30 mL) were added. The flask was then equipped with a Dean-Stark apparatus connected to a condenser and an external bubbler. The solution was then heated in an oil bath at $130^\circ C$ and stirred overnight. The mixture was cooled to room temperature and the Dean-Stark apparatus was replaced with a distillation setup to remove all volatiles via distillation.

Distillation yielded **1** as a dark colored oil. Yield 15.7 g (97.62%). 1H NMR (500 MHz, $CDCl_3$) δ = 7.50 (t, 4H, $J=7.4$ Hz), 6.96 (d, 4H, $J=7.0$ Hz), 6.79 (t, 2H, $J=6.8$ Hz), 2.85 (sept, 1H, $J=6.8$ Hz), 1.19 (d, 6H, $J=6.8$ Hz) $^{13}C\{^1H\}$ NMR (125 MHz, C_6D_6) δ = 152.4, 145.6, 134.4, 129.4, 129.2, 128.1, 119.4, 112.7, 36.2, 20.6.

2: To a flame-dried 100 mL Schlenk flask equipped with a magnetic stir bar, Ac_2O (5.3 mL, 0.055 mol, 2.6 equivalents) was added and then cooled on a water-ice bath. While stirring, formic acid (2.5 mL, 0.067 mol, 3.2 equivalents) was added dropwise. Upon completion of

addition, the ice bath was removed and replaced with an oil bath at 55°C and stirred for 1 hr. The solution was allowed to cool back to room temperature and then THF was added (10 mL). Hydrazone **1** (5.06 g, 0.021 mol, 1.0 equivalent) was dissolved in THF (20 mL) in separate flame-dried Schlenk flask. The hydrazone solution was then cannula transferred into the flask with formic acetic anhydride. The reaction was allowed to stir at room temperature until completion. All volatiles were then removed *in vacuo* to yield **2** as a white solid. Yield 5.2 g (93.06%). ¹H NMR (500 MHz, CDCl₃) δ = 8.09 (s, 1H), 7.96 (dd, 2H, J=1.4, 7.1Hz), 7.55 (tt, 1H, J= 1.2, 7.4Hz), 7.46 (t, 1H, J=7.7H), 7.18 (t, 2H, J=7.3Hz), 7.02 (m, 4H), 3.56 (sept, 1H, J=6.8Hz), 1.19 (d, 6H, J=6.8Hz) ¹³C {¹H} NMR (125 MHz, C₆D₆) δ = 186.2, 156.0, 141.1, 136.1, 132.9, 129.4, 128.7, 127.9, 125.9, 120.7, 37.4, 20.1.

Attempt to synthesize hemiaminal **5** from N-formyl hydrazone **2**: To a flame-dried 100 mL Schlenk flask equipped with a magnetic stir bar, KHMDS (1.71 g, 8.50 mmol, 1.5 equivalents) was added in a glovebox. The flask was taken out of the glovebox and THF (10 mL) was added and the solution was cooled on dry ice-acetone bath to -78°C. To the cooled flask, hydrazone **2** (1.51 mL, 5.67 mmol, 1.0 equivalent) was added via needle and syringe. The dry ice bath was removed and the reaction was stirred overnight. A crude sample taken to measure reaction progress by NMR showed the presence of hydrazone **1**.

Attempt to synthesize hemiaminal **5** from hydrazone **1**: To a flame-dried 100 mL Schlenk flask equipped with a magnetic stir bar, hydrazone **1** (2.66 mL, 0.008 mol, 1.0 equivalent) and Et₂O (20 mL) were added and then cooled to -78°C in a dry ice-acetone bath. While stirring, n-BuLi (2.5 M in hexanes, 10.5 mL, 0.019 mol, 2.2 equivalents) was added dropwise. During addition, the solution evolved gas. After completion of addition, the reaction was stirred for 1 hr. To the solution, ethyl formate (1.0 mL, 0.013, 1.5 equivalents) was added. The solution was

brought to stir at room temperature and stirred for 6 hrs. A crude sample taken to measure reaction progress by NMR showed the presence of hydrazone **1**.

3: To a flame-dried 250 mL Schlenk flask equipped with a stir bar, diisopropylamine (12.5 mL, 0.089 mol) and dry THF (50 mL) were added, and then cooled on a dry ice-acetone bath to approximately -80°C. nBuLi in hexanes (2.5 M, 35.7 mL, 0.089 mol) was added slowly via syringe and needle. The reaction was removed from the acetone bath and stirred at room temperature for 45 minutes, then cooled to -80°C. To a separate flame-dried Schlenk flask, ethyl isobutyrate (15 mL, 0.112 mol) and dry THF (20 mL) were added and mixed. The ester solution was then cannula transferred into the 250 mL flask containing LDA. The resulting solution was removed from the acetone bath and stirred at room temperature for 1 hour. In a separate Schlenk flask, benzoyl chloride (8.75 mL, 0.075 mol) and dry THF (50 mL) were added and mixed. The benzoyl chloride solution was then slowly cannula transferred into the 250 mL flask. The flask was then allowed to slowly warm up to room temperature and stirred overnight. The reaction was quenched with 100 mL water, then extracted with Et₂O (3 x 50 mL). The organic layer was then washed with water (2 x 25 mL) and dried with brine (1 x 25 mL) and MgSO₄. The solution was filtered, and all volatiles were removed in vacuo to yield **3** as a viscous yellow liquid (~90% yield, with residual THF). ¹H NMR (500 MHz, CDCl₃) δ = 7.83 (d, 2H, J=7.0Hz), 7.51 (t, 1H, J=7.0Hz), 7.41 (t, 2H, J=7.5Hz), 4.10 (q, 2H, J=7.3Hz), 1.53 (s, 6H), 1.03 (t, 3H, J=7.3Hz) ¹³C {¹H} NMR (125 MHz, C₆D₆) δ = 197.9, 175.2, 135.3, 132.8, 128.8, 128.5, 61.5, 53.4, 24.05, 24.01.

4: To a 100 mL round bottom flask equipped with a stir bar, phenylhydrazine (7.36 mL, 0.075 mol), **3** (15.00 g, 0.068 mol), and acetic acid (60 mL) were added, and the flask was equipped with a reflux condenser and external bubbler. The reaction was then and heated to

130°C with stirring overnight. Upon cooling to room temperature, the reaction was diluted with Et₂O (100mL) and the entire solution was washed with water (2 x 100 mL), the dried with brine (1 x 30 mL) and Na₂SO₄, filtered, and all volatiles were removed in vacuo. The resulting crude product was recrystallized from hot MeOH and water to yield **4** as an off white solid. The mother liquor can yield a second batch of recrystallized product, but with more impurities. Yield 4.25g (23.6% yield). ¹H-NMR (500MHz, CDCl₃): δ 8.068 (d, 2H, J=7.6Hz), 7.91-7.95 (m, 2H), 7.42-7.49 (m, 5H), 7.23 (t, 1H, J=7.4Hz), 1.61 (s, 6H). ¹³C-NMR (125MHz, CDCl₃): δ 177.4, 162.4, 138.3, 130.7, 130.5, 129.0, 128.9, 126.7, 125.3, 118.07, 49.9, 23.1.

5: To a flame-dried 100 mL Schlenk flask equipped with a stir bar, pyrazolone **4** (3.00 g, 0.011 mol) and LAH (0.107 g, 0.003 mmol) or LiBHET₃ (1 M in THF, 11 mL, 0.011 mol) were added in the glovebox. The flask was brought out of the box, attached to a Schlenk line, and cooled on an ice-water bath to approximately 0°C. Dry Et₂O (30 mL) was added. The reaction was stirred on ice bath for 2 hours. The reaction was quenched with EtOAc (10 mL) and then water (10 mL) and the left to stir for at least 30 minutes. The resulting slurry was filtered over celite on a frit, washing the cake with Et₂O (2 x 10 mL). The organic phase was separated from the aqueous, then dried with brine (1 x 15 mL) and MgSO₄. The solids were filtered off and volatiles were removed in vacuo. The crude product was purified by layering pentane over the crude or by recrystallization from pentane to yield hemiaminal **5** as an off white solid. The mother liquor can yield a second batch of product with reduced purity. *Caution: hemiaminal 5 is unstable in halogenated solvents exposed to oxygen, slowly transforming into a deep purple molecule whose identity is yet to be determined.* Yield 1.40g (41% yield). ¹H-NMR (500MHz, CDCl₃): δ 7.79 (d, 2H, J=7.9Hz), 7.30-7.42 (m, 6H), 6.93 (t, 1H, J=6.4Hz), 5.25 (d, 1H,

J=7.6Hz), 2.43 (br d, 1H, J=7.7Hz), 1.47 (s, 3H), 1.43 (s, 3H). ^{13}C -NMR (125MHz, CDCl_3): δ 153.6, 143.3, 132.0, 129.4, 128.8, 128.6, 126.8, 120.4, 114.2, 92.4, 51.3, 25.3, 18.0.

6: To a flame-dried 50 mL Schlenk flask equipped with stir bar, hemiaminal **5** (1.00 g, 3.75 mmol) and dry Et_2O (20 mL) were added, then cooled on a water-ice bath to approximately 0°C . Tf_2O (0.63 mL, 3.75 mmol) was added dropwise to the solution and continued to be stirred at 0°C for 15 minutes before removing the ice bath and stirring at room temperature for 1 hour to yield a faintly green suspension. The reaction was filtered using an oven-dried filter cannula, then washed with dry Et_2O (2 x 10 mL). The resulting off white solid **6** was dried thoroughly under vacuum before being brought into the glovebox. Yield 1.40g (93.6% yield). ^1H -NMR (500MHz, CDCl_3): δ 10.74 (s, 1H), 8.27 (m, 2H), 8.13 (d, 2H, J=8.4Hz), 7.74 (t, 1H, J=7.4Hz), 7.62-7.69 (m, 5H), 2.04 (s, 6H). ^{13}C -NMR (125MHz, CDCl_3): δ 183.9, 171.2, 135.4, 135.0, 133.4, 130.6, 129.9, 129.3, 125.9, 122.4, 120.7, 63.6, 21.2. ^{19}F -NMR (376MHz, CDCl_3): δ -78.3.

7: Pyrazolinium **6** was left in a sealed vial in the glovebox for seven days, slowly converting from an off-white powder to a red solid. *Alternatively: Pyrazolinium 6 (100 mg) was added to a Schlenk flask containing a magnetic stir bar and toluene (10 mL) and the solution was heated on an oil bath at 120°C overnight. All volatiles were removed in vacuo to give **7^{HOTf}** in quantitative yield.* ^1H -NMR (400MHz, CD_2Cl_2): δ 7.55-7.58 (m, 5H), 7.48-7.51 (m, 3H), 7.40-7.44 (m, 2H), 2.31 (s, 3H), 2.23 (s, 3H). ^{13}C -NMR (100MHz, CD_2Cl_2): δ 152.5, 141.7, 138.1, 131.4, 130.6, 130.3, 129.8, 129.4, 128.8, 126.7, 114.3, 11.1, 8.0.

8: In an Ar-filled glovebox, pyrazolinium **6** (1.00 g, 2.01 mmol, 1 equiv.) and KHMDS (0.50 g, 2.01 mmol, 1.0 equiv.) were added to a 100 mL Schlenk flask equipped with a magnetic stir bar. The flask was brought out of the glovebox, connected to a Schlenk line, and cooled to 0°C on a water-ice bath. To the flask, dry Et_2O (60 mL) was added. The reaction was stirred

overnight at room temperature with the flask open to the Schlenk line. Upon completion, the solution was filtered and then washed with water (2 x 20 mL). The organic layer was separated and dried with MgSO₄ and filtered. All volatiles were removed in vacuo with a Schlenk vacuum. The resulting yellow oil was stored in a glovebox until further use. Yield 0.56 g (57.7% yield). ¹H-NMR (500MHz, C₆D₆): δ 7.70 (d, 4H, J=7.2Hz), 7.00-7.09 (m, 8H) 6.93 (t, 4H, J=7.6Hz), 6.85 (d, 4H, J=7.0Hz), 6.68 (t, 2h, J=7.6Hz), 1.50 (s, 6H), 1.25 (s, 6H). ¹³C-NMR (125MHz, C₆D₆): δ 159.2, 140.9, 132.3, 128.8, 128.7, 127.7, 127.2, 121.5, 119.0, 52.1, 26.6, 26.2.

9: To a flame-dried 50 mL Schlenk flask equipped with magnetic stir bar, pyrazolinium **6** (0.100 g, 0.251 mmol, 1.0 equivalent) and NaOMe (0.020 g, 0.376 mmol, 1.5 equivalent) were added in a glovebox. The Schlenk flask was brought out of the glovebox and MeOH (10 mL) was added to the flask. After stirring for 1 hr, all volatiles were removed *in vacuo*. DCM (10 mL) was added to the residue, filtered, and then all volatiles were removed *in vacuo* to give **9**. Yield 0.053 g (75.71%). ¹H-NMR (500MHz, CDCl₃): δ 7.80 (d, 2H, J=6.6Hz), 7.27-7.41 (m, 9H) 6.93 (m, 1H), 5.11 (s, 1H), 3.19 (s, 3H), 1.52 (s, 3H), 1.44 (s, 3H). ¹³C-NMR (125MHz, CDCl₃): δ 156.0, 143.9, 132.0, 129.5, 128.8, 127.0, 120.3, 114.0, 97.9, 54.3, 50.8, 26.9, 17.6.

Attempt to obtain free EndersCAAC from **9** via vacuum pyrolysis: To a flame-dried 50 mL Schlenk flask equipped with magnetic stir bar, adduct **9** (0.053 g, 0.189 mmol, 1.0 equivalent) was added. The Schlenk flask was brought out and attached to a Schlenk line vacuum and the flask was heated at 130°C overnight. Upon cooling to room temperature, a dark color residue was observed.

10: To a flame-dried 100 mL Schlenk flask equipped with magnetic stir bar, pyrazole **4** (0.500 g, 1.89 mol, 1.0 equivalent) and Woollin's reagent (1.365 g, 2.57 mmol, 1.35 equivalents) were added in a glovebox. The Schlenk flask was brought out of the glovebox and PhMe (10

mL) was added to the flask. The flask was stirred for 48 hr at 130°C. Upon cooling to room temperature, the reaction was filtered. All volatiles were removed *in vacuo* to yield **10**. Yield 0.601 g (97.09% yield). ¹H-NMR (500MHz, CDCl₃): δ 8.12 (d, 2H, J=8.0Hz), 8.00 (d, 2H, J=7.7Hz), 7.48-7.54 (m, 4H), 7.25 (d, 2H, J=7.2Hz), 1.72 (s, 6H). ¹³C-NMR (125MHz, CDCl₃): δ 206.8, 172.8, 138.4, 131.2, 130.8, 130.5, 128.5, 127.5, 125.2, 124.9, 67.8, 27.1. ⁷⁷Se-NMR (76MHz, CDCl₃): δ 501.

Attempt to obtain free EndersCAAC from selenium-exchange reaction between **10** and free ^{Et}CAAC: To a flame-dried 50 mL Schlenk flask equipped with magnetic stir bar, adduct **10** (0.100 g, 0.306 mmol, 1.0 equivalent) and ^{Et}CAAC (0.095 g, 0.306 mmol, 1.0 equivalent) were added. The Schlenk flask was brought out and THF (10 mL) was added. The reaction was stirred for 1 hr at room temperature. An aliquot was taken to monitor the reaction by NMR.

^{Et}CAAC(Se) was observed (¹³C-NMR: δ217 ppm) and the disappearance of **10** was observed as well, however, the resulting spectrum contained multiple unknown species.

11: To a flame-dried 500 mL Schlenk flask equipped with a large magnetic stir bar, magnesium turnings (0.966 g, 0.039 mol, 2.5 equivalents) was added and the flask was evacuated and refilled twice with Ar. THF (50 mL) was then added. To the flask, 2,4,6-triisopropylbromobenzene (4.5 g, 0.016 mol, 1.0 equivalent) was added dropwise. If Grignard formation appeared to form slowly, two drops of 1,2-dibromoethane was added. Upon completion of addition, a condenser connected to the Schlenk line was attached and the reaction was heated at reflux for 4 hrs. The reaction was then brought to room temperature. In a separate flame-dried 100 mL Schlenk flask, (BocN)₂ (3.65 g, 0.016 mol, 1.0 equivalent) dissolved in THF (25 mL) and both flasks were cooled to -78°C. The Grignard solution was cannula transferred into the (BocN)₂ while stirring. The reaction was stirred for 1 hr before it was quenched with

AcOH (0.9 mL, 1.0 equivalent). The solution was then brought to room temperature and Et₂O (100 mL) and water (30 mL) were added. The organic phase was separated from the aqueous phase, dried with brine (20 mL), dried with MgSO₄, and filtered. All volatiles were removed *in vacuo* on a rotovap to yield a crude off-white solid.

To a flame-dried 100 mL Schlenk flask equipped with a large magnetic stir bar, the off-white solid (0.966 g, 0.039 mol, 2.5 equivalents) was added and the flask was evacuated and refilled twice with Ar. HCl in dioxanes (20 mL) was then added and the reaction stirred for 2 hours. The solution was then filtered and the solids washed with Et₂O (2 x 20 mL) to yield **11^{HCl}**. Yield 1.82 g (42.01% yield). NMR matched literature reported values.²⁶

12: To a 100 mL round bottom flask with a large magnetic stir bar, 2,6-dimethylaniline (5.10 mL, 0.041 mol, 1.0 equivalents), HCl (37% aqueous, 10.3 mL), and water (12 mL) were added and cooled on a water-ice bath. The flask was equipped with an addition funnel and a solution of NaNO₂ (3.20 g, 0.046 mol, 1.125 equivalents) in water (20 mL) was added dropwise into the aniline solution, taking care to not let the reaction heat up too much. Upon completion of addition, the reaction was stirred for 1 hr on ice, eventually solidifying into a red solid. Separately, in a 250 mL round bottom flask with a large magnetic stir bar, SnCl₂ dihydrate (18.71 g, 0.083 mol, 2.0 equivalents), HCl (30.9 mL), and water (12 mL) were added and cooled on ice. The contents of the aniline-diazonium flask were quickly added to the SnCl₂ flask, immediately becoming a pale yellow solid. The mixture was stirred overnight at room temperature. The reaction was then filtered and the solids washed with brine (2 x 10 mL). The solids were then thoroughly dried to yield **12^{HCl}**. Yield 3.21 g (44.89% yield). NMR matched literature reported values.²⁷

13: To a 100 mL round bottom flask equipped with a stir bar, hydrazine monohydrate (2.00 mL, 0.031 mol, 1.0 equivalent), ketoester **4** (6.82 g, 0.031 mol, 1.0 equivalent), and EtOH (40 mL) were added, and the flask was equipped with a reflux condenser and external bubbler. The reaction was then heated to 90°C with stirring overnight. Upon cooling to room temperature, all volatiles were removed *in vacuo*. The residue was dissolved in DCM (40 mL) washed with water (1 x 30 mL) and then dried with brine (1 x 30 mL) and Na₂SO₄. The solution was then filtered, and all volatiles were removed *in vacuo* to yield **13** as a white solid. Yield 5.11 g (87.64% yield). ¹H-NMR (500MHz, CDCl₃): δ 9.44 (br s, 1H), 7.79 (m, 2H), 7.42 (m, 3H), 1.51 (s, 6H). ¹³C-NMR (125MHz, CDCl₃): δ 181.2, 162.6, 131.35, 129.8, 128.7, 127.0, 51.4, 22.7.

14: To a flame-dried 250 mL Schlenk flask equipped with a stir bar, diisopropylamine (12.5 mL, 0.089 mol, 1.2 equivalent) and dry THF (50 mL) were added, and then cooled on a dry ice-acetone bath to approximately -80°C. nBuLi in hexanes (2.5 M in hexanes, 35.7 mL, 0.089 mol, 1.2 equivalents) was added slowly via syringe and needle. The reaction was removed from the acetone bath and stirred at room temperature for 45 minutes, then cooled to -80°C. To a separate flame-dried Schlenk flask, methyl cyclohexylcarboxylate (10.6 g, 0.074 mol, 1.0 equivalent) and dry THF (20 mL) were added and mixed. The ester solution was then cannula transferred into the 250 mL flask containing LDA. The resulting solution was removed from the acetone bath and stirred at room temperature for 1 hour. In a separate Schlenk flask, benzoyl chloride (8.75 mL, 0.075 mol) and dry THF (50 mL) were added and mixed. The benzoyl chloride solution was then slowly cannula transferred into the 250 mL flask. The flask was then allowed to slowly warm up to room temperature and stirred overnight. The reaction was quenched with 100 mL water, then extracted with Et₂O (3 x 50 mL). The organic layer was then

washed with water (2 x 25 mL) and dried with brine (1 x 25 mL) and MgSO₄. The solution was filtered, and all volatiles were removed in vacuo to yield **3** as a viscous yellow liquid (~56% yield, with residual THF). ¹H NMR (500 MHz, CDCl₃) δ = 7.77 (d, 2H, J=7.1Hz), 7.49 (t, 1H, J=7.1Hz), 7.39 (t, 2H, J=7.5Hz), 3.64 (s, 6H), 1.40-1.65 (m, 10H). ¹³C {¹H} NMR (125 MHz, C₆D₆) δ = 198.4, 174.5, 136.2, 132.5, 128.5, 128.4, 58.1, 52.6, 32.5, 25.5, 22.4.

15: To a 100 mL round bottom flask equipped with a stir bar, phenylhydrazine (7.36 mL, 0.075 mol), ethyl benzoacetate (11.78 mL, 0.068 mol), and EtOH (100 mL) were added and stirred overnight at 50°C. Upon cooling to room temperature, the reaction was filtered and the solids were washed with cold EtOH. The yellow solid was then thoroughly dried to yield **15**. Yield 13.08 g (81.44% yield). The resulting crude product was recrystallized from hot MeOH and water to yield **4** as an off white solid. The mother liquor can yield a second batch of recrystallized product, but with more impurities. Yield 4.25g (23.6% yield). NMR matched literature reported values.³²

16: To a 250 mL round bottom flask equipped with a stir bar, pyrazolone **15** (3.00 g, 0.013 mol, 1.0 equivalent), NaOH (0.56 g, 0.014 mol, 1.1 equivalents), 1,5-dibromopentane (1.90 mL, 0.015 mol, 1.2 equivalents), THF (80 mL), and DMSO (20 mL) were added and stirred for 16 hr at 40°C. Upon cooling to room temperature, the reaction was filtered and volatiles were removed *in vacuo* to yield **16** as a viscous oil. Yield 2.13 g (42.59% yield). ¹H NMR (500 MHz, CDCl₃) δ = 7.85 (d, 2H, J=8.0Hz), 7.78 (d, 2H, J=8.0Hz), 7.38-7.44 (m, 4H), 7.34 (t, 2H, J=7.2Hz), 5.97 (s, 1H), 4.25 (m, 2H), 3.45 (m, 2H), 2.03 (m, 4H), 1.85 (m, 2H). ¹³C {¹H} NMR (125 MHz, C₆D₆) δ = 155.1, 150.7, 138.7, 133.4, 129.0, 128.7, 128.3, 126.5, 125., 122.2, 71.8, 32.8, 31.0, 29.3, 27.7, 25.9.

17: To a 250 mL round bottom flask equipped with a stir bar, pyrazolone **15** (2.00 g, 8.46 mmol, 1.0 equivalent), LiOH (0.24 g, 9.31 mmol, 1.1 equivalents), 1,4-dibromobutane (1.30 mL, 10.15 mmol, 1.2 equivalents), and THF (50 mL) were added and stirred for 16 hr at 40°C. Upon cooling to room temperature, the reaction was filtered and volatiles were removed *in vacuo* to yield **17** as a solid. Yield 0.87 g (37.34% yield). ¹H NMR (500 MHz, CDCl₃) δ = 8.03 (d, 2H, J=9.0Hz), 7.85-7.87 (m, 2H), 7.41-7.47 (m, 5H), 7.20 (t, 1H, J=7.3Hz), 3.19 (m, 4H), 2.05 (m, 2H), 1.85 (m, 2H). ¹³C {¹H} NMR (125 MHz, C₆D₆) δ = 162.1, 130.4, 130.3, 128.9, 128.9, 126.1, 125.1, 119.2, 118.9, 68.1, 58.1 36.5, 33.9.

18: To a 500 mL round bottom flask equipped with a magnetic stir bar, benzoyl chloride (6.55 mL, 0.056 mol, 1.05 equivalents) was added dropwise to a stirred solution of aniline (4.9 mL, 0.054 mol, 1.0 equivalent) and NEt₃ (10.72 mL, 0.076 mol, 1.5 equivalents) in DCM and stirred for two hours at room temperature. The reaction was diluted with water. The organic phase was separated and the aqueous phase was extracted with DCM (3 x 100 mL). The organic phases were combined and washed with HCl (aq, 1 M, 100 mL) and saturated NaHCO₃ (1 x 100 mL). The organic phase was then dried with MgSO₄ and filtered. All volatiles were evaporated *in vacuo* on a rotovap. The crude solids were thoroughly washed with hexanes and then dried to yield **18**. Yield 8.01 g (72.55%). NMR matched literature reported values.³³

19: In a flamed-dried 100 mL round bottom flask equipped with magnetic stirbar, benzanilide **18** (1.00 g, 5.07 mmol, 1.0 equivalents), DMAP (0.031 g, 0.25mol, 0.05 equivalents), NEt₃ (1.06 mL, 7.60 mmol, 1.5 equivalents), and THF (30 mL) were added and cooled to 0°C. To the stirring solution, 2-bromo-2-methylpropanoyl bromide (0.94 mL, 7.60 mmol, 1.5 equivalents) was added dropwise. Upon completion of addition, the reaction was stirred at 60°C for 2 days. The reaction was quenched with water (30 mL) and extracted with

EtOAc (3 x 20 mL). The organic phase was separated and dried with brine (20 mL) and MgSO₄. The solution was then filtered through a short pad of celite before immediately being used.

20: In a flamed-dried 100 mL round bottom flask equipped with magnetic stirbar, imide **19** and DMSO (15 mL) were added. To the stirring solution, NaN₃ (0.989 g, 15.21 mmol, 3.0 equivalents) was added in one portion. The reaction was stirred at room temperature for 1 day. Upon cooling to room temperature, the reaction was quenched with water (50 mL) and the mixture was extracted with EtOAc (3 x 50 mL). The organic phases were combined and dried with brine (2 x 50 mL) and MgSO₄. The solution was then filtered and all volatiles removed *in vacuo*. The resulting residue was purified by trituration in hexanes (3 x 20 mL) to yield **20** as a white solid. Yield 0.208 g from **18** (13.31% yield).

21: In a 50 mL round bottom flask equipped with magnetic stirbar, azido **20** (0.208 g, 0.66 mmol, 1.0 equivalent) and PhMe (10 mL) were added. To the stirring solution, triphenylphosphine (0.42 g, 0.73 mmol, 1.1 equivalents) was added in one portion. The reaction was stirred at 80°C for 2 days. Upon cooling to room temperature, all volatiles were removed *in vacuo* and the residue was purified with a short silica column (1:1 hexanes/EtOAc) to yield **21** as a white solid. Yield 0.129 g (74% yield).

22: To a 250 mL round bottom flask equipped with a stir bar, 2,6-diisopropylaniline (10 mL, 0.053 mol, 1.0 equivalent) and toluene (60 mL). To the solution, benzoyl chloride (6.5 mL, 0.053 mol, 1.0 equivalent) was added all at once. The flask was then equipped with a condenser connected to an external bubbler and placed in an oil bath heated to 130°C. The reaction was stirred overnight. Upon cooling to room temperature, all volatiles were removed *in vacuo* on a rotovap. The resulting crude solid was recrystallized from EtOH. The solid was then dried

thoroughly on a vacuum line to yield **22** as a white solid. Yield 13.12 g (87.94% yield). NMR matched literature reported values.³⁴

24: To a 250 mL round bottom flask equipped with a stir bar, amino acid **23** (5.0 g, 0.049 mol) and MeOH (50 mL) were added, and the flask was cooled with a brine-ice bath to approximately 0°C. Using an addition funnel equipped with an external bubbler, SOCl₂ (7.00 mL, 0.097 mol) was added dropwise. Upon the completion of adding SOCl₂, the addition funnel was exchanged for a reflux condenser attached to an external bubbler and the reaction was stirred at 0°C for an additional 30 minutes. The ice bath was removed, and the reaction was heated at reflux for 2 hours. All volatiles were removed using a rotovap with the water bath at 60°C, scrapping the flask every so often. *Caution: do not use high vacuum in order to protect the rotovap vacuum pump.* CHCl₃ (10 mL) was then added to dissolve the crude product and the flask was heated to reflux for 15 minutes. Once more, all volatiles were removed via rotovap to yield **24** as a white solid. Yield 6.51 g (87.3% yield). ¹H-NMR (500MHz, CDCl₃): δ 8.97 (s, 3H), 3.82 (s, 3H), 1.73 (s, 6H). ¹³C-NMR (125MHz, CDCl₃): δ 171.8, 57.6, 53.6, 24.1.

25: To a flame-dried 100 mL Schlenk flask equipped with a stir bar, benzamide **22** (7.48 g, 0.027 mol) and SOCl₂ (11 mL, 0.159 mol) were added at room temperature. Upon completion of addition, the Schlenk flask was equipped with a reflux condenser attached to an external bubbler, then heated to 80°C for 2 hours. The reflux condenser was removed, and all volatiles were thoroughly removed using Schlenk line vacuum to yield a viscous yellow liquid. After removal of all volatiles, CHCl₃ (20 mL) was added to the imidoyl chloride intermediate. To a separate flame-dried 250mL Schlenk flask equipped with a stir bar, amino ester **24** (4.08 g, 0.027 mol) was added and dried under vacuum at 60°C for 1 hour. To the 250 mL flask, CHCl₃ (80 mL) and dry NEt₃ (11.1 mL, 0.079 mol, 3 equivalents) were added and the resulting suspension

was stirred at 0°C on an ice bath. The imidoyl chloride solution was added to the larger flask using cannula transfer. Upon completion of addition, the ice bath removed and the reaction was stirred overnight. The reaction was quenched with water (30 mL) and washed with 1 M HCl (1 x 30 mL), saturated NaHCO₃ solution (1 x 50 mL). The organic phase was then dried with brine (1 x 30 mL) and MgSO₄ before being filtered and all volatiles removed via rotovap to yield **25** as an off white powder. Yield 9.29 g (91.8% yield). ¹H-NMR (500MHz, CDCl₃): δ 7.19 (m, 5H), 6.91 (m, 3H), 4.93 (s, 1H), 3.75 (s, 3H), 2.99, (sept, 2H), 1.70 (s, 6H), 1.10 (d, 6H), 0.87 (d, 6H). ¹³C-NMR (125MHz, CDCl₃): δ 175.7, 152.5, 145.3, 138.5, 129.4, 128.2, 128.1, 122.6, 121.9, 56.7, 52.41, 27.9, 25.7, 24.8.

26: To a flame-dried 100 mL pressure Schlenk flask equipped with stir bar, amidine **25** was added and dried under vacuum for 30 minutes. To the flask, HCl in Et₂O (20 mL) was added via cannula and the flask was sealed. The flask was heated to 60°C overnight with stirring. *Caution: use a blast shield as an added safety measure.* The reaction was cooled to room temperature and transferred to a 10 0mL beaker containing a stir bar and saturated Na₂CO₃ solution (40 mL) and stirred for 30 minutes. The organic phase was separated, and the aqueous layer washed with Et₂O (1x 30 mL). The organics were combined and dried with brine (1 x 15mL) and MgSO₄, filtered, and all volatiles removed via rotovap to yield **26** as a white solid. Yield 3.25 g (71.3% yield). ¹H-NMR (500MHz, CDCl₃): δ 7.33-7.42 (m, 4H), 7.19-7.23 (m, 4H), 2.73 (sept, 2H), 1.56 (s, 6H), 1.15 (d, 6H), 0.93 (d, 6H). ¹³C-NMR (125MHz, CDCl₃): δ 186.5, 159.9, 146.5, 131.1, 130.2, 129.4, 129.4, 128.3, 124.4, 67.5, 28.9, 24.7, 24.5, 22.8.

27: To a flame-dried 100mL Schlenk flask equipped with a stir bar, imidazolone **26** (0.50 g, 2.68 mmol, 1.0 equivalents) and THF (20 mL) were added and was placed in a room temperature water bath. To the flask, DIBAL (1.0 M, 4.3 mL, 4.30 mmol, 1.5 equivalents) was

added dropwise via needle and syringe. Upon completion of addition, the reaction flask was removed from the water bath and placed in an oil bath at 60°C and stirred overnight. Upon reaction completion and cooling to approximately 0°C in a water-ice bath, EtOAc was added dropwise until excess DIBAL was quenched. Water (10 mL) and Et₂O (50mL) was added and the entire solution was filtered to remove aluminum salts. The solution was washed with water (1 x 30 mL) and the organic phase was separated from the aqueous phase. The organic phase was then dried with MgSO₄ and filtered. All remaining volatiles were removed *in vacuo* to yield **27** as a white solid. Yield 0.14 g (28.01% yield). ¹H-NMR (500MHz, CDCl₃): δ 7.33-7.42 (m, 3H), 7.18-7.24 (m, 5H), 5.35 (s, 1H), 2.72 (sept, 2H, J=6.8Hz), 1.54 (s, 6H), 1.14 (d, 6H, J=6.8Hz), 0.93 (d, 6H, J=6.8Hz). ¹³C-NMR (125MHz, CDCl₃): δ 160.04, 145.49, 131.2, 130.1, 129.3, 128.3, 124.4, 94.9, 49.5, 28.9, 24.8, 24.5, 22.8.

3.5.3 Computational Data

All calculations were performed with the Gaussian16 program package.³⁵ The theoretical approach is based on the framework of density functional theory (DFT). All calculations were performed with either the B3LYP³⁶ or MO-62X³⁷ functional and employing Pople *et al*'s 6-31G basis set³⁸ and Ahlrichs *et al*'s TZVP basis set.³⁹ The Gibbs energy corrections from frequency calculations and dispersion corrections were added to the single-point energies to obtain the Gibbs free energies in solution. Gibbs free reaction energies and enthalpies were calculated for standard conditions ($P = 1 \text{ atm}$, $T = 298 \text{ K}$) and are unscaled.

Table 3.1. DFT Calculated Thermodynamic Data of EndersCAAC and IsoEndersCAAC. Calculated at MO-62x//def2-TZVP.

Molecule	Thermodynamic Data
EndersCAAC	Zero-point correction= 0.353849 (Hartree/Particle)
	Thermal correction to Energy= 0.371528
	Thermal correction to Enthalpy= 0.372472
	Thermal correction to Gibbs Free Energy= 0.306880
	Sum of electronic and zero-point Energies= -883.273212
	Sum of electronic and thermal Energies= -883.255533
	Sum of electronic and thermal Enthalpies= -883.254589
	Sum of electronic and thermal Free Energies= -883.320181
IsoEndersCAAC	Zero-point correction= 0.183071 (Hartree/Particle)
	Thermal correction to Energy= 0.191987
	Thermal correction to Enthalpy= 0.192931
	Thermal correction to Gibbs Free Energy= 0.150069
	Sum of electronic and zero-point Energies= -383.193261
	Sum of electronic and thermal Energies= -383.184345
	Sum of electronic and thermal Enthalpies= -383.183401
	Sum of electronic and thermal Free Energies= -383.226263

Table 3.2. DFT Calculated Geometric Data of EndersCAAC and IsoEndersCAAC. Calculated at MO-62x//def2-TZVP.

Molecule	Geometric Data
EndersCAAC	N 0.38525 -1.04115 0.00003
	C -0.75399 -0.43284 0.00002
	N 1.37217 0.01105 -0.00001
	C -0.57034 1.09226 0.00001
	C 0.93844 1.25361 -0.00003
	C -1.99915 -1.22723 -0.00003
	C 2.74401 -0.40748 -0.00001
	C 3.74714 0.56824 -0.00064
	C 3.07503 -1.76458 0.00062
	C 4.41947 -2.14073 0.00063
	C 5.42688 -1.17725 0.00001
	C 5.08261 0.17748 -0.00062
	H 5.85907 0.93689 -0.00111
	H 3.45240 1.61069 -0.00110
	H 6.47066 -1.47650 0.00002
	H 4.67464 -3.19639 0.00112
	H 2.28785 -2.50635 0.00109
	C -1.92184 -2.63501 -0.00030
	C -3.27317 -0.63408 0.00017
	C -4.42753 -1.41794 0.00012
	C -4.33364 -2.80806 -0.00014
	C -3.07291 -3.41311 -0.00035
	H -0.94343 -3.10107 -0.00048
	H -2.98910 -4.49591 -0.00056
	H -5.40076 -0.93633 0.00028
	H -5.23276 -3.41708 -0.00018
	H -3.37555 0.44332 0.00038
	C -1.14292 1.76634 -1.28590
	C -1.14273 1.76631 1.28605

Table 3.2. DFT Calculated Geometric Data of EndersCAAC and IsoEndersCAAC. Calculated at MO-62x//def2-TZVP (Continued).

	C -0.98198 3.29318 1.26580 H -0.64193 1.34254 2.16400 H -2.20403 1.51076 1.38221 C -0.98216 3.29321 -1.26564 H -2.20424 1.51079 -1.38191 H -0.64226 1.34259 -2.16394 C -1.59066 3.91205 0.00013 H -1.45418 3.71476 -2.16146 H 0.08392 3.53836 -1.31251 H -2.67946 3.75289 0.00021 H -1.43661 4.99745 0.00013 H 0.08411 3.53833 1.31252 H -1.45387 3.71471 2.16170
IsoEndersCAAC	C -0.83262 0.73068 -0.00001 N 0.34919 1.16536 -0.00001 N -0.87054 -0.71953 -0.00001 C 0.33137 -1.25012 -0.00002 C 1.22080 -0.02734 0.00000 C -2.09984 -1.50508 -0.00001 H -2.96809 -0.85179 0.00001 H -2.12487 -2.13630 0.88439 H -2.12489 -2.13628 -0.88442 C -2.08095 1.54144 0.00001 H -1.81257 2.59339 0.00001 H -2.68584 1.32480 0.88157 H -2.68585 1.32480 -0.88154 C 2.08638 -0.01182 1.25960 H 1.46469 -0.02423 2.15503 H 2.69271 0.89333 1.26927 H 2.73358 -0.88678 1.27287 C 2.08643 -0.01179 -1.25957 H 1.46479 -0.02418 -2.15502 H 2.73363 -0.88675 -1.27283 H 2.69276 0.89336 -1.26919

3.6 Acknowledgements

Chapter 3, in part, is as of publication of this dissertation, currently ongoing as a project between Victor T. Wang, Mohand Melaïmi, and Guy Bertrand. Without the input and assistance of Mohand Melaïmi and Guy Bertrand, this project would not have gone this far. Additionally, this chapter contains unpublished work by Nahal Soltani who paved the initial route to the

EndersCAAC iminium. Finally, this chapter contains unpublished work by Vojtech Docekal who solved how to get to the isoEndersCAAC hemiaminal.

3.7 References

- (1) Melaimi, M.; Jazzar, R.; Soleilhavoup, M.; Bertrand, G. Cyclic (Alkyl)(Amino)Carbenes (CAACs): Recent Developments. *Angew. Chem. - Int. Ed.* **2017**, *56* (34), 10046–10068. <https://doi.org/10.1002/anie.201702148>.
- (2) Proetto, M. T.; Alexander, K.; Melaimi, M.; Bertrand, G.; Gianneschi, N. C. Cyclic (Alkyl)(Amino)Carbene (CAAC) Gold(I) Complexes as Chemotherapeutic Agents. *Chem. – Eur. J.* **2021**, *27* (11), 3772–3778. <https://doi.org/10.1002/chem.202004317>.
- (3) Ung, G.; Rittle, J.; Soleilhavoup, M.; Bertrand, G.; Peters, J. C. Two-Coordinate Fe⁰ and Co⁰ Complexes Supported by Cyclic (Alkyl)(Amino)Carbenes. *Angew. Chem. - Int. Ed.* **2014**, *53* (32), 8427–8431. <https://doi.org/10.1002/anie.201404078>.
- (4) Arrowsmith, M.; Braunschweig, H.; Celik, M. A.; Dellermann, T.; Dewhurst, R. D.; Ewing, W. C.; Hammond, K.; Kramer, T.; Krummenacher, I.; Mies, J.; Radacki, K.; Schuster, J. K. Neutral Zero-Valent s-Block Complexes with Strong Multiple Bonding. *Nat. Chem.* **2016**, *8* (9), 890–894. <https://doi.org/10.1038/nchem.2542>.
- (5) Hoffmann, R. Building Bridges Between Inorganic and Organic Chemistry (Nobel Lecture). *Angew. Chem. Int. Ed. Engl.* **1982**, *21* (10), 711–724. <https://doi.org/10.1002/anie.198207113>.
- (6) Frey, G. D.; Lavallo, V.; Donnadiu, B.; Schoeller, W. W.; Bertrand, G. Facile Splitting of Hydrogen and Ammonia by Nucleophilic Activation at a Single Carbon Center. *Science* **2007**, *316* (5823), 439–441. <https://doi.org/10.1126/science.1141474>.
- (7) Martin, D.; Canac, Y.; Lavallo, V.; Bertrand, G. Comparative Reactivity of Different Types of Stable Cyclic and Acyclic Mono- and Diamino Carbenes with Simple Organic Substrates. *J. Am. Chem. Soc.* **2014**, *136* (13), 5023–5030. <https://doi.org/10.1021/ja412981x>.
- (8) Tolentino, D. R.; Neale, S. E.; Isaac, C. J.; Macgregor, S. A.; Whittlesey, M. K.; Jazzar, R.; Bertrand, G. Reductive Elimination at Carbon under Steric Control. *J. Am. Chem. Soc.* **2019**, *141* (25), 9823–9826. <https://doi.org/10.1021/jacs.9b04957>.
- (9) Hudnall, T. W.; Moerdyk, J. P.; Bielawski, C. W. Ammonia N–H Activation by a N,N'-Diamidocarbene. *Chem. Commun.* **2010**, *46* (24), 4288. <https://doi.org/10.1039/c0cc00638f>.
- (10) Hudnall, T. W.; Bielawski, C. W. An N, N' -Diamidocarbene : Studies in C - H Insertion , Reversible Carbonylation , and Transition-Metal Coordination Chemistry. **2009**, *373* (2), 16039–16041.
- (11) Siemeling, U.; Färber, C.; Bruhn, C.; Leibold, M.; Selent, D.; Baumann, W.; Hopffgarten, M. von; Goedecke, C.; Frenking, G. N-Heterocyclic Carbenes Which Readily Add Ammonia , Carbon Monoxide and Other Small Molecules ., *Chem. Sci.* **2010**, *1* (6), 697–704. <https://doi.org/10.1039/C0SC00451K>.
- (12) Chu, T.; Nikonov, G. I. Oxidative Addition and Reductive Elimination at Main-Group Element Centers. *Chem. Rev.* **2018**, *118* (7), 3608–3680. <https://doi.org/10.1021/acs.chemrev.7b00572>.

- (13) Peltier, J. L.; Tomás-Mendivil, E.; Tolentino, D. R.; Hansmann, M. M.; Jazzar, R.; Bertrand, G. Realizing Metal-Free Carbene-Catalyzed Carbonylation Reactions with CO. *J. Am. Chem. Soc.* **2020**, *142* (43), 18336–18340. <https://doi.org/10.1021/jacs.0c09938>.
- (14) Jazzar, A. R.; Bourg, J. B.; Dewhurst, R. D.; Donnadieu, B.; Bertrand, G.; Jazzar, R.; Bourg, J. B.; Dewhurst, R. D.; Donnadieu, B.; Bertrand, G. Intramolecular “Hydroiminiumation and -Amidiniumation” of Alkenes: A Convenient, Flexible, and Scalable Route to Cyclic Iminium and Imidazolium Salts. *J. Org. Chem.* **2007**, *72* (9), 3492–3499. <https://doi.org/10.1021/jo0703909>.
- (15) Benhamou, L.; Chardon, E.; Lavigne, G.; Bellemin-Laponnaz, S.; César, V. Synthetic Routes to N-Heterocyclic Carbene Precursors. *Chem. Rev.* **2011**, *111* (4), 2705–2733. <https://doi.org/10.1021/cr100328e>.
- (16) Kosai, T.; Ishida, S.; Iwamoto, T. A Two-Coordinate Cyclic (Alkyl)(Amino)Silylene: Balancing Thermal Stability and Reactivity. *Angew. Chem.* **2016**, *128* (50), 15783–15787. <https://doi.org/10.1002/ange.201608736>.
- (17) Alder, R. W.; Blake, M. E.; Chaker, L.; Harvey, J. N.; Paolini, F.; Schütz, J. When and How Do Diaminocarbenes Dimerize? *Angew. Chem. Int. Ed.* **2004**, *43* (44), 5896–5911. <https://doi.org/10.1002/anie.200400654>.
- (18) *NHC-CAAC Heterodimers with Three Stable Oxidation States - Munz - 2016 - Angewandte Chemie - Wiley Online Library.* <https://onlinelibrary.wiley.com/doi/full/10.1002/ange.201607537> (accessed 2023-08-01).
- (19) Enders, D.; Breuer, K.; Kallfass, U.; Balensiefer, T. Preparation and Application of 1,3,4-Triphenyl-4,5-Dihydro-1H-1,2,4-Triazol-5-Ylidene, A Stable Carbene. *Synthesis* **2003**, *2003* (8), 1292–1295. <https://doi.org/10.1055/s-2003-39409>.
- (20) Tomás-Mendivil, E.; Hansmann, M. M.; Weinstein, C. M.; Jazzar, R.; Melaimi, M.; Bertrand, G. Bicyclic (Alkyl)(Amino)Carbenes (BICAACs): Stable Carbenes More Ambiphilic than CAACs. *J. Am. Chem. Soc.* **2017**, *139* (23), 7753–7756. <https://doi.org/10.1021/jacs.7b04640>.
- (21) Das, A.; Elvers, B. J.; Nayak, M. K.; Chrysochos, N.; Anga, S.; Kumar, A.; Rao, D. K.; Narayanan, T. N.; Schulzke, C.; Yildiz, C. B.; Jana, A. Realizing 1,1-Dehydration of Secondary Alcohols to Carbenes: Pyrrolidin-2-Ols as a Source of Cyclic (Alkyl)(Amino)Carbenes. *Angew. Chem. Int. Ed.* **2022**, *61* (28), e202202637. <https://doi.org/10.1002/anie.202202637>.
- (22) Lorkowski, J.; Serrato, M. R.; Gembicki, M.; Mauduit, M.; Bertrand, G.; Jazzar, R. A Straightforward Access to Cyclic (Alkyl)(Amino)Carbene Copper (I) Complexes. *Eur. J. Inorg. Chem.* **2023**, *26* (15), e202300074. <https://doi.org/10.1002/ejic.202300074>.
- (23) Buron, C.; Stelzig, L.; Guerret, O.; Gornitzka, H.; Romanenko, V.; Bertrand, G. Synthesis and Structure of 1,2,4-Triazol-2-Ium-5-Ylidene Complexes of Hg(II), Pd(II), Ni(II), Ni(0), Rh(I) and Ir(I). *J. Organomet. Chem.* **2002**, *664* (1), 70–76. [https://doi.org/10.1016/S0022-328X\(02\)01924-1](https://doi.org/10.1016/S0022-328X(02)01924-1).
- (24) Çetinkaya, E.; Hitchcock, P. B.; Küçükbay, H.; Lappert, M. F.; Al-Juaid, S. Carbene Complexes: XXIV22For Part XXIII, See Ref. 1. No Reprints Available.. Preparation and Characterization of Two Enetetramine-Derived Carbenerhodium(I) Chloride Complexes RhCl(LR)₃ and [RhCl(COD)LR] and the Preparation and X-Ray Structures of the Enetetramine L2R and Its Salt [L2R][BF₄]₂. *J. Organomet. Chem.* **1994**, *481* (1), 89–95. [https://doi.org/10.1016/0022-328X\(94\)85013-5](https://doi.org/10.1016/0022-328X(94)85013-5).

- (25) Junor, G. P.; Lorkowski, J.; Weinstein, C. M.; Jazzar, R.; Pietraszuk, C.; Bertrand, G. The Influence of C(Sp³)H–Selenium Interactions on the ⁷⁷Se NMR Quantification of the π -Accepting Properties of Carbenes. *Angew. Chem.* **2020**, *132* (49), 22212–22217. <https://doi.org/10.1002/ange.202010744>.
- (26) Dong, S.; Frings, M.; Cheng, H.; Wen, J.; Zhang, D.; Raabe, G.; Bolm, C. Organocatalytic Kinetic Resolution of Sulfoximines. *J. Am. Chem. Soc.* **2016**, *138* (7), 2166–2169. <https://doi.org/10.1021/jacs.6b00143>.
- (27) Liu, X.; Liang, J.; Yu, Y.; Han, X.; Yu, L.; Chen, F.; Xu, Z.; Chen, Q.; Jin, M.; Dong, C.; Zhou, H.-B.; Lan, K.; Wu, S. Discovery of Aryl Benzoyl Hydrazide Derivatives as Novel Potent Broad-Spectrum Inhibitors of Influenza A Virus RNA-Dependent RNA Polymerase (RdRp). *J. Med. Chem.* **2022**, *65* (5), 3814–3832. <https://doi.org/10.1021/acs.jmedchem.1c01257>.
- (28) Yin, J.; Buchwald, S. L. Palladium-Catalyzed Intermolecular Coupling of Aryl Halides and Amides. *Org. Lett.* **2000**, *2* (8), 1101–1104. <https://doi.org/10.1021/ol005654r>.
- (29) Kang, S.-K.; Lee, S.-H.; Lee, D. Copper-Catalyzed N-Arylation of Amines with Hypervalent Iodonium Salts. *Synlett* **2000**, *2000* (7), 1022–1024. <https://doi.org/10.1055/s-2000-6673>.
- (30) Chen, Z.; Guo, Y.; Niu, H.; Wang, J.; Li, J.; Li, C.; Qiao, R. Development of a New Synthetic Route of the Key Intermediate of Irbesartan. *Org. Process Res. Dev.* **2022**, *26* (8), 2438–2446. <https://doi.org/10.1021/acs.oprd.2c00113>.
- (31) Wu, L.; Burgess, K. Syntheses of Highly Fluorescent GFP-Chromophore Analogues. *J. Am. Chem. Soc.* **2008**, *130* (12), 4089–4096. <https://doi.org/10.1021/ja710388h>.
- (32) Yan, C.; Theodorescu, D.; Miller, B.; Kumar, A.; Kumar, V.; Ross, D.; Wempe, M. F. Synthesis of Novel Ral Inhibitors: An in Vitro and in Vivo Study. *Bioorg. Med. Chem. Lett.* **2016**, *26* (23), 5815–5818. <https://doi.org/10.1016/j.bmcl.2016.10.021>.
- (33) Li, C.; Zhang, K.; Ma, H.; Wu, S.; Huang, Y.; Duan, Y.; Luo, Y.; Yan, J.; Yang, G. An Optimized Ni-Catalyzed Chan-Lam Type Coupling: Enantioselective Access to Chiral N-Aryl Sulfinamides. *Chem. – Eur. J.* **2022**, *28* (70), e202202190. <https://doi.org/10.1002/chem.202202190>.
- (34) O’Broin, C. Q.; Guiry, P. J. Synthesis of 2-Amino-1,3-Dienes from Propargyl Carbonates via Palladium-Catalyzed Carbon–Nitrogen Bond Formation. *Org. Lett.* **2020**, *22* (3), 879–883. <https://doi.org/10.1021/acs.orglett.9b04413>.
- (35) Frisch, M. J.; Trucks, G. W.; Cheeseman, J. R.; Scalmani, G.; Caricato, M.; Hratchian, H. P.; Li, X.; Barone, V.; Bloino, J.; Zheng, G.; Vreven, T.; Montgomery, J. A.; Petersson, G. A.; Scuseria, G. E.; Schlegel, H. B.; Nakatsuji, H.; Izmaylov, A. F.; Martin, R. L.; Sonnenberg, J. L.; Peralta, J. E.; Heyd, J. J.; Brothers, E.; Ogliaro, F.; Bearpark, M.; Robb, M. A.; Mennucci, B.; Kudin, K. N.; Staroverov, V. N.; Kobayashi, R.; Normand, J.; Rendell, A.; Gomperts, R.; Zakrzewski, V. G.; Hada, M.; Ehara, M.; Toyota, K.; Fukuda, R.; Hasegawa, J.; Ishida, M.; Nakajima, T.; Honda, Y.; Kitao, O.; Nakai, H. Gaussian 09.
- (36) Becke, A. D. Density-functional Thermochemistry. III. The Role of Exact Exchange. *J. Chem. Phys.* **1993**, *98* (7), 5648–5652. <https://doi.org/10.1063/1.464913>.
- (37) Zhao, Y.; Truhlar, D. G. The M06 Suite of Density Functionals for Main Group Thermochemistry, Thermochemical Kinetics, Noncovalent Interactions, Excited States, and Transition Elements: Two New Functionals and Systematic Testing of Four M06-Class Functionals and 12 Other Functionals. *Theor. Chem. Acc.* **2008**, *120* (1), 215–241. <https://doi.org/10.1007/s00214-007-0310-x>.

- (38) Rassolov, V. A.; Ratner, M. A.; Pople, J. A.; Redfern, P. C.; Curtiss, L. A. 6-31G* Basis Set for Third-Row Atoms. *J. Comput. Chem.* **2001**, *22* (9), 976–984. <https://doi.org/10.1002/jcc.1058>.
- (39) Schäfer, A.; Horn, H.; Ahlrichs, R. Fully Optimized Contracted Gaussian Basis Sets for Atoms Li to Kr. *J. Chem. Phys.* **1992**, *97* (4), 2571–2577. <https://doi.org/10.1063/1.463096>.

Chapter 4 – An Air-Persistent Radical Cation

4.1 Introduction

Electron rich olefins (Figure 4.1) are organic reductants that have applications in photoelectronic and photovoltaic devices, electrically conductive materials for organic field-effect transistors, and as chemical sensors. The most studied of these are the tetrathiafulvalene (TTF) **A** and related derivatives.¹ The TTF **A** displays three isolable oxidation states from the neutral, cation radical, and dication states. The tetraazafulvalenes (TAF) **B**₁ are unstable as they can exhibit the Wanzlick equilibrium, disassociating into their corresponding imidazole-2-ylidene N-heterocyclic carbene (NHC) monomers.² More recently, tethered TAF **B**₂ were shown to be more strongly reducing organic reductants.³ TAF **B**₂ also features two very close redox potentials, effectively rendering **B**₂ a two-electron reductant. Inspired by the carbene dimerization route to TAFs, Munz *et al* reported the synthesis and electronic properties of enetriamines (ETA) **C** which are NHC and cyclic (alkyl) (amino) carbene (CAAC) heterodimers.⁴ Further reports by Jana *et al* and Munz *et al* have determined the major effects that contribute to the successful isolation of each of the three oxidation states.^{5,6} Finally, enediamines (EDA) **D**₁ and **D**₂ were reported by Jana *et al* and Lombardi *et al*, respectively and are formally CAAC homodimers.^{7,8} These EDA also exhibit two redox events and at higher potentials, as expected due to the decreased stabilizing effect of the adjacent nitrogen atoms.

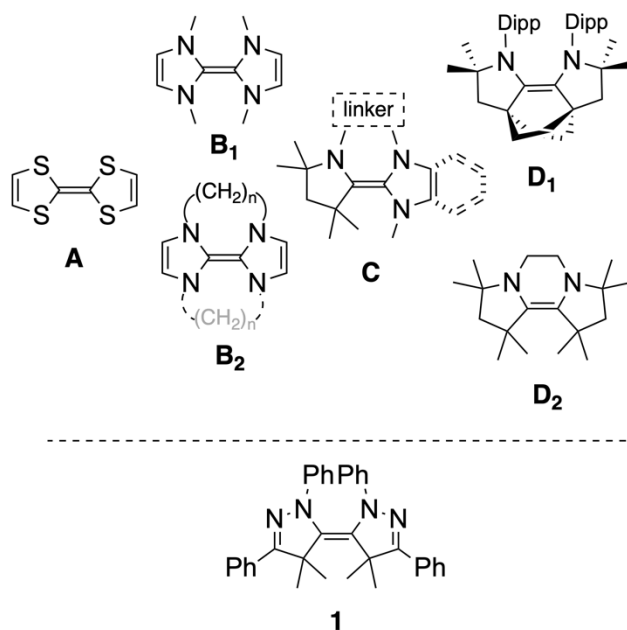


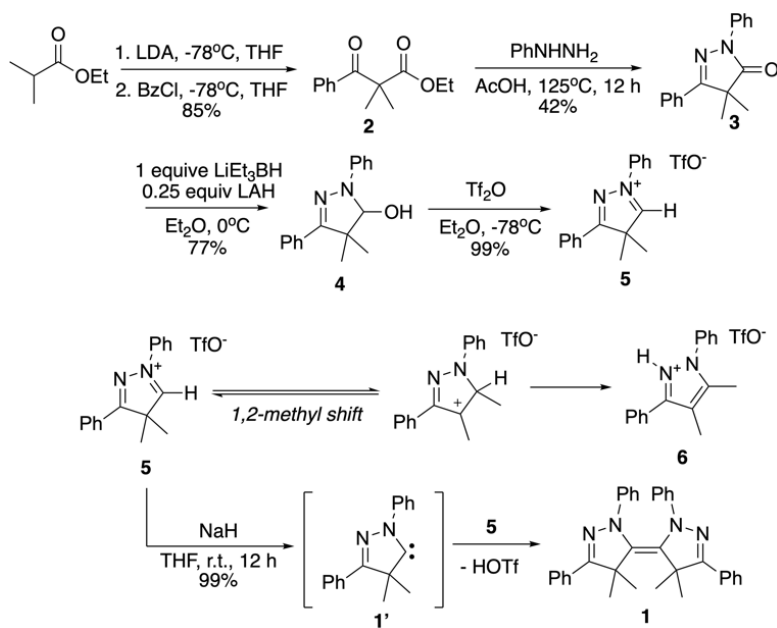
Figure 4.1. Tetrathiafulvalenes (**A**), tetraazafulvalenes (**B**), enetriamines (**C**), enediamines (**D**), and the herein reported novel EDA 3,3'-bipyrazolyliidene scaffold (**1**).

So far, efforts to access electron rich olefins via carbene dimerization has focused on using NHCs and CAACs. What interesting properties may emerge when other carbenes are utilized? Herein we report the synthesis of novel EDA dimer **1**, which can be thought of as the dimer of two small pyrazolyliidene carbenes, and its redox properties and reactivity. The extended conjugation provided by the carbon-nitrogen double bond in the pyrazolyliidene core is key to the air-persistent nature of the radical cation and spectroscopic features that facilitates easy identification of the redox states of dimer **1**. Their solid-state structures and electronic properties are discussed based on NMR, cyclic voltammetry, X-ray crystallography, EPR, and DFT calculations.

4.2 Synthetic Route to 3,3'-Bipyrazolyliidene

The bipyrazolyliidene structure was synthesized in a five-step synthesis (Scheme 4.1). First, a Claisen condensation of ethyl isobutyrate and benzoyl chloride yielded ketoester **2** as a

viscous, yellow oil. Ketoester **2** was then cyclized with phenylhydrazine in refluxing acetic acid to yield pyrazolone **3** as an off-white solid. Pyrazolone **3** can then be reduced with lithium aluminum hydride or lithium triethylborohydride to yield hemiaminal **4** as a white solid. Treating hemiaminal **4** with one equivalent of triflic anhydride in diethyl ether quantitatively yields pyrazolinium salt **5** as an off-white fluffy solid. In our work, we discovered that pyrazolinium **5** will rearrange into pyrazolium **6** through a 1,2-methyl shift and a subsequent deprotonation. This process is thought to be catalyzed by the presence of adventitious triflic acid not removed during workup, or by the basic imine nitrogen in the backbone. As a result, it is not recommended to store pyrazolinium **5** for greater than one day. Deprotonation of pyrazolinium **5** with sodium hydride quantitatively yields dimer **1** as a yellow oil. Dimer **1** is stable under inert conditions and has a half-life of 2 hours in ambient atmosphere, as measured by UV-vis spectroscopy. The overall yield of this synthetic route from ethyl isobutyrate to dimer **1** is 26.9%. Other bases such as KHMDS and KOtBu can be used to deprotonate pyrazolinium **5**, but due to the highly electrophilic iminium carbon and low levels of steric bulk surrounding the carbon, the addition product is formed as a byproduct. As reported in previous papers,^{4,9} dimer **1** is most likely formed from the free carbene **1'** immediately reacting with another equivalent of pyrazolinium **5** and a subsequent deprotonation by a second equivalent of base to yield the dimerized carbene. Single crystals of X-ray diffraction quality were obtained by dissolving dimer **1** in minimal pentane and leaving the solution in a -40°C freezer for several weeks.



Scheme 4.1. Synthesis of Dimer **1**.

4.3 Characterization

The NMR spectra of dimer **1** displays several identifiable peaks compared to its precursors and to other carbene dimers. The internal C=C bond has a chemical shift of δ 127.2 ppm versus δ 177.3, 92.9, and 172.9 ppm chemical shifts of the carbon atom in lactam **3**, hemiaminal **4**, and pyrazolinium **5** precursors, respectively. These chemical shifts are in general agreement with similar CAAC-derived compounds¹⁰ apart from the pyrazolinium carbon shift; the CAAC pyrrolidinium carbon shift is more downfield at δ 192 ppm.¹¹ The internal C=C bond of dimer **1** is also found in the same range as the previously reported carbene homo- and heterodimers. For comparison, the C=C bond in the Munz untethered heterodimer **C** has a shift of δ 127.7 ppm,⁴ the C=C bond in the Jana tethered CAAC homodimer has a shift of δ 126.9 ppm,⁷ and the Roesler CAAC homodimer has a shift of δ 126.7 ppm.⁸ Interestingly, the chemical shift of the imine carbon changes in the same direction as the carbenic carbon as well: δ 162.4 ppm in lactam **3**, δ 155.9 ppm in hemiaminal **4**, δ 183.5 ppm in pyrazolinium **5**, and δ 159.2 ppm

in dimer **1**. Additionally, the geminal methyl groups on the quaternary carbon adjacent to the internal double bond are non-equivalent, displaying two signals each integrating to six hydrogens at δ 1.25 and 1.50 ppm in ^1H -NMR and δ 26.1 and 26.6 ppm in ^{13}C -NMR, suggesting that the pyrazolidine rings may have a flexible puckered rather than a planar conformation.

2-D NMR experiments assisted in deconvoluting the dimer **1** NMR spectra and in establishing the assignments of multiple proton and carbon peaks. Through one-bond through-bond interactions ($^1J_{\text{H-C}}$) the ^1H - ^{13}C heteronuclear multiple quantum coherence (HMQC) experiment (Figure 4.2) established that one of the δ 1.25 ppm shift in ^1H -NMR and δ 26.6 ppm shift in ^{13}C -NMR is associated with one of the methyl groups and the δ 1.50 ppm shift in ^1H -NMR and δ 26.1 ppm shift in ^{13}C -NMR are associated with the other methyl group. While ^1H -NMR and ^{13}C -NMR shifts of alkyl groups are not perfectly correlated, the upfield shift of the δ 1.25 ppm methyl may be due to electronic shielding from a distant part of the molecule.

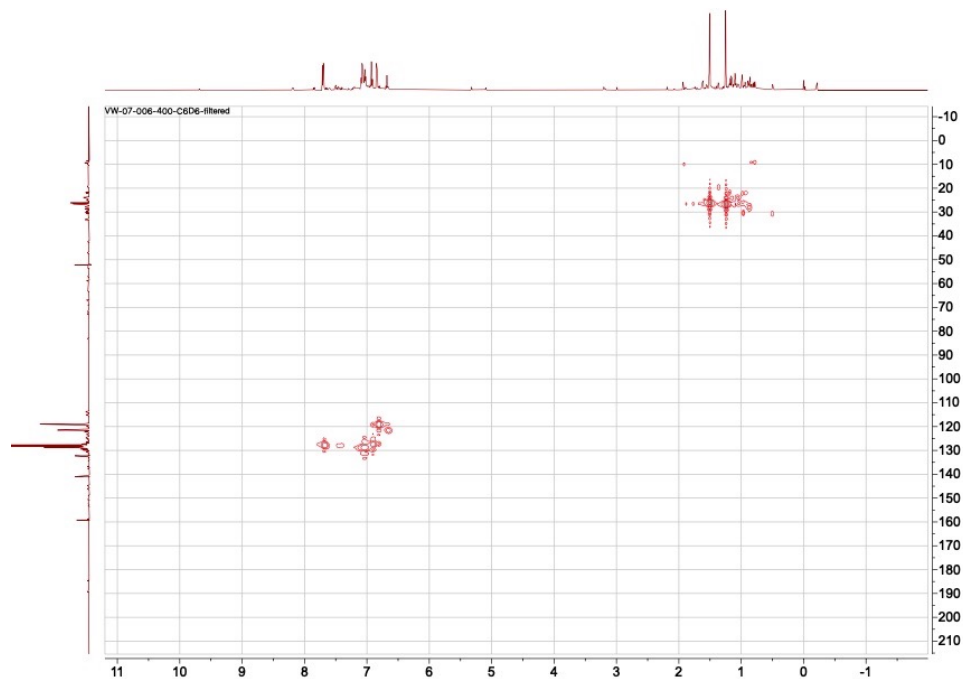


Figure 4.2. ^1H - ^{13}C HMQC NMR Spectrum of Dimer **1**.

The ^1H - ^{13}C heteronuclear multiple bond correlation (HMBC) experiment (Figure 4.3) revealed through multi-bond through-bond interactions ($^n\text{J}_{\text{H-C}}$ where $n > 1$) that the methyl protons were interacting not only with the carbons of the other methyl protons and the quaternary carbon, but also with the imine carbon at $\delta 159.2$ ppm and a carbon at $\delta 127.2$ ppm, definitively assigning this peak to the dimer **1** internal C=C bond. The ^1H - ^{13}C HMBC experiment also revealed interactions between the aromatic carbon and hydrogen atoms.

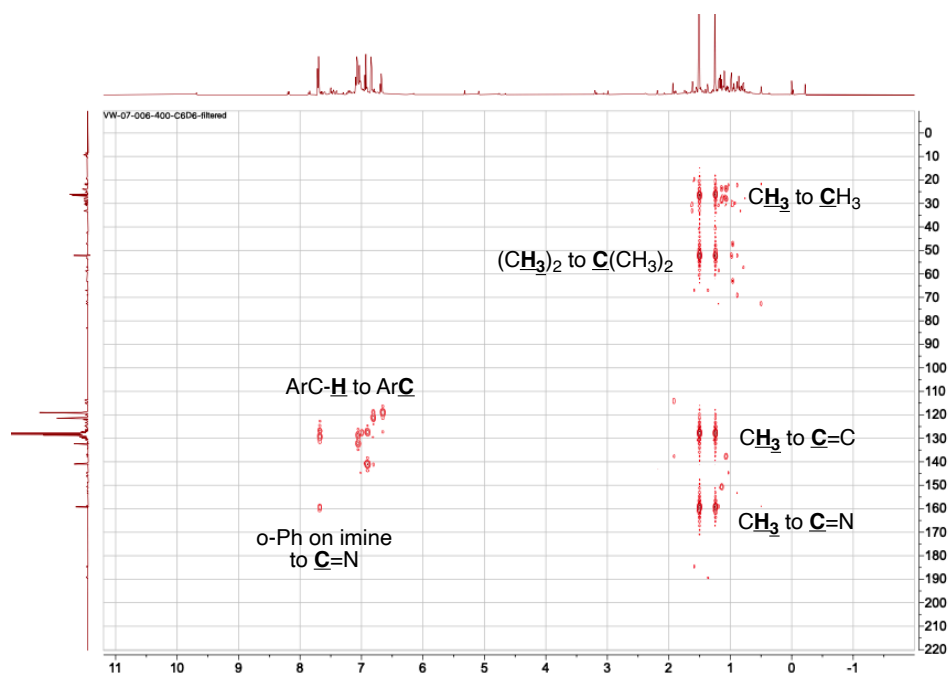


Figure 4.3. ^1H - ^{13}C HMBC NMR Spectrum of Dimer **1** with Interactions Labeled.

Finally, the 2-D homonuclear nuclear Overhauser effect spectroscopy (NOESY) (Figure 4.4) revealed that there are methyl-methyl and aromatic-aromatic through-space interactions, as expected, but through-space interactions between the methyl hydrogens and the aromatic hydrogen with the $\delta 7.70$ ppm chemical shift, which corresponds to the ortho-hydrogens of the C-phenyl group. Noticeably, these are no through-space interactions with upfield aromatic hydrogens were detected, indicating that the dimer is more likely to be the Z conformation, where the quaternary carbons are on the same side of the internal C=C bond, than the E

conformation, where the quaternary carbons are on opposite sides of the internal C=C bond. The 2-D nuclear interactions are summarized in Figure 4.5.

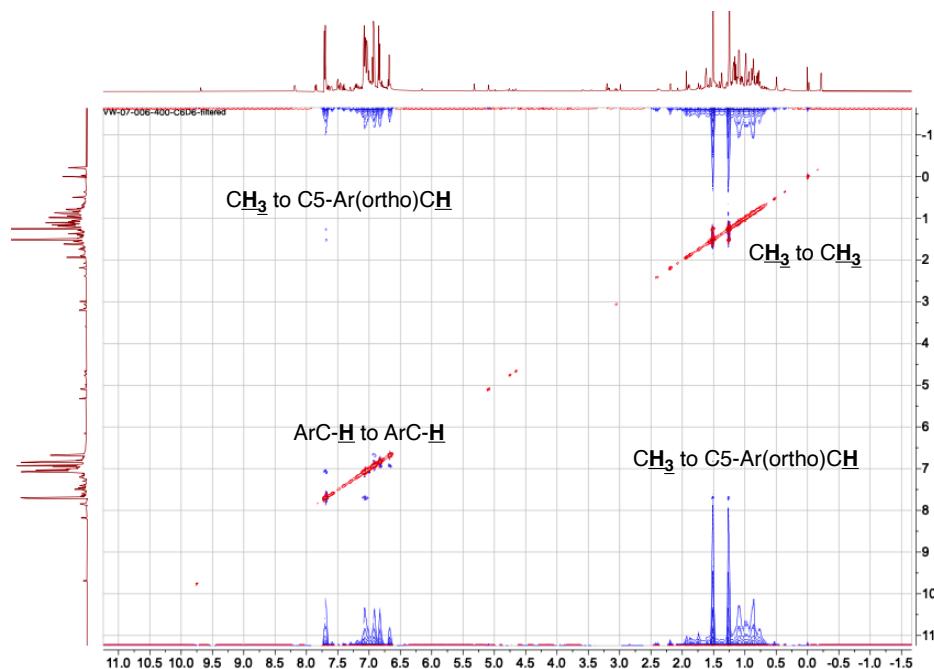


Figure 4.4. Homonuclear 2-D NOESY NMR Spectrum of Dimer 1 with Non-Cross Peak Interactions Labelled.

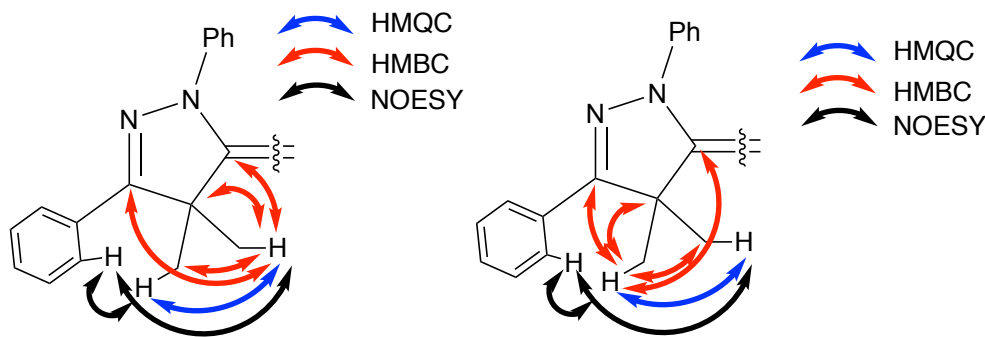


Figure 4.5. Summary of 2-D Nuclear Interactions of Dimer 1 by Each Geminal Methyl.

The cyclic voltammogram of dimer **1** showed two reversible one-electron processes at -0.623 V and -0.216 V vs. SCE (Figure 4.6). For comparison, the voltammograms of ETA **C** and EDA **D**₂ display two waves at $E_{1/2} = -0.01$ V and +0.33 V vs. SCE and -0.88 V and -0.07 V vs. SCE, respectively.^{4,8} The lack of a third nitrogen around the internal C=C bond can explain the anodic shift of the dimer **1** oxidation potentials relative to that of ETA **C**. Simultaneously, the

presence of two imine moieties in conjugation with the enediamine system can explain the cathodic shift of the dimer **1** oxidation potentials relative to that of EDA **D2**. Meanwhile, TTF **A** has two oxidation potentials at $E_{1/2}=+0.32$ V and $+0.71$ V vs. SCE.¹ Thus, dimer **1** and TTF **A** have similarly spaced oxidation potentials and **1** may have potential applications as a more reducing TTF.

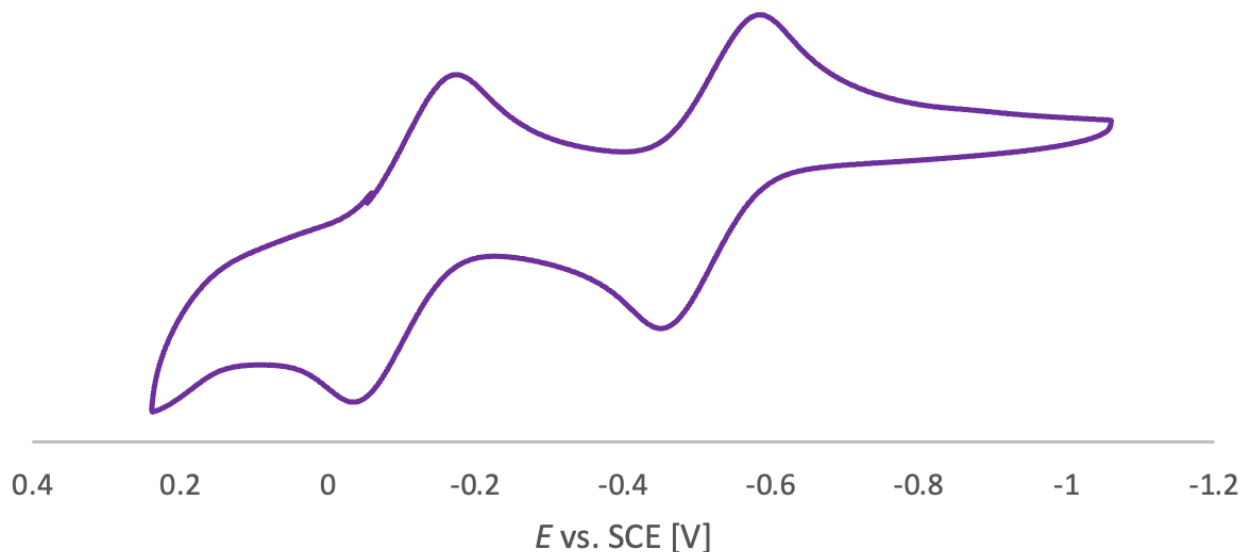
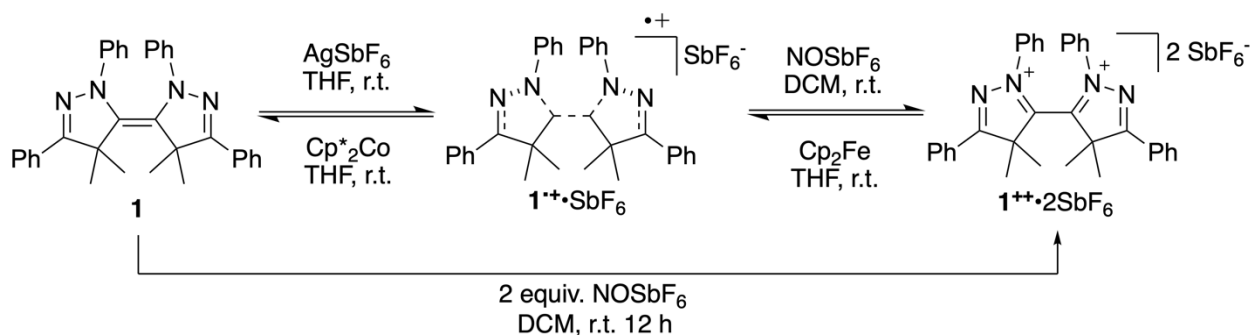


Figure 4.6. Cyclic voltammogram of bipyrazolylidene **1** ($n\text{Bu}_4\text{NPF}_6$ 0.1 M in THF, 100 mVs^{-1} , vs. SCE).

In agreement with the oxidation potentials obtained from cyclic voltammetry, dimer **1** was chemically oxidized with one equivalent of AgSbF_6 in THF to yield radical cation $\mathbf{1}^{\bullet+}\cdot\text{SbF}_6$ as an NMR-silent intensely purple oil (Scheme 4.2). Fortuitously, radical cation $\mathbf{1}^{\bullet+}\cdot\text{SbF}_6$ is air-persistent enough that it can be purified with silica gel column chromatography. Radical cation $\mathbf{1}^{\bullet+}\cdot\text{SbF}_6$ is stable when stored under inert conditions and has a half-life of 33 hours under ambient atmosphere, as measured by UV-vis. Radical cation $\mathbf{1}^{\bullet+}\cdot\text{SbF}_6$ was further oxidized with one equivalent of NOSbF_6 in CH_2Cl_2 to yield dication $\mathbf{1}^{2+}\cdot\text{SbF}_6$ as a red solid. Dication $\mathbf{1}^{2+}\cdot 2\text{SbF}_6$ can also be synthesized from dimer **1** directly by using two equivalents of NOSbF_6 in CH_2Cl_2 and stirring overnight. Dication $\mathbf{1}^{2+}\cdot 2\text{SbF}_6$ can be reduced to radical cation $\mathbf{1}^{\bullet+}\cdot\text{SbF}_6$ with

one equivalent of ferrocene in THF. Radical cation $1^{\bullet+}\cdot\text{SbF}_6$ can be reduced to dimer **1** with one equivalent of decamethylcobaltocene (Cp^*_2Co) in THF. Single crystals of radical cation $1^{\bullet+}\cdot\text{SbF}_6$ and dication $1^{2+}\cdot 2\text{SbF}_6$ to obtain their solid-state structure have so far been elusive. One possible explanation for this difficulty could be due to the existence of atropisomers of $1^{\bullet+}\cdot\text{SbF}_6$ and $1^{2+}\cdot 2\text{SbF}_6$. With axial chirality derived from the central C-C bonds of $1^{\bullet+}\cdot\text{SbF}_6$ and $1^{2+}\cdot 2\text{SbF}_6$, it is possible that the energy to the barrier of rotation around the central C-C bond is just small enough that the two stereoisomers can interconvert in solution (*vide infra*), causing the molecules to oil or powder out of solution rather than form orderly crystals.



Scheme 4.2. Synthesis of Monocation $1^{\bullet+}\cdot\text{SbF}_6$ and dication $1^{2+}\cdot 2\text{SbF}_6$.

The most striking feature of the solid-state structure of dimer **1** is that the two pyrazolidine rings of the core structure are vertically offset by approximately 1.2 Å (Figure 4.7). The geometry around the internal C=C bond resembles that of trans bent alkenes, a geometric motif more commonly seen in main group double bonds (B=B, Si=Si, Ge=Ge, etc.) and in strained alkenes like bridgehead alkenes and trans cycloalkenes.¹² Alternatively, the geometry of the internal C=C can be construed as the final geometry of two carbene monomers approaching each other in a carbene dimerization direct mechanism.⁹ The length of the internal C=C bond is 1.360 Å and longer than that of molecules **C** and molecule **D₂** (1.346 Å and 1.332 Å, respectively) even though the dimer has less sterically demanding N-phenyl groups rather than the N-Dipp groups of molecules **C** and **D₂**, perhaps indicating the steric environment around the

internal C=C bond is hindering a shorter C=C bond. The sum of the bond angles around nitrogen adjacent to the internal C=C bond, nitrogen atoms 1 and 2, are essentially planar [$\Sigma(\text{CN1C}) = 357.3^\circ$; $(\text{CN2C}) = 357.8^\circ$] compared with that of molecules **C** and **D**² [$\Sigma(\text{CN2C}) = 328.85^\circ$; $\Sigma(\text{CN3C}) = 330.66^\circ$, and $\Sigma(\text{CN1C}) = 356.1^\circ$; $\Sigma(\text{CN2C}) = 355.9^\circ$, respectively], indicating that greater conjugation and donation between the p(N) lone pairs and the internal C=C bond π -orbitals, which may also explain the longer length of the internal C=C bond. The torsion angle between the two bipyrazolylidene (as measured by atoms N1, C1, C1', and N1') is only 2.6° , which is small compared to the torsion angle of **C**⁴ (12.9°) but like that of **D**₂⁷ (2.9°). The solid-state structure reveals that the two N-phenyl groups have parallel displaced π -stacking interactions with each other, providing a stabilizing factor that favors the cis bipyrazolylidene conformation to the trans conformation in which the N-phenyl groups are on opposite sides of the internal C=C bond. Finally, the shortest distance between the C-phenyl ortho proton and one of the geminal methyl groups is 2.127 Å, which can explain the observed NOESY interaction between the geminal methyl groups and the aromatic hydrogen peak at $\delta 7.70$ ppm. The Nuclear Overhauser Effect is typically observed when interacting nuclei are less than 5.0 Å apart. Because both geminal methyl groups are observed to interact through space with the $\delta 7.70$ ppm peak, this suggests that, in the solution-state, the pyrazolylidine core exhibits some conformational flexibility.

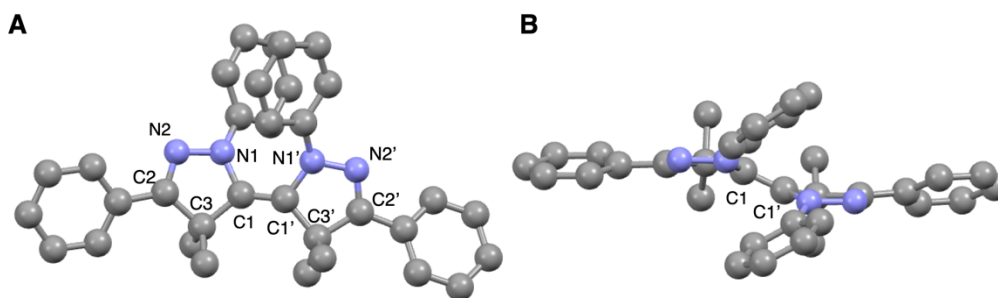


Figure 4.7. Solid-state structure of dimer **1** (a) top view and (b) side view. Hydrogen atoms omitted for clarity.

X-band electron paramagnetic resonance (EPR) measurement (Figure 4.8) of radical cation $\mathbf{1}^{\bullet+} \cdot \text{SbF}_6$ in THF show that the unpaired electron couples with two distinct pairs of nitrogen atoms. Simulation of the spectra allowed for the extraction of isotropic hyperfine couplings with each unique nitrogen atoms ($a_{\text{N1}} = 7.55$ MHz and $a_{\text{N2}} = 1.08$ MHz).

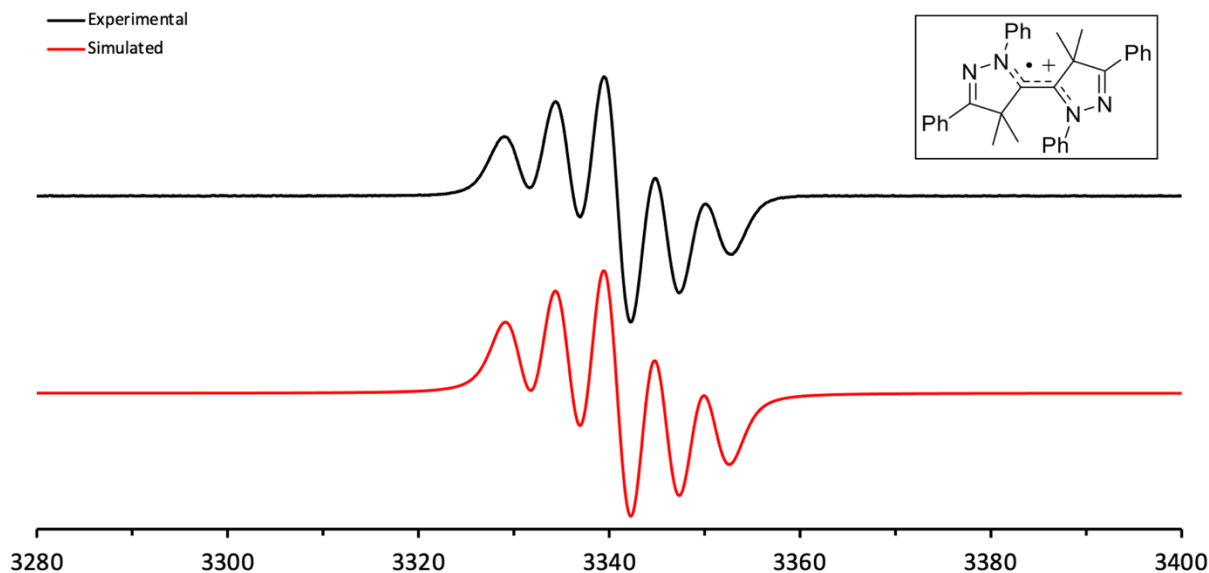


Figure 4.8. Experimental and simulated room-temperature EPR spectra of $\mathbf{1}^{\bullet+} \cdot \text{SbF}_6$.

Density functional theory (DFT) calculations were utilized to allow further understanding of the bipyrazolylidene system and predict what the structures of $\mathbf{1}^{\bullet+} \cdot \text{SbF}_6$ and $\mathbf{1}^{2+} \cdot 2\text{SbF}_6$ may look like (Figure 4.9). The structures of **1**, $\mathbf{1}^{\bullet+} \cdot \text{SbF}_6$, and $\mathbf{1}^{2+} \cdot 2\text{SbF}_6$ were optimized from the

single-crystal X-ray structure dimer **1** using Gaussian16¹³ program and performed with the hybrid functional U/B3LYP¹⁴ and the basis set TZVP.¹⁵ The functional-basis set combination was chosen to facilitate comparison with DFT calculations in relevant literature.^{5,7,8} In the optimized structures, the internal C-C bonds and the imine C=N bonds increase in length as the molecules become more oxidized from 1.360, to 1.410, and 1.462 Å and from 1.281, to 1.291, and 1.303 Å, respectively. The torsion angle of the three molecules also increases with increasing oxidation state from 2.6°, to 26.8°, and 47.7°. Finally, the bond between the internal alkene carbon and the adjacent nitrogen shortens as oxidation state increases from 1.411, to 1.361, and 1.317 Å.

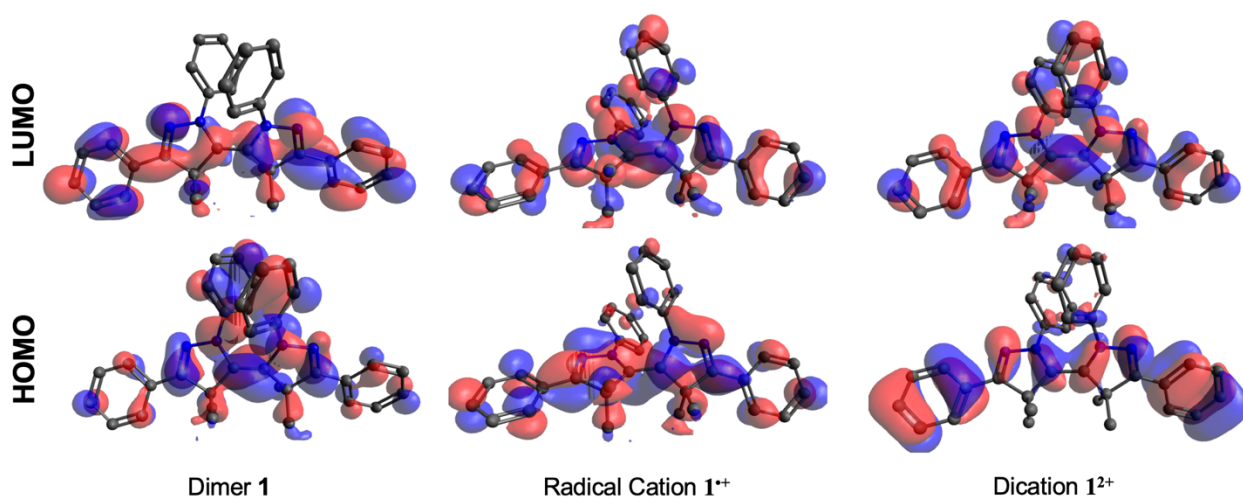


Figure 4.9. Representations of DFT calculated HOMO and LUMO (α -SOMO and β -SOMO for Radical Cation) of Dimer **1**, Radical Cation **1⁺**, and Dication **1²⁺**. Hydrogen atoms omitted for clarity.

A conformational analysis study was used to study the barriers of rotation of **1⁺** and **1²⁺**. The molecules were rotated around their internal C-C bond at dihedral angle increments of 15° based on the dihedral angle of N1-C1-C1'-N1' and the Hartree-Fock energy of each conformation was calculated (Figure 4.10). The analyses predict that the energy needed to overcome the rotational barrier is 20.99 kcal/mol for radical cation **1⁺** and 19.72 kcal/mol for

dication $\mathbf{1}^{2+}$. The global energy maxima, or highest energy conformation, of each molecule occurs when the N-phenyl and geminal methyl groups are eclipsed. In both molecules, the smaller local maxima occur when the pyrazolylidene rings are orthogonal to each other. The elongated internal C-C bond and increased distance of its flanking substituents of dication $\mathbf{1}^{2+}$ explains why its observed local maxima are lower in energy compared to that of radical cation $\mathbf{1}^{\bullet+}$. The IUPAC defines atropisomers as having a half-life of at least 1000 seconds at a given temperature, which corresponds to an energy barrier of approximately 22 kcal/mol at 300 K or 27°C.¹⁶ These two molecules are barely under the limit at the standard pressure and temperature parameters that the conformational analyses were conducted.

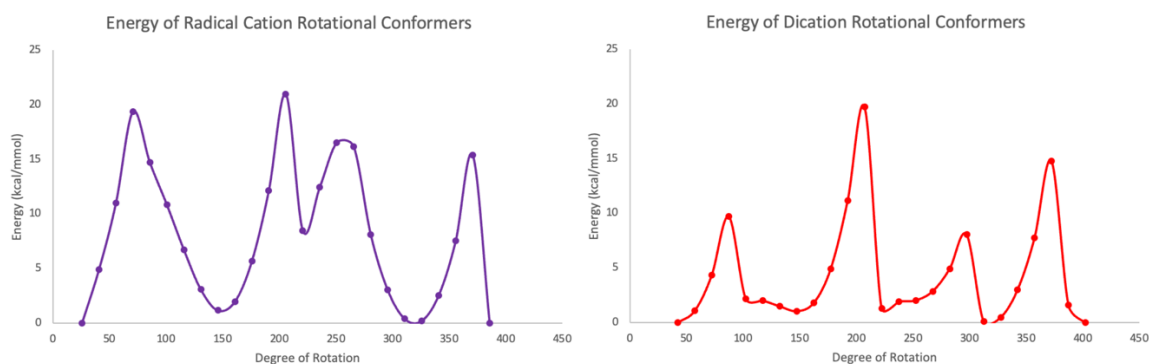


Figure 4.10. Calculated Barrier to Rotation of Radical Cation $\mathbf{1}^{\bullet+}$ and Dication $\mathbf{1}^{2+}$.

The Mulliken population analysis calculates the partial charge and spin density on each atom in the molecule. The analysis of radical cation $\mathbf{1}^{\bullet+}$ confirms that the unpaired electron spin density is distributed over both pyrazolylidene rings with significant spin density on the carbonic carbon and the adjacent nitrogen atom (Figure 4.11B). In all, the unpaired electron spin is well stabilized through the delocalization to eight of the core atoms. The differing amounts of spin density of both nitrogen atoms is consistent with the observed EPR hyperfine coupling constants.

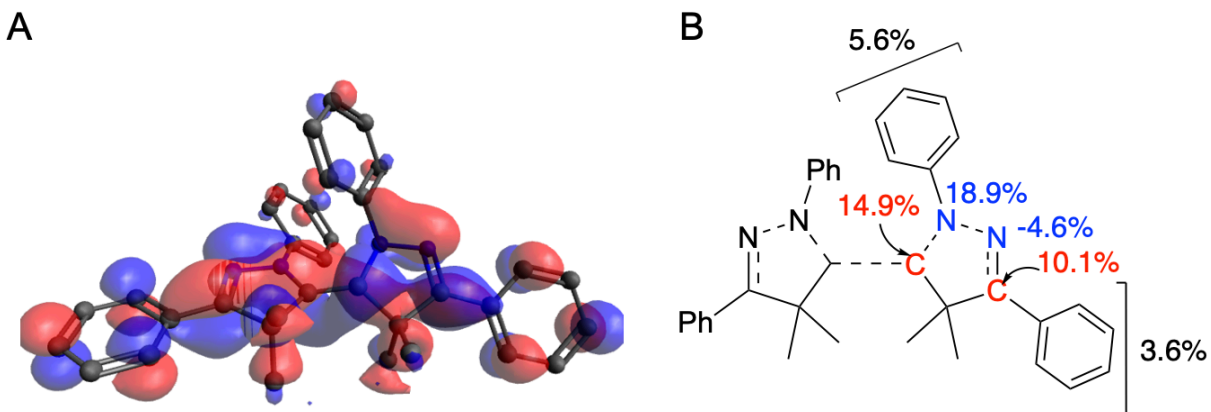


Figure 4.11. Representation of DFT Calculated (a) α -SOMO of Radical Cation $\mathbf{1}^+$ and (b) Spin Densities by Mulliken Population Analysis. As the molecule is symmetric, spin densities are shown only for the right half of radical cation $\mathbf{1}^+$.

4.4 Conclusions

In summary, the bipyrazolylidene framework introduces a unique structural motif for further development of reducing electron rich olefins. The air-persistent character of the derived radical cation can be attributed to the extended conjugation that the bipyrazolylidene system provides. As expected with the removal of one nitrogen atom, dimer $\mathbf{1}$ features a more positive pair of reversible redox potentials, especially compared with reported ETAs, and on par with EDAs derived from CAAC homodimers. The solid-state structure of dimer $\mathbf{1}$ contains offset pyrazolylidene rings and the internal C=C bond has the *Z* configuration, likely stabilized by parallel displaced π -stacking interactions of the N-phenyl groups. The EPR spectrum and DFT suggest that unpaired electron spin resides at both pairs of nitrogen atoms, with the nitrogen atom directly adjacent to the internal C=C bond containing more spin density than the imine nitrogen atom. Additionally, DFT calculations tantalizingly hint at radical cation $\mathbf{1}^+$ and dication $\mathbf{1}^{2+}$ existing as atropstereoisomers as the barrier of rotation across the internal C-C bond may lock the molecules in two inconvertible conformation states. In terms of outlook for the three

oxidation states of dimer **1**, the imine C=N bond may be of interest to spectroscopists who study chiral radicals as the C=N bond is highly distinctive in IR spectroscopy and can be used to monitor the electronic states of the radical cation and dication. Radical cation **1**^{•+} may be a prime candidate as a spintronics material, should the solid-state structure ever be fully characterized, whether by manipulating environmental conditions or by introducing additional steric hinderance to finally reach the defined atropisomer threshold.

4.5 Experimental

4.5.1 General Methods

All manipulations were performed using standard glovebox and Schlenk techniques. Glassware was dried in an oven overnight at 150 °C or flame-dried, and solvent were dried and degassed before use. Benzene, THF, diethyl ether, and n-pentane were freshly distilled over Na metal. Hexanes, dichloromethane, and chloroform were freshly distilled over CaH₂. All reactions with dimer **1** were set up in an argon-filled glovebox.

Deuterium-labeled solvents (d₆-benzene (C₆D₆) and d-chloroform (CDCl₃) were purchased from Cambridge Isotope Laboratories and were freshly distilled over CaH₂. NMR: Multinuclear NMR data were recorded on a Varian INOVA 500 MHz or a JOEL ECZL 400 MHz at UCSD. Chemical shifts (δ) are reported in parts per million (ppm) and are referenced to residual solvent signals (¹H, ¹³C). Coupling constants J are given in hertz (Hz). NMR multiplicities are abbreviated as follows: s = singlet, d = doublet, t = triplet, q = quartet, sext = sextet, sept = septet, m = multiplet, br = broad. All spectra were recorded at 298 K unless otherwise noted.

Electrochemical experiments were performed with an analyzer from CH Instruments (Model 620E) with platinum working and auxiliary electrodes. The reference electrode was built from a silver wire inserted in a small glass tube fitted with a porous Vycor frit and filled with a AgNO₃ solution in acetonitrile (0.01 M). Ferrocene was used as a standard, and all reduction potentials are reported with respect to the $E_{1/2}$ of the Fc⁺/Fc redox couple.

Single crystal X-Ray diffraction data were collected on a Bruker Apex II-CCD detector using either Mo-K α radiation ($\lambda = 0.71073 \text{ \AA}$) or Cu-K α ($\lambda = 1.54178$). Crystals were selected under oil, mounted on nylon loops then immediately placed in a cold stream of N₂. Structures were solved and refined using SHELXTL and Olex2 software. All hydrogen atoms were included in the refinement in calculated positions depending on the connecting carbon atoms. Visualized structures were generated with Mercury or Avogadro.

4.5.2 Synthetic Procedures

2: To a flame-dried 250 mL Schlenk flask equipped with a stir bar, diisopropylamine (12.5 mL, 0.089 mol) and dry THF (50 mL) were added, and then cooled on a dry ice-acetone bath to approximately -80°C. nBuLi in hexanes (2.5 M, 35.7 mL, 0.089 mol) was added slowly via syringe and needle. The reaction was removed from the acetone bath and stirred at room temperature for 45 minutes, then cooled to -80°C. To a separate flame-dried Schlenk flask, ethyl isobutyrate (15 mL, 0.112 mol) and dry THF (20 mL) were added and mixed. The ester solution was then cannula transferred into the 250 mL flask containing LDA. The resulting solution was removed from the acetone bath and stirred at room temperature for 1 hour. In a separate Schlenk flask, benzoyl chloride (8.75 mL, 0.075 mol) and dry THF (50 mL) were added and mixed. The benzoyl chloride solution was then slowly cannula transferred into the 250 mL flask. The flask

was then allowed to slowly warm up to room temperature and stirred overnight. The reaction was quenched with 100 mL water, then extracted with Et₂O (3 x 50 mL). The organic layer was then washed with water (2 x 25 mL) and dried with brine (1 x 25 mL) and MgSO₄. The solution was filtered, and all volatiles were removed in vacuo to yield **2** as a viscous yellow liquid (~90% yield, with residual THF). ¹H NMR (500 MHz, CDCl₃) δ = 7.83 (d, 2H, J=7.2Hz), 7.51 (t, 1H, J=7.0Hz), 7.41 (t, 2H, J=7.2Hz), 4.10 (q, 2H, J=7.3Hz), 1.53 (s, 6H), 1.03 (t, 3H, J=7.3Hz). ¹³C {¹H} NMR (125 MHz, C₆D₆) δ = 197.9, 175.2, 135.3, 132.8, 128.8, 128.5, 61.5, 53.4, 24.05, 24.01.

3: To a 100 mL round bottom flask equipped with a stir bar, phenylhydrazine (7.36 mL, 0.075 mol), **2** (15.00 g, 0.068 mol), and acetic acid (60 mL) were added, and the flask was equipped with a reflux condenser and external bubbler. The reaction was then heated to 130°C with stirring overnight. Upon cooling to room temperature, the reaction was diluted with Et₂O (100mL) and the entire solution was washed with water (2 x 100 mL), the dried with brine (1 x 30 mL) and Na₂SO₄, filtered, and all volatiles were removed in vacuo. The resulting crude product was recrystallized from hot MeOH and water to yield **3** as an off white solid. The mother liquor can yield a second batch of recrystallized product, but with more impurities. Yield 4.25g (23.6% yield). ¹H-NMR (500MHz, CDCl₃): δ 9.068 (d, 2H), 7.91-7.95 (m, 2H), 7.42-7.49 (m, 4H), 7.23 (t, 1H), 1.61 (s, 6H). ¹³C-NMR (125MHz, CDCl₃): δ 177.4, 162.4, 138.3, 130.7, 130.5, 129.0, 128.9, 126.7, 125.3, 118.07, 49.9, 23.1.

4: To a flame-dried 100 mL Schlenk flask equipped with a stir bar, lactam **3** (3.00 g, 0.011 mol) and LAH (0.107 g, 0.003 mmol) or LiBHEt₃ (1 M in THF, 11 mL, 0.011 mol) were added in the glovebox. The flask was brought out of the box, attached to a Schlenk line, and cooled on an ice-water bath to approximately 0°C. Dry Et₂O (30 mL) was added. The reaction

was stirred on ice bath for 2 hours. The reaction was quenched with EtOAc (10 mL) and then water (10 mL) and the left to stir for at least 30 minutes. The resulting slurry was filtered over celite on a frit, washing the cake with Et₂O (2 x 10 mL). The organic phase was separated from the aqueous, then dried with brine (1 x 15 mL) and MgSO₄. The solids were filtered off and volatiles were removed in vacuo. The crude product was purified by layering pentane over the crude or by recrystallization from pentane to yield hemiaminal **4** as an off white solid. The mother liquor can yield a second batch of product with reduced purity. *Caution: hemiaminal 4 is unstable in halogenated solvents exposed to oxygen, slowly transforming into a deep purple molecule whose identity is yet to be determined.* Yield 1.40g (41% yield). ¹H-NMR (500MHz, CDCl₃): δ 7.79 (d, 2H), 7.30-7.42 (m, 6H), 6.93 (t, 1H), 5.25 (d, 1H), 2.43 (d, 1H), 1.47 (s, 3H), 1.43 (s, 3H). ¹³C-NMR (125MHz, CDCl₃): δ 153.6, 143.3, 132.0, 129.4, 128.8, 128.6, 126.8, 120.4, 114.2, 92.4, 51.3, 25.3, 18.0.

5: To a flame-dried 50 mL Schlenk flask equipped with stir bar, hemiaminal **4** (1.00 g, 3.75 mmol) and dry Et₂O (20 mL) were added, then cooled on a water-ice bath to approximately 0°C. Tf₂O (0.63 mL, 3.75 mmol) was added dropwise to the solution and continued to be stirred at 0°C for 15 minutes before removing the ice bath and stirring at room temperature for 1 hour to yield a faintly green suspension. The reaction was filtered using an oven-dried filter cannula, then washed with dry Et₂O (2 x 10 mL). The resulting off white solid **5** was dried thoroughly under vacuum before being brought into the glovebox. Yield 1.40g (93.6% yield). ¹H-NMR (500MHz, CDCl₃): δ 10.74 (s, 1H), 8.27 (m, 2H), 8.13 (d, 2H), 7.74 (t, 1H), 7.62-7.69 (m, 5H), 2.04 (s, 6H). ¹³C-NMR (125MHz, CDCl₃): δ 183.9, 171.2, 135.4, 135.0, 133.4, 130.6, 129.9, 129.3, 125.9, 122.4, 120.7, 63.6, 21.2.

6: Iminium **5** was left in a sealed vial in the glovebox for seven days, slowly converting from an off-white powder to a red solid. *Alternatively: Iminium 5 (100 mg) was added to a Schlenk flask containing a magnetic stir bar and toluene (10 mL) and the solution was heated on an oil bath at 120°C overnight. All volatiles were removed in vacuo to give 6 in quantitative yield.* ¹H-NMR (400MHz, CD₂Cl₂): δ 7.74 (d, 2H), 7.51 (t, 4 H) 7.33-7.46 (m, 4H), 2.31 (s, 3H), 2.23 (s, 3H). ¹³C-NMR (100MHz, CD₂Cl₂): δ 150.7, 140.7, 137.6, 134.7, 129.4, 128.8, 128.6, 128.0, 127.6, 125.1, 11.3, 9.9.

1: Method 1 – In an Ar-filled glovebox, pyrrolidinium **5** (1.00 g, 2.01 mmol, 1 equiv.) and NaH (0.121 g, 5.03 mmol, 2.5 equiv.) were added to a 100 mL Schlenk flask equipped with a magnetic stir bar. The flask was brought out of the glovebox, connected to a Schlenk line, and cooled to 0°C on a water-ice bath. To the flask, dry Et₂O (60 mL) was added. The reaction was stirred overnight at room temperature with the flask open to the Schlenk line. Upon completion, the solution was filtered and then washed with water (2 x 20 mL). The organic layer was separated and dried with MgSO₄ and filtered. All volatiles were removed in vacuo with a Schlenk vacuum. The resulting yellow oil was stored in a glovebox until further use. Yield 0.56 g (57.7% yield).

Method 2 – In an Ar-filled glovebox, 1⁺•SbF₆ (40 mg, 0.053 mmol, 1 equiv.) and Cp*₂Co (18 mg, 0.055 mmol, 1.05 equiv.) were added to a 20 mL scintillation vial equipped with a magnetic mini stir bar. Dry THF (5 mL) was added, and the reaction was stirred for 1 hr at room temperature. All volatiles were removed in vacuo. The product was extracted from the residue with C₆D₆.

$^1\text{H-NMR}$ (500MHz, C_6D_6): δ 7.70 (d, 4H, $J=7\text{Hz}$), 7.00-7.09 (m, 8H), 6.93 (t, 4H, $J=7\text{Hz}$), 6.85 (d, 4H, $J=7\text{Hz}$), 6.68 (t, 2H, $J=7\text{Hz}$), 1.50 (s, 6H), 1.25 (s, 6H). $^{13}\text{C-NMR}$ (125MHz, C_6D_6): δ 159.2, 140.9, 132.3, 128.8, 128.7, 127.7, 127.2, 121.5, 119.0, 52.1, 26.6, 26.2.

$^1\text{H-NMR}$ (500MHz, CDCl_3): δ 7.82 (d, 4H, $J=7\text{Hz}$), 7.40-7.48 (m, 6H), 7.02 (t, 4H, $J=7\text{Hz}$), 6.82 (t, 2H, $J=7.8\text{Hz}$), 6.63 (d, 4H, $J=8\text{Hz}$), 2.03 (s, 12H), 1.73 (s, 12 H). $^{13}\text{C-NMR}$ (125MHz, CDCl_3): δ 159.5, 140.3, 131.7, 128.8, 128.6, 127.5, 127.2, 127.1, 121.0, 118.5, 52.3, 26.9, 26.4.

$1^+\cdot\text{SbF}_6$: Method 1 – In an Ar-filled glovebox, dimer **1** (0.30 g, 0.52 mmol, 1 equiv.) and AgSbF_6 (0.215 g, 0.62 mmol, 1.2 equiv.) were added to a 50 mL Schlenk flask equipped with a magnetic stir bar. The flask was brought out of the glovebox and connected to a Schlenk line. To the flask, dry DCM (10 mL) was added. The reaction was stirred overnight at room temperature. The solution was filtered and purified by column chromatography (silica gel) by first eluting all other organic compounds with EtOAc/hexanes (1:2) and the eluting the radical cation with DCM/MeOH (9:1). Fractions containing the radical cation were combined and the organic layer was dried with MgSO_4 and filtered. All volatiles were removed in vacuo with a Schlenk vacuum. The resulting deep purple oil was stored in a glovebox until further use. Yield 0.14 g (36.5% yield).

Method 2 - In an Ar-filled glovebox, $1^{2+}\cdot 2\text{SbF}_6$ (40 mg, 0.041 mmol, 1 equiv.) and Cp_2Fe (8.5 mg, 0.045 mmol, 1.1 equiv.) were added to a 20 mL scintillation vial equipped with a magnetic mini stir bar. Dry DCM (5 mL) was added, and the reaction was stirred for 1 hr at room temperature. All volatiles were removed in vacuo. The product was extracted from the residue with C_6D_6 .

$1^{2+} \cdot 2\text{SbF}_6$: Method 1 – In an Ar-filled glovebox, radical cation $1^{+\bullet} \cdot \text{SbF}_6$ (0.14 g, 0.19 mmol, 1 equiv.) and NOSbF_6 (0.056 g, 0.21 mmol, 1.1 equiv.) were added to a 50 mL Schlenk flask equipped with a magnetic stir bar. The flask was brought out of the glovebox and connected to a Schlenk line. To the flask, dry DCM (10 mL) was added. The reaction was stirred overnight at room temperature with the flask open to the Schlenk line. The solution was filtered with a cannula filter into a dry receiving Schlenk flask. All volatiles were removed in vacuo with a Schlenk vacuum. The resulting red solid was stored in a glovebox until further use. Yield 0.15 g (81.1% yield).

Method 2 - In an Ar-filled glovebox, dimer **1** (0.10 g, 0.20 mmol, 1 equiv.) and NOSbF_6 (0.112 g, 0.42 mmol, 2.1 equiv.) were added to a 50 mL Schlenk flask equipped with a magnetic stir bar. The flask was brought out of the glovebox and connected to a Schlenk line. To the flask, dry DCM (10 mL) was added. The reaction was stirred overnight at room temperature with the flask open to the Schlenk line. The solution was filtered with a cannula filter into a dry receiving Schlenk flask. All volatiles were removed in vacuo with a Schlenk vacuum. The resulting red solid was stored in a glovebox until further use. Yield 0.12 g (61.6% yield).

$^1\text{H-NMR}$ (500MHz, CD_3CN): δ 8.30 (d, 4H, $J=8.6\text{Hz}$), 4.93 (t, 4H, 7.5Hz), 7.77 (t, 4H, $J=7.5\text{Hz}$), 7.51 (t, 4H, $J=7.5\text{Hz}$), 7.18 (d, 4H, $J=7.5\text{Hz}$), 2.43 (s, 6H), 2.38 (s, 6H). $^{13}\text{C-NMR}$ (125MHz, CD_3CN): δ 189.2, 164.4, 136.9, 136.4, 132.4, 131.2, 126.2, 125.0, 69.3, 26.4, 22.8.

4.5.3 Crystallographic Data

Olex2 software¹⁷ was used for the resolution, refinement, and generation of crystallographic information files of every structure. The structures were solved with the ShelXS9¹⁸ structure solution program using Direct Methods and refined with the ShelXL9¹⁷

refinement package using Least Squares minimization. During the final stages of the refinements, all the positional parameters and the anisotropic temperature factors of all the non-H atoms were refined. The H atoms were geometrically located and their coordinates were refined riding on their parent atoms.

Molecule 1c	
Empirical formula	C ₃₄ H ₄₃ N ₄
Formula weight	496.63
Temperature/K	100.15
Crystal system	monoclinic
Space group	P 1 21/c 1
a/Å	10.730(3)
b/Å	22.353(6)
c/Å	11.307(3)
α/°	90
β/°	91.009(9)
γ/°	90
Volume/Å ³	2711.7(14)
Z	4
ρ _{calc} /g/cm ³	1.216
μ/mm ⁻¹	0.482
F(000)	1056
Crystal size/mm ³	0.46 × 0.37 × 0.25
Radiation	MoKα (λ = 0.71073)
2θ range for data collection/°	7.146 to 136.57
Index ranges	-11 ≤ h ≤ 11, -15 ≤ k ≤ 15, -16 ≤ l ≤ 16
Reflections collected	4854
Independent reflections	3281 [R _{int} = 0.0422, R _{sigma} = 0.0425]
Data/restraints/parameters	5563/0/370
Goodness-of-fit on F ²	1.036
Final R indexes [I ≥ 2σ (I)]	R ₁ = 0.0397, wR ₂ = 0.0965
Final R indexes [all data]	R ₁ = 0.0486, wR ₂ = 0.1023
Largest diff. peak/hole / e Å ⁻³	0.22/-0.21

4.5.4 Computational Data

All calculations were performed with the Gaussian16 program package.¹³ The theoretical approach is based on the framework of density functional theory (DFT). All calculations were

performed with the B3LYP functional and employing Pople *et al*'s 6-31G basis set¹⁹ and Ahlrichs *et al*'s TZVP basis set.¹⁵ The orbitals and energies of dimer **1** was calculated from the X-ray structure and from further geometry optimization from the X-ray structure. The geometries and energies of radical cation and dication **1^{•+}** and **1²⁺** calculated initially from ab initio structures that were pre-optimized using the Avogadro software and without constraints at the levels of theory. The Gibbs energy corrections from frequency calculations and dispersion corrections were added to the single-point energies to obtain the Gibbs free energies in solution. Gibbs free reaction energies and enthalpies were calculated for standard conditions ($P = 1$ atm, $T = 298$ K) and are unscaled and are given in the following Table 4.1. TD-DFT calculations were calculated at the levels of theory mentioned above to obtain electronic transitions in the near IR to UV wavelength regions but are not discussed here. Cartesian coordinates for the optimized structures are given in the following Table 4.2.

Table 4.1. DFT Calculated Thermodynamic Data of **1**, **1^{•+}** and **1²⁺** Calculated at B3LYP//TZVP.

Molecule	Thermodynamic Data
Dimer 1	Zero-point correction= 0.575947 (Hartree/Particle) Thermal correction to Energy= 0.608841 Thermal correction to Enthalpy= 0.609786 Thermal correction to Gibbs Free Energy= 0.510192 Sum of electronic and zero-point Energies= -1533.726003 Sum of electronic and thermal Energies= -1533.693109 Sum of electronic and thermal Enthalpies= -1533.692165 Sum of electronic and thermal Free Energies= -1533.791759
Radical Cation 1^{•+}	Zero-point correction= 0.578047 (Hartree/Particle) Thermal correction to Energy= 0.610579 Thermal correction to Enthalpy= 0.611524 Thermal correction to Gibbs Free Energy= 0.513701 Sum of electronic and zero-point Energies= -1533.558118 Sum of electronic and thermal Energies= -1533.525586 Sum of electronic and thermal Enthalpies= -1533.524641 Sum of electronic and thermal Free Energies= -1533.622464
Dication 1²⁺	Zero-point correction= 0.581443 (Hartree/Particle) Thermal correction to Energy= 0.613283 Thermal correction to Enthalpy= 0.614228 Thermal correction to Gibbs Free Energy= 0.518960 Sum of electronic and zero-point Energies= -1533.348555 Sum of electronic and thermal Energies= -1533.316714 Sum of electronic and thermal Enthalpies= -1533.315770

Table 4.1. DFT Calculated Thermodynamic Data of **1**, **1⁺** and **1²⁺** Calculated at B3LYP//TZVP (Continued).

	Sum of electronic and thermal Free Energies=	-1533.411038
--	--	--------------

Table 4.2. DFT Calculated Geometric Data of **1**, **1⁺** and **1²⁺**. Calculated at B3LYP//TZVP.

Molecule	Geometric Data
Dimer 1	N -2.77896 0.46699 -0.23507 C -3.00631 -0.76967 0.03537 C -1.72328 -1.59809 0.18416 C -0.67566 -0.48977 -0.10843 N -1.42266 0.68345 -0.34534 C 0.67566 -0.48976 0.10872 N 1.42268 0.68346 0.34551 C 1.72327 -1.59817 -0.18361 C 3.00630 -0.76973 -0.03500 N 2.77897 0.46697 0.23528 C -1.56392 -2.07639 1.65055 H -2.19669 -2.93737 1.86276 H -1.82762 -1.28267 2.35048 H -0.53588 -2.36496 1.84733 C -1.74430 -2.79579 -0.78758 H -2.62454 -3.41227 -0.60847 H -0.87125 -3.43240 -0.65497 H -1.77617 -2.45995 -1.82459 C 1.74422 -2.79564 0.78841 H 0.87115 -3.43224 0.65592 H 1.77607 -2.45956 1.82534 H 2.62444 -3.41220 0.60948 C 1.56401 -2.07680 -1.64990 H 0.53603 -2.36559 -1.84665 H 2.19695 -2.93770 -1.86193 H 1.82758 -1.28317 -2.34999 C 4.40616 -1.23502 -0.10417 C 4.79090 -2.42942 -0.72915 C 5.41515 -0.44930 0.48256 C 6.74537 -0.83665 0.43383 C 7.11104 -2.02655 -0.19425 C 6.12655 -2.81860 -0.77277 H 4.05706 -3.06425 -1.20095 H 5.13749 0.46867 0.98179 H 7.50075 -0.21262 0.89598 H 8.14963 -2.33143 -0.22826 H 6.39402 -3.74530 -1.26570 C -4.40618 -1.23497 0.10416 C -5.41499 -0.44925 -0.48288 C -4.79112 -2.42937 0.72900 C -6.12679 -2.81854 0.77223 C -7.11110 -2.02648 0.19343 C -6.74523 -0.83658 -0.43455 H -5.13718 0.46871 -0.98204 H -8.14970 -2.33135 0.22712 H -7.50047 -0.21255 -0.89692 H -4.05743 -3.06424 1.20100 H -6.39441 -3.74525 1.26506 C -1.05970 1.80694 -1.13329 C -1.77342 3.00133 -0.97871

Table 4.2. DFT Calculated Geometric Data of **1**, **1⁺** and **1²⁺**. Calculated at B3LYP//TZVP (Continued).

	C -1.46304 4.10411 -1.76057 C -0.43267 4.04230 -2.69842 C 0.27283 2.85445 -2.85257 C -0.03615 1.73842 -2.08024 H -2.56931 3.05158 -0.24954 H -2.02279 5.02217 -1.62858 H -0.18777 4.90776 -3.30130 H 1.06884 2.78584 -3.58429 H 0.50540 0.81608 -2.22528 C 1.05973 1.80706 1.13332 C 0.03615 1.73868 2.08025 C -0.27282 2.85481 2.85243 C 1.77348 3.00141 0.97861 C 1.46311 4.10430 1.76033 C 0.43271 4.04263 2.69817 H -0.50542 0.81637 2.22538 H -1.06885 2.78630 3.58415 H 2.56939 3.05156 0.24945 H 2.02288 5.02232 1.62824 H 0.18782 4.90816 3.30093
Radical Cation 1⁺	N 2.76575 0.43034 0.44072 C 3.01350 -0.77805 0.05829 C 1.73862 -1.58999 -0.18336 C 0.69307 -0.50367 0.13020 N 1.39364 0.59295 0.52720 C -0.69309 -0.50366 -0.13007 C -1.73867 -1.58994 0.18354 N -1.39363 0.59296 -0.52714 N -2.76574 0.43038 -0.44070 C -3.01354 -0.77799 -0.05822 C 1.61783 -2.02613 -1.66588 H 1.92507 -1.22669 -2.34006 H 0.59248 -2.29515 -1.90298 H 2.23982 -2.89480 -1.86833 C 1.71116 -2.80309 0.77688 H 2.58173 -3.43102 0.59787 H 0.82680 -3.41535 0.61925 H 1.73737 -2.48261 1.81843 C -1.71122 -2.80314 -0.77657 H -1.73741 -2.48277 -1.81815 H -2.58180 -3.43103 -0.59749 H -0.82687 -3.41540 -0.61885 C -1.61793 -2.02594 1.66611 H -1.92522 -1.22644 2.34021 H -0.59258 -2.29492 1.90327 H -2.23991 -2.89461 1.86861 C 4.41055 -1.22560 -0.03408 C 4.79033 -2.42453 -0.65467 C 6.12828 -2.79495 -0.72590 C 7.11268 -1.98076 -0.17811 C 6.75049 -0.78776 0.44606 C 5.41881 -0.41485 0.52037 H 5.14222 0.50605 1.01394 H 8.15382 -2.27272 -0.23302 H 7.50979 -0.15062 0.88162

Table 4.2. DFT Calculated Geometric Data of **1**, **1⁺** and **1²⁺**. Calculated at B3LYP//TZVP (Continued).

	H 4.05539 -3.07705 -1.09885 H 6.39845 -3.72327 -1.21287 C 0.95596 1.76999 1.20779 C 1.60319 2.97748 0.94650 C -0.04523 1.69331 2.17447 C -0.41956 2.84213 2.85989 C 0.20898 4.05541 2.59468 C 1.22360 4.11649 1.64266 H 1.72119 5.05557 1.43777 H 2.39015 3.01611 0.20737 H -1.19238 2.78219 3.61534 H -0.08292 4.94662 3.13520 H -0.50679 0.74561 2.41123 C -0.95590 1.76996 -1.20776 C 0.04531 1.69321 -2.17441 C 0.41968 2.84199 -2.85987 C -0.20883 4.05530 -2.59473 C -1.22347 4.11645 -1.64274 C -1.60311 2.97747 -0.94654 H -2.39008 3.01616 -0.20744 H 0.50686 0.74549 -2.41112 H 1.19253 2.78201 -3.61530 H 0.08311 4.94648 -3.13528 H -1.72104 5.05555 -1.43790 C -4.41060 -1.22553 0.03404 C -5.41878 -0.41486 -0.52068 C -4.79046 -2.42436 0.65476 C -6.12843 -2.79476 0.72587 C -6.75046 -0.78775 -0.44650 C -7.11275 -1.98066 0.17781 H -4.05559 -3.07681 1.09914 H -8.15389 -2.27261 0.23263 H -6.39866 -3.72300 1.21294 H -5.14211 0.50596 -1.01437 H -7.50971 -0.15068 -0.88227
Dication 1²⁺	N -2.71017 0.38986 -0.72286 C -3.02260 -0.74762 -0.16899 C -1.78230 -1.55277 0.21012 C -0.71621 -0.52562 -0.14596 N -1.32875 0.48556 -0.72734 C 0.71622 -0.52561 0.14591 C 1.78233 -1.55273 -0.21021 N 1.32875 0.48556 0.72731 N 2.71017 0.38988 0.72283 C 3.02262 -0.74758 0.16893 C -1.71272 -1.97549 1.69674 H -2.09869 -1.19757 2.35362 H -0.68866 -2.20021 1.98492 H -2.29467 -2.87834 1.85966 C -1.71742 -2.78400 -0.74579 H -2.59567 -3.40216 -0.57201 H -0.83730 -3.38830 -0.54747 H -1.71983 -2.47644 -1.79064 C 1.71750 -2.78400 0.74566 H 1.72000 -2.47648 1.79053

Table 4.2. DFT Calculated Geometric Data of **1**, **1⁺** and **1²⁺**. Calculated at B3LYP//TZVP (Continued).

H	2.59573	-3.40217	0.57178
H	0.83736	-3.38828	0.54739
C	1.71272	-1.97541	-1.69684
H	2.09871	-1.19749	-2.35371
H	0.68865	-2.20011	-1.98501
H	2.29463	-2.87829	-1.85978
C	-4.42215	-1.12617	-0.05445
C	-4.84444	-2.27512	0.63680
C	-6.19352	-2.58067	0.73429
C	-7.14308	-1.75246	0.14365
C	-6.73955	-0.61124	-0.55024
C	-5.39684	-0.29904	-0.65200
H	-5.08534	0.58096	-1.19624
H	-8.19518	-1.99529	0.22061
H	-7.47654	0.03025	-1.01518
H	-4.13411	-2.93219	1.11198
H	-6.50331	-3.46660	1.27250
C	-0.79305	1.63971	-1.38978
C	-1.40156	2.87334	-1.16170
C	0.25788	1.49488	-2.29311
C	0.73482	2.62086	-2.94881
C	0.15693	3.86551	-2.71120
C	-0.90996	3.98814	-1.82365
H	-1.36359	4.95429	-1.64849
H	-2.22997	2.95207	-0.47281
H	1.54032	2.51988	-3.66372
H	0.52816	4.73879	-3.23135
H	0.65940	0.51860	-2.52280
C	0.79302	1.63968	1.38977
C	-0.25792	1.49481	2.29308
C	-0.73490	2.62078	2.94880
C	-0.15704	3.86544	2.71121
C	0.90987	3.98811	1.82368
C	1.40150	2.87333	1.16171
H	2.22992	2.95210	0.47284
H	-0.65942	0.51852	2.52275
H	-1.54041	2.51976	3.66369
H	-0.52830	4.73871	3.23137
H	1.36348	4.95427	1.64854
C	4.42218	-1.12612	0.05445
C	5.39681	-0.29912	0.65227
C	4.84454	-2.27493	-0.63699
C	6.19363	-2.58047	-0.73440
C	6.73953	-0.61131	0.55060
C	7.14313	-1.75239	-0.14348
H	4.13427	-2.93191	-1.11239
H	8.19524	-1.99521	-0.22036
H	6.50347	-3.46629	-1.27274
H	5.08526	0.58077	1.19666
H	7.47647	0.03009	1.01576

4.6 Acknowledgements

Chapter 4 is adapted, in part from Victor T. Wang, Mohand Melaiimi, and Guy Bertrand “A 3,3’-Bipyrazolylidene Air-Persistent Radical Cation” that is in manuscript preparation. Permission to use images and data was obtained from Mohand Melaiimi and Guy Bertrand. The dissertation author was the first author of the manuscript.

4.7 References

- (1) Bendikov, M.; Wudl, F.; Perepichka, D. F. Tetrathiafulvalenes, Oligoacenes, and Their Buckminsterfullerene Derivatives: The Brick and Mortar of Organic Electronics. *Chem. Rev.* **2004**, *104* (11), 4891–4946. <https://doi.org/10.1021/cr030666m>.
- (2) Böhm, V. P. W.; Herrmann, W. A. The “Wanzlick Equilibrium.” *Angew. Chem. Int. Ed.* **2000**, *39* (22), 4036–4038. [https://doi.org/10.1002/1521-3773\(20001117\)39:22<4036::AID-ANIE4036>3.0.CO;2-L](https://doi.org/10.1002/1521-3773(20001117)39:22<4036::AID-ANIE4036>3.0.CO;2-L).
- (3) Shi, Z.; Thummel, R. P. N,N’-Bridged Derivatives of 2,2’-Bibenzimidazole. *J. Org. Chem.* **1995**, *60* (18), 5935–5945. <https://doi.org/10.1021/jo00123a034>.
- (4) *NHC-CAAC Heterodimers with Three Stable Oxidation States - Munz - 2016 - Angewandte Chemie - Wiley Online Library*. <https://onlinelibrary.wiley.com/doi/full/10.1002/ange.201607537> (accessed 2023-08-01).
- (5) Messelberger, J.; Grünwald, A.; Goodner, S. J.; Zeilinger, F.; Pinter, P.; Miehlich, M. E.; Heinemann, F. W.; Hansmann, M. M.; Munz, D. Aromaticity and Sterics Control Whether a Cationic Olefin Radical Is Resistant to Disproportionation. *Chem. Sci.* **2020**, *11* (16), 4138–4149. <https://doi.org/10.1039/D0SC00699H>.
- (6) Mandal, D.; Dolai, R.; Kumar, R.; Suhr, S.; Chrysochos, N.; Kalita, P.; Narayanan, R. S.; Rajaraman, G.; Schulzke, C.; Sarkar, B.; Chandrasekhar, V.; Jana, A. Influence of N-Substitution on the Formation and Oxidation of NHC–CAAC-Derived Triazaalkenes. *J. Org. Chem.* **2019**, *84* (14), 8899–8909. <https://doi.org/10.1021/acs.joc.9b00774>.
- (7) Kumar Nayak, M.; Suhr, S.; Chrysochos, N.; Rawat, H.; Schulzke, C.; Chandrasekhar, V.; Sarkar, B.; Jana, A. Tethered CAAC–CAAC Dimers: Oxidation to Persistent Radical Cations and Bridging-Unit Dependent Reactivity/Stability of the Dications. *Chem. Commun.* **2021**, *57* (10), 1210–1213. <https://doi.org/10.1039/D0CC07385G>.
- (8) Lombardi, B. M. P.; R. Pezoulas, E.; A. Suvinen, R.; Harrison, A.; S. Dubrawski, Z.; S. Gelfand, B.; M. Tuononen, H.; Roesler, R. Bis[Cyclic (Alkyl)(Amino)Carbene] Isomers: Stable Trans -Bis(CAAC) versus Facile Olefin Formation for Cis -Bis(CAAC). *Chem. Commun.* **2022**, *58* (45), 6482–6485. <https://doi.org/10.1039/D2CC01476A>.

- (9) Alder, R. W.; Blake, M. E.; Chaker, L.; Harvey, J. N.; Paolini, F.; Schütz, J. When and How Do Diaminocarbenes Dimerize? *Angew. Chem. Int. Ed.* **2004**, *43* (44), 5896–5911. <https://doi.org/10.1002/anie.200400654>.
- (10) Das, A.; Elvers, B. J.; Nayak, M. K.; Chrysochos, N.; Anga, S.; Kumar, A.; Rao, D. K.; Narayanan, T. N.; Schulzke, C.; Yildiz, C. B.; Jana, A. Realizing 1,1-Dehydration of Secondary Alcohols to Carbenes: Pyrrolidin-2-Ols as a Source of Cyclic (Alkyl)(Amino)Carbenes. *Angew. Chem. Int. Ed.* **2022**, *61* (28), e202202637. <https://doi.org/10.1002/anie.202202637>.
- (11) Lavallo, V.; Canac, Y.; Präsang, C.; Donnadiou, B.; Bertrand, G. Stable Cyclic (Alkyl)(Amino)Carbenes as Rigid or Flexible, Bulky, Electron-Rich Ligands for Transition-Metal Catalysts: A Quaternary Carbon Atom Makes the Difference. *Angew. Chem. - Int. Ed.* **2005**, *44* (35), 5705–5709. <https://doi.org/10.1002/anie.200501841>.
- (12) Borden, W. T. Pyramidalized Alkenes. *Chem. Rev.* **1989**, *89* (5), 1095–1109. <https://doi.org/10.1021/cr00095a008>.
- (13) Frisch, M. J.; Trucks, G. W.; Cheeseman, J. R.; Scalmani, G.; Caricato, M.; Hratchian, H. P.; Li, X.; Barone, V.; Bloino, J.; Zheng, G.; Vreven, T.; Montgomery, J. A.; Petersson, G. A.; Scuseria, G. E.; Schlegel, H. B.; Nakatsuji, H.; Izmaylov, A. F.; Martin, R. L.; Sonnenberg, J. L.; Peralta, J. E.; Heyd, J. J.; Brothers, E.; Ogliaro, F.; Bearpark, M.; Robb, M. A.; Mennucci, B.; Kudin, K. N.; Staroverov, V. N.; Kobayashi, R.; Normand, J.; Rendell, A.; Gomperts, R.; Zakrzewski, V. G.; Hada, M.; Ehara, M.; Toyota, K.; Fukuda, R.; Hasegawa, J.; Ishida, M.; Nakajima, T.; Honda, Y.; Kitao, O.; Nakai, H. Gaussian 09.
- (14) Becke, A. D. Density-functional Thermochemistry. III. The Role of Exact Exchange. *J. Chem. Phys.* **1993**, *98* (7), 5648–5652. <https://doi.org/10.1063/1.464913>.
- (15) Schäfer, A.; Horn, H.; Ahlrichs, R. Fully Optimized Contracted Gaussian Basis Sets for Atoms Li to Kr. *J. Chem. Phys.* **1992**, *97* (4), 2571–2577. <https://doi.org/10.1063/1.463096>.
- (16) Alkorta, I.; Elguero, J.; Roussel, C.; Vanthuyne, N.; Piras, P. Chapter 1 - Atropisomerism and Axial Chirality in Heteroaromatic Compounds. In *Advances in Heterocyclic Chemistry*; Katritzky, A., Ed.; Advances in Heterocyclic Chemistry; Academic Press, 2012; Vol. 105, pp 1–188. <https://doi.org/10.1016/B978-0-12-396530-1.00001-2>.
- (17) Dolomanov, O. V.; Bourhis, L. J.; Gildea, R. J.; Howard, J. a. K.; Puschmann, H. OLEX2: A Complete Structure Solution, Refinement and Analysis Program. *J. Appl. Crystallogr.* **2009**, *42* (2), 339–341. <https://doi.org/10.1107/S0021889808042726>.
- (18) Sheldrick, G. M. A Short History of SHELX. *Acta Crystallogr. A* **2008**, *64* (1), 112–122. <https://doi.org/10.1107/S0108767307043930>.
- (19) Rassolov, V. A.; Ratner, M. A.; Pople, J. A.; Redfern, P. C.; Curtiss, L. A. 6-31G* Basis Set for Third-Row Atoms. *J. Comput. Chem.* **2001**, *22* (9), 976–984. <https://doi.org/10.1002/jcc.1058>.